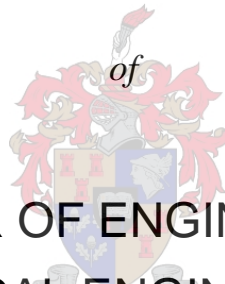# Technical and economic comparison of pyrolysis and pelleting for valorisation of pulper rejects from a secondary tissue mill, as alternative to disposal

by

Joshua Lourens Nel

Thesis presented in partial fulfilment
of the requirements for the Degree

of

MASTER OF ENGINEERING
(CHEMICAL ENGINEERING)

in the Faculty of Engineering
at Stellenbosch University

Supervisor
Prof. Johann Görgens

Co-Supervisor
Dr. François-Xavier Collard

March 2021

DECLARATION

By submitting this thesis electronically, I declare that the entirety of the work contained therein is my own, original work, that I am the sole author thereof (save to the extent explicitly otherwise stated), that reproduction and publication thereof by Stellenbosch University will not infringe any third party rights and that I have not previously in its entirety or in part submitted it for obtaining any qualification.

Date: March 2021

I

PLAGIARISM DECLARATION

1. Plagiarism is the use of ideas, material, and other intellectual property of another's work and to present is as my own.

2. I agree that plagiarism is a punishable offence because it constitutes theft.

3. I also understand that direct translations are plagiarism.

4. Accordingly, all quotations and contributions from any source whatsoever (including the internet) have been cited fully. I understand that the reproduction of text without quotation marks (even when the source is cited) is plagiarism.

5. I declare that the work contained in this assignment, except where otherwise stated, is my original work and that I have not previously (in its entirety or in part) submitted it for grading in this module/assignment or another module/assignment.

Initials and surname: J, L Nel

Date: 25 February 2021

Dedication

"This thesis is dedicated to my parents, Danté and Prue, whose no waste philosophy inspired me. Even if I had to stand in buckets while showering with lukewarm, solar-powered water that would eventually be used for watering the garden."

Abstract

South African paper mills are researching solutions to divert commercial and industrial waste (C&IW) from landfills. This problem is driven by increasing landfill fees, and pressure from the Department of Environmental Affairs and corporate policy.

This study evaluates two recycling methods for one C&IW from secondary tissue mills, known as pulper rejects. Pulper rejects are rich in plastics and contain some fibres. The methods of recycling included secondary (pelleting) and tertiary recycling (pyrolysis) to convert rejects into marketable solid recovered fuel (SRF) and condensable product (fuel oil), respectively.

Rejects were pretreated through drying, milling, extracting ferrous metal, and pelleting. The Ø6 mm pellets underwent analysis to test the technical, economic, and environmental factors according to two British SRF standards. The results from analyses proved the pellets to be feasible for cofiring as SRF in the primary burner of cement kilns. This was possible due to the high lower-heating value (LHV of 29.7 MJ/kg), low ash content (8.65 wt.%), and specific concentration of mercury, which was lower than the maximum permissible concentration according to the Air Quality Act 39 of 2004 (0.0574 mg/MJ).

Comparatively, the pellets were subject to pyrolysis for conversion to condensable product, char, and gas. The highest condensable product yield of 62.4 wt.% was achieved at 500 °C on bench-scale and the condensable product was 70% wax and the rest, oil. Consequently, temperatures from 450 to 550 °C were tested on pilot-scale, with a condensable product yield of 51.9 wt.% being achieved at 500 °C. This product contained wax, organic phase oil and aqueous phase oil being 47.6, 20.6 and 31.8 wt.% of the total, respectively. The wax and organic phase oil had a higher heating value (HHV) of 38.9 and 43.6 MJ/kg, respectively and formed the fuel oil product. The gross-energy conversion (GEC) represented the energy transfer from feedstock to products. At 500 °C, the GEC to char and condensable product from bench-scale and pilot-scale was 86.5% and 74.1%, respectively with the difference attributed

to the aqueous phase oil reported for pilot-scale. However, the separation of aqueous phase resulted in improved oil HHV from 20.6 MJ/kg (bench-scale) to 43.6 MJ/kg (pilot-scale).

Techno-economic models were developed for the pelleting and pyrolysis processes to compare profitability at mill capacity. The pelleting process was developed according to the recovery factor transform function method to evaluate multiple pelleting lines with the SRF selling price based off its LHV. The pyrolysis process was developed on Aspen Plus, using pilot-scale data, and the price of char and fuel oil determined according to their HHV.

Neither process was profitable with the economic settings. The minimum fuel selling price (MFSP) of SRF calculated at 25% discount rate was R6 269/ton and more than 5.16 times the current price (R1 214/ton). Similarly, the MFSP for fuel oil was R29 137/ton and 5.85 times the current price (R4 978/ton). Hence, unless waste disposal fee is drastically increased or feedstock capacity increased, both processes will remain unprofitable.

Opsomming

Suid-Afrikaanse papiermeule doen navorsing om oplossings te vind wat kommersiële en industriële afval (C&IW) weg van vullisterreine af lei. Die probleem word aangedryf deur verhoogde vullisterreinfooie, en druk van die Departement van Omgewingsake en korporatiewebeleid.

Hierdie studie evalueer twee herwinningsmetodes vir een C&IW uit sekondêre weefselmeule, bekend as pulpmasjienuitskot. Pulpmasjienuitskot is ryk in plastiek en bevat sommige vesels. Die metodes van herwinning sluit in sekondêre (korreling) en tersiêre herwinning (pirolise) om uitskot in bemarkbare soliede, herwinde brandstof (SRF) en kondenseerbare produk (brandstofolie), onderskeidelik, om te keer.

Uitskot is voorbehandel deur droging, malery, ekstrahering van ysterhoudende metale, en korreling. Die Ø6 mm korrels het analise ondergaan om die tegniese, ekonomiese en omgewingsfaktore na aanleiding van twee Britse SRF-standaarde te toets. Die resultate van die analises het bewys dat die korrels bruikbaar is vir ko-ontbranding as SRF in die primêre brander van sementoonde. Hierdie was moontlik as gevolg van die hoë laer-verhittingswaarde (LHV van 29.7 MJ/kg), lae asinhoud (8.65 wt.%), en spesifieke konsentrasie van kwik wat laer was as die maksimum toelaatbare konsentrasie na aanleiding van die Lug Kwaliteit Beleid 39 van 2004 (0.00574 mg/MJ).

In vergelyking, is die korrels onderwerp aan pirolise vir omsetting na kondenseerbare produk, verkoolsel en gas. Die hoogste kondenseerbare produk met 'n opbrengs van 62.4 wt.% is bereik by 500 °C op banktoetsskaal en die kondenseerbare produk was 70% was en die res, olie. Vervolgens is die temperature van 450 tot 550 °C getoets op loodsskaal, met kondenseerbare produkopbrengs van 51.9 wt.% wat bereik is by 500 °C. Hierdie produk het was, organiese fase-olie en waterige fase-olie bevat, wat 47.6, 20.6 en 31.8 wt.% van die totaal verteenwoordig, onderskeidelik. Die was en organiese fase-olie het 'n hoër verhittingswaardes (HHV) van 38.9 en 43.6 MJ/kg gehad, onderskeidelik, en het die brandstof-

olie produk gevorm. Die bruto-energie-omsetting (GEC) het die energie-oordrag van voermateriaal na produkte verteenwoordig. By 500 °C was die GEC na verkoolsel en kondenseerbare produk van banktoetsskaal en loodsskaal 86.5% en 74.1%, onderskeidelik met die verskil toegeskryf aan die waterige fase-olie gerapporteer vir loodsskaal. Die skeiding van waterige fase-olie het egter tot verbeterde olie HHV gelei, van 20.6 MJ/kg (banktoetsskaal) na 43.6 MJ/kg (loodsskaal).

Tegno-ekonomiese modelle is ontwikkel vir die korreling- en piroliseprosesse om winsgewendheid by meulekapasiteit te vergelyk. Die korrelingproses is ontwikkel na aanleiding van die herwinningsfaktor se transformeringsfunksiemetode om verskeie korrelinglyne met die SRF-verkoopsprys te vergelyk, gebaseer op sy LHV. Die piroliseproses is ontwikkel op Aspen Plus, deur loodsskaaldata te gebruik, en die prys van verkoolsel en brandstofolie is bepaal na aanleiding van hul HHV.

Nie een van die prosesse was winsgewend met die ekonomiese omgewing nie. Die minimum brandstofverkoopprys (MFSP) van SRF wat bereken is by 25% afslagkoers was R6 269/ton en meer as 5.16 keer die huidige prys (R1 214/ton). Soortgelyk was die MSFP vir brandstofolie R29 137/ton en 5.85 keer die huidige prys (R4 978/ton). Daarom, behalwe as afvalwegruimingfooie drasties verhoog of voermateriaalkapasiteit toeneem, sal beide prosesse nie-winsgewend bly.

Acknowledgements

Table of contents

List of figures

List of tables

Glossary

Aromatics	- Stable compounds with an aromatic ring in their molecular structure
ASTM	- American Society for Testing and Materials
BFD	- Block-flow diagram
Biorefinery	- A plant that converts biomass or waste into platform chemicals
BTX	- Benzene, Toluene and Xylene
ca.	- (lat: *circa*). Meaning "about"
CAPEX	- Capital expenditure of a project.
Coarse rejects	- Type of paper mill reject waste. Also called pulper rejects.
C&IW	- Commercial and Industrial waste
EC	- Energy conversion from feed to products
EU	- European Union
FCI	- Fixed capital investment
Fibres	- Lignocellulosic fibres
Fluff	- Non-pelleted, dried, shredded waste material.
GC/MS	- Gas chromatography/ Mass spectrometry
GEC	- Gross energy conversion, ratio of energy of the products to feedstock
HDPE	- High density polyethylene,
HHV	- Higher heating value
HMF	- Hydroxymethyl furfural
HMWC	- Heavy molecular weight compounds, enriching the wax, or solid phase
IRR	- Internal rate of return
ktpa	- kiloton per annum
LDPE	- Low density polyethylene
LGA	- Levoglucasan
LHV	- Lower heating value
LMTD	- Log mean temperature difference
LMWC	- Low molecular weight compounds, typically enriching the gas phase
MBT	- Mechanical-biological treatment
MFSP	- Minimum fuel selling price
Monomer	- Molecule that is bonded to other identical molecules to form a polymer
MSW	- Municipal Solid Waste

NCG	- Non-condensable gas
NEC	- Net energy conversion, which includes process energy too
NPV_{25}	- Net-present value after 25 years
Olefins	- Hydrocarbons with at least one multiple bond
Oligomer	- Chain of 2 to 5 monomers, e.g. two (dimers), three (trimers), etc.
OPEX	- Operating expenditure (annual) of a project.
PAHs	- Poly-aromatic hydrocarbons
PAMSA	- Paper Manufacturer's Association of South Africa
Paraffins	- Straight-chain/ branched hydrocarbons with no multiple bonds.
PE	- Polyethylene
PET	- Polyethylene terephthalate
PFD	- Process-flow diagram
Polymer	- Molecule of high molecular mass, composed of repeated monomers
PONA	- Paraffin, olefin, naphthene, aromatic
RFTF	- Recovery factor transfer function
PP	- Polypropylene
PS	- Polystyrene
PVC	- Polyvinyl chloride
RDF	- Refuse derived fuel
SRF	- Solid recovered fuel
Subcoal®	- Name of rejects processed into commercial secondary fuel pellets
TEA	- Techno-economic analysis
TCI	- Total capital investment
TGA	- Thermogravimetric analysis
viz.	- (lat: *videlicet*). Meaning "namely"
WC	- Working capital
WGSR	- Water gas-shift reaction
w.r.t	- with respect to
WDF	- Waste-derived fuel, an umbrella term for solid fuels from waste

Chapter 1: Introduction to Research

1.1. Background context and problem statement

From 2015 to 2017, the South African pulp and paper industry on average, contributed to 0.5%, 4.0%, and 21.5% of the national, manufacturing, and agricultural GDP, respectively [1], [2]. These statistics represent the scale of the pulp and paper industry and why most mills are required to track their social and environmental responsibilities. One of the core responsibilities of this industry is the minimization of waste and the elimination of landfill waste.

This core responsibility is not only being incentivized by corporate policy but is becoming a growing problem for South African paper mills due to the accelerating cost of landfill gate fees, restrictions on the landfilling of wet, organic waste and pressure from the South African Department of Environmental Affairs (SADEA). The landfill gate fee has been increasing yearly at *ca.* 7.5% per year due to the increasing loss of landfill air space and there is legislation in progress concerning banning the landfill of organic waste with a moisture content greater than 40 wt.% [3]–[5]. The SADEA published a National Environmental Management Waste Act (NEMWA) Section 28 notice in December 2017 requiring the pulp and paper industry to "develop and submit an industry waste management plan on how the respective industries will manage their waste" [6]. Although this statement was withdrawn two years later due to the passing of the then Minister of Environmental Affairs [5], it is expected that these requirements will resurface.

The study presented in this document focuses on a commercial and industrial waste (C&IW) stream, *viz.,* pulper rejects, from a secondary tissue mill in Johannesburg. Secondary mills use recycled paper, containing plastics and other waste, instead of pulp as feedstock and hence their produced waste is "highly heterogeneous with particles of varying moisture content, particle size and density" [7]. Despite these factors, in comparison to other wastes, like municipal solid waste (MSW), rejects are favored due to their higher energy content, lower chlorine content, more homogenous composition, and better access and workability from a contractual or procurement perspective [5], [8]. These characteristics apply for other C&IW streams and substantiate why C&IW is the second most recycled waste in South Africa, after metal, whereby 77% of all C&IW is recycled [9].

In South Africa, recycling processes are predominantly economically driven and hence should be shown to be profitable. If waste is recycled into an energy carrier it is helpful to compare the energy input for the manufacturing process to the energy extracted from the products to check whether less energy is used for the manufacture than what is gained [10]. Recycling methods are grouped as primary, secondary, tertiary, or quaternary recycling [11] and several industrial partners have

released preliminary reports showing how all the methods except primary recycling might be possible for recycling pulper rejects [7], [12]–[14].

Both primary and secondary recycling is referred to as "conversion to product" types of recycling [13]. Primary recycling uses mechanical separating techniques to isolate products with the same properties as the uniform, uncontaminated material [11]. The primary recycling of pulper rejects is discouraged due to its heterogeneity and the tendency of paper and plastics to clump together, making their separation almost impossible. Conversely, secondary recycling also uses separating units but results in a mixed product of lower value, such as secondary fuel or waste-derived fuels (WDF) [11]. The conversion of pulper rejects to WDF and its counterparts like refuse-derived fuel (RDF) or solid-recovered fuel (SRF) has had commercial success and patents describing its process. SRF from C&IW has been reported to have a higher lower-heating value (LHV) than SRF from construction waste or MSW [15]–[17]. The Dutch company, N+P recycling, has produced secondary fuel pellets, according to SRF standards called Subcoal® [18], [19], made for co-firing in cement kilns for clinker production. A patent also exists for cofiring WDF into boilers for electricity generation [20]. European standards have been developed to ensure that SRF is economically, technically, and environmentally suitable for cofiring in cement kilns or powerplants [10], [21].

Tertiary or chemical recycling employs chemical treatment to produce higher-value products from waste [22]. An example of tertiary recycling is depolymerizing mixed, contaminated waste through pyrolysis to create a fossil fuel substitute (e.g. heavy fuel oil) [11], [22]. Tertiary recycling is sometimes referred to as "conversion to energy-carrier" recycling. The tertiary recycling of pulper rejects into fuel oil is feasible due to its high plastic content (over 60 wt.%) resulting in substantial liquid yields of more than 50 wt.%, with high energy content [23]–[26], [27], [28]. Conversely, the process has been reported to be profitable when the rejects from multiple mills are combined, at 19 kilotons per annum (ktpa), which is 5.5 times greater than the current capacity (3.5 ktpa), evident of the processes' reliance on scales of economy [29]. Quaternary or energy recycling is not used to produce a physical product, like fuel, but instead to recover energy, most likely as electricity through an incineration process [11], [22]. It is a "conversion to energy" type of recycling [13] and is often integrated with tertiary or secondary recycling plants to produce the energy required for the process.

1.2. Research aim and questions

The goal of this research is to test which of the two recycling methods is best for the diversion of pulper rejects from landfill. The two recycling methods to be compared are the pyrolysis of rejects to produce fuel oil (tertiary recycling) and the pelleting of the rejects (secondary recycling) into a waste-derived fuel (WDF), specifically solid-recovered fuel (SRF). Literature contains several articles on the experimental results from the bench-scale pyrolysis of rejects [23]–[25], one for the techno-economics relating to the pyrolysis of rejects [29], or pyrolysis of biomass with a similar capacity to

the current mill [30]. Literature also has various article for the pelleting of MSW to form a WDF, usually RDF [31]–[33]. To the best of the author's knowledge, only one comparative study exists for the economic comparison between pyrolysis and pelleting processes [34]. However, this comparative study was for a biomass feedstock and used normalized data from other authors [34]. In contrast, the current study uses a C&IW feedstock and data gathered experimentally.

The problem to be addressed - which recycling method is best for the pulper rejects, is three-fold. The first aspect of the study involved treating pulper rejects through drying, extracting ferrous metals, milling, and pelleting. The treated reject pellets were then tested according to factors specified in the Waste Resources and Action Program (WRAP) classification scheme [35], which is an improvement to the SRF standard, BS EN 15359: 2011 [10], because it is ideal for small-scale SRF producers (>100 ktpa) [35]. The characteristics of SRF could be used to determine its application in industry and technology. Whereby, cement kilns were targeted as a customer due to their drive for high substitution rates with alternative fuel, as seen in European markets [36], [37]. Although, if SRF is used in South African cement kilns, its emissions must adhere to the Air Quality Act 39 of 2004 [38].

Through pyrolysis, pulper rejects are capable of being converted into a condensable product consisting of a wax and organic oil phase of high energy content. It is well-known that the condensable product can be heterogenous and might contain aqueous phase oil, containing mainly water. Hence, the second aspect was performing pyrolysis experiments on bench and pilot-scale setups to determine how scaling up will affect product yield, most importantly condensable product, and its composition. In addition, the effect of temperature on process gross and net energy conversions, should be tested to show how temperature (the main driving mechanism of pyrolysis) influences the transfer of energy from feedstock to products. The results from the pilot-scale pyrolysis of rejects provide a fairer and more reliable comparison to the results expected on commercial scale.

The third aspect involved assessing the profitability of either process at the mill capacity of 3.48 ktpa of wet, pulper rejects. The pelleting process followed the recovery factor transform function (RFTF) matrix method and required the composition (fibre, plastic, moisture, metal content, etc.) of the as-received rejects [32], [39]. The RFTF method could evaluate multiple pelleting lines and calculate the LHV of SRF, so that selling price could be determined [40]. Using the CAPEX and OPEX requirement, the selling price of SRF could be compared to the minimum fuel selling price (MFSP) to assess profitability. MFSP, at 25% discount rate, was calculated according to the discounted cash flow method. Conversely, the pyrolysis process required the composition of rejects, and pilot-scale product yields. This data was input into an Aspen Plus model for determining the mass and energy balance data. The results from Aspen could then be used for determining CAPEX and OPEX requirements. The experimental HHV was used to calculate the selling price of the char and fuel [41], which could be compared to the MFSP at 25% discount rate for evaluating profitability.

1.3. Scope and limitations of the investigation

The scope of this research is to test the technical and economic conversion of pulper rejects into solid recovered fuel (SRF) and condensable product (fuel oil) from pyrolysis. The limitations included:

- Exclusion of incineration tests to determine the effectiveness of SRF as an alternative fuel in the cement industry. Hence, the suitability of the SRF as a non-hazardous fuel is only based off characterization tests stipulated in BS EN 15359 and WRAP classification.
- Similarly, the specific gas concentrations (mg/MJ) for heavy metals content in the SRF were calculated from absolute concentrations (mg/kg) and transfer factors as specified according to SRF standards [42]. The specific gas concentration was then tested against the permissible concentrations specified in the South African Air Quality Act 39 of 2004 [38].
- Batch pyrolysis was performed for bench-scale experiments, while semi-continuous pyrolysis was performed for pilot-scale. Inherent differences between the reactor types are expected.
- The pyrolysis fuel oil was the wax and organic phase oil *sans.* aqueous phase oil. Whereby, the composition of the three phases (and fuel oil) used for the techno-economic analysis were based off literature values and not determined experimentally, due to time constraints.
- The techno-economics for the pelleting and pyrolysis process did not consider the environmental aspects of either process, because a full life-cycle assessment was not performed. The low carbon tax in South Africa at R127 per ton is expected to not significantly influence OPEX for either process or necessitate a carbon-capture stage.

1.4. Chapter Overview

This thesis is organized into 8 chapters to answer the research aims. **Chapter 2** is the literature review, which initially provides context to the paper mill waste. Thereafter, each recycling method is introduced, and the pelleting process is explained w.r.t the SRF standards and how SRF is used in cement kilns. The pyrolysis of both plastics and fibres is explored by investigating the product yields and condensable phase composition at tested temperatures and the literature review ends with a summary of techno-economic studies on pyrolysis and pelleting. **Chapter 3** reiterates the study objectives by clearly defining the respective sub-objectives. **Chapter 4** defines the experiment methodology followed, including the characterization tests, classification of SRF and methodology for bench-scale and pilot-scale pyrolysis. The results for the experimental work including the characterization, SRF tests, and pyrolysis experiments are detailed in **Chapter 5**. **Chapter 6** deals with the methodology followed for the techno-economic analysis (TEA) of both processes and provides the results for the TEA study. **Chapter 6** shows how the most appropriate pelleting and pyrolysis conversion lines were selected and provides a breakdown of results for the best pelleting and pyrolysis process and lastly, comparing the processes. **Chapter 7** provides the conclusions, based off the study aims, and provides recommendations for the work going forward.

4

Chapter 2: Literature Review

2.1. Context to the paper mill waste stream

2.1.1. Introduction to the secondary fibre mills

The paper and pulp industry involves processing timber into pulp, in a pulp mill, and then subsequently, processing pulp into paper-based products with paper mills. In addition to pulp, wastepaper can be recycled to make paper-based products. Paper mills that use recovered paper are known as secondary fibre mills and ones using pulp, primary fibre mills. Secondary pulp mills are cheaper to run and have less of an environmental impact than primary mills. However, the fibres can be recycled a maximum of six times [43], [44], and are usually recycled less than three times globally [45]. Secondary mills generate more than triple the amount of waste compared to primary fibre mills [46], especially in the form of rejects, which are non-existent in primary mills [47]. The quality and quantity of feedstock can vary depending on the source of the waste and time of year, for instance, higher proportions of wrapping and packaging paper occur during the festive season [47]. Figure 2.1 shows the flow of materials for the two types of fibre mills and its wastes including primary, deinking, secondary sludge, and rejects [48].
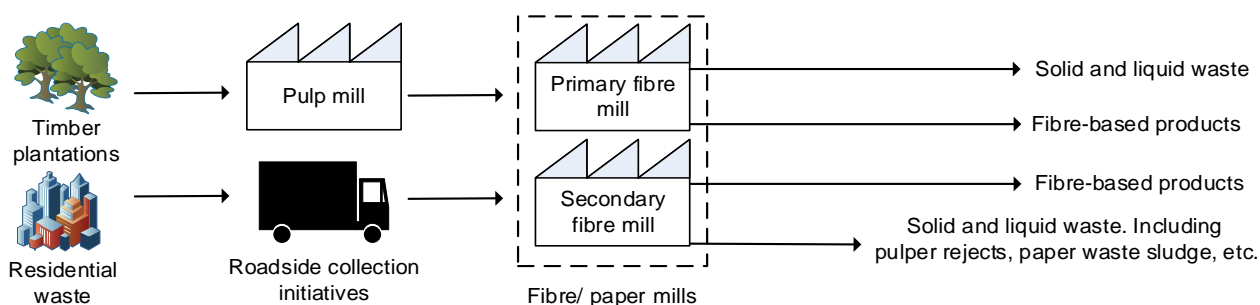
Figure 2.1: The material flow from raw material to finished product for pulp and paper mills.

Waste from secondary mills can be divided into two types of waste, *viz.*, rejects, and sludge. Rejects can be either coarse or fine and sludge can be deinking or effluent [13], [46]. For this study, only the coarse rejects that are separated early in the process line are considered.

2.1.2. Context of studied pulper rejects

Office-grade paper is typically the main feedstock for secondary tissue mills [43], [47]. Whereby, South African secondary tissue mills use 3 of the 16 paper grades as feed, being heavy letter 1 (HL1), heavy letter 2 (HL2), and common mixed waste (CMW) [49]. HL1 and HL2 form the two highest grades of recovered paper and consist of printed or unprinted paper without heavy printing [49]. CMW is less desirable as it can contain magazines with heavily printed paper or glossy paper and hence, more inorganics are expected [49], [50]. Whereby, using the CMW paper grade as feedstock will change the colour of wet-lap or final pulp, making it duller and grey in appearance.

Coarse rejects are separated early in the process line from the small fibres that are sent downstream for processing into pulp. The paper grade feedstock is stored as recovered paper bales and placed on a scale measuring mass intake, using a forklift. The mass of feed is measured to calculate the amount of chemicals and water to be added to the pulper [43]. The conveyor scale drops the feed into a high-density pulper, mixing with water and chemicals. The slurry is sent to the scalping screen which, depending on the density of the components, splits the stream into three products; light rejects, heavy rejects and accepts. The heavy rejects fall into the scalping screen conveyor screw which dumps the material into a trash container forming some of the pulper rejects. The light rejects are transported vertically under pressure into the drum screen which separates the material into accepts and rejects depending on particle size. The larger particles (rejects) that do not fall through the drum are sent to the scalping screen conveyor screw to reside in the trash container of pulper rejects. The accepts from the drum screen are recycled back to the high-density pulper and the accepts from the scalping screen are sent to the pulper dump chest for downstream processing. Coarse rejects are named 'pulper rejects' by some researchers because they are extracted directly after the high-density pulping unit [43]. The process explained above is shown in Figure 2.2.
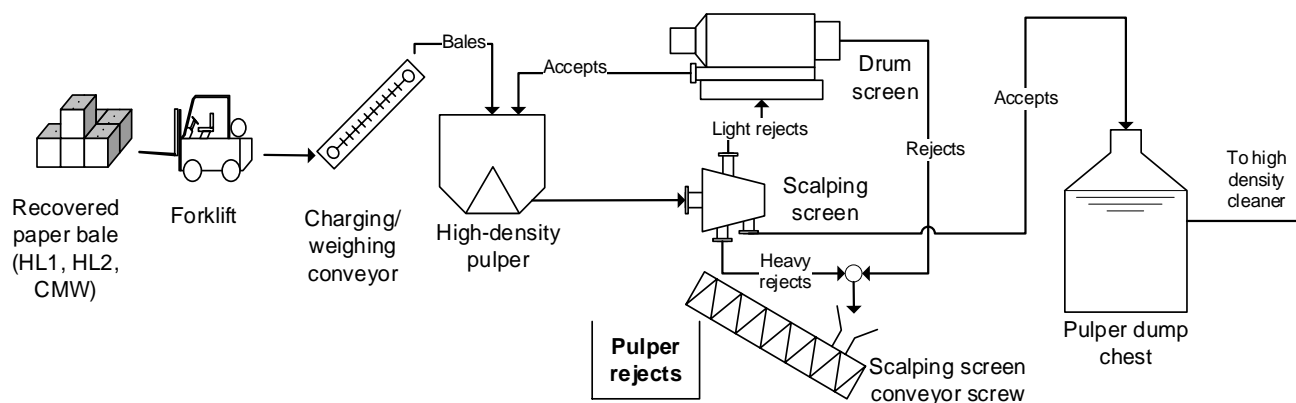
Figure 2.2: The process to extract the course/ pulper rejects from the process line

It has been reported by the paper mill that 6 wt.% of the recovered paper ends up as pulper rejects [51]. This is congruent to the value reported by another researcher at 6.5 wt.% [46]. The pulper rejects are comprised of heavy rejects from the scalping screen (e.g. cloth, metals, and glass) and light rejects from the drum screen (e.g. LDPE, PP, fibres, etc.) [47]. When the pulper rejects are dumped into the trash container, they have a very high moisture content, of at least 40 wt.% [23], [26], [52]. Pulper rejects are dewatered by a compactor or screw/ belt press and left to dry in a rain-free area to marginally decrease their moisture content before being landfilled [47]. Thermal drying techniques like forced convection or conduction are necessary to further lower the moisture content.

2.2. Composition of pulper rejects

2.2.1. Components of pulper rejects

Dried, pulper rejects consist of three main groups of components, *viz.,* plastics, biomass, and inorganics. Most researchers agree that pulper rejects are mainly comprised of plastics, making them the primary & secondary paper mill waste stream of highest energy content and lowest ash content [13]. Two researchers who have compartmentalized pulper rejects, found their plastic content to range between 70 to 77 wt.%, [23], [52]. Although, another researcher has identified rejects from a secondary board mill to be 16% plastics [26], [43], demonstrating that samples can have a wide plastic content range. Biomass and natural polymers in the form of fibres, textiles, wood, and leather are typically present as the second-largest group of materials, as seen in Figure 2.3 [23], [43]. Figure 2.3 provides an example of the composition of pulper rejects from one secondary mill [23]. Two researchers calculated the biomass content as being around 17 to 18 wt.% [52] and another as *ca.* 25 wt.% [23]. The biomass composition of rejects is calculated manually or through a selective dissolution method [52], which has been proven to work [53]. The third group of the pulper rejects are inorganics. In Figure 2.3, inorganics are presented as metals, including both ferrous and non-ferrous metals together, and other inorganics like sand or glass. Inorganics can also be present as part of plastic and biomass (e.g., inks, dyes, and fillers present in paper). Inorganics are minimized as much as possible through ballistic or magnetic separation because they are incombustible.
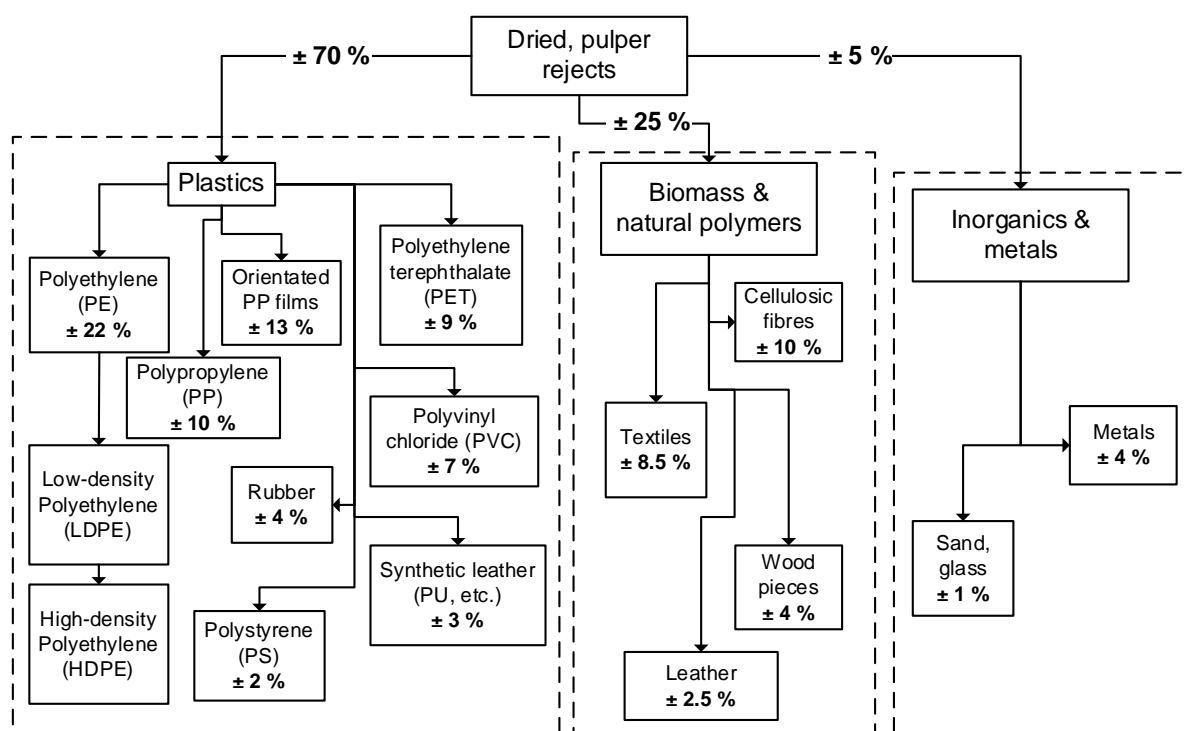
Figure 2.3: Approximate composition of pulper rejects gathered from a secondary paper mill [23]

Due to the heterogeneous composition of pulper rejects, and that waste streams differ greatly from one source to another, many researchers describe waste in terms of its proximate, ultimate, and/ or heating value analysis. These analyses provide insight into the chemical and thermal properties of the feedstock [54] and assist in predicting success as a fuel source. For proximate analysis, the moisture - and ash content describes the incombustible part of the stream. A low moisture and ash content will favour a better fuel source. Conversely, the fixed carbon and volatile matter content represent the organic, combustible part. Whereby a high content of each refers to material with good burning capabilities or a good fuel source. Volatile matter is the fraction of organics that volatize at extreme temperatures and fixed carbon is the carbon available after devolatization of the sample. Most plastics are typically entirely volatile matter, while biomass is more evenly balanced depending on the source (for instance wood typically contains 15 - 20 wt.% of fixed carbon and more than 70 wt.% volatile matter) [55]. Materials of high fixed carbon content are also successful fuels because they have long burning times but even fuel oils with no fixed carbon can too be successful fuels [56].

The link between the results from ultimate analysis and its success as a fuel source is less clear but typically material with a high carbon (C) content is a good fuel source, because large amounts of heat are released when C bonds are broken [56]. Researchers have found a linear relationship to exist between the C content and energy content of fuel [57], [58]. The presence of hydrogen (H) also contributes to the heating value but can cause loss of efficiencies because it can react to form water in flue gas [57], [59]. The presence of oxygen is less desired because it directly correlates to samples of lower energy content because C-O bonds release less energy than C-C or C-H bonds. In addition, incombustible water will form if H and O are present in the sample, and if no H is present the O will produce CO_2. The presence of nitrogen (N), sulphur (S), and chlorine (Cl) are rarer than the other components and are usually less than 1 wt.% combined in biomass sources [55], [60], [61]. Typically, N, S, and especially Cl, are undesired in the sample due to health and safety concerns. The emissions produced from the combustion of each can be harmful if not controlled, with the presence of N and S being directly proportional to the pollutant groups NO_x and SO_x in their emissions [62], [63] and the presence of Cl leading to the formation of hydrochloric gas, which is toxic if inhaled .

2.2.2. Plastics in pulper rejects

The six common thermoplastics make up 80% of all plastics used worldwide and are typically generated in residences and offices [64]. These plastics include PET, LDPE, PVC, HDPE, PP, and PS. Plastics are polymers which means they are molecules of high relative molecular mass, which are structurally comprised of repetitions of monomer units from low relative molecular mass [65]. The monomers present in each of the six common thermoplastics are shown in Figure 2.4. From the monomers, the carbon, hydrogen, oxygen (PET), and chlorine (PVC) can be calculated and be shown to be almost identical to that of the ultimate analysis, presented in Table 2.1. In addition the

difference in the polymer branching between LDPE and HDPE is illustrated in Figure 2.4 where HDPE polymers is generally linear and unbranched and LDPE is highly branched [66].
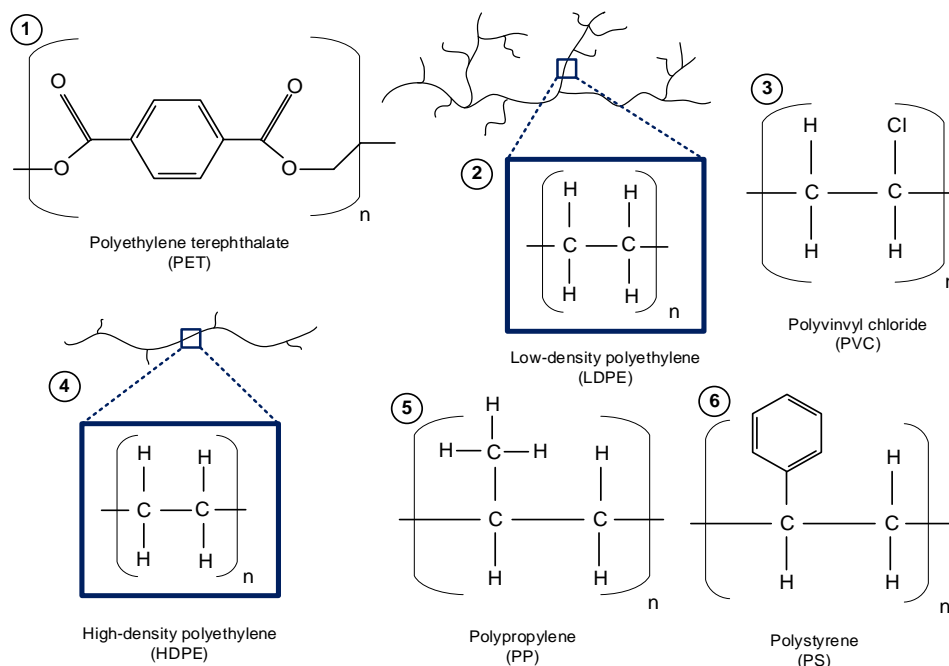
Figure 2.4: The monomers present in the plastics polymers

Table 2.1: Proximate, ultimate (wt.%), and heat (MJ/kg) analysis of different plastics.

Plastic Type		PET	HDPE	PVC	LDPE	PP	PS	*SL
Proximate Analysis	Moisture	0.61	0	0.57	0.30	0.21	0.28	0.20
	Ash	0.50	0.80	0.2	0.20	1.61	0.00	4.40
	VM	85.0	97.9	94.6	99.7	97.9	99.6	87.10
	FC	13.5	0.02	5	0	0.46	0.16	8.30
Ultimate Analysis	C	62.5	85.1	41.8	85.6	83.8	92.0	63.30
	H	4.20	15.3	5.73	14.3	13.8	7.85	6.30
	N	0	0.01	0.02	0.05	0	0.34	6.00
	O	33.3	0	2.92	0.05	0.20	0.52	17.60
	Cl	0	0	49.5	0	0.06	0	
	S	-	0.13	0.015	0.20	0.50	0	0.10
Energy values	C/H	14.9	6.14	7.48	6.01	6.09	11.7	10.05
	LHV	22.2	43.01	22.3	-	41.0	-	-
	HHV	23.2	43.97	22.8	46.6	46.4	42.1	26.06
References		[67], [68]	[67], [68];	[67], [69];	[69], [70]	[67], [69], [71]	[69], [72];	[73]

Notes: *SL; synthetic leather, usually comprised of polyurethane

Table 2.1 also shows the proximate analysis and higher-heating value (HHV) of the plastics. There is very little moisture and ash in all plastics as shown in Table 2.1 with the plastics having relatively high VM of >94 wt.%, except for PET which is still 85% [60]. These four plastics are also only

comprised of H & C, with a high C composition of 83% to 92% and low H composition of 8% to 14% [69]. These characteristics directly correlate to these plastics having high calorific values of 41 to 46 MJ/kg [67], [69]. The two plastics which contain a significant proportion of heteroatoms, being chlorine for PVC and oxygen for PET have a significantly lower energy content of 23 MJ/kg. It is understood that PVC is a major component of construction and demolition waste [74], and usually not found in packaging and single-use plastics as expected for pulper rejects.

2.2.3. Biomass components in pulper rejects

Biomass components, present in the pulper rejects, are mostly comprised of lignocellulosic fibres. Lignocellulose is comprised of three main natural polymers, *viz.;* cellulose, hemicellulose, and lignin, which together constitute the cell wall of all hardwoods, softwoods, grasses and other agricultural residues [75], [76]. Apart from the three polymers, there are also minor amounts of other organic (e.g. extractives) and inorganic material necessary for the proper functioning of the once-living organism of the tree [61]. Although the 'washed-out' fibres are the result of processed biomass, they still contain the main polymers, in different proportions to the raw wood. Softwoods such as conifer trees are typically used for paper production due to their higher cellulose content and longer fibres. The softwood timber beneath the bark used for paper production has a cellulose content of *ca.* 45%, compared to the hardwoods at *ca.* 40% [61]. The papermaking process of office-grade paper increases the cellulose content of pulp [77]–[79] to values around 75% [68], [80]. The bleached pulp production of the papermaking process removes part of the lignin as paper sludge and hence the lignin content of the paper is less and paper will be predominantly cellulose and hemicellulose [81].

Cellulose is a straight-chained, unbranched polysaccharide comprised of repeating cellobiose monomers [82], [83]. The cellobiose monomer is comprised of two β-glucopyranose units connected by an oxygen element as shown in Figure 2.5. Therefore each cellulose polymer has the molecular formula, $(C_6H_{10}O_5)_n$, where "n" refers to the degree of polymerisation [82]. The degree of polymerisation of cellulose can reach 5000 which is far greater than that of lignin or hemicellulose [84]. Cellulose can hold moisture because its fibrils have a large surface area of 100 to 200 m^2/g to entrain water and its structure contains high amounts of hydroxyl groups (as shown in Figure 2.5), that have strong hydrogen bonds with water, keeping water "bound on the fibril surface" [85], [86]. Cellulosic fibres are expected to have 6% to 8% moisture at conditions of moderate humidity [86].

Hemicellulose, unlike cellulose, is a heteropolysaccharide meaning that it is comprised of different kinds of monosaccharides [83]. In 1961, Aspinall defined hemicellulose to be a polysaccharide chain comprised of four or five of the following six monosaccharide units; D-xylose, D-mannose, D-glucose, D-galactose, or other glycosyls. The other glycosyls were later found to be L-arabinose and D-glucuronic acid. The degree of polymerisation of hemicellulose is 200 or less and it is more branched than cellulose [87]. The random amorphous structure of hemicellulose, of general molecular formula

10

($[C_5(H_2O)_4]_n$) gives rise to its weaker structure and hence why its hydrolyses in the presence of a weak acid or base, resulting in it not being as predominant as cellulose in paper [84].
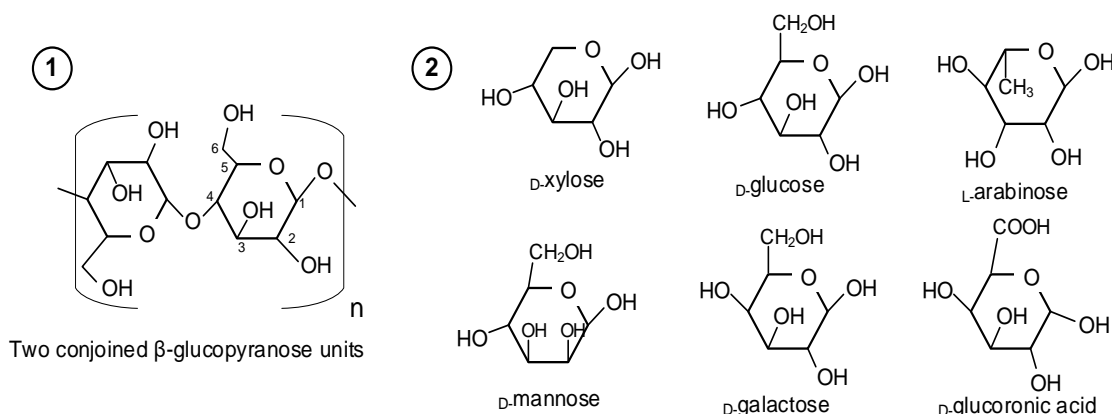
Figure 2.5: Monomer of cellulose on the left (1) and the common monomers of hemicellulose on the right (2)

The C, H, and O content of blank printing paper (BPP) and cotton cloth is similar to cellulose, representative of its high composition thereof, as shown in Table 2.2 [82]. Lignocellulosic biomass samples do not have an HHV greater than 20 MJ/kg. Whereby, BPP has a low HHV of 13.5 MJ/kg that due to its low lignin content and high ash content (inorganics present in labels and inks of the fibre) [50]. The reason why biomass has a lower HHV than plastics is from its higher O content ranging between 40 to 50 wt.%, as shown in Table 2.2. However, an advantage that biomass has over plastics (as shown in Table 2.2), is its lack of N, S, and Cl components, which each barely exceed 0.4%. Hence the emission control for the incineration or pyrolysis of biomass is less stringent than plastics due to its minimized NO_x, SO_x, or harmful dioxins pollution. Only leather, made up of collagen polymers, has a high N content of 6% and an S and Cl content of 1% to 2% [55].

Table 2.2: Proximate, ultimate (wt.%) and heat (MJ/kg) analysis of different natural polymers in pulper rejects

Material		*BPP	Cloth	HWRF	Wood	Rubber	Leather
Proximate Analysis	Moisture	0.00	-	4.80	4.80		7.46
	Ash	10.70	1.05	1.80	1.64	10.19	21.16
	VM	79.3	87.9	87.60	83.10	67.39	57.12
	FC	9.98	11.0	10.60	15.26	22.43	14.26
Ultimate Analysis and energy content values (C/H & HHV)	C	45.12	47.6	49.90	50.33	85.01	42.01
	H	5.31	6.30	6.00	6.11	8.27	5.32
	N	0.38	0.82	0.30	0.36	0.85	5.98
	O	48.90	45.1	43.30	43.04	4.12	22.83
	Cl	0.00	0.65	0.00	0.27	1.62	-
	S	0.28	0.13	0.00	0.11	1.56	1.00
	C/H	8.50	7.55	8.32	8.24	10.28	7.90
	HHV	13.51	17.08	-	19.60	32.00	16.85

References	[60]	[55]	[61]	[55]	[55]	[55]

Notes: *BBP: blank printing paper

2.3. Introduction to pelleting and pyrolysis for recycling

2.3.1. A brief introduction to pelleting

Waste streams such as commercial and industrial waste (C&IW) and municipal solid waste (MSW) can be converted into a secondary fuel, known as waste-derived fuel (WDF). WDF is an umbrella term used to describe unspecified waste which has been processed to increase its heating value [35]. A well-established type of WDF is refuse-derived fuel (RDF) which is typically converted to a type (like a powder, fluff, pellet etc.) according to an ASTM classification [88], [89]. The ASTM standard lists 7 types of RDF, and specifies particle sizing restrictions for 3 (coarse, fluff and powder) of the 7 RDF types [88], [89]. However, this standard does not consider any other environmental or economic factors [90]. Instead, there are European standards for a type of RDF known as solid recovered fuel (SRF), which is a defined type of RDF according to a quality management system (QMS). Consequently, SRF has been shown to have improved quality from a cofiring perspective when compared to RDF [91]. Figure 2.6 shows how C&IW can be converted into WDF. Figure 2.6 also shows how WDF, RDF, and SRF are linked to each other [90]. The production of waste is usually inevitable but waste like scrap metals can be sold to generate sales, as shown in Figure 2.6.
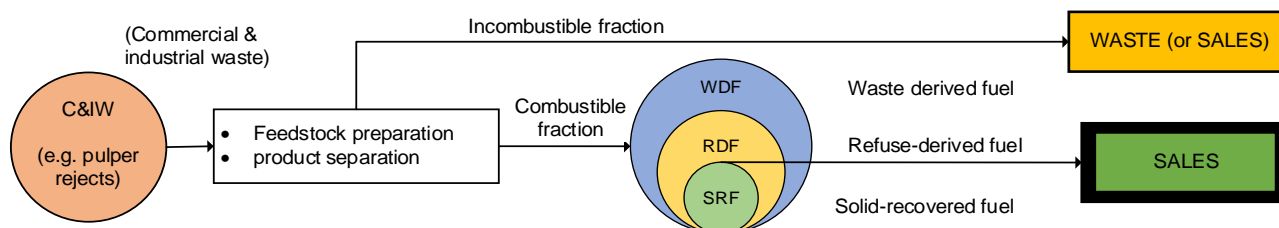
Figure 2.6: Onion diagram for the link between refuse-derived fuel (RDF) and solid-recovered fuel (SRF)

C&IW (e.g. pulper rejects), might be a good source for SRF conversion because they will require a shorter process line than waste fractions like MSW, because C&IW is expected to have a smaller fraction of incombustible matter and produce less waste requiring disposal [5], [8]. The only drawback of using pulper rejects as SRF is its very high as-received moisture content [12]. However, this can be overcome with effective dewatering processes like compaction and thermal drying.

2.3.1.1. Solid-recovered fuel (SRF)

The main customers of SRF would include the cement industry and powerplants [46], [92] The use of SRF in cement kilns is double-sided as it supplies the required energy demand, while its ash and residue from combustion are mixed with the cement clinker, adding to its volume [93]. Whereby, SRF can be co-processed with limestone in a kiln operating at a maximum temperature of 1450 °C to produce clinker, a precursor to Portland cement [94], [95]. The SRF with high volatile matter makes it easy to ignite but combust quickly due to low fixed carbon content [96]. European cement plants

12

were first spurred on to use substitute SRF with coal due to growing supply resultant of increasing waste disposal fees and willingness to reach a high substitution rate of coal [8].

2.3.2. A brief introduction to pyrolysis

Pyrolysis is a method of thermally degrading organics into three products (char, condensable product, and non-condensable gas) at moderately temperature (400 to 700 °C) and in an inert environment (No O_2). The elevated temperature and lack of oxygen prevent combustion, but still breaks some degree of polymer bonds within and between the organic monomers causing the unstable radicals to quickly co-react forming more stable, but shorter chain polymers (*viz.* oligomers) and other compounds [62], [97]. These oligomers have a much lower molecular weight than the original polymer and will vaporize at the reactor temperature [62], causing them to exit the reaction zone as volatiles to enter the condensation train. Condensable product is the fraction of condensed volatile products present as a liquid or wax at the temperature and pressure set in the condensers [97]. Volatiles that do not condense are called non-condensable gases (NCG) and the third product is a solid char made up of inorganics and more stable molecules that are not volatized at the pyrolysis temperature and pressure and left as a residue.

2.3.2.1. Condensable product

Condensable product is typically the most desirable product because it can substitute some fuel oils and if upgraded, transportation fuels [98], [99]. The physical and chemical properties of the condensable product are mainly dependent on the feedstock composition (plastics, lignocellulosic fibres or both), but also the pyrolysis conditions [99], [100] It is expected that the non-catalytic, pyrolysis of pulper rejects will yield condensable product similar to fuel oil because its composition will be mainly short and long aliphatic hydrocarbons present as oil and wax, respectively [24], [101], [102]. Commercial fuel oils, like heavy fuel oil (HFO), can have a high viscosity and be used for heating and steam generation applications [103], [104]. While, fuel oils with lower viscosity (more oily) can also be used for heating applications or substitute marine fuel oil [105], [106]. A problem associated with highly viscous liquid fuels is that they can repolymerize over time, making the storage and transportation of the fuel more difficult [47].

2.4. Conversion of pulper reject into solid recovered fuel (SRF) pellets

The following section describes SRF standards, pellet production, use of SRF in cement kilns and some information regarding the process lines for production of secondary fuels in literature.

2.4.1. Standards related to SRF

As is, pulper rejects have negative economic value due to their heterogeneous composition which makes them only good for disposal [52], but through effective pretreatment and conditioning, the pulper rejects can be upgraded to SRF, fit for resale [31], [107], [108]. In addition to the pretreatment

steps outlined in section 2.4.3, the pretreated material can be conditioned into pellets or briquettes to enhance its transportability, flowing capability, and unify the particle size of the product [54].

2.4.1.1. The British Standard, BS EN 15359, 2011

There are no South African standards for RDF or SRF, but there is a British standard for classifying waste as SRF [10]. This standard is BS EN 15359, 2011 [10] and it outlines a QMS followed to allow pretreated waste to be classified as SRF [91]. This standard is the same as UNI CEN/TS 15359 and ISO/TC 300 [109]. SRF is sourced from non-hazardous waste (e.g., C&IW) and BS EN 15359, 2011 is involved in the production, classification, and trade of SRF, but not its use as shown in Figure 2.7.
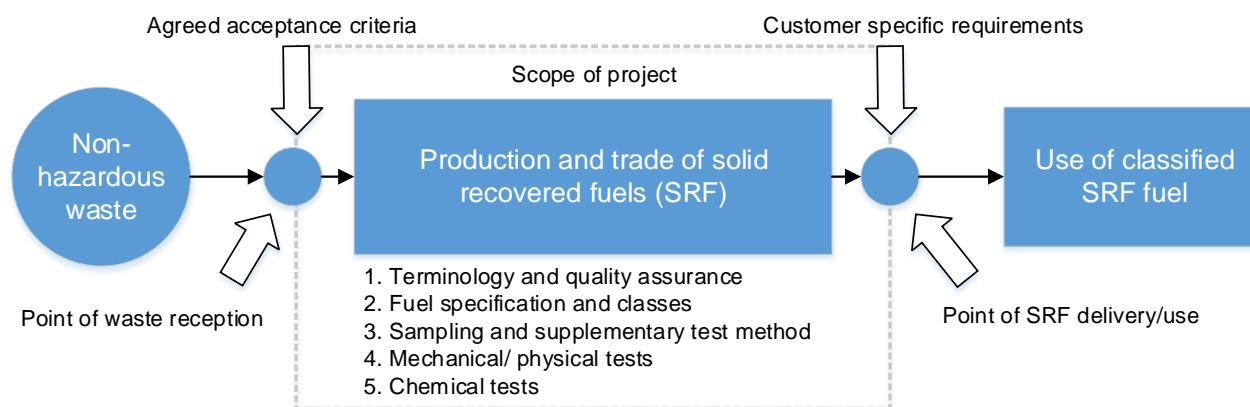
Figure 2.7: The scope, standardization, and tests of SRF from waste. As adapted from BS EN 15359 [10]

All SRF classification tests are performed on the pretreated sample that is to be sold to the customer [109] or "material at delivery" [21]. The standard BS EN 15359, 2011 classifies waste according to the technical, economic, and environmental factors [10]. The factors are each determined by the following attributes: chlorine composition for the technical factor, lower-heating value (LHV) for the economical factor, and mercury composition for the environmental factor. The environmental factor depends on the mercury attribute, because unlike other heavy metals, mercury will volatize and exit as emissions while the rest will be incorporated as clinker if burned in a cement kiln [42]. The reason why the other attributes are used for each factor is explained in Sections 2.4.1.3 to Section 2.4.1.5. Additionally, each attribute should be tested routinely to ensure that the quality of the SRF does not change with the changing seasons [33], [110].

2.4.1.2. The Waste Resources and Action Program (WRAP) classification scheme

The WRAP classification scheme is a more comprehensive standard for small scale producers of SRF that produce less than 100 kilotons per annum (ktpa) [35]. Similar to BS EN 15359, 2011 [10], the WRAP classification scheme classifies SRF according to its technical, environmental, and economic factors [35]. Although, the WRAP classification scheme includes a further 2 attributes per factor to ensure the eligibility of the waste as SRF. The 3 attributes for each of the 3 factors is shown in Table 2.3. Whereby, the 1 factor that was used for BS EN 15359, 2011 is included in Table 2.3 as

bold text [10]. The WRAP classification scheme also made an adjustment to the LHV of standard BS EN 15359, 2011 whereby class 5 initially was only required to attain 3 MJ/kg which was increased to 6.5 MJ/kg as shown in Table 2.3. The WRAP classification scheme classifies each attribute for the factors from class 1 to class 5 as shown in Table 2.3, where class 1 represent the best possible classification and class 5, the worst possible classification.

Table 2.3: The classification scheme as displayed in the WRAP classification guide [35]

Factor	Attribute	Statistical measure	Unit	Class				
				1	2	3	4	5
Economical	Biomass cont.	Mean	wt.% (ar)	≥ 90	≥ 80	≥ 60	≥ 50	< 50
	LHV	**Mean**	**MJ/kg (ar)**	**≥ 25**	**≥ 20**	**≥ 15**	**≥ 10**	**≥ 6.5**
	Moisture cont.	Mean	wt.% (ar)	≤ 10	≤ 15	≤ 20	≤ 30	< 40
Technical	Bulk density	Mean	kg/m^3 (ar)	> 650	≥ 450	≥ 350	≥ 250	≥ 100
	Cl content	**Mean**	**wt.% (d)**	**≤ 0.2**	**≤ 0.6**	**≤ 1.0**	**≤ 1.5**	**≤ 3.0**
	Ash content	Mean	wt.% (d)	≤ 10	≤ 20	≤ 30	≤ 40	≤ 50
Environmental	**Mercury (Hg)**	**Median**	**mg/MJ (ar)**	**≤ 0.02**	**≤ 0.03**	**≤ 0.08**	**≤ 0.15**	**≤ 0.50**
		80th perc.	**mg/MJ (ar)**	**≤ 0.04**	**≤ 0.06**	**≤ 0.16**	**≤ 0.30**	**≤ 1.00**
	Cadmium (Cd)	Median	mg/MJ (ar)	≤ 0.1	≤ 0.3	≤ 1.0	≤ 5.0	≤ 7.5
		80th perc.	mg/MJ (ar)	≤ 0.2	≤ 0.6	≤ 2.0	≤ 10	≤ 15
	Sum of heavy metals (HM)	Median	mg/MJ (ar)	≤ 15	≤ 30	≤ 50	≤ 100	≤ 190
		80th perc.	mg/MJ (ar)	≤ 30	≤ 60	≤ 100	≤ 200	≤ 380

*(ar) – "as received"; (d) – "dry"; Cont. – content

2.4.1.3. Economic factor

The economic factor is represented by the biomass content, lower heating value (LHV) and moisture content. The presence of biomass is generally favoured in waste, since biomass sources need CO_2 to photosynthesize, their combustion yields no net CO_2 emissions [111] - provided that there is no CO_2 release associated with the pre-treating or transport of the biomass source. According to the standard, a high biomass content relates to a feedstock that is incentivized as fuel through renewable obligations certificates (ROC) in the European Union (EU) [35]. A high biomass content is favoured for South African SRF due to minimizing carbon tax and eligibility for funding. In South Africa, CO_2 emissions from the biomass fraction of solid fuels are not charged according to the carbon tax bill, but CO_2 emissions for the non-biomass fraction are expected to pay [112]. Funding incentives are available through the Industrial development corporation (IDC) and Department of Trade, Industry and Competition (DTIC) for biofuel production facilities, which refers to fuel from biomass but not mixed plastic and biomass waste [5], [113]. Contrarily, there are examples of plastic-rich SRF having

shown no adverse effects on ash quality or emissions when cofired with 90% coal [114], [115]. Additionally, polyolefin plastics are generally more suitable than all other plastics when used for alternative fuel generation because they present less challenges while firing [116]. Indeed, the high plastic content lowers the biomass content attribute, but its presence significantly improves the LHV of the SRF [37]. LHV is possibly the most important characteristic of SRF when cofired in cement kilns [90] and despite the standard showing calorific values as low as 6.5 MJ/kg being appropriate for sale as SRF [35], there is debate among researchers to what is acceptable. Researchers typically agree that SRF of high energy content (or LHV) over *ca.* 18 MJ/kg should be co-fired in cement kilns [36], [90], [117]. Conversely, SRF with LHV below *ca.* 18 MJ/kg has been reported as suitable for firing in lignite coal boilers [90], [117]. Lastly, the moisture content is an economical attribute because it is related to LHV and should be as low as possible before cofiring to improve the LHV [35], [118].

2.4.1.4. Technical factor

The technical factor is represented by three attributes; ash content, chlorine content and bulk density [35]. The ash content of paper sludge is particularly representative of alkali metals, e.g. alum (Al(Ⅲ)SO$_4$) used for pH control in paper making [119], [120]. Generally the ash content of plastics is very low, being less than 2 wt.% [67]–[70]. Ash content is regarded as technical factor because if the cofired material has a high ash content, it might cause fouling and slagging problems in boilers, causing damage [121]. Likewise a high content of chlorine could induce corrosion on the surface of boiler equipment [120], [122]. The bulk density of pulper rejects when it is milled and dried is known as fluff and has been reported to have a bulk density of 150 to 200 kg/m^3 [20]. Bulk density a technical factor because it can cause feeding problems depending on the technology [122]. Generally, the densities of SRF when presented as baled fluff, soft or hard pellets and is between 240 to 350 kg/m^3 according to review of SRF used in European cement kilns and powerplants [90]. Generally the density is best improved in a pellet mill, which increases the bulk density to values of 350 kg/m^3 [41] to 400 kg/m^3 [20], [123]. The bulk density of coal has been reported as 800 to 900 kg/m^3 for bituminous coal and 560 to 600 kg/m^3 for lignite coal [41].

2.4.1.5. Environmental factor

The environmental factors are an important quality requirement as the cofiring of coal with SRF can lead to the emission of volatile, submicron particles that can be difficult to control [124]. Mercury is the most volatile of the heavy metals [42], [91], and has been observed to deposit on gaseous filters [125]. Hence it is necessary to avoid any WDF that have significant mercury content. Typically, if a fuel has an attribute in the environmental factor of class 3 or higher it is discouraged for use in certain industries or technologies in the EU [42]. The specific concentration (mg/MJ) is used for the environmental attributes instead of absolute concentrations (mg/kg), so that SRFs with varying calorific value can be compared and tested [35], [42]. Whereby, SRF of high energy content was generally reported to yield absolute concentrations of heavy metals that were too high before the

correlation was used [42]. The median and 80th percentile are used instead of the mean value, because the normal distribution for heavy metal composition is skewed to the right [35], [42].

2.4.2. SRF from pulper rejects

2.4.2.1. Effect of composition, water content and fines content on pelleting

The strength and uniformity of pellets can differ greatly depending on the composition of feedstock [126], [127]. It is known that woody biomass chips can be easily pelletized due to the high lignin content that acts as a binder [128]–[132], but plastic alone will not form strong pellets and binders must be added to increase particle cohesion to create stronger pellets [126], [133]. Despite, most lignin being removed through the paper production process, paper and paper mill sludge can still act as good binding agent for mixed plastic waste or woody biomass [134], [135]. The lignocellulosic fibre can be added within the range of 4 to 27 wt.%, as reported in a study, to improve particle binding to produce pellets [134], [135]. Pulper rejects have been reported to have a lignocellulosic fibre content from 17 to 25 wt.% and hence within range for successful particle bonding [23], [52].

The moisture content of the pulper rejects should be reduced to between 8% and 18% before densification is appropriate [136], [137]. Although it is expected that, the smaller the particles, the better the binding between the particles, a fines content with typical size less than 500 µm should be between 10 to 20 wt.% of the rejects [138]. Fines content within this range enhances pellet bonding by occupying pore spaces between larger particles, benefitting pellet strength [138]. Conversely, samples with higher fines content will deteriorate the pellet quality and energy content [138]. The rest of the material should have a particle sizes less than 5 or 6 mm for adequate pelleting [130]. One researcher confirmed milled, pulper reject fluff with a particle size of 5 mm or less created strong feasible pellets [123]. If pulper rejects are shown to pelletize appropriately, they can be pelletized or briquetted depending on the size and shape of the individual particles required. According to an international ISO standard for biomass fuel, pellets are cylindrical and have a diameter of less than 25 mm [139], while briquettes have a diameter greater than 25 mm and are not restricted to being cylindrical and can be ovoid or pillow-shaped [139].

2.4.2.2. Energy content of rejects

The energy content of pulper rejects is highly dependent on the plastic and water content. Typically, rejects from secondary mills have HHVs from 18 to 28 MJ/kg [43], [47] which increases to 23 to 28 MJ/kg when dried and inorganic contaminants, extracted [12]. The influence of plastic content was demonstrated when rejects from a secondary board mill stream with an approximated plastic composition between 50 to 60 wt.% plastics had an HHV of 22.5 MJ/kg, whilst rejects from the same mill but a higher plastic content had an HHV of 28.8 MJ/kg [24], [25]. Generally, the HHV of pulper rejects from secondary tissue mills are higher than those from newsprint and even board mills (despite similarities in composition) and reported by one researcher as 24.8 MJ/kg when air dried as

seen in a secondary, K-C tissue mill [43]. Higher HHV have been reported by a further 2 researchers. Whereby, the HHV of pulper rejects from a secondary tissue mill in literature was recorded between 28 to 31 MJ/kg [23] and 30 MJ/kg for another paper mill [28].

2.4.2.3. Commercial examples of waste-derived fuels from pulper rejects

Although most of the RDF pelleting process are for MSW, there are a few examples in literature and industry of RDF pelleting processes using pulper rejects as feedstock. An example of the on-site production of RDF pellets are Rofire® pellets, made from the pulper rejects attained from the Smurfit Kappa mill in Roermond, Netherlands [13], [14], [28]. The Smurfit Kappa paper mill is a no-waste paper mill that produces RDF pellets from its rejects, and there have been two examples of researchers using the pellets as feedstock for their gasification and pyrolysis experiments [27], [28].

Internationally, only one Dutch company called N+P Recycling was found to be involved in the off-site production of secondary fuel pellets from pulper rejects. The pellets are called Subcoal® and their patented process of SRF pellet production has maintained the commercial-scale operation of 8 to 9 t/h of Subcoal® since 2013 [140]. Subcoal® has been shown to have a bulk density from 400 to 450 kg/m^3, with an average pellet diameter of Ø8 mm and length of 30 mm [20], [123]. In addition, their high VM content reported between 60 to 86 wt.% and their high LHV value over 20 MJ/kg displays their large plastic content [123]. Patents have been developed for the co-firing of Subcoal® with coal in industrial furnaces [20], with authors showing that Subcoal® to produce less CO_2 emissions than coal on a GJ basis and even had a positive CO_2 balance due to the CO_2 saved from the transport of substituted coal [18].

The substitution of fossil fuel with alternative fuels is growing in European countries whereby the Netherlands and Belgium have the highest substitution of alternative fuels with rates of 85% and 60% in 2011, respectively [141], consequent of these countries' commitment to reducing their CO_2 emissions according to the Kyoto Protocol agreement of 1997. In comparison, the USA substituted 8% of its fossil fuels in 2004 [141] and South Africa 13% as of 2014 [142].

2.4.2.4. Application of SRF according to attributes

The attributes of the SRF from the pulper rejects can be used to determine for what industry and technology the SRF would be used for. The application of the SRF was generally determined by its LHV and particle size [143], but recently Austrian researchers have summarized the use of SRF in which industry and preferred technology depending on several attributes [144], [145]. The result of their findings was recorded as a table as shown in Table 2.4 where lower heating value (LHV), particle size (PS), ash content, chlorine (Cl) and sum of heavy metals (HM) content all contribute to the application of the SRF. As seen in Table 2.4, the firing of alternative fuels can be done in cement kilns for clinker production or boiler for power generation [144], [145].

Interest has been shown by cement companies in South Africa like Lafarge, AfriSam and Pretoria Portland Cement (PPC) to substitute their coal with alternative fuel like SRF [146]. Co-processing of SRF for cement clinker production is typically is done at two locations in the process line: in the main or primary burner (PFB) or in the calciner [147]. As shown in Table 2.4, the best quality SRF (highest LHV, small PS and low ash content) is most suited for firing in the PFB, while the calciner is generally suitable for SRF of lower LHV and larger PS [144], [145]. The PFB can accept alternative fuels, because the associated high temperature aids ignition of fuel [147]. However, high flame temperatures are required in the PFB and that is why only SRF with a very high LHV is recommended [147]. It is understood that most of these cement companies could accept SRF fuel from a technical standpoint, because they use long dry kilns [148], as primary burners (PFB), which provide enough residence time during the flight phase to support ignition [147].

As shown in Table 2.4, lower quality fuels can be used for power generation from SRF including grate-fired and fluidized bed incinerators [117], whereby grate systems are capable of processing SRF of particle size up to 30 cm but fluidized bed incinerators can handle only 8 cm particles [117]. Table 2.4 shows that low quality SRF could be used for the hot disc cement kiln (HDF) technology [149], but it must be noted that this technology is not yet implemented in South Africa [148].

Table 2.4: Application of SRF in certain industries depending on SRF attributes [144], [145]

Attribute	Unit	PFB (Cement)	HDF (Cement)	Boilers		Calciner (Cement)	Coal Powerplant (Power)
				Grate firing	Fluidized bed		
LHV	MJ/kg	20 - 25	14 - 16	11 - 16	11 - 16	11 - 18	11 - 15
PS	mm	10 - 30	< 120	20 - 100	< 300	50 - 80	< 50
Ash	wt.%	< 10	20 - 30	< 20	*	*	< 35
Cl	wt.%	0.8 - 1.0	0.6 - 0.8	0.8 - 1.0	0.8 - 1.0	< 0.8	< 1.5
HM	wt.%	< 1	*	1 - 2	< 3	0	< 1

* PBF - Primary burner cement kiln: HDF – Hot disc Cement kiln:

2.4.2.5. Use of SRF in cement kilns

The building sector is the third-largest producer of CO_2 emissions, and responsible for 10% of the total CO_2 emissions worldwide, which are predominantly from concrete manufacture [111], [150]. It is estimated that 80% of emissions from the construction industry are from cement manufacture which, can be split into the decarbonation of limestone (58% of emissions), and the combustion of fossil fuels for heating (42%) [111]. Decarbonation is the result of high temperatures in clinker production (up to 1500 °C), which causes accelerating conversion of limestone (67% of clinker) to CO_2 as seen in Equation 2.1 [151].

$$CaCO_3(s) \xrightarrow{\text{heat}} CaO\ (s) + CO_2(g)$$ Equation 2.1

The combustion of fossil fuels also produces significant CO_2 emissions, and the emission factor can vary significantly depending on the fuel source used. South Africa has a huge reliance on coal, whereby 93% of electricity nationwide was generated from coal in 2000, which fractionally decreased to 90% in 2017 [152], [153]. Similarly, coal is used as the main fuel source in the South African cement industries [148], [154]. The cost of fuels plays a significant role in determining feasibility because 30% to 40% of the OPEX can be linked to the purchase of fossil fuels required for cofiring for clinker production [96], [155]. The comparison of the CO_2 emissions for fossil and alternative fuels that can be used in the cement industry is shown below [111] and the relative price of each fossil and alternative fuel is also provided [154]. From Table 2.5, it should be evident how alternative fuels like SRF can drastically decrease the net CO_2 emissions of a cement production line, with a cheaper free-on-board cost.

Table 2.5: Comparison of alternative and fossil fuel types w.r.t CO_2 emissions and pricing

Type	Fuel	Net CO_2 emission (g CO_2/MJ)	*Relative price (€/GJ)
Fossil fuel	**Petcoke	101	**0.6
Fossil fuel	Coal	96	0.5 – 1.2
Fossil fuel	Natural gas	54	2 - 6
Alternative fuel	Waste tires	85	0
Fuel oil	Fuel oil	74	4 - 7
Alternative fuel	Plastic	75	0
Alternative fuel	RDF	9	Dependent
Alternative fuel	Biomass	0	0 – 1.5

Note: * Price does not include transport; **estimation based from half the (maximum) cost of coal [96]

Coal and pet coke are pulverized to an average particle size less than 100 μm before being used as fuel in a boiler or cement kilns [20]. This minimizes process inefficiencies and quickens the rate of combustion for volatiles and char [156]. Unfortunately, SRF cannot be pulverized to this small particle size because their particles are non-spherical and plastics are resistant to shear stresses [157]. Modern kilns that are made to process feedstocks like SRF can handle pellets, as long as their particle size is less than 10 mm according to one source [110] and even 30 mm according to another source [36]. Typically, higher feed rates of SRF are required for modern kilns to compensate for the longer ignition times and lowered heat and combustion release rates associated with large SRF pellets when compared to pulverized coal [158].

2.4.3. Process line architecture

Many process units for MSW processing are borrowed from the mineral processing industry and hence there are no strict heuristics for MSW processing or SRF conversion lines [32], [159]. Ten process lines from literature are shown in Table 2.6. Process lines 1 to 3 show lines proposed by

Andritz™ for the manufacture of RDF from C&IW specifically, paper mill rejects. Process lines 5, 6, 7, and 9 indicate proposed lines for the conversion of MSW to RDF [7], [32], [160] and the rest are for 'landfill mining' of MSW to achieve multiple by-products [107], [161], [162]. Line 8 and 10 refer to the 'landfill mining' cases involving separating MSW into various fractions for resale instead of a single concentrated organic fraction, such as RDF. Almost all the process lines, including the rejects line, show extensive use of magnetic separators highlighting their importance in removing ferrous material. Their extensive use is evident of their effectiveness and cheap cost relative to other units. RFD produced from lines 5 to 7 had a "disposal cost" [31] indicating that there was uncertainty in the European market regarding RDF in 2002 and hence they had an attached disposal cost instead of a selling price. Although nowadays, even in developing countries like India, the price of high-quality RDF with an LHV of *ca.* 19 MJ/kg ranges between Rs.1 800 – Rs.3 600 per ton (or R360 - R720 per ton assuming an exchange rate of 5 Rs./ZAR) [40]. The price of RDF is expected to be variable depending on its perceived value in the market but should be still competitive against the fuels that are currently being used for the cement kilns or powerplants. The process lines in Table 2.6 mostly use magnetic separation (MS), shredding (S), or a Trommel (T)/ Pre-trommel (PT). Fewer lines used hand-sorting conveyor (HS), ballistics classification (BC), air classification (ACC), hammermilling (M), pelleting (P), or compaction (DE) and only line 8 used eddy-current separation (ECS).

Table 2.6: Comparison of various RDF process lines as seen in the literature

Line	Line configuration	Description
1	MS-BC-*DE-S-MS-MS-HS-WB	Production of fuel from pulper and light rejects [7].
2	S-MS-BS-*DE-S-MS-MS-T-HS-WB	Production of fuel from various mill rejects [7].
3	S-MS-BS-ACC-T-dD-P-T-WB	Line for converting C&IW to SRF pellets [160].
4	BC-MS-S-ACC-T	Solid waste sorting process at 21 tph MSW [161].
5	S-T-MS-M-T	RDF conversion line from MSW, shown to yield lowest OPEX of tested process lines (line 10) [32].
6	S-T-MS-S-T-M-T	RDF conversion line from the same study which showed to have second lowest OPEX (line 11) [32].
7	T-HS-MS-S-T-M-T	Another line identified as viable for converting MSW to RDF from Caputo, 2002 (line 2) [32].
8	T-M-PT-MS-ECS-BC	Landfill mining case for MSW [162]. In this case, the bar sizer is assumed to be a trommel.
9	S-T-dD-M-S-P-WB	RDF conversion line from MSW, as proposed by the Indian ministry of housing affairs [40].
10	HS-HS-T-MS-HS-S	Mechanical sorting line for the landfill mining of RDF from MSW (option 1) [107].

2.4.3.1. Hand-sorting

Hand-sorting is useful for separating plastics (like PET bottles or PVC pipes), glass, or metal [159]. The use of a hand-sorting line might be an effective process unit, considering the low minimum wage

for non-skilled workers in South Africa [163]. Additionally, hand-sorting would provide employment to these workers in the surrounding community. It is encouraged to place a hand-sorting unit early in the process line to extract inorganics (e.g. glass) that might damage units downstream [32].

2.4.3.2. Dewatering/ Compacting

Although some of the process lines could produce RDF of low moisture content like Line 3 and 9, which both used a hot-air dryer (dD) [40], [160], the majority of the process lines use no thermal drying and only mechanical dewatering. Indeed, pulper rejects have a moisture content between 40 to 60 wt.% [13], [26], [43], and although mechanical dewatering can reduce moisture content of rejects by 20 to 50 wt.% [164], [165], the inclusion of thermal drying is a necessity [12], [164].

2.4.3.3. Thermal drying

Thermal drying of paper mill rejects is most favored in rotary drum-dryers or conveyor belt dryers [164], [166]. A rotary drum dryers has been reported in one study to reduce the moisture content of de-inking sludge to as low as 3 wt.% [43]. Rotary drum dryers can use heated air or flue gases from combustion as utility to dry wet feed [43]. In addition to direct drying with exhaust gases or air, the heat for drying can be supplied indirectly with a steam-tube dryer [164], [167]. Direct dryer are optimal when incoming air temperature is from 110 to 150 °C, and blown counter-current to the feed [164]. Thermal drying has been shown to make up *ca.* 70% of the OPEX for the pretreatment section [168].

2.4.3.4. Metal separation

Metal (ferrous or non-ferrous) can cause damage to equipment downstream units, especially for shredders, dryers, the pellet press die, and boilers [7]. Typically, large, ferrous metals can be captured via an inexpensive, over-belt magnet [7], [169]. Indeed, around 80 wt.% of ferrous metals can be recovered from MSW with a single magnet, but typically two magnetic separators are placed in series to maximize extraction [167]. Magnetic separation should be employed before shredding because large ferrous material are easier to extract than smaller particles [7]. Conversely, non-ferrous particles (e.g. aluminum or copper) can be extracted with an eddy current separator [7].

2.4.3.5. Shredding and sieving

The purpose of shredding is to convert the sample to smaller, uniform particle size [7]. It is important to correctly place the shredding unit in the process as it will influence other unit operations (e.g. shredding must be a precursor for fine metal sorting in eddy current separation) [7]. Screening and sieving usually occur in collaboration with shredding. The particles of desired size will fall through a mesh (static or vibrating) and if not fallen through, recycled back to the shredder [7].

2.4.3.6. Ballistic separation

Ballistic separation is the separation of stones, bricks, and other coarse, non-combustible material from the rejects [7]. Due to the small quantity of these materials in the coarse rejects representative sample, it is assumed that an almost negligible fraction of bricks, sand, and glass will be present and

hence the need for a ballistic separator is most likely redundant. Air classification can also be used as well to separate light materials "lights" from heavy material "heavies".

2.4.3.7. Pellet mill operation

A pellet mill is used to produce many pellets continuously. The pellet mill uses a die with hundreds to thousands of cylindrical press channels (resembling counterbores drilled through the die), two rollers, and a motor to force raw material into the press channels and extrude the raw material through the press channels, making many pellets simultaneously. Pellet mills are referred to as die and roller mills and can have two designs, being the flat-die or ring-die. The flat-die design uses a rotating, horizontal, solid circular die and a fixed roller rested on the die to extrude the pellets through the press channels. The flat-die is used for pilot-scale operations due to its simpler design and lightweight structure [170], [171]. The ring die uses the same mechanism as the flat die but is more popular for higher capacities from 2.5 to 5 ton/h [172]. Instead of the die being horizontal and a solid circular disk, it is a thick, vertical ring as shown in Figure 2.8. From Figure 2.8, it is seen that the ring has many press channels, with each press channel having three sections; an opening to feed material into a channel, an active channel for extruding the material through the channel, and the inactive press channel. The inactive press channel part is used to maintain the strength of the ring but does not influence densification.
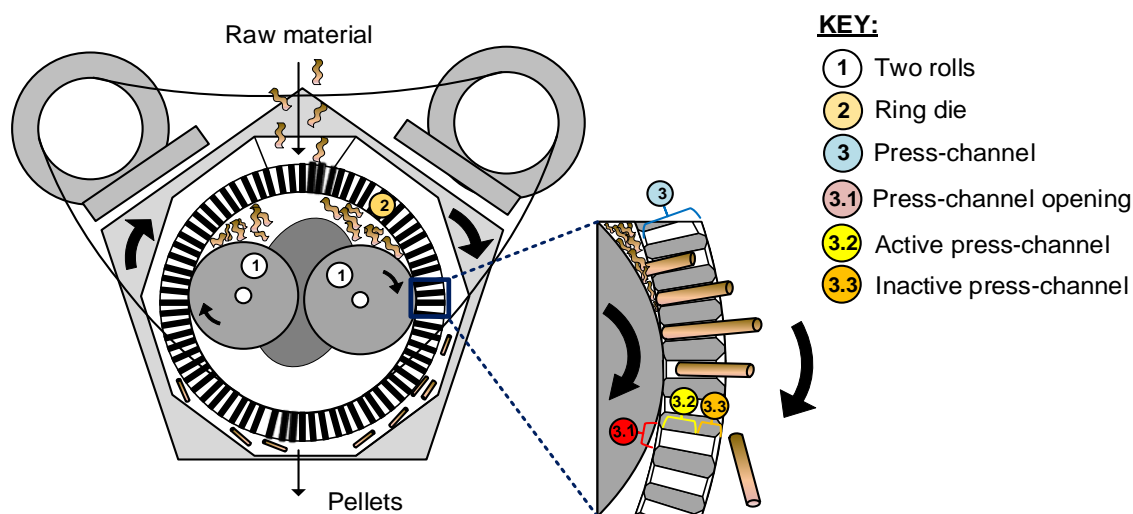
Figure 2.8: Ring die press machine and mechanism, redrawn from [173]

The strength of biomass pellets was improved for a ring-die pellet mill using an optimal speed of rotation of 150 to 250 rpm and a gap width between the roller and die set to between 2 and 4 mm, whereby increasing the gap size also advertently increased pellet mill capacity [134], [174]. The produced pellets were also shown to be strongest when their die diameter was sized between Ø4.8 to Ø9.5 mm and the length to diameter ratio was 8:1 to 10:1 [134]. Although it should be noted that decreasing the die diameter increased the power requirements and decreased the capacity of the pellet mill, which had determinantal effects on upscaling the process (lowering OPEX) [175]. The

pressure exerted in the pellet die is typically greater than what is needed to make strong pellets and is recorded as being between 200 and 350 MPa [176].

Friction caused from the operation of the roller on the die can cause the temperature of the die and press-channels to reach *ca.* 100 °C and 130 °C, respectively [173]. The temperature of the die and press channels can be recorded from thermographs using Infrared (IR) cameras [130], [177]. Biomass is best pelleted when the die temperature is maintained between 80 to 100 °C to melt the plant waxes (that serve as pellet adhesive) without allowing degradation [130], [177]. However, plastics can withstand higher temperatures above 100 °C, causing the plastic to partially melt and produce even stronger pellets [178], [179].

2.5. Conversion of pulper rejects into fuel oil

The following section describes the literature surrounding the pyrolysis of fibres, plastics and rejects.

2.5.1. Factors influencing pyrolysis

2.5.1.1. Definitions used for pyrolysis

The following bullet points describe the difference between batch and continuous reactors and solid and vapor residence time. The heating rate is also defined:

- Batch reactors are setups where material is fed into a unit and held for the reactor duration.
- Continuous or semi-continuous reactors introduce the solid feed into a reaction zone for a limited time before eventually transporting the feedstock out of the reaction zone.
- The solid residence times is the length of time that solids are held in the reaction zone. It can be controlled by reaction duration that feedstock is held in a batch-reactor or the speed at which the solids are kept within the reaction zone section of a continuous reactor.
- The length of time that the volatiles remain in the reactor zone is known as the vapor residence time and it can be controlled with the inert gas flowrate.
- The heating rate is the speed at which the feedstock material reaches the set temperature of the pyrolysis reactor.

2.5.1.2. Difference between batch, bench-scale, and continuous, pilot-scale reactor

Batch-scale setups use long solid residence times to facilitate complete conversion of the feedstock to pyrolysis products. As the thermal degradation temperature is reached, the feedstock becomes volatile and able to condense downstream with aid from an inert gas. At the end of the reactor duration the setup is opened, and char and condensable product is collected. Conversely, kilogram-scale experiments are often continuous, so shorter solids residence times than batch setup are expected and because there is much more feed in kilogram-scale setups, it is expected that there will be greater heat, mass, and phase-transfer limitations [180], [181]. For these reasons, the

evolution of volatiles and condensation of pilot-scale setups is not as efficient as batch-scale, but indeed a better comparison to continuous operation on industrial scale [180], [181].

2.5.1.3. Temperature

Temperature is undoubtedly the most important operating variable, as bond breakage and cracking is always easier at higher temperature, being the main driving mechanism of pyrolysis reactions [182], [183]. Researchers have proved temperature to have the largest influence on product yield and composition for the pyrolysis of biomass [184], [185] and polyolefins [183], [186]. The experiments also showed that holding time or the solids residence time had the second largest influence on product distribution and composition for the batch pyrolysis of biomass and plastic [183]–[186]. Pyrolysis of fibres and plastics is usually performed at temperatures above 400 °C, to allow the components to volatize but less than 700 °C to prevent excessive polyaromatic hydrocarbons (PAHs) release and avoid excessive energy use. Due to the significant influence of temperature on the product distribution and product composition – the pyrolysis of feedstocks is most typically tested over a range of temperatures.

2.5.1.4. Solids residence time

Solids residence times should be long enough to allow the complete conversion of the sample. If it is too short, not all the volatiles will be released, which will decrease the yield of condensable product [186]–[189]. At lower temperature with slower conversion rate the solids residence time must be long enough to yield maximum yield [189], but if temperature increases, thermal degradation quickens and the solids residence time can be shorter [186]–[189]. A solids residence of 30 minutes should be sufficient for the batch pyrolysis of a sample at temperatures around 500 °C [25], [190].

2.5.1.5. Vapor residence time

Albeit less than temperature, the volatile residence times has a major impact on the pyrolysis product distribution and composition [183], [186], whereby longer vapor residence times enhance secondary reactions that convert primary products into secondary products such as NCG [191]. The different primary and secondary products for biomass and plastics are detailed in section 2.5.3.1 and 2.5.4.2, respectively. The volatile residence time can be controlled by the flowrate of the inert, sweeping gas and although higher flowrates prevent secondary reactions, too high flowrates prevent volatiles from condensing in the condensation train and lower the condensable product yield. For instance, the fast pyrolysis on a bench-scale, batch reactor was shown to produce significantly higher oil yield at a lower nitrogen gas flowrate of 0.5 L/min, compared to 2 L/min for a pure plastic feedstock [192].

2.5.1.6. Heating rate

Heating rate and pyrolysis type are linked together whereby a pyrolysis type is named according to its heating rates, *viz.,* slow, and fast pyrolysis refer to pyrolysis using slow and fast heating rates, respectively. Heating rate can be coupled with variables like particle size, carrier gas flowrate (vapor

residence time), and temperature to target a desired product [193], [194]. The product yields and operating conditions to maximize the main product for fast, slow, and intermediate pyrolysis are detailed in Table 2.7 for the example of lignocellulosic fibres.

Slow pyrolysis uses a heating rate typically between 6 and 60 and less than 100 °C/min [195]–[200], to yield relatively low liquid yields of *ca.* 30 wt.% [201], [202], that can contain up to 70 wt.% water [203]. Intermediate pyrolysis uses higher heating rates around 100 °C/min and residence times between 10 and 30 seconds [202], to produce higher liquid yields of *ca.* 50 wt.% [202]. Generally, fast pyrolysis of biomass favors a liquid yield of *ca.* 75 wt.% with a water content of *ca.* 25 wt.% [203]. Fast pyrolysis uses heating rates higher than 100 °C/min being typically within the region of 10 to 200 °C/s [195]–[200] and very short residence times of 1 to 5 seconds, coupled with small particle size [181], [194], [195] to aid heat penetration, avoiding undesirable secondary reactions and hence produce high liquid yields.

Table 2.7: Comparison of slow, intermediate, and fast pyrolysis of lignocellulosic fibres w.r.t favourable conditions

Type	Heating rate (°C/min)	Temperature (°C)	Residence time (s)	Typical yields (wt.%)		
				Liquid	Char	Gas
Slow	6 - 60	200 - 400	100 - 300	10 – 35	25 - 90	5 - 55
Intermediate	60 - 100	400 - 700	10 – 30 s	50	25	25
Fast	> 100	400 - 700	0.5 – 5	50 – 75	10 – 35	10 - 25

2.5.1.7. Particle size of feedstock

The particle size of feed is often altered for pilot-scale experiments. While fine particles (<1 mm) are used for fast pyrolysis, the feedstock is sometimes pelleted to sizes with a diameter between 4 and 8 mm size to improve its bulk and packing density [24], [25], [204]. The highest liquid yield occurred for paper mill sludge when it was pelleted to a Ø6 mm diameter [204]. Briquetting the feedstock (Ø >25 mm) is expected to have negative effects on the pyrolysis liquid yield and most likely enhance char yield compared to smaller pellet diameters [193], [194]. This is because the larger briquettes will need a longer time for the heat to penetrate through the material, which inadvertently causes thermal lag and mass transfer limitations [193], [194]. Conversely, using small pellets that are quickly heated at high temperature will promote faster depolymerization and volatile release [205].

2.5.2. Thermal degradation of components in pulper rejects

Thermogravimetric analysis (TGA) can assist in choosing the pyrolysis experimental temperatures. Based on the evolution of the sample mass subject to temperature increase in an inert atmosphere with limited heat or mass transfer limitations [206], the results from TGA inform about the temperature needed to thermally degrade the sample in a non-isothermal, inert atmosphere. The

curve showing mass loss with temperature is the thermogravimetric (TG) curve and it is derived w.r.t the temperature to get the derivative (dTG) curve, or temperature of maximum mass loss.

2.5.2.1. Thermal degradation of plastic

Table 2.8 shows the degradation temperature ranges and peaks for different plastics when exposed to a constant heating rate of 10 °C/min in TGA. Faster heating rates shift peak temperature to a higher value, due to thermal lag [61] [193], [194]. As shown in Table 2.8, PVC is the least thermally stable, followed by PS, then PET, PP, LDPE, and lastly HDPE [207], [208]. Five of the six common thermoplastics thermally degrade with a single degradation step between 350 and 500 °C, with the peak degradation temperatures occurring between 410 and 480 °C [209]. PVC is the only one of six plastics with two degradation steps. The first step is known as dehydrochlorination and occurs between 280 and 290 °C and the second step occurs between 460 to 480 °C [207], [210].

Table 2.8: Thermal degradation peaks and ranges for plastic types at 10 °C/min heating rate.

Plastic	Melting temperature (°C)	Degradation temperature (°C)	Peak temp. (°C)		Reference
			1st	2nd	
PET	260	380 - 520	440	-	[208]
LDPE	135 - 140	400 - 500	470	-	[207], [211]
PVC	> 140	280 - 520	280 - 290	460 - 480	[209], [211]
HDPE	134	400 - 520	480	-	[207], [209], [212]
PP	140 - 160	410 - 460	430 - 440	-	[207], [213]
PS	150 - 220	350 - 480	410 - 440	-	[207]

2.5.2.2. Thermal degradation of lignocellulose constituents

Unlike the narrow, distinct degradation peaks exhibited for most of the plastic polymers (except PVC), the thermal degradation of lignocellulose biomass exhibits several, often non-distinct, thermal degradation peaks. The thermal degradation mechanisms of lignocellulosic materials, including fibre-based products (e.g. paper and boards), can be divided into several stages depending on the constituents which are mainly affected, *viz.* moisture, hemicellulose, cellulose and lignin [84], [211], [214], [215]. Moisture evolution is characterised by an endothermic reaction occurring above 100 °C and fully complete by 220 °C [84] and dried, lignocellulosic samples typically experiences two thermal degradation steps. The first step represents hemicellulose degradation and the next cellulose degradation, with lignin degradation usually having no distinct peak [209], [211], [216].

Due to the heteropolysaccharide and amorphous nature, hemicellulose degrades at a lower temperature than cellulose. Pure hemicellulose as extracted xylan has been shown to experience two degradation ranges. At a heating rate of 10 °C/min, xylan thermally degrades between 150 and 260 °C with a peak degradation temperature of 235 °C [212]. The second peak was observed between 245 and 345 °C, with a maximum at 286 °C [212]. Other researchers reported hemicellulose to thermally degrade with a single step from 220 to 315 °C, experiencing peak degradation around

268 °C [84], [217]. For instance, hemicellulose extracted from softwood and hardwoods were found to experience a single-step thermal degradation, with a peak degradation temperature at 310 and 280 °C, respectively [218].

Pure cellulose has a single thermal degradation step and begins to thermally degrade from 260 or 280 °C [212], [219], only experiencing accelerated decomposition above 310 °C with a peak between 330 and 360 °C [67], [209], [212], [216], [217], [219]. Indeed, lignocellulosic fibres of high cellulose content of 75 wt.% and more, such as office and waste paper, newspaper, boards, and cottons [68], [80], were observed to have only one degradation peak within a narrow range of 350 and 370 °C for 10 °C/min despite containing some hemicellulose or lignin [67], [209], [217]. Whilst, blank printing paper with an ash content of 10 wt.% was observed to have a second peak at around 720 °C evident of $CaCO_3$ decomposition [60].

2.5.2.3. Thermal degradation of paper mill waste

The thermal degradation of paper mill waste streams generally shows two or three distinct peaks due to the presence of fibres, plastics and inorganics. Paper mill rejects were shown to degrade at around 250 °C with a first peak between 320 to 380 °C corresponding to the fibrous fraction in the sample [24], [52]. The second peak was associated with the degradation of plastics and began at 420 °C, with a maximum between 450 and 500 °C [24], [52]. This peak is typical of polyolefins such as LDPE or HDPE [24], [209], [211], [213]. Some samples display a third peak observed at temperatures above 700 °C, corresponding to the degradation of inorganics present in the fibres. This peak is usually small for plastic rejects but can be larger for samples with high fibre content such as paper waste sludge [209], [220]. The reaction responsible of the peak is due to the degradation of $CaCO_3$ (often used as a filler) into carbon dioxide and calcium oxide as in Equation 2.2. It was observed that glossy paper with a 27 wt.% ash content, had a peak temperature 5 °C less than office paper [67], [209], [214]. Increased ash content is observed to decrease peak degradation temperature due to the enhanced heat transfer from the catalytic effect [209], [220].

$$CaCO_3 \ (s) \rightarrow CO_2 \ (g) + \ CaO \ (s) \qquad\qquad\qquad\qquad \text{Equation 2.2}$$

2.5.3. Pyrolysis of lignocellulosic fibres

The pyrolytic mechanism for lignocellulose fibres and biomass is introduced and thereafter the different product is introduced with emphasis on the condensable product.

2.5.3.1. Pyrolytic mechanisms of biomass and lignocellulosic biomass

Although the pyrolysis of lignocellulosic fibre yields three main products (condensable product, char, and NCG), many complex reactions and intermediary products occur. Instead, researchers have grouped primary reactions as reactions that produce primary products, secondary reactions as those which produce secondary products. For biomass or lignocellulosic fibres, primary reactions usually

occur between 200 to 450 °C while secondary reactions are favoured from 500 to 800 °C [83]. Typically, the primary pyrolysis products are desired and secondary reactions, converting primary products into secondary products such as NCG are undesired. Conditions that restrict secondary and ternary reactions include using a quench zone to quickly cool down volatiles post-reaction and a high flowrate to shorten volatile residence time [221]. Figure 2.9 shows the pyrolysis mechanisms for biomass & cellulose. Scheme 1 (left) is the well-established mechanism of biomass pyrolysis known as the two-stage, semi-global mechanism. This mechanism shows that NCG, tar, and char are all primary pyrolysis products formed by cracking, depolymerizing/ fragmentation, and recombination reactions, respectively [83]. Further secondary reactions on the tar can occur to form more NCG and char via subsequent cracking and recombination reactions [58], [83].

Anca-Couce, 2016, proposed the model as shown on the right (2) of Figure 2.9 to describe the mechanisms of cellulose pyrolysis. This model uses the Waterloo-mechanism [223], Broido-Shafizadeh model [224], [225], and updates made by Piskorz and Banyasz [226]–[228] to describe these products and formations. For this mechanism, primary reactions on cellulose form primary char of low hydrogen content, (along with NCG and H_2O) and the intermediate product, active cellulose, by recombination and depolymerization reactions, respectively. Thereafter active cellulose can be converted to NCG and tar, consisting mainly of levoglucosan, through fragmentation reactions [222]. Both reactions are still referred to as primary reactions and both products can be further converted to secondary NCG, secondary tar, and secondary char. The secondary tar phase product is due to further cracking and depolymerization reactions at elevated temperatures. The secondary char is also formed synchronously with CO_2, H_2O, and volatile PAH [222], [229].
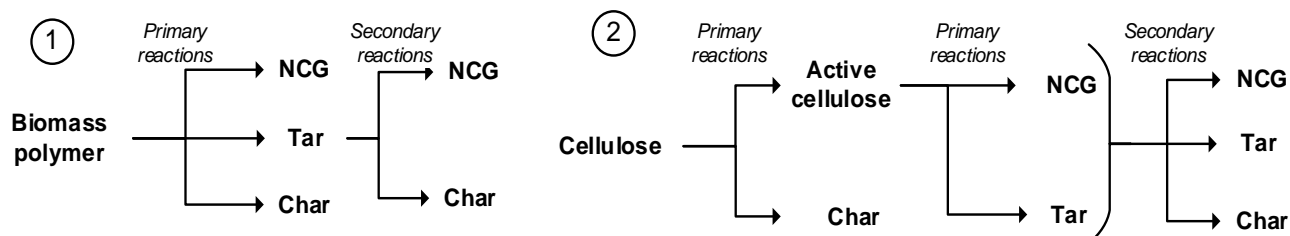
Figure 2.9: Mechanisms for pyrolysis, representing the scheme for (1) biomass and (2) for cellulose.

2.5.3.2. Non-condensable gas (NCG)

NCG from biomass and sometimes RDF or SRF (if the plastic content is low) tends to consist primarily of CO_2, CO, and CH_4 [165], [230], [231]. Whereby at temperatures below 500 °C, as much as 60% of NCG can be low-energy CO and CO_2, but as the temperatures is increased to 500 °C, the methane content peaks at *ca.* 10 vol.%, causing the energy content of NCG to maximize at this temperature [100], [221], [229], [230], [232].

2.5.3.3. Char

Char from biomass is a solid product shown to consist mainly of inorganics (ash in proximate analysis), fixed carbon and some volatile matter. Char from biomass pyrolysis is from cyclization reactions, meaning that although char can consist of unconverted feedstock, it will still be present at high temperatures - even for low ash containing feedstocks [214]. In addition to the highly cyclized carbon structures, solid char has been shown to contain most of the inorganics present in the feedstock, like glass and metals, that remain involatile due to their high degradation temperature [100], [233]. Whereby, the ash content of char from high ash content paper has been recorded as high as 60 wt.% [214]. At the low temperature of 300 °C, the char yield is observed to be favored and maximized with a yield between 40% and 45% for a paper feedstocks [234], [235]. Increasing the temperature to 425 °C was shown to decrease the char yield to between 30 to 33 wt.% [234], [235]. The heating value of char decreases with increasing temperature. This observation has been deemed responsible from the decreasing H/C ratio of the char with increasing temperature [236].

2.5.3.4. Bio-oil yield

The condensable product from the pyrolysis of lignocellulosic fibres and biomass is known as bio-oil. The batch pyrolysis of lignocellulosic fibres, in the form of waste paper or PWS, produces bio-oil with yields *ca.* 50 wt.% from 400 to 450 °C [234], [235], [237]. The slow pyrolysis of paper waste from 325 to 425 °C was reported to maximize condensable product yield at around 400 °C with a yield between 48 and 53 wt.% [234], [235]. Another researcher reported a lower bio-oil yield of *ca.* 40 wt.% at the higher temperature of 500 °C for the slow pyrolysis of recycled paper sludge [238]. While, the fast pyrolysis of PWS of low ash content (LAPWS) was reported to achieve a maximum bio-oil yield of 45 wt.% at 425 °C [237]. This yield was significantly lower than the bio-oil yield attained for the same regarding PWS of high ash content (60 wt.%), and at a lower temperature of 340 °C [237]. The maximum oil yields experienced at lower temperature are believed to be due to the inks and fillers (inorganics) present in the paper waste that have a catalytic effect, enhancing conversion of primary tar to secondary NCG at higher temperatures [234], [235].

2.5.3.5. Bio-oil composition

Some researchers have observed bio-oils produced from the pyrolysis of fibres to contain two distinct phases with different densities [230], [234], [239]. A darker phase is present as an organic phase and is generally assumed to contain mainly compounds derived from lignin that are insoluble in water [239]. The other phase is a lighter, more transparent aqueous phase containing water and water-soluble compounds, that are generally derived from carbohydrates [239]. The aqueous phase from pyrolysis of different biomass sources is mainly water, with a water content between 40 and 70 wt.% [102], [190], [240], [241]. Bio-oil from biomass is observed to be susceptible to ageing, *viz.,* the bio-oil repolymerizes during storage and increases its water content due to release of volatiles [242].

Carbohydrate-derived molecules such as formic acid, acetol and acetic acid are water-soluble and present from the pyrolysis of most biomass samples [234], [243]. Although, as the samples become more like lignocellulosic fibre (e.g. PWS), the carbohydrate-derived compounds will typically consist predominantly of levoglucosan (LGA) and glycolaldehyde [204]. It has been observed that carbohydrate-derived compounds like LGA, 5-hydroxymethylfurfural (5-HMF), formic-acid and acetic acid can make up as much as 20 wt.% of the aqueous phase bio-oil from fibres [239], [240]. LGA is typically the main component of bio-oil from pyrolysis of fibres, and its presence is typically associated with the degradation of cellulose [228], [244]. Although one researchers observed the presence of inorganics to drastically reduce the LGA composition by two or three times [245], another confirmed high-ash PWS to actually have higher LGA concentration and maximized at lower temperature [204]. Although LGA is derived from carbohydrates, it is argued to be water-insoluble [234] and dissolve in the organic phase. The lignin derived compounds are typically in lower concentrations than carbohydrate derived compounds, even for woody biomass sources [240], [243]. Woody biomass was observed to produce bio-oil containing between 1 and 2.5 wt.% for each of the lignin-derived compounds; $_{2,6}$-methoxy-$_4$-propenyl phenol, vanillin and $_{2,6}$-Dimethoxy phenol [240]. Conversely, bio-oil from corn stover and cob was observed to contain between 1 and 2 wt.% of each phenol and guaiacol [243]. Similarly, the most abundant lignin-derived components in bio-oil from PWS, had compositions of 1 wt.% each observed for guaiacol, phenol and apocynin [204].

2.5.3.6. Bio-oil energy content

When produced at bench-scale, the amount of produced bio-oil is typically too small to separate into various fractions and researchers have still been able to calculate the heating value without separation. It has been observed that the HHV of bio-oil from LAPWS was shown to range between 17.4 to 22 MJ/kg [204]. The bio-oil from paper waste had a similar HHV of 23 MJ/kg and consisted of a variety of compounds of length C_6 to C_{18} consisting of lignin and carbohydrate-derived compounds and trace amounts of alkanes and alkenes [235]. The HHV of bio-oil will not change as significantly as the char because the H/C ratio of bio-oil was observed to remain constant [236].

2.5.4. Pyrolysis of individual plastics

Plastics are generally favorable as pyrolysis feedstock due to their capability to increase condensable vapor yield and increase the heating value of the feedstock and subsequent pyrolysis products. However, not all plastic are beneficial and generally only the plastics containing no heteroatoms (i.e. compounds with only C-C and C-H bonds), *viz.,* polyethylene (LDPE and HDPE), polypropylene (PP) and polystyrene (PS) are favorable in the feedstock [209].

2.5.4.1. Problem plastics

PET is unfavorable as pyrolysis feedstock because it has a high oxygen content of 33%. This high oxygen content results in high NCG yields with significant CO and CO_2 concentration [232], [246],

[247]. Consequently. the condensable product yield of PET is between 13 and 23 wt.% at temperatures around 500 °C [247], [248] and the condensable product is corrosive due to the significant concentrations of its monomers present - benzoic acid and vinyl terephthalate [249], [250]. A challenge PET introduces is the production of a yellow solid powder containing oxygenates and organic acids known to cause blockages in reactor systems due to its high boiling point [192], [248]. This solid powder is believed to be the monomer of PET – Terephthalic acid (TPA), that has a tendency to condenses within the piping [251] due to its boiling point of 400 °C. The pyrolysis of PET at around 500 °C has been observed to produce condensable product with yields between 13 and 23 wt.%, despite its high volatile matter content [247], [248]. The liquid from PET pyrolysis is corrosive, due to the high composition of benzoic acid and vinyl terephthalate, both monomers of PET [249], [250]. Increasing the temperature from 500 to 600 °C was shown to lower benzoic acid composition in the liquid by *ca.* 25% to 40% but liquid yield was still far less than 50 wt.% [247], [248]. The presence of PVC is unfavorable in the pyrolysis feedstock because its degradation yields hazardous and corrosive HCl gas and chlorinated compounds (e.g. chlorobenzene), in NCG [210], [252], [253]. The release of HCl is due to the first degradation step (dehydrochlorination) of PVC resulting in the significant release of Cl^- ions, that may react to form HCl which is toxic if inhaled [254]. Both HCl and chlorobenzene have been observed to be evident in the NCG from PVC pyrolysis [255], furthermore the liquid yield of PVC pyrolysis is low at 500 °C [246], [255].

2.5.4.2. Pyrolytic mechanisms of plastics

In Figure 2.10, reaction scheme 1 (left) shows a mechanism for the thermal decomposition of polyolefins (PP and PE) [256]. This mechanism shows how polyolefins are thermally degraded into primary wax product through primary reactions [183], [256]–[258], like polymer chain scission [259]. Mechanism 2 (Figure 2.10) was observed to be the best predictor of product distribution out of 8 schemes for the fast pyrolysis of polyethylene [257]. Mechanism 2 is believed to be better than mechanism 1 because it does not only assume wax as a primary product, but also oil and NCG [257]. In addition, waxes can lend to higher amounts of liquid oil by secondary reaction [257].
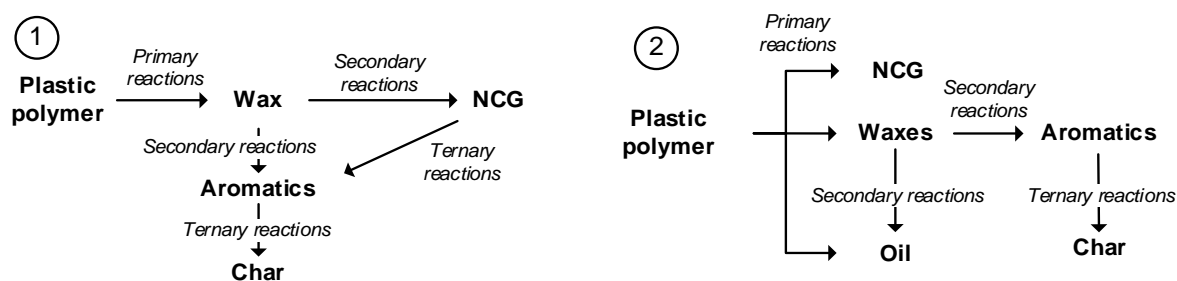
Figure 2.10: Mechanisms for pyrolysis, representing the scheme for (1) plastic pyrolysis and (2) for PE.

The secondary reactions of mechanism 1 involved 'cracking' wax into lower molecular weight compounds (LMWC), being alkanes and alkenes enriching the NCG phase [256], [258]. In mechanism 1, it was proposed that when LMWC alkanes and alkenes are thermally unstable (at a

higher temperature) they can convert into aromatic compounds, like BTX (benzene, toluene & xylene) [71], [256], [258]. These cyclization reaction are from Diels-Alder and dehydrogenation reactions [71], [260]. Lastly, for both mechanisms 1 and 2, it is established that ternary reactions can further cyclize aromatics to char with a polycyclic structure [256], [258], which can occur at prolonged residence times or even high temperatures [261], [262]. Mechanism 2 disregards secondary cracking reactions of wax to NCG, by only considering aromatics forming reactions and char formation. As shown for the pyrolysis of fibres, if cracking reactions are favoured for long enough, they will convert components in the oil phase into LMWC that enrich the NCG phase [83]. Hence, the fact that mechanism 2 disregards reactions converting wax and oil into NCG might be a cause for contention.

2.5.4.3. Gas

Generally, the NCG yield from plastics is the product of second highest yield (after condensable product), but for PET and PVC it is the main product. PET and PVC both produce NCG with a yield over 50 wt.% at temperatures around 500 °C. The NCG from the slow pyrolysis of PET at 500 °C ranged between 52 to 65 wt.% [263] and another study compared the pyrolysis of PVC and PET at 500 °C and observed the plastics to produce NCG at a yield of 88 and 77 wt.%, respectively [249].

The pyrolysis of polyolefins (PE and PP) and PS between the temperatures of 400 and 600 °C will generally produce NCG with a yield between 5 to 20 wt.% [255], but was highly dependent on the temperature, as well as heating rate and pressure. It was observed that lower pressures in batch reactors [262] or longer solids residence time (150 min) [206] caused the thermal degradation of LDPE to occur at lower temperature. Hence, the temperature of 425 °C was observed to maximize condensable product yield from LDPE pyrolysis, resulting in an NCG yield of 10 wt.% [262]. Likewise, at the lowest tested temperature of 450 °C from another experiment, the observed NCG yield from LDPE pyrolysis was 16 wt.% [206]. Conversely, both batch experiments were shown to yield much higher NCG yields between 40 to 47 wt.% at 500 °C, exhibiting severe secondary cracking to NCG [206], [262]. Likewise, the NCG yield from the pyrolysis of PP was observed to be 44 wt.%, at the pyrolysis temperature of 600 °C and 20 wt.% at the temperature of 500 °C [264].

The HHV of NCG from polyolefins and PS is high, often exceeding 40 MJ/kg because the monomers in the feedstock contain no heteroatoms, allowing the composition of the NCG to be observed as 80 wt.% alkanes and 20 wt.% alkenes of length C_1 to C_5 [261]. The plastic LDPE was shown to yield NCG having a calorific value just less than methane gas. i.e. 42 MJ/kg [206], [262]. This NCG from LDPE was maximized at 500 °C possibly due to the high concentration of C_3 and C_4 species at this temperature [206], [262]. Even for pure plastics, the small presence of carbon oxides in the NCG have been observed and argued to be the result of air pockets inside the reactor [206].

2.5.4.4. Char

The char yields from the fast pyrolysis of polyethylene and polypropylene between the temperatures of 400 to 600 °C tends to be less than 5 wt.% overall. LDPE pyrolysis over 400 °C was observed to produce negligible char yields [206], [262]. Likewise, no char yield was observed from the pyrolysis of HDPE at 500 or 600 °C [264]. Similarly, the batch pyrolysis of PP was observed to achieve only a 2 wt.% char yield at 430 °C [261], [265], and a 3.5% char yield at 450 °C [266]. Indeed, most literature states that that the fast pyrolysis of plastics results in low char yields, but the slow pyrolysis of plastic can result in higher char yields that even show an increase in char yield, especially for PS.

Polystyrene is well-known to be the plastic with lowest degradation temperature with the highest condensable product yields often exceeding 90 wt.%, but as the temperatures increases past this point the char yield of PS has been observed to sometimes increase [262], [267]. Whereby at 400 to 425 °C, when the char yield was less than 5 wt.%, increasing the temperature to 500 °C caused the char yield from PS to increase to 27 and 30 wt.% [262], [267]. This phenomenon is believed to be due to secondary and ternary reaction that are enhanced at longer solids residence times, causing the aromatic ring structure to condense. Likewise, the long solids residence time also caused the same phenomenon to occur for the batch pyrolysis of LDPE, which went from having negligible char yield at 425 °C to a char yield of 16 wt.% at 500 °C [262].

2.5.4.5. Condensable product yield

Polyolefins and PS have high volatile matter content exceeding 90 wt.% and consequently able to produce high yields of condensable product for temperatures between 400 to 600 °C [255]. Generally, all the plastics, except PE and sometimes PP [268], [269] will condense into a liquid oil [262], [264], [266]. Indeed, both PE and PP are typically converted into a mainly waxy product during pyrolysis between 400 to 600 °C and short solid residence times [183], [256]–[258] [266] [264].

Researchers who have compared the pyrolysis of different plastic wastes, all have observed PS to have the highest condensable product yield at temperatures below 500 °C [261], [266], [270]. For temperatures below 500 °C, the condensable product yield from PS pyrolysis has been observed to be no less than 80 wt.% and maximized at lower temperatures than the other plastics. At 425 °C, when the wax yield from the batch pyrolysis of LDPE was 25 wt.%, the oil yield from PS was observed as 81 wt.% [266]. The same temperature (425 °C) for a batch reactor was observed by another researcher to convert PS to oil with a conversion yield of 97% [262]. Whilst, increasing the temperature to 450 and 500 °C, caused the yield to decrease to 80 and 67 wt.%, respectively [262].

LDPE is generally observed as the polyolefin with the lowest temperature to maximize condensable product yield, whereby condensable product (wax) is also observed to be maximized below 500 °C. Whereby, the wax yield from the pilot-scale, batch pyrolysis of LDPE was observed to decrease from 84 wt.% at 450 °C to 60 wt.% at 500 °C [206]. Bench-scale, batch reactors were capable of higher

conversions to wax product with a yield of 90 wt.% at the temperature of 425 °C [262]. Increasing the temperature to 450 °C, caused the wax yield to decrease to 72 wt.% [262]. Although the chemical composition of LDPE and HDPE is identical, the wax yield from HDPE tends to be maximized at slightly higher temperatures than LDPE [271]. It was observed from the fast, batch pyrolysis of HDPE that the condensable product yield increased from 3.1 to 75 wt.% for the temperature increase from 400 to 450 °C [272]. The batch pyrolysis of HDPE from 400 to 550 °C was observed to produce condensable product yields of 72 and 79 wt.% at 500 and 550 °C, respectively [273]. The pyrolysis of HDPE was studied from 500 to 600 °C with the maximum condensable product yield occurring at 500 °C with a yield of 79 wt.% and most of the condensable product being wax (83 wt.%) [264].

PP is typically observed to be the plastic with highest condensable product yields for temperatures of 500 °C and above. This has been demonstrated using a batch reactor at 500 °C with a solids residence time of 60 minutes, where the pyrolysis of PP had a condensable product yields of 95 wt.%, while HDPE and PS were converted to a lower condensable product at a yield of 93 and 71 wt.%, respectively [267]. The condensable product from the batch pyrolysis of PP was observed to maximize at a temperature of 488 °C, with a yield of 86 wt.% and increasing the temperature to 525 °C, produced a yield of 81 wt.% [274], [275]. Similarly, a condensable product yield of 83% was observed for the batch pyrolysis of PP at 500 °C for one hour [276].

2.5.4.6. Condensable product composition

PS is well-known to provide oil comprised of its aromatic monomer units. Styrene is the main component of PS pyrolysis oil with yields in the range of 50 to 85 wt.% obtained in range of 350 to 600 °C [277]–[279]. In batch reactors, when solids residence time is extended, the styrene has been observed to convert into mainly ethylbenzene, and toluene [262], [267]. It was observed at 500 °C, that around 30 and 35 wt.% of oil was comprised of toluene and ethylbenzene, respectively [262], [267]. In addition, a small amount of PS in a sample was shown to thoroughly improve the aromatics content of the condensable product, whereby if 10 wt.% of the feedstock contained PS, the oil from pyrolysis contained 8.3 wt.% aromatics [269].

The production of wax is favoured in short residence times and associated with the incomplete degradation of polyolefins [83], [271], [280]. However, if the solids residence time is extended and temperature increased, wax may be converted into oil [257], [262]. The condensable product from polyolefins are mainly aliphatic hydrocarbons with some aromatics [268], [269]. Typically, the condensable product from polyolefins has a higher concentration of alkanes than alkenes [261], [262], [267]. A study reported the condensable product from the pyrolysis of PE and PP to contain 70 and 57 vol.% alkanes, respectively [261]. Likewise, the same condensable product from PE and PP was observed to contain 22 and 34 vol.% alkenes, respectively [261], thereby leaving the aromatics to make up the less than 10 vol.% condensable product. Other researchers have

described the aromatics content of the condensable product from fast pyrolysis of polyolefins at 500 °C to be negligible [102], [268], [269]. However, increasing the solids residence times for the batch pyrolysis of PE and PP was shown to increase the aromatic fraction due to the promotion of secondary reactions [262], [271].

The condensable product from the pyrolysis of PP is not always waxy in viscosity [266], with a C_9 olefin known as 2,4-dimethylhept-1-ene being shown to comprise up to 25 wt.% of the condensable product composition [281]. The liquid from PP pyrolysis can contain other such hydrocarbons such C_5 olefin, C_6 olefin, several C_{15} olefin and some C_{21} olefins [282].

The condensable product from LDPE, with an HHV between 39 to 40 MJ/ kg was shown to have a higher calorific value than the condensable product from PS, with an HHV of 37 MJ/kg [262]. This is believed to be due to aromatic compounds, which have lower calorific value than aliphatic compounds, even when both compounds contain the same number of C atoms [262]. Other studies have also confirmed the HHV of PE or PP wax to be between 35 to 44 MJ/kg for temperatures from 400 to 600 °C [271], [274], [283], and the wax from LDPE was observed to be marginally higher than wax from HDPE, with the HHV of wax from HDPE ranging between 36 to 40 MJ/kg [271].

2.5.5. Product yields from pulper rejects

The addition of plastics to other waste streams, like lignocellulosic fibres has a positive impact on the energy content of the feed, resulting in pyrolysis products of higher energy content. In addition, adding plastic to fibres increases condensable product yield while decreasing gas and char yield.

2.5.5.1. Overview of pyrolysis products

Lignocellulosic fibres (cotton textiles or paper fibres) and polyolefins (PE & PP) are estimated to constitute most of the pulper rejects [23], and hence the condensable product will be mainly from degradation of these two components. Figure 2.11 shows the condensable product produced at different pyrolysis temperatures for fibres and polyolefins. In Figure 2.11, the degradation pathways for fibres and polyolefins is represented as a red and yellow line, respectively.
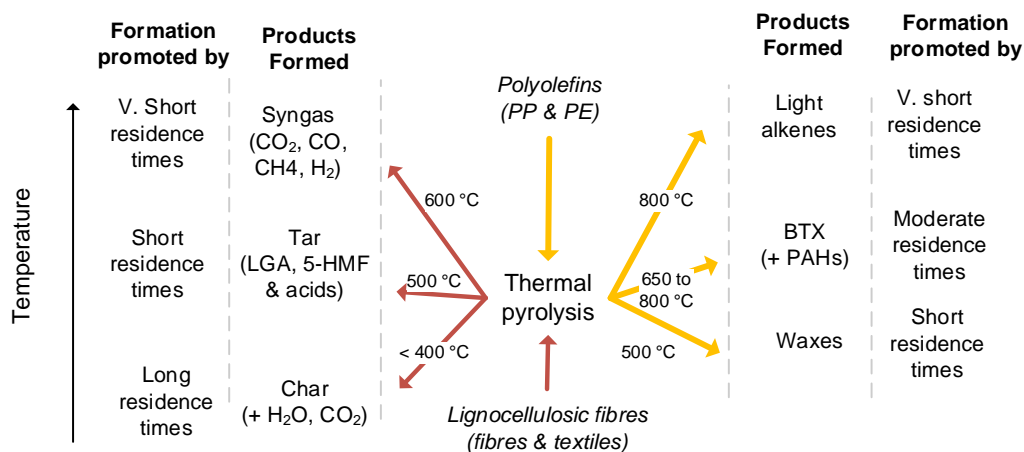
Figure 2.11: The main products produced at certain temperatures and the other variables that influence the products

At temperatures less than 400 °C, it is typically believed that the moisture will be fully evolved from the sample forming an aqueous phase oil product and char product containing mainly unconverted feedstock [24], [27]. The water content in bio-oil has been shown to be *ca.* 70 wt.% at 300 °C, which decreases to between 40 and 50 wt.% at 700 °C [284]. Cellulose would have begun degrading into its carbohydrate-derived components, too [100]. This temperature would only partially volatize the plastic products. The fast pyrolysis of polyolefins at temperatures around 500 °C is known to convert polyolefins into wax [271] and fibres into organic phase oil (tar) and aqueous phase oil [230]. The fraction of aromatic hydrocarbons, *viz.,* benzene, toluene, xylene (BTX) in condensable product from polyolefins can be present, albeit in small quantities at 500 °C [262], [271]. The increase in temperature from 650 to 800 °C, is associated with the conversion of wax into BTX [71], [101], [259], [262]. The composition of BTX in condensable product has been observed to increase from 10 wt.% at 650 °C to more than 50 wt.% at 750 °C [71]. Although aromatic components like BTX and others (e.g. ethyl-benzene) can be a valuable source of chemicals [100], [233], [262], their production is associated with the production of polyaromatic hydrocarbons (e.g. naphthalene) which can be toxic if inhaled. Additionally, increasing the pyrolysis temperature past 650 °C will require higher energy demand than 500 °C and result in condensable product of lower energy content due to the high aromatic hydrocarbon composition instead of high aliphatic hydrocarbon composition [275].

2.5.5.2. Condensable product yield

The non-catalytic conversion of pulper rejects into condensable product has been performed by four researchers on bench-scale [23]–[26], but to the best of the author's knowledge – none have tested the tested the pilot-scale pyrolysis of paper rejects alone. One researcher tested the co-pyrolysis of stem wood with rejects fed in a ratio of 80:20 [28]. A problem that arises for pilot-scale pyrolysis of rejects is the difficulty in controlling the homogeneity of the condensed product [285], which if sold as fuel oil - should not separate by gravity into light and heavy oil components [286].

It has been observed that for paper mill rejects of different plastic to fibre ratios, that the high plastic fractions (identified from the higher volatile matter content) produced condensable product with higher yields and greater HHV than rejects of lower plastic content [24], [25]. The presence of wax (C_{20+} alkanes) as condensable product is associated with the fast pyrolysis of polyolefins [240] and can be evident from the increasing wax content in condensable product for feedstocks with higher plastic content [24], [25]. The slow, batch pyrolysis of rejects was performed at 300, 425 and 550 °C, where it was observed that the condensable product yield to be maximized at 550 °C with a yield between 46 and 48 wt.% [24]. Conversely the fast, batch pyrolysis of the same rejects was performed at 350, 450 and 550 °C and condensable product yield was observed to maximize also at 550 °C, but with a higher yield from 58 to 59 wt.% [25]. For both articles, no wax was seen at the lowest tested temperature of 300 or 350 °C and the aqueous phase dominated the condensable product at

37

this temperature [24], [25]. The wax phase was evident during fast pyrolysis experiments, whereby it was observed that 85 to 90 wt.% of the condensable product was wax at 550 °C [25].

2.5.5.3. Char

The slow pyrolysis of the high-plastic, reject stream at 300 °C was shown to produce a solid residue with a yield of 76 wt.%, consisting of char and unconverted material [24]. Increasing the temperature to 425 °C, was shown to substantially decrease the solid residue yield to 41 wt.%, and further convert the material into aqueous phase oil and char [24]. Conversely, the fast pyrolysis of rejects yielded lower char yields than slow pyrolysis, whereby the char yield was decreased from 32 to 27 wt.% for the increase in temperature from 450 to 550 °C [25]. The decreased pyrolysis temperature not only lowers the char yield but lowers the HHV of the char from 35 to 33 MJ/kg and to 22 MJ/kg for the temperature change from 350 to 450 to 550 °C, respectively [25]. The low temperature of 300 °C was shown to maximize the gross energy conversion for pyrolysis whereby between 84 and 93 wt.% of the energy in the rejects was converted to the solid residue fraction [24].

2.5.5.4. Gas

Due to the high plastic content, NCG from rejects is expected to have similar characteristics to the NCG from mixed plastics, but also expected to contain carbon oxides like CO_2 and CO due to the lignocellulosic fibre fraction [83], [287]. Although, the NCG from the fast pyrolysis of plastic is typically made up of alkanes and alkenes of carbon length C_1 to C_4 [165], [229], [262], [288], components with carbon length C_5 to C_6 have been observed in the NCG from mixed plastic pyrolysis [233], [262]. Whereby, a high presence of PE or PS in the feedstock was reported to increase the HHV of the NCG to around 44 MJ/kg [262]. Temperature has been shown to also affect the composition of NCG in mixed plastic pyrolysis, whereby increasing the pyrolysis temperature was observed increase the composition of CO, H_2 and CH_4 in the NCG but decreases CO_2 composition [230].

2.5.6. Condensable product phases from rejects

2.5.6.1. Wax product

Waxes are aliphatic hydrocarbons (alkanes and alkenes) typically greater than C_{20} and up to C_{36} [268], [271] to C_{40} [262]. The largest fraction of alkanes and alkenes from the pyrolysis of PE was observed to be within C_{19} to C_{23} [262] and forms the reason why most condensable product yield from PE pyrolysis is wax, as observed when wax comprised between 83 wt.% [264] and 90 wt.% [273] of the condensable product yield.

The pyrolysis of Tetra Pak is expected to be similar to pulper rejects because like rejects, Tetra Pak is a combination of plastic film, lignocellulosic fibres and aluminum in similar compositions [102]. The wax from the pyrolysis of Tetra Pak at 500 °C had a "prevalent paraffinic character", containing mainly aliphatic hydrocarbons (alkanes and alkenes) [102]. However, the exact composition was not determined because the method of component identification was through H-NMR which only

determines the number of bonds [102]. The average molecular weight of Tetra Pak wax was 443 g/mol, representing an aliphatic hydrocarbon with a carbon length between C_{31} and C_{32} [102]. This was less than that from LDPE observed in the same study with an average molecular weight of 531 g/mol or hydrocarbon with length between C_{36} and C_{37} [102]. The lower average molecular weight for Tetra Pak could be due to the secondary cracking that is enhanced due to the catalytic effect of aluminium.

Although wax is expected from the pyrolysis of PE alone, carbonyl groups (C=O) have been observed in wax from the pyrolysis of Tetra Pak, which was possibly due to the interaction between fibres and plastics [102]. Generally, this could be the reason why the HHV of waxes from the fast pyrolysis of rejects with higher fibres content had an HHV of 31 to 33 MJ/kg, while the wax from rejects with less fibres, and more plastic had an HHV of 40 to 41 MJ/kg [25]. Conversely the wax from the pyrolysis of fibre and plastic was recorded as only around 17 MJ/kg [24]. The condensable product containing wax from the pyrolysis of plastic film was observed to liquefy at temperatures of 60 °C, due to its melting point [289] and hence capable of transport by pump [229].

2.5.6.2. Oil phase

The oil from the pyrolysis process is all the condensable product that is not wax. Generally, slow pyrolysis of mixed biomass and plastic streams like MSW [280] or pulper rejects [24] will generally degrade the wax into oil, leaving a high energy oil phase. Conversely, fast pyrolysis of MSW [280] and Tetra Pak [102] was observed to produce condensable product with three phases – wax, water-rich phase (aqueous) and a hydrocarbon rich, oily phase (organic).

The aqueous phase from these mixed streams is generally from the pyrolysis of lignocellulosic fibres containing a high oxygen content. Due to this high water content, the HHV of the aqueous phase has been reported to be too low to be determined by bomb calorimetry [100]. Aqueous phase from the co-pyrolysis of biomass with plastics was reported to be inferior to the aqueous phase from biomass alone, being attributed to hydrogen-transfer of PE to biomass, enhancing water formation reactions by hydrodeoxygenation [240], [290]. Therefore, the water in aqueous phase is likely to be increased in the presence of plastics [240]. Co-pyrolysis of plastics with biomass was reported to produce pyrolysis liquid with far lower aromaticity than from the bio-oil from biomass alone [290].

The co-pyrolysis of biomass with plastics improves the quality of condensable product by lowering the oxygen content of the oil, causing the heating value to increase [290]. The organic phase oil from rejects is from the depolymerization of plastics and fibres [234]. The slow pyrolysis of rejects of varying plastic content was shown to produce oil with an HHV maximized at 15 MJ/kg [25]. This lower HHV is attributed to the water content present in oil, decreasing the HHV. Conversely, organic phase has been reported to have a high energy content, when it is distinct from the aqueous phase, whereby an HHV of between 37 to 43 MJ/kg has been reported [24]. The high HHV of the organic

phase can be attributed to its composition - comprised of straight chain n-alkanes in the range of C_8 to C_{19}, like diesel [290]. Pure plastics generally produces organic oil with alkanes with length C_8 to C_{10} and C_{13} to C_{17} [283], that is still present even when the plastic content in feed is low [240]. When co-pyrolyzed with biomass, it has been seen that plastics (at 50% of feed) cause the aliphatic fraction of the pyrolysis oil to increase from 14% (biomass alone) to 70% when co-fed with PE [290].

2.6. Techno-economic assessments

The conversion of pulper rejects into a marketable product will not only reduce the amount of C&IW sent to landfill but potentially capable of producing extra income to the paper mill. The techno-economic analysis (TEA) method is used for measuring the energetic demands of an upscaled process, as well as predicting financial profitability for a long-term project before commissioning. Typically, the discounted cash flow method is used to test profitability [291].

2.6.1. Conversion of waste to waste-derived fuels

There are several techno-economic analyses for the conversion of MSW to WDF pellets [31], [32] [107], also sometimes referred to as mechanical treatment (MT) operations. Researchers have compared MT operations to waste-to-energy scenarios to compare the effect of incinerating the waste to sell electricity [292], [293], while others have included 'landfill-mining' scenarios to separate many plastics and raw materials individually and sell them (primary recycling) and only produce a small fraction of mixed WDF product (secondary recycling) [162], [294]. Primary recycling is typically more profitable than secondary recycling is [33], but as previously mentioned - almost impossible to do for pulper rejects. The conversion of MSW into SRF is scarce in literature with researchers having difficulty in classifying processed MSW into RDF due to its low organic content.

Of the models that are involved in the production of a WDF alone, a few have used the "recovery factor transform function (RFTF) matrix" to compare different process lines of the same feedstock [32], [39], [90], [108], [162]. The RFTF matrix requires the waste stream to be split into components and each component assigned qualities (e.g. ash content, moisture, HHV) [32], [162]. Thereafter, the process units in series will affect each component resulting in a unique WDF product for each process line [31], [32]. Typically the purchase cost of equipment (PCE) is taken from similar studies and a scaling factor of 0.8 is appropriate for solids-handling equipment [295], [296]. The total capital investment (TCI) of WDF conversion lines is observed to be calculated according to a Lang factorial method [31] that is modified from the typical Lang Factors for solids-handling processes [297]. At capacity of 250 kilotons/year, the capital expenditure (CAPEX) was reported between €1 to €2 million, which increased to €7 to €8 million when a bio-drying unit was included [8].

For one comparative study, it was reported it was more profitable for European treatment facilities to incinerate low quality WDF, like RDF from MSW, and sell the electricity to the grid than sell the RDF to end user [31], [33]. However, this is possibly due to the uncertainty of the use of RDF in the

European market at the time (2002) [31], [33], and that the SRF is sold as a "disposal fee" [31]. The disposal fee for the RDF from MSW mentioned in the above article was €33.5/ton [31], [32]. Indeed, the sale of RDF is usually from governments incentivizing their use in industry, as seen in an article whereby in 2004 the German government was paying industries a "disposal fee" of €10 to €60/ton of fuel accepted [108]. This disposal fee should at least equate to the production costs.

A desired internal rate of return (IRR) is specified according to the overall risk of a project and the IRR for SRF conversion line has been specified to be as low as 5% [33], [298] to 10% [146], [299], and associated with a project of very low risk. The profitability of MT processes are still very reliant on scale of economies [300], as observed from a study whereby the minimum RDF selling price for a 200 t/h pellet RDF plant was recorded as €5/ton, and less than that for a 25 t/h pellet RDF plant, with a minimum RDF selling price of €13/ton [31]. The results from that study were congruent to another study, where the production costs have been estimated at €5 - €15/ton [8]. A more recent study has shown the cost for processing waste into RDF to range from €32, €23 to €15/ton for a 10, 20 and 80 t/h plant, respectively [107].

2.6.2. Thermo-chemical conversion facility

Annexed thermochemical conversion facilities have been modelled using software such as Aspen Plus and then the profitability tested with MS Excel. Generally, the TEA processes are either modelled according to a selling price of fuel and the key profitability indicators given, or a desired IRR is met through specifying a minimum fuel selling price (MFSP). Typically, the latter will provide an easy means of assessment against commercial fuel oil prices.

The TCI of pyrolysis processes has been shown to be costed according to a modified Lang factorial method, for a 'biorefinery' processes [301] and this method has been used for the pyrolysis of paper mill rejects [29], as well as for the pyrolysis of biomass [302]–[304]. The costing is calculated through splitting the PCE to 'inside battery limits' (ISBL) and 'outside battery limits' OSBL costs and assigning Lang Factors accordingly [295]–[297], [302]. The working capital for the pyrolysis process is assumed as 5% of the fixed capital cost (FCC) [29], [296], [302], [305], [306].

The same paper mill rejects that were tested on slow [24] and fast, batch pyrolysis [25] were input into a TEA model, using the small capacity of 550 kg/h of wet rejects, and shown to be unprofitable [29]. The profitability was compared by identifying the difference between the minimum fuel selling price (MFSP) to attain a discount rate of 9.5%, and that of commercial fuels ($15.9/GJ) [29]. At a capacity of 550 kg/h, the MFSP of the plastic-rich rejects were 2.4 times the price of commercial fuel and the fibre-rich rejects were 4 times the price of commercial fuel [29]. Combining the rejects from two neighbouring paper mills, would make the TEA profitable at a capacity of 2400 kg/h proving its reliance on scales of economy [29]. Another South African article tested the feasibility for converting tire waste into fuel oil at a low capacity of 145 kg/h [307]. The optimistic fuel selling price of R14.65

41

per litre was used to demonstrate profitability with a net-present value of R7.6 million after 15 years (NPV_{15}) [307]. In addition, profitability was attained by selling not only the oil, but steel at a price of R2.5 per kg, char, and accepting a gate fee for the collection of tires. Hence, this article describes an optimistic market for high-sulphur pyrolysis oil in South Africa and a means of comparison for equipment cost and product selling prices in South Africa [307].

Another study on the small-scale pyrolysis of dried biomass at a capacity of 200, 600 and 1000 kg/h showed that pyrolysis, coupled with a combined heat and power (CHP) unit to sell electricity, is not profitable [30]. The idea to sell electricity was believed to be due to the high char yields (50 to 70 wt.%) and low condensable product yield (10 to 30 wt.%) [30]. The on-site generation of electricity was later described as being a poor investment in comparison to purchasing electricity from the grid [30]. Hence profitability could only be attained if the 1000 kg/h choice was coupled with an increase of 50% for char selling price and the TCI and material cost was decreased by 50% and 20%, respectively [30]. The market value for char has been shown to be highly variable in literature depending on its use. Char from biomass can be sold as biochar due to absorptive properties [308]. Biochar has been reported to cost $5.06/kg in the U.K market (R83.72/kg, considering the exchange rate of 16.54 ZAR/US $) [30], but lower prices of *ca.* $0.30/kg (R4.96/kg) have been reported for South African char [308]. Adding plastic to biomass will make char less desirable as an absorbent because molten or charred plastic reduces the microporous surface area of char [240].

2.6.3. Comparison between pelleting and pyrolysis

Although there have been several reports published by companies like Andritz or VNP which have outlined the possible recycling methods for rejects [7], [12]–[14], articles focused on the technical and economic comparisons between pyrolysis and pelleting are in short supply.

To the best of the author's knowledge, there is only one article that has focused as a comparative study of the techno-economics of pyrolysis and pelleting of a waste stream (biomass) [34]. This article dealt with pyrolysis, pelleting and torrefaction as pretreatment methods and supply chain logistics (not considered for this study) for each conversion method [34]. Using normalized data from other literature, the article compared the pelleting and pyrolysis process w.r.t the gross – and net energy conversion (GEC & NEC), production costs on a mass (R/ton $_{product}$) and energy basis (R/GJ $_{product}$) and specific CAPEX requirement (M€/MW$_{th}$). The gross energy conversion (GEC) is an indication of the energy contained in the feedstock compared to the energy of the products, while the net energy conversion (NEC) is the GEC but includes the process energy (i.e., energy for heating, drying, etc.). The results for the pretreatment part of the comparison is shown in Table 2.9, whereby the CAPEX, specific CAPEX and production costs for the pyrolysis process is more than the pelleting process [34]. The GEC of the pyrolysis process was lower than the pelleting process, because the lower-heating value (LHV) of the oil (17 MJ/kg) was only fractionally higher than the LHV of wood

pellets (15.8 MJ/kg) [34]. Subsequently, the NEC for the pyrolysis process was also lower than the pelleting process, although the difference between the GEC and NEC in Table 2.9 for the pyrolysis process is only 2% [34], and contentious considering the high energy requirement of pyrolysis.

Table 2.9: Technical and economic comparison for the pelleting and pyrolysis process, as adapted from [34]

	Variable	Unit	Pelleting process	Pyrolysis process
Technical	Feedstock	-	Wet wood chips	Dry, wood (3 mm)
	Product	-	Pellets	Bio-oil
	LHV	MJ/kg	15.8	17.0
	Mass density	kg/m^3	500 to 650	1200
	GEC	%	92.2	66.0
	NEC	%	84.0	64.0
Economic	Specific CAPEX	M€/MW $_{th}$	0.15	0.40 to 1.16
	OPEX	€/ton	41	75 to 150
		€/GJ	6 to 12	3.4

2.7. Conclusions and gaps in literature

The following section summarizes the literature and identifies the gaps in the literature.

2.7.1. Pelleting of pulper rejects

Rejects contain 60 to 80 wt.% polyolefin plastics, 10 to 20 wt.% fibres and 5 to 10 wt.% ferrous metals. This waste can be converted to waste-derived fuel (WDF) by concentrating the organic fraction through extracting ferrous metal and reducing the moisture. WDF is an umbrella term that includes refuse-derived fuel (RDF) and solid-recovered fuel (SRF). WDF can be called SRF if it is assigned a class code according to a classification from the WRAP classification scheme (An improved BS EN 15359 made for small-scale RDF producers). SRF with high energy content, low ash and moisture content is suitable for firing in the primary burners of cement kilns but should be compared against South African Air quality emissions to ensure its eligibility for cofiring.

2.7.2. Pyrolysis of pulper rejects

Pyrolysis involves thermally treating waste at temperatures from 400 to 700 °C in anaerobic conditions to breakdown polymers into shorter chain monomers. The pyrolysis of feeds with high volatile matter content, like plastics, produces high yields of condensable product with higher energy density and homogeneity than the feedstock. The pyrolysis of fibres at *ca.* 500 °C produces condensable product with two phases, being aqueous phase containing mainly water and tarry phase product containing mainly LGA. The fast pyrolysis of polyolefins (PE and PP) at 500 °C is reported to convert between 60 to 80 wt.% of the rejects into condensable product, rich in wax. The batch, pyrolysis of rejects on bench-scale could produce condensable products (wax and oil) with yields between 55 to 65 wt.%. Several studies have been performed with paper mill waste on pilot-

scale using the "thermo-catalytic reactor" and "Pyro-reformer reactor" at Aston University, but all tests have either been for gasification resulting in condensable product of high aromatic content, or pyrolysis but with a paper-rich, rejects. Additionally, none of these tests have provided a comparison of the pilot-scale experiments to bench-scale with emphasis on product yield or energy contents.

2.7.3. Comparative TEA for the pelleting and pyrolysis processes

The RFTF matrix is a means of comparing different waste-to-WDF conversion lines w.r.t to the impact that different process units and their order have on produced WDF. Due to the unknown market of some WDF, some waste-to-WDF lines have used a "disposal fee" for processing the waste instead of a selling price to establish profitability. Pyrolysis processes, modelled on Aspen Plus, are highly sensitive to feedstock capacities. Whereby, the TEA of a pyrolysis process was unprofitable at a capacity of 4.32 ktpa of pulper rejects. In comparison, the current study assumes a lower capacity of 3.48 ktpa. To the best of the author's knowledge, only one comparative study exists between the pyrolysis and pelleting pretreatment methods, but this process was based off normalized literature and for a biomass stream where the energy content of the bio-oil (17 MJ/kg) was only fractionally greater than the pellets (15.8 MJ/kg).

Chapter 3: Research Aims and Objectives

3.1. Aim and objectives of study

The aim of this study is to determine which recycling method; pyrolysis or pelleting, is more suitable for diversion of pulper rejects from landfill. This research aim is fulfilled according to three objectives.

Objective 1: To evaluate the suitability of solid-recovered fuel (SRF) derived from pulper rejects for use as alternative fuel in South African cement kilns. This would entail the following:

- Identify what the pretreatment steps are to process rejects into waste-derived fuel (WDF).
- Calculate the composition of the wet rejects and WDF, for characterization and for use in the pelleting and pyrolysis techno-economic analysis.
- Evaluate whether the produced WDF will adhere to the classification for solid-recovered fuels (SRF) according to BS EN 15359 and WRAP classification scheme.
- Determine whether the classified SRF can be used for cofiring in South African cement kilns according to its chemical qualities and permissible heavy metals content.

Objective 2: Assess the product yield and energy distribution from the pilot-scale pyrolysis of pulper rejects and how these variables differ from the bench-scale pyrolysis. This would entail the following:

- Compare the product distribution yield for the batch, bench-scale pyrolysis of rejects to the results gathered by a researcher who only pyrolyzed rejects on the bench-scale setup.
- Compare the gross-energy conversion (GEC) at bench-scale to the comparative study.
- Determine the product distribution yield for the pilot-scale pyrolysis and identify the phases present in the condensable product phase.
- Determine the energy content of each of the separated phases, explained above.
- Evaluate the GEC and net-energy conversion (NEC) of the pilot-scale pyrolysis setup.

Objective 3: To evaluate which conversion process is more profitable at the mill capacity of 3.48 kilotons per annum (ktpa) of wet rejects. This would entail the following:

- Determine a composition for the wet and dry rejects so that the pelleting process can be modelled according to the recovery factor transfer function matrix (RFTF) method.
- Define a product yield for each pyrolysis temperature, by assigning model components to the phases of the condensable products, so that the process can be modelled in Aspen Plus.
- Attaining a suitable correlation to be used for the pricing of char, fuel oil and SRF products.
- Develop a model for each process, so that the minimum fuel selling price (MFSP) can be determined from the revenue, CAPEX and OPEX using the discounted cash flow method.

Chapter 4: Experimental Methodology

4.1. Research project overview

The research approach for the study was illustrated in Figure 4.1. As shown in Figure 4.1 the research approach has been separated into an experimental and simulation section. The experimental section would fulfil the technical comparison between the two conversion technologies (objective 1 and 2) and the simulation work would fulfil the economic comparison (objective 3).

The research approach (Figure 4.1) shows how the 200 kg was initially pre-treated and underwent characterization analysis to test its suitability as fuel. The technical feasibility of converting the pulper rejects into SRF has been evaluated according to testing the pre-treated waste with its compliance to SRF standards outlined in the standard, BS EN 15359, 2011 and WRAP classification scheme. If the sample were shown to comply within the standards for its technical, economic, and environmental factors, the pre-treated pulper rejects could be categorized as a class code of SRF. Thereafter, the environmental factors should be compared to the maximum, permissible gas concentrations specified in Air Quality Act 39 of 2004 for use in the cement or power industry [38].

Conversely the technical feasibility of converting pulper rejects into pyrolysis condensable product consisted of scaling up the pyrolysis from bench-scale to pilot-scale. The bench-scale pyrolysis gave yields and energy conversions for the pyrolysis temperatures and confirmed results collected by a colleague on the same apparatus for rejects of high plastic content [24], [25]. The results from bench-scale would provide the temperature range to be tested to maximize condensable product yield and energy conversion for pilot-scale. The condensable product from pilot-scale would be enough to separate the low energy aqueous phase from the high energy wax and organic oil phase (fuel oil).

The methodology for economic feasibility of each process is in Chapter 6. The pelleting process was modelled according to the RFTF matrix method, to produce an SRF product, in Microsoft (MS) Excel. The pyrolysis process was modelled in Aspen Plus V8.8 to attain the mass and energy balance data. This data was subsequently used in MS Excel to calculate the profitability of the process. The LHV determined the price of the SRF and the HHV determined the price of char and fuel oil. These selling prices were then compared against the minimum fuel selling price (MFSP) required to attain an internal rate of return (IRR) of 25%, to determine profitability. The MFSP required to attain an IRR of 10% was compared too, as seen for some pyrolysis and pelleting techno-economic analyses.

These research goals were achieved keeping in mind that a bench- and pilot-scale pyrolysis unit are available in the Department of Process Engineering and there is limited equipment for testing combustion characteristics. Hence the implications of incinerating the waste turned SRF is not included, but compliance of environment factors to the Air Quality Act 39 of 2004 assumes feasibility.
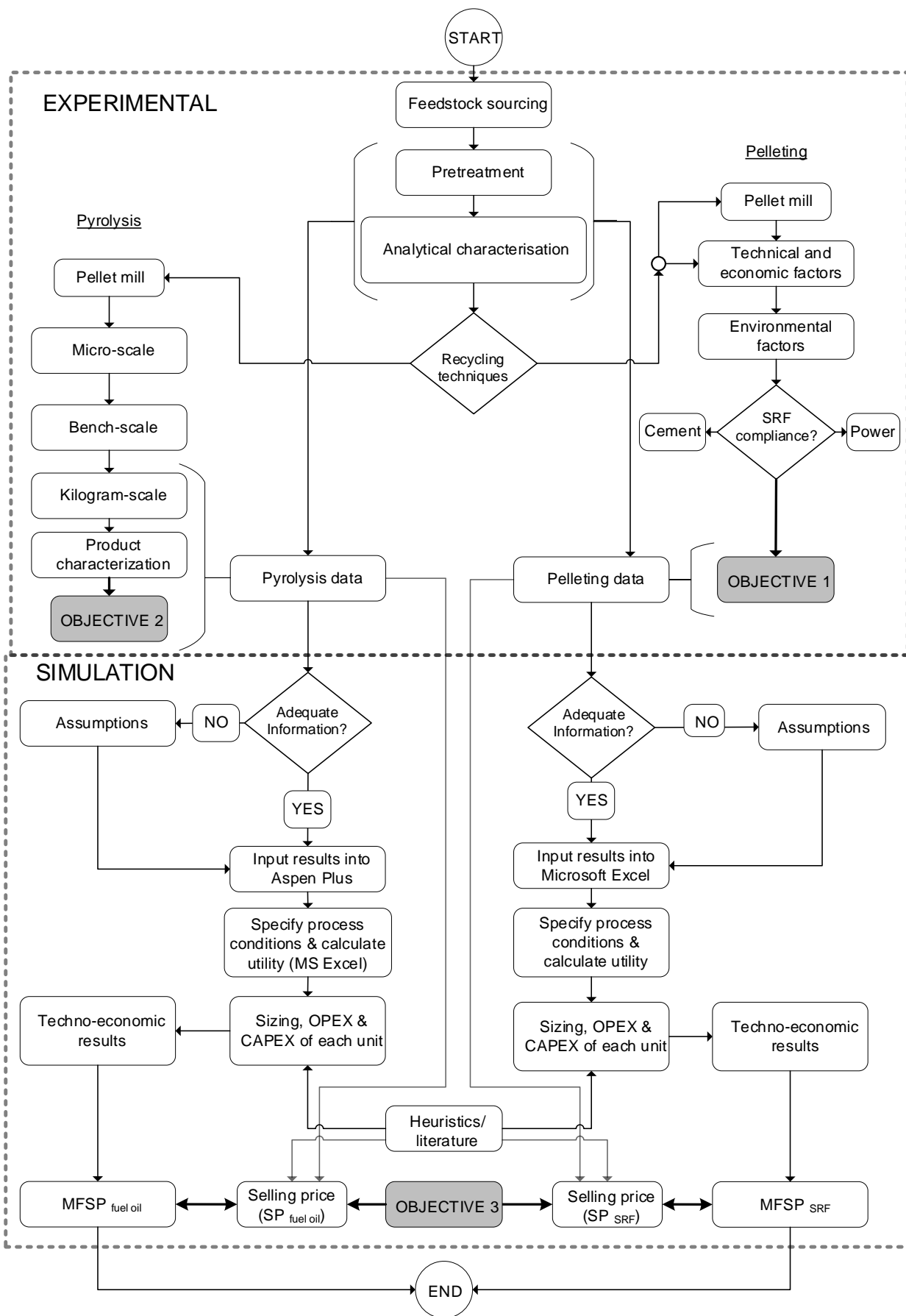
Figure 4.1: Research approach

4.1.1. Feedstock sourcing and pre-treatment

The pulper rejects used for this study were from the recycled fibre process (RFP) of the Kimberly-Clark (K-C), Enstra mill. These rejects are isolated after the pulping section and are typically baled to be sent to landfill. Four bags of coarse rejects each of mass around 50 kg were couriered to the Department of Process Engineering, Stellenbosch University. The bulk sample was air-dried using fast-moving air in a tunnel greenhouse for two months. The sample was turned over every week to aid drying and all ferrous metal was removed using a permanent magnet. The dried sample, without metal, was then milled down to 4 mm particle size using a knife-mill and 4 mm screen. This dried, milled pulper rejects is referred to as fluff [179]. The feedstock for the pyrolysis experiments at bench-scale and pilot-scale were Ø6 mm pellets made from pelletizing fluff in an ABC HANSEN pellet mill (Model 200). The material was pelleted to increase its packing density.

4.1.1.1. Moisture content

The moisture content of the as-received sample was determined from the difference in weight of wet 50 g samples upon delivery and after 18 to 24 hours of oven drying at 70 °C. Additionally, the moisture content of the air-dried material waste was determined with a ML-50 Moisture Analyzer.

4.1.1.2. Ferrous metal content

The mass composition of ferrous metal was determined from the mass of ferrous metal collected through magnetic separation and the mass of dried and wet rejects. The mass of the material was weighed on scale with 0.001 kg tolerance.

4.1.1.3. Sub-sampling method

Sub-sampling is the method of obtaining a representative sample of smaller size to perform characterization, pelleting and pyrolysis trials. The sub-sampling method for the characterisation tests involved the cone-and-quarter procedure until *ca.* 200 g of fluff was available. Cone-and-quartering involved mixing and piling the sample together, flattening the sample out in the shape of a circle, and evenly dividing the circle into four quarters. Two opposite sides of quarter are discarded, and the 2 other quarters are mixed to begin cone-and-quarter sampling again. The tests for pelleting attributes were typically taken from the 200 g representative sample, otherwise grab samples were used (e.g., bulk density, ash content and lower heating value). The feedstock used for the pyrolysis tests were taken as grab samples from the pelleted material (Ø6 mm pellets).

4.1.2. Analytical characterization

The characterisation tests described refer to particle size, proximate, ultimate, higher heating value (HHV) analysis of the feedstock and pyrolysis products. Proximate and ultimate analysis was performed on fluff because small sample mass is required (20 mg), and a single Ø6 mm pellet is too heavy. Particle size analysis was performed to attain fractions with different particle sizes (most analyses require uniform size) and produce a particle size distribution (PSD) for the fluff.

4.1.2.1. Particle size analysis

Particle size analysis was performed through sieve analysis following ASTM D4749. Sieves were collected from the Hydrometallurgy Room (Process Engineering Lab) and 9 sieves with the following diameters were used: 500, 850, 1000, 1400, 2000, 2800, 4000, 5600, 8000 µm. Four 50 g samples of fluff were used to attain the separated size fractions and particle size distribution (PSD) of the fluff. Fluff of particle size under 500 µm are fines and most chemical analyses were performed on particles of size 1000 - 1400 µm. The PSD was a cumulative passing distribution curve with d_{50} and d_{80} values to indicate diameters allowing 50 and 80 wt.% of particles passing through, respectively.

4.1.2.2. Ultimate analysis

The ultimate analysis was performed on fluff (<1400 µm) in accordance with ASTM D5291-92 using an Elementar Vario EL Cube Elemental Analyser. Ultimate analysis determined the content of Carbon, Hydrogen, Nitrogen and Sulphur present in the sample.

4.1.2.3. Proximate analysis

Proximate analysis was performed on fluff (<1400 µm) and pyrolysis char (unknown size) from pilot-scale experiments. Proximate analysis for both samples was in accordance with ASTM E1131:2015, using the Discovery TGA 5500 apparatus. A sample of 20 mg was required for the fluff and char and N_2 and O_2 carrier gas at a flowrate of 70 ml/min.

4.1.2.4. HHV determination

The HHV of the feedstock (single pellet) and pyrolysis char was tested in accordance with the ASTM standard D5865-11a, using a bomb calorimeter (Cal2K Eco Calorimeter). The bomb calorimeter was calibrated using benzoic acid. The HHV analysis of the condensable product from pyrolysis (oil or wax) was performed using gelatine capsules for both bench and pilot-scale experiments.

4.2. Conversion of rejects to pyrolysis condensable product

4.2.1. Micro-scale pyrolysis

Samples of fluff (<1400 µm) and fines (<500 µm) were decomposed in an inert atmosphere via thermogravimetric analysis to observe thermal degradation without mass or heat transfer limitations.

4.2.1.1. Decomposition profiles

The thermal decomposition profiles of fluff and fines was determined using the Discovery TGA 5500, with a 20 mg sample and N_2 as carrier gas at flowrate of 80 ml/min. The mass loss of the sample was measured at a constant time with a heating rate of 10 °C/min. The thermal degradation of the fluff was representative of the pyrolysis feedstock because the mass of a single Ø6 mm pellet exceeds 20 mg and the fines was tested as a means of comparison against the larger particles. Trios™ Software was used to generate the data for the thermal degradation (TG) curve for the four samples. This data was imported into Matlab™ software and the derivative thermal degradation

(dTG) curves were generated with a derivative and smoothing function. The dTG curves represent the rate of mass loss of the sample at changing temperatures.

4.2.1.2. Approximation of composition

The TG and dTG curves show estimates for how complete pyrolysis will be at specific temperatures and hence the areas under the dTG curves were used to approximate relative composition of the lignocellulosic fibres, polyolefins and other organic residue depending on their peak degradation temperatures. This method was followed to approximate the quantity of PET and LDPE in mixed plastic [192], and although not accurate [309], provides a rough estimation. The MATLAB program code used to calculate the relative area under each deconvoluted peak is shown in Appendix A.1.

4.2.2. Bench-scale pyrolysis experiments

Bench-scale pyrolysis experiments were performed from the pyrolysis temperature of 350 to 550 °C, with experiments at the temperature of 350, 500 and 550 °C performed in duplicate, due to small variability within results. The experiments at 450 °C was performed in triplicate, due to greater variability within results. Hence, 9 experiments were used for the results on bench-scale. The bench-scale pyrolysis experiments were performed in a batch, stainless-steel tubular reactor. The dimensions of the horizontal tubular reactor were an outside diameter and length of 110 and 450 mm, respectively. The one side of the reactor was connected to a N_2 purge and the other, was the exit of the reactor connected to the downstream condensation train. The condensation train consisted of a stainless-steel pot at ambient conditions, two metal condensers chilled with water connected by a stainless-steel collection pot submerged in dry-ice (-79 °C) and an electrostatic precipitator. The produced NCG was collected in Tedlar bags and analysed through gas chromatography. Figure 4.2 shows the bench-scale pyrolysis setup, where Table 4.1 describes each labelled unit and its function in the bench-scale pyrolysis reaction according to Figure 4.2.

4.2.2.1. Calibration

The pyrolysis temperature was carefully controlled through induction heating and measured by infra-red (IR) temperature measurement and displayed on the screen of the PLC (see Figure 4.2). Prior to every run, the temperature was calibrated by adjusting the emissivity ($0 < \epsilon < 1$) on the back of the PLC. The reactor was then heated, and the temperature measured with two thermocouples, placed where the sample boat would be placed, to see if the emissivity needed to be adjusted so that the temperature read by the PLC was the same as that read by the thermocouples.

4.2.2.2. Experiment

A sample of 30 g of Ø6 mm pulper reject pellets were placed in the sample boat and loaded into the reactor. The sample was heated at a constant heating rate of *ca.* 200 °C/min to the desired pyrolysis temperature and once attained, the sample was subjected to the pyrolysis temperature for a holding time of 30 minutes, as set on the PLC. To carry the volatiles through the condensation setup while

maximizing condensation, the N_2 flowrate was adjusted to 0.5 L/min for all bench-scale pyrolysis experiments. The holding time of 30 minutes and the N_2 flowrate of 0.5 L/min was reported as appropriate for converting plastics to condensable product for this reactor setup [192]. When the sample was undergoing degradation, the volatiles were evolved from the reaction zone and into the condensation system consisting of an ambient temperature collection pot, two condenser using cooling water at 5 °C and another metal collection pot submerged in dry ice (-79 °C). The first collection pot predominantly collected wax product and the condenser, second pot and 12-kV electrostatic precipitator (ESP) collected predominantly oil product. At the 30-minute mark, the heater was turned off to allow the reactor to cool down and N_2 flowrate was turned off after a further 10 minutes to allow any volatiles still in the system to condense. The extra 10 minutes allowed the reactor temperature to drop below 300 °C preventing any further pyrolysis reactions.

4.2.2.3. Condensable product (wax vs. oil) and char fraction

The condensable product yield was split into wax and oil depending on where the condensable product was collected. The wax yield was the difference in mass of units 6 to 9 (Figure 4.2), as shown in Equation 4.1 where "f" and "i" mean final and initial and refer to unit weights before and after the experiment, respectively. The oil yield was the difference in mass of units 10 to 14 and is calculated similarly to the wax yield but considering units 10 to 14 instead of units 6 to 9. The char yield was determined from the difference in mass of Unit 5, from before and after each run. The units described in the above section are shown in Figure 4.2 and a description of each given in Table 4.1.

$$\text{wax yield (wt. \%)} = \frac{(\text{unit6}_f - \text{unit6}_i) + (\text{unit7}_f - \text{unit7}_i) + (\text{unit8}_f - \text{unit8}_i) + (\text{unit 9}_f - \text{unit 9}_i)[g]}{\text{mass}_{feed}[g]} \qquad \text{Equation 4.1}$$

4.2.2.4. Non-condensable gas (NCG) fraction

For the bench-scale pyrolysis experiments the NCG was sampled throughout the 30-minute run and prolonged 10 minutes post-run in 5 L Tedlar-bags. Each bag was filled for 3 minutes before being replaced by another. At the end of each run, the composition of the NCG could be analysed through gas chromatography (G.A.S CompactGC 4.0). Gas chromatography was used to quantify the concentration of N_2, CO, CO_2, CH_4, H_2 C_2H_4, C_2H_6, C_3 group, C_4 group and C_5 groups. The mass of each gas component could be calculated according to the volume of produced gas compared to the volume of N_2 in the sample (of known flowrate [0.5 L/min]) and the molecular weight (M_W) of each gas component. Due to the high temperature and low-pressure system, the gas is assumed ideal. Each gas fraction could be calculated according to Equation 4.2.

$$m_X = \frac{\text{Vol. \% (X)}}{\text{Vol.\% (N}_2)} \cdot \frac{N_2 \text{ flow rate [L/min]}}{\text{Ideal gas volume [L/mol]}} \cdot M_W[g/mol] \qquad \text{Equation 4.2}$$

Comparing the summation of the products, (i.e., mass of the gas produced, the condensable product and the solid char) to the feedstock, will determine the mass balance closure. Whereby if the mass balance closure equals 100%, this means that the mass of the products is identical to the feedstock.
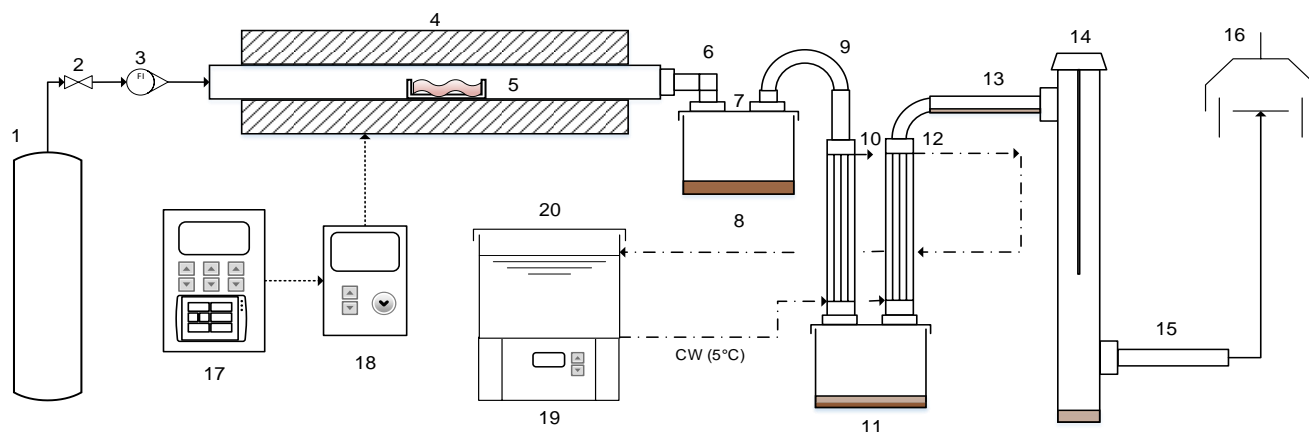
Figure 4.2: The batch, bench-scale pyrolysis unit.

Table 4.1: The description and function of each unit from Figure 4.2

Unit	Description	Function
1	Nitrogen tank	Supply Nitrogen (N_2)
2	Gate valve	Open & close N_2 supply
3	Flowmeter	Maintain N_2 flowrate at 0.5 L/min
4	Induction reactor	Heat reactor to pyrolysis temperature
5	Glass sample boat with sample	Hold 30 g sample for batch reaction duration.
6	Metal elbow connection (MEC)	Connection between reactor and Pot 1
7	Lid + Gasket of pot 1	Connection between MEC and Pot 1
8	Pot 1	Collect the condensable product (wax)
9	U-bend connection	Connection between Pot 1 and MC1
10	Metal condenser 1 (MC1)	Condense volatiles using chilled water (5 °C)
11	Pot 2	Collect the condensable product (oil)
12	Metal condenser 2 (MC2)	Condense volatiles using chilled water (5 °C)
13	Rubber hosepipe	Connection between MC2 and ESP
14	Electrostatic precipitator (ESP)	Condense remaining volatiles (oil)
15	Rubber pipe to extractor	Send non-condensable gases to extractor hood
16	Extraction duct	Extraction of NCG from lab
17	PLC	Control and adjust the reactor parameters
18	Heater	Turn on pyrolysis unit
19	Chiller	Chill the recirculated water to 5 °C
20	Buffer tank	Collect the recirculated water

4.2.3. Pilot-scale pyrolysis experiments

4.2.3.1. Description

Three temperatures were tested on pilot-scale (450, 500 and 550 °C). The experiment at 450 °C was performed in duplicate and the experiments at 500 and 550 °C were performed in triplicate due to higher variation within groups. Hence, 8 experiments were used for the results from pilot-scale.

The pilot-scale experiments were performed on a kilogram-scale, rotary-kiln reactor. The pilot-scale unit is semi-continuous and comprised of a hydraulic feeding section, a rotating kiln reactor, a char-pot, a four-part condensation train, a chiller, two gas towers and a PLC (to control various temperatures, rotation speed, vacuum pump, and view alarms). For example, the temperature of the reactor and two trace heaters can be controlled via the PLC.

Figure 4.3, shows the PFD of the pilot-scale unit. The feeding section uses two pneumatically operated valves to minimize O_2 contamination. After feeding, the sample is pushed by a hydraulic piston into the reactor zone. When the hydraulic piston is back into its starting position the feeding valves open again to introduce more feed. The top pneumatic feed hopper opens every 72 seconds, introducing more feed into the reactor zone. The rotary kiln reactor is electrically heated to the set temperature by the PLC. The feedstock is transported along the length of the reactor via screw baffles, where it is chemically decomposed into volatiles. The solid char falls into the char collection pot. The temperatures of the char collection pot and pipework to condensation train are set to a temperature of 300 °C and 350 °C, respectively to prevent condensation of heavy volatiles. Condenser 1 is submerged in water and the temperature is controlled between 25 and 35 °C. Condenser 2 to 4 are submerged in chilled water maintained at 5 to 10 °C. A vacuum pump was used to displace the NCG fraction into the gas towers. NCG that collects in the collection tower is used to calculate volume and subsequent mass of NCG produced during each run. A gas sampling valve (Unit 24 in Figure 4.3) after the four-stage condensation train allows the operator to sample gas with Tedlar bags throughout the experiment.

Each run was fed 2 kg over a period of 1.5 hours. The gas was collected, and the volume produced recorded for a further 2 hours before turning off the N_2 rotameter and reactor unit. The unit was left overnight to cool down and the retort remained rotating to transfer the char to the char-pot. The following day, char yield was calculated according to the mass difference of unit 7 and mass of char collected in the reactor. A fitting was used on a vacuum cleaner to extract the remaining char directly from the reactor through the inspection eye (Unit 6 in Figure 4.3). The liquid yield was calculated according to the difference in mass of units 10, 11, 13, 14, 16, 17, 19 – 23 from Figure 4.3 before and after the experiment. The liquid from each condenser was collected and stored in the fridge.

4.2.3.2. Non-condensable gas fraction

Unlike bench-scale the NCG was not sampled throughout the pilot-scale experiments. Instead, the gas collection towers were used to calculate the volume of gas produced by displacing the water of the collection tower and recording the volume and time it took for the collection tower to fill up with NCG and sweeping gas (1 L N_2/min). While one collection tower was filling with gas, and thus displacing the water, the other tower was being filled up with water so that it could be used next.

To find the composition of the gas produced throughout the run, a 5 or 10 L Tedlar bag was attached to the gas sampling point (after the condensation train) and the valve opened to introduce the representative sample of NCG. The representative sample was taken when the tower was half full to get a fair test for NCG composition of every full collection tower. Given the mol composition from GC and the volume recorded in the gas collection tower, it is possible to calculate the mass of the gas component. It assumed that the gas behaves ideally (occupies 22.4 L/mol), as shown in Equation 4.3. The total mass of NCG per run was calculated from the summation of gas components (Equation 4.4) excluding N_2 and O_2. Once the mass composition of NCG is calculated, the energy content of NCG can be calculated according to the weighted average method as shown in Equation 4.5 for LHV_{NCG}. Both the HHV and LHV values are shown in Table 4.2 [310], [311].

$$m_{gas,i} = \frac{mol\ comp._i\ (\%)}{1} \times \frac{V_{tower}\ (dm^3)}{1} \times \frac{mol_{idl.gas}\ (mol)}{22.4\ (dm^3)} \times \frac{mol.weight_i(g)}{(mol)} \times \frac{1\ (kg)}{1000(g)} \qquad \text{Equation 4.3}$$

$$m_{gas} = \sum_{i=1}^{n} m_{gas,i}\ (kg) \qquad \text{Equation 4.4}$$

$$LHV_{gas} = \sum_{i=1}^{n} \frac{m_{gas,i}\ (kg)}{m_{gas,tot}\ (kg)} \times LHV_{gas,i} \qquad \text{Equation 4.5}$$

Table 4.2: Energy content (LHV and HHV) of the components present in the syngas

Component	CO	CH_4	H_2	CO_2	C_2H_6	C_2H_4	C_3	C_4	C_5
LHV (MJ/kg)	9.09	50.0	120	0	47.6	47.1	43.1	45.7	45.3
HHV (MJ/kg)	10.1	55.5	142	0	51.9	50.3	50.0	49.4	49.0

4.2.3.3. Char characterization

The char from each run was divided into two fractions, *viz.,*

- The char extracted from inside the reactor with a vacuum, referred to as "vacuum char".
- The char extracted from the charpot, referred to as "charpot char".

The HHV of char was calculated from the yield and HHV of the two char types as in Equation 4.6.

$$HHV_{tot.char}\left(\frac{MJ}{kg}\right) = \left(HHV_{charpot}\left(\frac{MJ}{kg}\right) \times \frac{Y_{charpot}\ (\%)}{Y_{tot.char}(\%)}\right) + \left(HHV_{vacuum}\left(\frac{MJ}{kg}\right) \times \frac{Y_{vacuum}\ (\%)}{Y_{tot.char}(\%)}\right) \qquad \text{Equation 4.6}$$
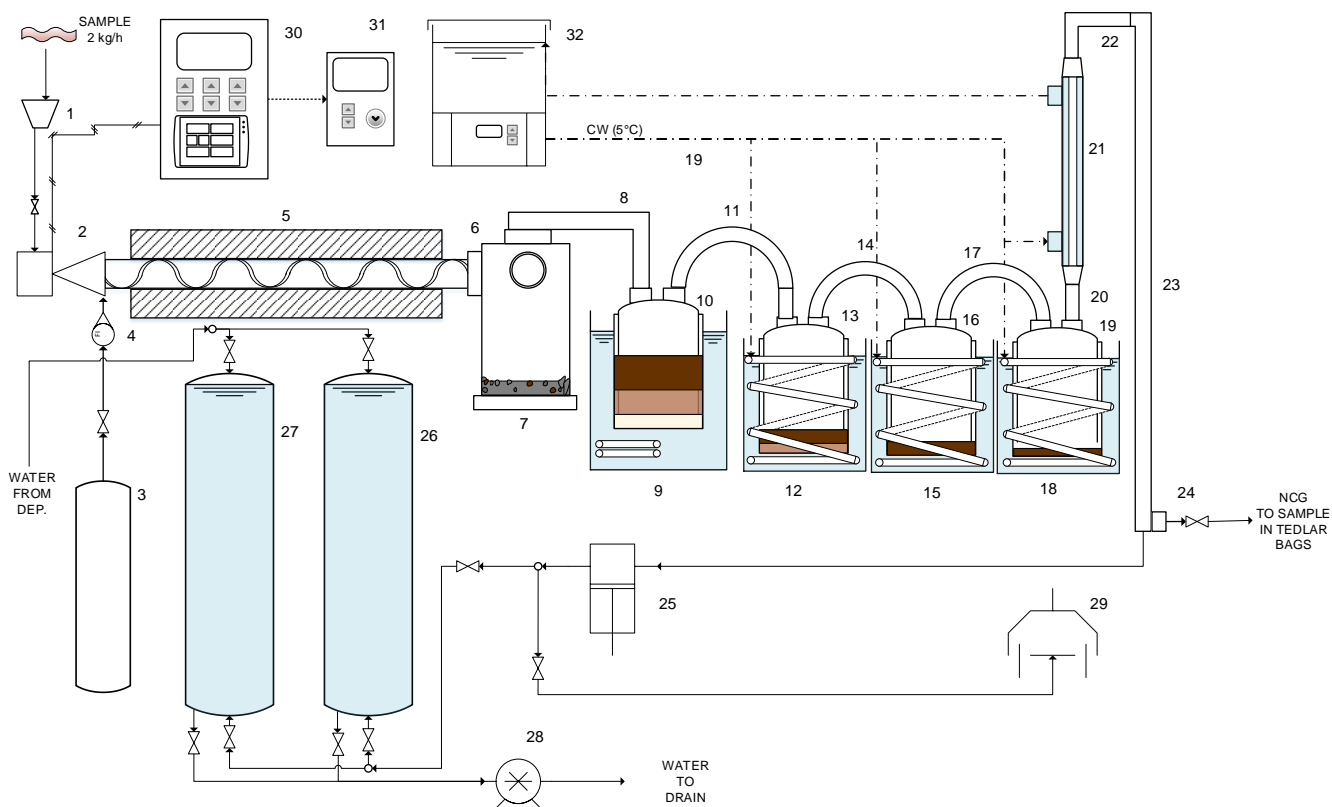
Figure 4.3: The PFD of kilogram-scale pyrolysis unit

Table 4.3: The description of each unit in kilogram-scale pyrolysis unit

Unit	Description	Unit	Description
1	Loading hopper	17	Silicone piping connection 3
2	Motor & hydraulically driven piston	18	Condenser 4 tank and chilling coils
3	Nitrogen tank	19	Condenser 4 vessel (5 L)
4	Flowmeter & flow adjuster	20	Silicone piping connection 4
5	Pyrolizer retort with screw baffles	21	Liebig condenser using CW from C4
6	Char-pot with inspection eye	22	Silicone with PVC elbow
7	Char-pot lid + gasket	23	Silicone piping
8	Pipework to condensation train (quench)	24	PVC T-valve/ nozzle for NCG sampling
9	Condenser 1 tank and heating element	25	Vacuum pump to aid NCG collection
10	Borosilicate condenser 1 vessel (8 L)	26	Gas collection tower 1
11	Silicone piping connection 1	27	Gas collection tower 2
12	Condenser 2 water tank and chilling coils	28	Submersible pump for displaced water
13	Condenser 2 glass vessel (5 L)	29	Extraction hood for NCG extraction
14	Silicone piping connection 2	30	PLC to control parameters, alarms
15	Condenser 3 water tank and chilling coils	31	Heater controls reactor temperature
16	Condenser 3 vessel (5 L)	32	Chiller provides refrigerator for CW

4.2.3.4. Condensable product characterization

Due to the significantly higher mass yield of liquid products from pilot-scale, this liquid could be further separated if needed. It was clear from physical inspection alone, that liquid from pilot-scale was made up of at least two clear immiscible fractions and even within the condenser, major differences in the HHV and water content were noticed and so a more effective and empirical methods of water content and HHV determination were chosen. The liquid was separated into three fractions as explained in section 4.2.4 and the analysis of each fraction was done separately. Similar to the char, the HHV of condensable product was calculated as a weighted average (Equation 4.7)

$$HHV_{fuel\ oil}\left(\frac{MJ}{kg}\right) = \left(HHV_{organic\ (phase)oil}\left(\frac{MJ}{kg}\right) \times \frac{Y_{organic\ oil\ (\%)}}{Y_{tot.\ fuel\ oil}(\%)}\right) + \left(HHV_{wax}\left(\frac{MJ}{kg}\right) \times \frac{Y_{wax\ (\%)}}{Y_{tot.\ fuel\ oil}(\%)}\right) \quad \text{Equation 4.7}$$

4.2.3.5. Gross – and net energy conversion

The gross energy conversion (GEC) is an indication of how energy is transferred from the feedstock to the products. The overall gross energy conversion (GEC $_{overall}$) is the summation of the GEC of the char and liquid products, as shown in Equation 4.8. The GEC for each product was calculated as the product of its mass and its HHV in comparison to the product of the feedstock mass of the feedstock and its HHV, as shown by Equation 4.9.

$$GEC_{overall}(\%) = GEC_{char}(\%) + GEC_{wax}(\%) + GEC_{org\ oil}(\%) + GEC_{NCG}(\%) \qquad \text{Equation 4.8}$$

$$GEC_{overall}(\%) = \frac{mass_{char}(kg) \times HHV_{char}(MJ/kg)}{mass_{feed}(kg) \times HHV_{feed}(MJ/kg)} + \cdots + \frac{mass_{NCG}(kg) \times HHV_{NCG}(MJ/kg)}{mass_{feed}(kg) \times HHV_{feed}(MJ/kg)} \qquad \text{Equation 4.9}$$

The net energy conversion (NEC) is like GEC but includes the energy requirements of the pilot-scale unit as shown in Equation 4.11. The energy consumption for each run was recorded by a 3 phase, 4 wire energy meter that read the units as kWh. For each run, time (h:m:s), and units (kWh) on the meter were recorded; before the element was turned to begin heating, once pyrolysis temperature was achieved and the sample was ready to be fed, and lastly once the pyrolysis experiment was finished and setup turned off. When all material had been fed into the reactor, the time and energy meter were recorded so that energy consumption as a function of material fed could be calculated.

$$Q_{products}(MJ) = \sum_{i=1}^{n} HHV_i\left(\frac{MJ}{kg}\right) \times mass_i(kg) \qquad \text{Equation 4.10}$$

$$NEC_{overall}(\%) = \frac{Q_{products\ (MJ)} - Q_{pyrolysis\ unit\ (MJ)}}{Q_{feed\ (MJ)}} \qquad \text{Equation 4.11}$$

4.2.4. Condensable product separation

The production of condensable product from the pyrolysis of the rejects on pilot-scale resulted in high volumes (more than 1L) of condensable product that was spread over four different condensers. These condensers are represented by units 10, 13, 16 and 19 in Figure 4.3. Condenser 1 and 2 (units 10 and 13, respectively) were demonstrated to contain at least 85 wt.% of the total

condensable product for all the runs. The condensable product from these two condensers was observed to be heterogenous containing wax and oil that had differences in viscosity and density. These differences warranted physical separation, whereby the condensable product initially underwent vacuum filtration (VF) to separate the oil from the wax. The oil was then sent to phase separation (PS) to split the oil into organic phase and aqueous phase oil. Consequently, the condensable product was subdivided into three phases.

4.2.4.1. Vacuum filtration (Separation of wax from oil)

As shown in Figure 4.4, the first separation involved the vacuum filtration (VF) of the condensable product from condenser 1 and 2 into wax and oil. VF of oil from wax, was done with a vacuum pump, hose, Büchner flask, filter paper and Büchner funnel as set-up according to Figure 4.4 .The second Büchner flask was used to avoid oil collecting in the pump. Approximately 100 mL of condensable product was slowly poured into the funnel ensuring the filtering paper was wet before adding the rest. In vacuum conditions, the oil would collect in the vacuum flask and every 5 minutes the condensable product remaining in the funnel was mixed with a metal spatula (without damaging the filtering paper) to aid separation. Separation was assumed to be complete when filtration had lasted at least 40 minutes and the time between each drop of oil into the Büchner flask was longer than 15 seconds. When both conditions were met, the vacuum pump was turned off and the difference between the mass of the assembled pieces was taken as a result. All the viscous liquid remaining in the funnel was wax and the liquid collected in the flask was oil, as shown in Figure 4.4.

4.2.4.2. Phase separation (Separation of aqueous phase oil from organic phase oil)

The collected oil from the vacuum filtration consisted of a distinct aqueous and organic fraction. The aqueous fraction was light yellow and transparent and had a higher density than the organic fraction. The organic fraction was entirely opaque and brown to black in colour. An example of the different fractions of oil from vacuum filtration can be seen in Figure B-6. The second separation involved the liquid-liquid separation of aqueous phase oil and organic phase oil due to their different densities. This was done with a separatory funnel as shown in picture 2 of Figure 4.4. This separation, *viz.* decantation of the organic phase PO from the aqueous phase, was done with a Laboratory stand, clamp, cone-shaped separatory funnel and two beakers as shown in Figure 4.4 (labelled 2). The typical procedure for using the separation funnels involved adding all collected pyrolysis oil into the flask, shaking the flask with intermittent pressure release, and allowing the sample to stand for ten minutes. Typically, the different fractions could be identified after a few minutes. A pre-weighed beaker was then filled with the fraction of higher density (aqueous phase) and another beaker with the organic fraction. It was confirmed that the material of higher density was the aqueous phase because it was tested as incombustible according to the bomb calorimeter when testing for HHV. Once each phase was separated, the wt.% and HHV can be determined. The HHV of each fraction was identified with the bomb calorimeter, as explained in Section 4.1.2.4.
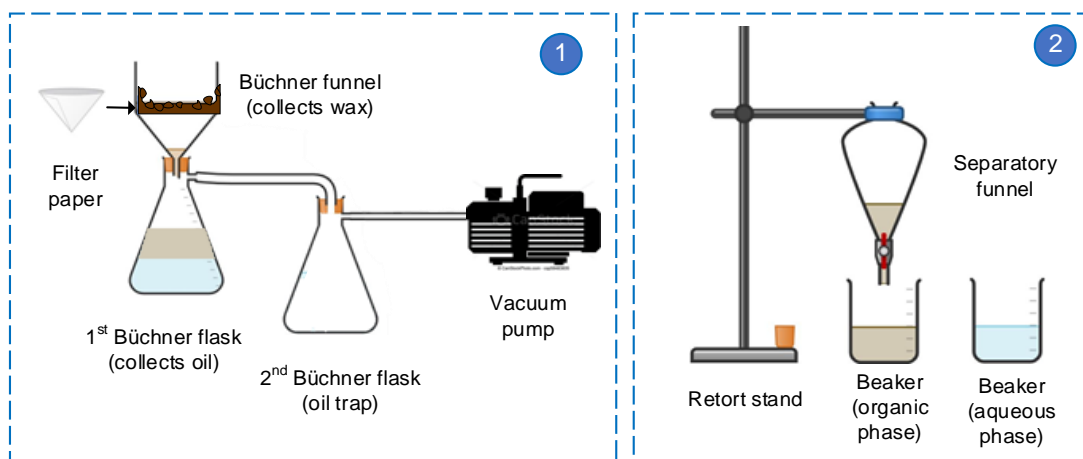
Figure 4.4: Vacuum filtration set-up (left, labelled 1) and phase separatory funnel setup (right, labelled 2)

4.3. Compliance of rejects to solid-recovered fuel (SRF) standards

The production of SRF is done according to the Standards, BS EN 15359, 2011 [10] and more comprehensively in the WRAP classification scheme [35]. The current facility has a proposed rejects capacity of 3.48 ktpa and hence should follow the WRAP classification scheme, suited for facilities processing less than 100 ktpa [35]. All quality tests are performed on the as-received sample or "material at delivery" [21]. The three factors are each determined by the three attributes below.

- Economic: Biomass content (BM) – Lower-heating vale (LHV) – Moisture (M)
- Technical: Bulk density (BD) – Chlorine content (Cl) – Ash content
- Environmental: Mercury content (Hg) – Cadmium content (Cd)– Sum of heavy metal (HM)

4.3.1. Economic factor of the WRAP classification scheme

4.3.1.1. Biomass content (BM) attribute

The biomass content attribute is assumed as the lignocellulosic fibre fraction. The approximate composition was determined according to Section 4.2.1.2, and was calculated as a percentage of the organic fraction of the pulper rejects.

4.3.1.2. Lower-heating value (LHV) attribute

The LHV of dry material (LHV_{dry}) was calculated according to the HHV of the dry pellet (HHV_{dry}) and the hydrogen ($x_{H,dry}$), oxygen ($x_{O,dry}$) and nitrogen ($x_{N,dry}$) mass fractions (wt.%) [312]. Equation 4.12 shows the equation used for the conversion from HHV to LHV from CEN/TS 15400 [312].

$$LHV_{dry} = HHV_{dry} + 6.15 \times x_{H,dry} - 0.8 \times \left[x_{O,dry} + x_{N,dry} \right] - 218.3 \times x_{H,dry} \qquad \text{Equation 4.12}$$

4.3.1.3. Moisture content (M) attribute

The moisture content of the air-dried fluff and Ø6 mm pellets were measured in a ML-50 Moisture Analyzer from the A&D Company. Samples of size between 2 to 3 g were used in the analyser with the temperature set to 110 °C and recorded for 60 minutes or until rate of evaporation was 0.0 %/min.

4.3.2. Technical factor of the WRAP classification scheme

4.3.2.1. Bulk density (BD) attribute

The bulk density was measured in 1000 mL measuring cylinder and the volume of pellets occupied measured against the weight of the pellets and done in triplicate. Conversely, unit density was measured by individually measuring the weight of 7 pellets on a scientific balance with 0.001 g sensitivity and measuring the length and diameter of each pellet with a vernier.

4.3.2.2. Chlorine content (Cl) attribute

Chlorine content of solids was calculated according to ASTM D4208, involving five steps [313]:

1. Combustion of the solid in a bomb calorimeter filled with 2 to 3 MPa of oxygen.
2. Diluting the combustion reside with 2% Na_2CO_3 solution to react with chloride product.
3. Washing out the inside cylinder of bomb with water.
4. Collect all the washings in a beaker and adjust the ionic strength with $NaNO_3$ solution.
5. Determining total chloride content through measuring the potential of the solution with chlorine ion-selective electrode, from potentiometric titration with $NaNO_3$ solution.

4.3.2.3. Ash content (ash) attribute

The ash content was determined by the NREL method, whereby a sample of pellets weighing 1.5 g was placed in a muffle furnace and exposed to isothermal oxidation at 575 °C for four hours [314]. The weight of the crucible after four hours of oxidations was used to determine the ash content.

4.3.3. Environmental factor of the WRAP classification scheme

The environmental attributes were comprised of the mercury (Hg), cadmium (Cd), and sum of heavy metals (HM) content. The absolute concentration of the environmental attributes was determined, and a calculation used to convert absolute concentration to specific gas concentration. Thereafter, each specific gas concentration was assessed against the maximum, permissible concentration specified for the application of the SRF according to the Air Quality Act 39 of 2004, to check eligibility.

4.3.3.1. Determination of absolute concentration (mg/kg)

The sum of heavy metals (HM) consisted of the addition of the following nine heavy metals: vanadium, chromium, manganese, cobalt, nickel, copper, arsenic, antimony, and lead. Initially, the absolute concentration (mg/kg) of the environmental attributes were determined by inductively coupled plasma mass spectrometry (ICP-MS). 5 replicates of reject fluff (<1000 μm) were required for ICP-MS to attain the mean, median, 80th percentile values. All samples underwent acid digestion in a microwave digester using HNO_3 before ICP-MS was carried out using an Agilent 7900 ICP-MS.

4.3.3.2. Conversion to specific concentrations (mg/MJ)

The Hg, Cd and HM content used for BS EN 15359 and WRAP classification scheme required the mass concentration of the environmental attributes as specific mass concentrations (mg/MJ). Hence

the mass compositions (C_m) identified from ICP analysis must be converted to specific mass concentration (C_S) by using the LHV of the SRF (MJ/kg) as shown in Equation 4.13.

$$C_S = C_m \times {}^1\!/_{LHV}$$

Equation 4.13

4.3.3.3. Adherence of SRF to Air Quality Act

The use of SRF is favoured in certain industries and technologies depending on its technical, economic, and environmental factors. Whereby, the recommended SRF quality for certain technologies is shown in Table 2.4 on page 19. Additionally, the environmental attributes of the SRF must be shown to adhere to the South African air quality legislation. Whereby as shown in Equation 4.14, the maximum specific concentration of the three attributes (C_s) can be calculated according to the permissible gas concentration (C_e), the specific volume of the emitted gas (V_s) and the transfer factor (TF) [42]. The Air Quality Act 39 of 2004 provides the permissible concentration of emitted gas (C_e) according to Hg, Cd and sum of HM content [38]. The specific volume of gas for a mixed PE and lignocellulosic fibre stream is 0.563 m^3/MJ [42]. The transfer factor represents the fraction of metal that will be released to the atmosphere when incinerated in a cement kiln or power plant [38], [315]. Table 4.4 provides the permissible concentration (C_e) and transfer factor (TF) for three metal types and two technologies and provides the reference from where the information was collected.

$$C_s = C_e \times V_S \times {}^1\!/_{TF}$$

Equation 4.14

Table 4.4: The permissible specific concentration of heavy metals and their transfer factors according to industry.

Attribute	Symbol	*Specific conc. [C_e] (mg/m^3)	Transfer factor [TF]		Calculated [C_S] (mg/MJ)	
			Power	Cement	Power	Cement
Mercury	Hg	0.05	5%	49.0%	0.563	0.0574
Cadmium	Cd	0.05	0.5%	1.873%	5.63	1.50
Sum of HM	HM	0.05	0.05%	0.05%	56.3	56.3
Source		[38]	[315]		-	-

*Specific concentration is provided for the standard conditions: 273 K, 101.3 kPa, 10% O_2

4.4. Data and Statistical analysis

4.4.1. Error bars

The data presented in the results section is the mean from at least two data values. To validate the consistency of the results, the error was represented as one standard deviation with the function "STD.DEV.S" used on MS Excel - represented as a tolerance "±" in Chapter 5. Sample standard deviation (s) is calculated according to the sum of square of the difference between the points and their mean ($\bar{x}$) while considering number of observations (N) and represented in Equation 4.15.

$$s = \sqrt{\frac{\sum_{i=1}^{N}(x_i - \bar{x})^2}{N-1}}$$

Equation 4.15

4.4.2. Significance between groups (ANOVA testing)

Significance between groups of results was determined using single-factor ANOVA from the Data Analysis Tool pack in MS Excel. The default alpha level (α) of 0.05 was assumed for the ANOVA testing and the default null hypothesis (H_0) is shown in Equation 4.16, where there is no difference in the mean values for the results at different temperatures. Consequently, the alternative hypothesis (H_A) as shown for Equation 4.17, is that the mean values between groups are statistically different [316]. If the *p-value* was shown to be greater than 0.05, the H_0 was not rejected, and hence there was no significant difference between the data. Conversely, if the *p*-value is smaller than 0.05 or the F value is larger than F_{crit}, the H_0 can be rejected and H_A accepted (values are significantly different).

$$H_O: \mu_{450\,°C} = \mu_{500\,°C} = \mu_{550\,°C}$$

Equation 4.16

$$H_A: \mu_{450\,°C} \neq \mu_{500\,°C} \neq \mu_{550\,°C}$$

Equation 4.17

4.4.3. Significance within groups (Post-hoc analysis)

If it was proved that the groups of experimental data were statistically different, a post-hoc analysis should be followed to determine which groups are statistically different to each other. The method followed for the post-hoc analysis was the Tukey-Kramer method because it can be used for groups of unequal sample size [316]–[318]. The number of pairwise comparisons between groups can be calculated according to Equation 4.18 based on the number of groups (k) for the results (e.g. 3 if tests at 450 °C, 500 °C and 550 °C are performed). The significance of each pairwise comparison is determined according to the comparison of the calculated q statistic and its respective q_{crit} statistic. The q statistic is the absolute difference between the mean of either group divided by the standard error (SE) as shown in Equation 4.19. Additionally, the equation used to calculate SE is shown in Equation 4.20 and is dependent on the mean square error within groups (MS_w) from the ANOVA table and sample size of the two groups (n_i and n_j) [319]–[321]. Lastly, once the q statistic for each pairwise comparison has been calculated, it must be compared to the critical q (q_{crit}) statistic according to the studentized range distribution for q, which is a function of the number of groups (k) and degrees of freedom within groups (df), as shown in the ANOVA [321]. The q_{crit} value for the experiments on pilot and bench-scale data were 4.60 and 5.22, respectively at an alpha value of 0.05 (the same as that for the ANOVA testing).

$$\text{No. of pairwise comparisons} = \frac{(k) \times (k-1)}{2}$$

Equation 4.18

$$q = \frac{\text{abs}[\bar{x}_i - \bar{x}_j]}{SE}$$

Equation 4.19

$$SE = \sqrt{1/2 \times MS_w \times (1/n_i + 1/n_j)}$$

Equation 4.20

Chapter 5: Experimental Results

Chapter 5 refers to the experimental work that was done to address objectives 1 and 2, following the methodology of **Chapter 4**.

5.1. Pulper Reject characterization

5.1.1. Moisture and scrap content of pulper rejects

The delivered, 200 kg sample of pulper rejects was split into four bags, weighed and air-dried. The moisture content (MC) of the as-received sample from the mill was determined as 46.4 ± 2.2 wt.% when oven-drying five 50 g samples. The 2 months of air drying reduced the as-received weight by 37.4 ± 2.2 wt.%. Additionally, oven drying further reduced the MC to the equilibrium MC (MC when evaporation seizes) of 5.9 ± 0.3 wt.%. The result for the moisture reduction of air drying is similar to the value of 35 wt.% reported for another waste-to-fuel sample [322]. The MC of the 5 samples of as-received pulper rejects is between 40 and 60 wt.% and congruent to literature [52].

Ferrous metal was extracted from the bulk sample using a permanent magnet. Figure 5.1 shows how the ferrous wires become entangled in the fibres but due to their large size, they can be easily extracted with a magnet. The ferrous metal composition was calculated as 11.3 and 7.2 ± 0.5 wt.% on a dry and wet basis, respectively, which is higher than what is reported elsewhere [23].

Figure 5.1: The delivered 200 kg sample (left), extracted ferrous metal (middle) and air-dried, shredded rejects (right)

5.1.2. Thermochemical decomposition curves

Figure 5.2 shows the thermal degradation (TG) curve for four samples at a constant heating rate of 10 °C/min under inert atmosphere. The same figure on the right shows the derivative thermal degradation (dTG) curves for the same curves. The 4 samples consist of two samples of the pelleted pulper rejects and two samples of the non-pelleted fines (particle size >500 μm). For both the pulper rejects and their fines, thermal degradation begins at 250 °C and is almost complete by *ca.* 520 °C.

All four curves show two major distinct mass loss regions. The first begins at 200 °C and is complete by 400 °C and relates to thermal degradation of lignocellulosic fibre. The main peak for this temperature range relates to the degradation of cellulose around 350 °C and for all four curves, a

shoulder is seen at *ca.* 300 °C, which corresponds to the degradation of the small content of hemicellulose present in fibres [67], [209], [217]. From Figure 5.2, it is evident that the temperature increase from 250 to 400 °C results in the significant mass loss of 40 to 50 wt.% for the fines content. Conversely, the pulper reject pellets experienced a mass loss of between 11 to 20 wt.%. This result shows that the fines have a higher fibre content than the larger particles, as described elsewhere [23], [53]. The second major degradation range from 400 to 500 °C represents the thermal degradation of plastics [207], [208]. The degradation of the pulper rejects is significantly more exaggerated in comparison to the fines within this range. All four curves show maximum degradation at *ca.* 470 °C, corresponding to PE [207], [209], [211], [212]. The second sample of pulper rejects has a shoulder off the main peak at 440 °C, probably most likely due to the presence of PP or PET [208]. The fines experience between 30 to 35 wt.% mass loss within this plastic degradation region and the pulper rejects, between 75% to 85% mass loss. Depending on the targeted properties of the pyrolysis products, temperatures from 350 °C (degradation of fibre fraction only) to 550 °C (degradation of both fibre and plastic fractions) could be tested on bench-scale.
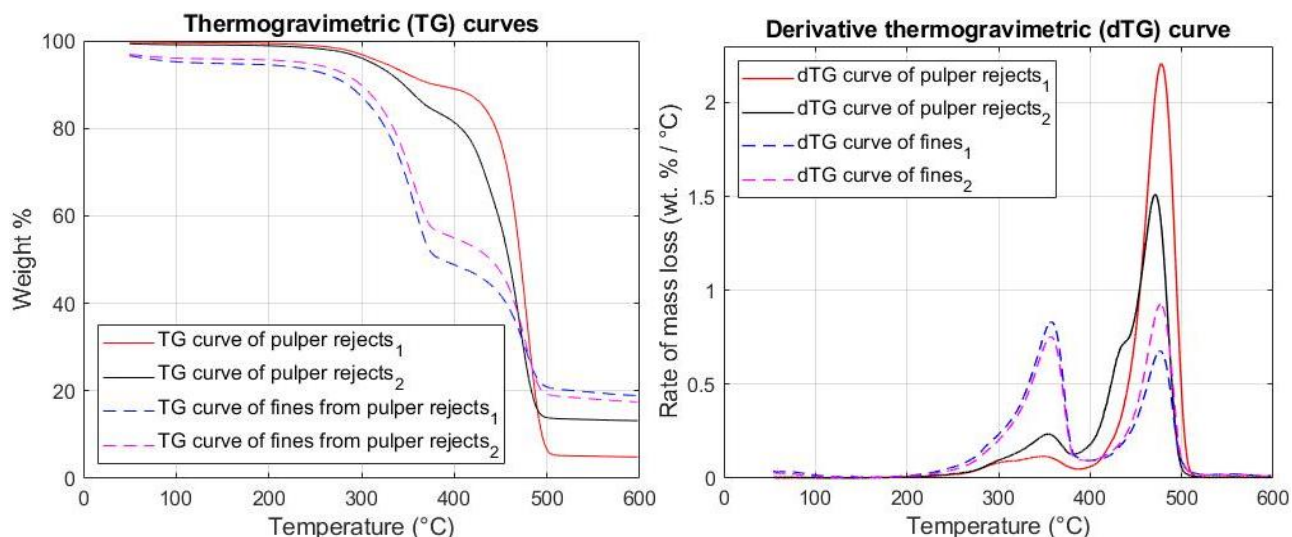
Figure 5.2: TG (left) and dTG curves (right) of pulper rejects and their fines

The two dTG curves of the pulper rejects have been shown individually in Figure 5.3 and a gaussian distribution plot has been plotted under the two main peaks. The area of the deconvoluted gaussian peaks representing the organic fractions; lignocellulosic fibres and PE relates to 11.1 ± 4.8 wt.% and 71.3 ± 13.2 wt.% of the total area under the curves, respectively as shown in Table 5.1. These areas do not include the shoulders of the peaks which could account for other organic residues (OOR), such as PET, as shown in Table 5.1. Hence the balance of the area was attributed to OOR as seen in Table 5.1. Although this method is not entirely accurate, especially for feed containing lignin [309], it has been used to approximate the quantity of LDPE and PET in mixed plastic [192]. The method for approximating the composition of plastics in the organic fraction will correspond closely to the mass loss of plastics from TGA because the volatile matter content of all plastics is almost 100 wt.%

63

and hence almost all plastic will volatize when thermally degraded [67]–[70]. Fibres in the form of paper and cloth contained 79 and 88 wt.% volatile matter content, respectively and hence not all fibres that are thermally degraded will volatize [55], [60]. Therefore, the approximation method is less accurate for fibres than plastics. Nevertheless, the approximated fibres composition as shown in Table 5.1 is 11.1 ± 4.8 wt.% and marginally less than the fibres composition observed in other rejects samples being around 17 to 18 wt.% [52] and up to *ca.* 25 wt.% of the total, dried rejects stream [23]. In Table 5.1, the plastics content is calculated as 71.3 ± 13.2 wt.% of the organic fraction and similar to the plastic content of other pulper rejects between 70 and 77 wt.% [23], [52].
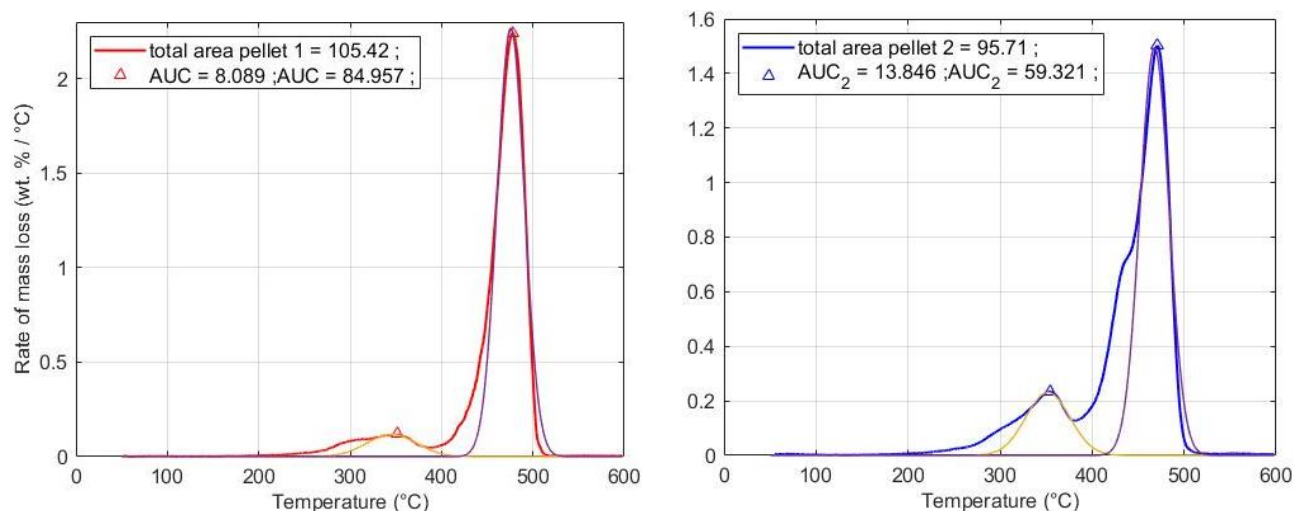
Figure 5.3: The deconvoluted peaks and their areas of the two pulper reject samples

Table 5.1: Approximate composition of the dried, organic fraction of pulper rejects

Material	Lignocellulosic fibre	Plastics (PE)	OOR (PET, wood, etc.)
Designation	First peak - 350 °C	Second peak - 470 °C	Remaining area
Composition (wt.%)	11.1	71.3	17.6

5.1.3. Proximate and ultimate analysis of pulper rejects

Table 5.2 provides the proximate and ultimate analysis results of the air-dried, milled pulper rejects and compares them to sources in literature. The four samples used for comparison is RDF sourced from Interwaste [323], pulper rejects from a Kimberly-Clark (K-C) secondary tissue mill in the U.K [43], [324], one of the three rejects from a South African secondary board mill shown to have highest plastic content [24], [25], [325] and pulper rejects from a secondary board mill based in Spain [52].

The proximate analysis corresponds closely to other samples containing biomass and plastic together as seen in Table 5.2. The volatile matter content of the rejects was determined as 87.6 wt.% and is shown in Table 5.2 to be marginally higher than the other tested mill rejects (82 to 85 wt.%), evident of the relatively high plastic content of the sample under study.

Table 5.2: Proximate and Ultimate analysis of the pulper rejects in comparison to other samples

Study	SRF fluff	[323]	[43]	[24], [25]	[52]
Proximate Analysis (wt.%)					
Volatile matter (m.f)	87.6 ± 0.52	82.7	82.2	85.08	82.5
Fixed Carbon (m.f)	4.84 ± 0.55	6.07	9.1	7.53	8.2
Ash (m.f) 700 °C	7.57 ± 0.35	11.25 [*1]	6.7 [*2]	5.3 [*2]	-
Ash (o.d) 575 °C	8.65 ± 0.01	-	-	-	9.3 [*3]
Ultimate Analysis (wt.%) (m.f)					
Nitrogen (N)	0.31 ± 0.09	0.35	0.5	-	0.29
Carbon (C)	58.4 ± 1.6	58.09	70.5	66.98	58.3
Hydrogen (m.f) (H)	8.20 ± 0.33	9.38	8.3	11.16	8.4
Sulphur (S)	0.0805 ± 0.03	-	< 0.1	-	0.13
Chlorine (Cl)	-	-	-	-	-
Oxygen (**balance) (O)	24.7 ± 3.5	20.93	13.9	21.56	22.26

KEY: (o.d) – oven dried; (m.f) – dry/ moisture-free; (a.f) – ash free; (**balance) – O% = 100%-N%-C%-H%-S%-ash%; The ash determined at [*1] - 750 °C (crucible method); [*2] – 700 °C (proximate analysis); [*3] – 550 °C (BS EN 15403)

As shown in Table 5.2, the ash content of rejects is determined as 8.65 and 7.57 wt.% according to the NREL method (575 °C) and proximate analysis method (700 °C), respectively. Hence, the ash content for the rejects is congruent to literature as seen from the ash content of coarse rejects being between 7 to 9 wt.% for three examples [52]. Whereby, another researcher showed ash content to decrease from 15 to 7 wt.% when plastic to fibre ratio in the rejects increased [325]. The increased ash content for more fibrous streams indicates the higher fraction of inorganics present in the fibrous part of the sample [325].

The ultimate analysis of this reject sample is shown in Table 5.2, where the C and H content of this sample was 58.4 and 8.20 wt.%, respectively. As shown in Table 5.2, this determined C content is on the lower range from that observed by other researchers who characterized pulper rejects and recorded C contents between 50 to 70 wt.% possibly due to rejects of varying plastic content [52], [325]. As shown in Table 5.2, The H content of the pulper rejects was determined as 8.38 wt.% and almost identical to the results gathered from two other researchers with a H content of 8.3 wt.% [43] and 8.4 wt.% [52]. Lastly, the oxygen content of the pulper rejects was calculated as 24.7 wt.% as seen in Table 5.2, where it can be seen to be higher than all the other paper mill rejects samples. This higher O content determined from the balance of the ultimate analysis. A high O content is generally unfavourable because it displaces the C content and lowers the energy content of the fuel. The N and S contents were insignificant at a mere 0.31 and 0.08 wt.%, respectively as shown in Table 5.2. The low N content indicates that the incineration of the rejects or its pyrolysis products will produce minimal NO_X emissions. Likewise, the very low S content indicates that the incineration of rejects or its pyrolysis products will produce negligible SO_X emissions. From Table 5.2, it is seen

that the ultimate analysis for this study is identical to rejects generated from the Holmen secondary board mill of Fuenlabrada, Spain [52]. This result establishes proof that rejects from secondary brown board and tissue mills are similar in composition [324], due to similar feedstocks being old corrugated containers and office grade paper for board and tissue mills, respectively [47].

5.1.4. Energy content evaluation

The energy content of the feedstock plays one of the most important factors in the evaluation of its potential as an energy product. The HHV of the air-dried pulper rejects ranged between 31 to 32 MJ/kg and was shown to have a mean value of 31.5 ± 0.4 MJ/kg. Hence, despite the higher oxygen content observed from the ultimate analysis, the HHV of these pulper rejects were higher than any rejects seen in literature. The HHV of 31.5 MJ/kg surpassed the HHV of a plastic-rich rejects stream from another South African mill, with an HHV of 28.8 MJ/kg [24], [25]. Similarly, the HHV of the rejects used in this study was marginally greater than the HHV observed for rejects collected from other secondary tissue mills, with values ranging from 28 to 31 MJ/kg [23], [28].

5.1.5. Conclusion

The composition of the pulper rejects is required for the Techno-economic analysis (TEA). The main findings from Section 5.1 are provided as 6 bullet points below, viz.:

- Moisture content of the as-received sample was estimated as 46.4 ± 2.2 wt.%.
- The ferrous metal content was shown to comprise 7.2 ± 0.5 wt.% of the wet feedstock.
- Dried rejects have a moisture content of 5.9 ± 0.2 wt.% and an HHV of 31.5 ± 0.4 MJ/kg.
- The content of ferrous metal in the dried rejects is 12.7 wt.%.
- The composition of the organic fraction was estimated from the average area under the deconvoluted peak areas of the dTG curves, whereby it was evident that the plastic content will probably be 70 wt.% or more of the organic fraction for the dried rejects.

5.2. Conversion to SRF pellets

The conversion of the pulper rejects into Ø6 mm SRF pellets involved milling the dried pulper rejects, identifying the particle size distribution (PSD) of the fluff, and then pelleting the fluff. Finally, some analytical tests were conducted to assess the economic, technical, and environmental factors.

5.2.1. Particle size distribution

The particle size distribution (PSD) of the fluff has been represented as a cumulative passing distribution as shown in Figure 5.4. The d_{50} and d_{80} particle size of the fluff represents the diameter size that allows 50 and 80 wt.% of the particles to pass through, respectively. The d_{50} and d_{80} particle size for the fluff, shown in Figure 5.4, was 3220 and 5340 µm, respectively and shows that not all the fluff that passed through the 4 mm screen had a particle size less than 4000 µm according to

sieve analysis. Hence, the non-sphericity of plastic particles [90], [157] was evident from 30.1 wt.% of particles having a particle size greater than 4 mm, despite passing through 4 mm knife-mill screen.
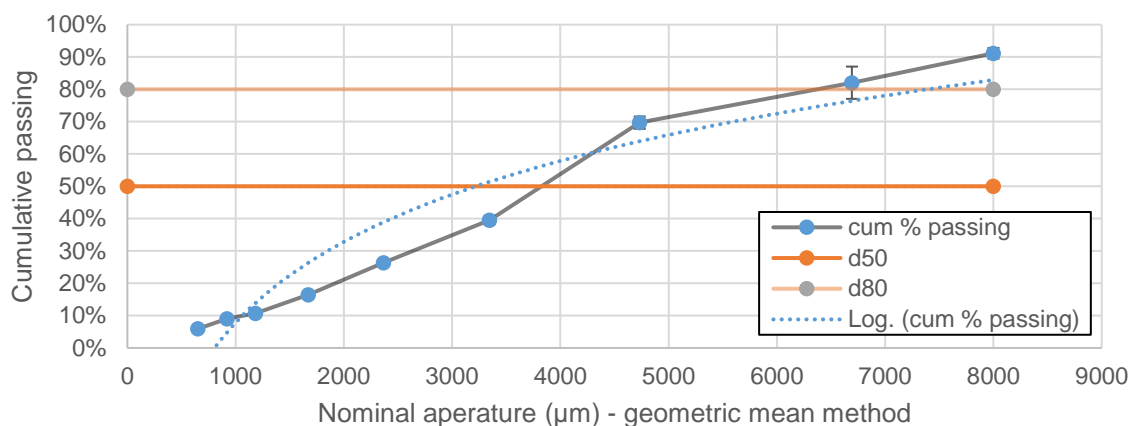
Figure 5.4: Cumulative % size distribution plot of air-dried material, milled to 4 mm in the knife-mill

In Figure 5.4, it was observed that on average 5.95 wt.% of the sample were fines with a particle size less than 500 µm. The fines were mainly made of fibres and had a higher ash content than the rejects as explained in section 5.1.2. Hence, the relatively large O content and small C content observed in ultimate analysis compared to other rejects (despite high HHV) might be attributed to fines being used for analysis instead of larger, more representative samples. This might be possible because ultimate analysis uses a small sample mass (<20 mg) and smaller particles are observed to have not only increasing ash content [221], but lignocellulosic fibres content [23]. This problem might be overcome through performing more replicates (larger sample size) for ultimate analysis.

5.2.2. Classification of SRF

The classification of SRF is evaluated according to the economic, technical, and environmental factor, with each factor represented by three attributes. All nine attributes are represented by 5 classes, whereby class 1 and 5 represents the best and worst possible classification, respectively.

5.2.2.1. Economic attributes of SRF

The first economic factor of this classification system is the fraction of biomass in the sample. The biomass content is assumed to be the same as the paper content (PPC) in the rejects, that was explained in section 5.1.2. Whereby, even all ferrous metal is removed, and the moisture content is reduced to 5.9 wt.%, the rejects still contain less than 30 wt.% fibres and far less than the 50% minimum limit to achieve class 4. Despite the specification of the biomass content in class 5, there are examples of SRF with more plastic than biomass [13], [14], [27], [28], [326].

Fortunately, the high plastic content improves the lower heating value (LHV) - another economic attributes of the SRF. As described in Section 5.1.4, the HHV of the air-dried pulper rejects was recorded as 31.5 ± 0.4 MJ/kg. The LHV, calculated from the HHV, moisture, H, O and N contents,

was recorded as 29.7 MJ/kg and in class 1 for the LHV attribute as seen in Table 5.3. The air-drying of the sample reduced the moisture content to 5.9 wt.% and when pelleted, it was seen that the moisture content was further reduced to 3.6 ± 0.7 wt.% and in class 1. The moisture of the pellets was less than the fluff possibly due to the pressing in densification and the heat from friction causing some of the water within the particles to evaporate [327]. The results from the tests for the economic factors of SRF are shown in Table 5.3 whereby the LHV and moisture content attributes are both in class 1, but the biomass content attribute is in class 5.

Table 5.3: Economic attributes of the solid-recovered fuel (SRF) according to WRAP classification scheme [35]

Classification characteristic	Statistical measure	Unit	Class				
			1	2	3	4	5
Biomass content	Mean	wt.% (a.r)	≥ 90	≥ 80	≥ 60	≥ 50	< 50 ✓
LHV	Mean	MJ/kg (a.r)	≥ 25 ✓	≥ 20	≥ 15	≥ 10	≥ 6.5
Moisture content	Mean	wt.% (a.r)	≤ 10 ✓	≤ 15	≤ 20	≤ 30	< 40

5.2.2.2. Technical attributes of SRF

The second factor of concern for SRF is the technical factor represented by bulk density (BD), chlorine (Cl) and ash content attributes according to the WRAP classification scheme [35]. Pelleting the rejects not only standardizes its particle size after processing, but also increases the packing or bulk density of the sample. Although another researcher had "rehydrated the shredded plastics with 40% water" prior pelleting to get effective pellets [325], it was seen that for this feedstock (even for the same pellet mill), the addition of water resulted in pellets of amorphous shape. Instead, only spraying water with a spray bottle was sufficient to aid lubrication of the flat pellet die and produce good quality, Ø6 mm pellets from the rejects. The reason why the pellets made with less water had better particle cohesion than those with excess can be attributed to increased friction between the metal die and roller. The friction transferred heat to the rejects causing the plastics to partially melt and result in pellets with a "molten shell" increasing their shape and strength [178]. The difference between pellets made by adding 40% water and using the spray bottle is shown in Figure 5.5.
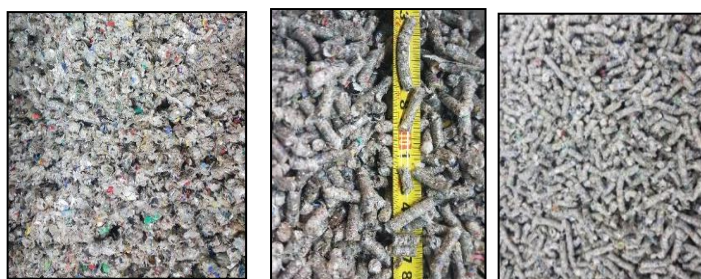
Figure 5.5: The pellets made from adding water (left), and only sprayed water (middle and right).

The pellets were made with a Ø6 mm die and shown to have a mean unit density of 700 kg/m^3 but with a high standard deviation (SD) of ± 200 kg/m^3, due to the heterogeneity of the pulper rejects. The large standard deviation for unit density is not unexpected as evident from other researchers

[128], [170]. Conversely, the mean bulk density of the Ø6 mm pulper reject pellets was 354 ± 3.61 kg/m^3 and had smaller variation within the triplicated result than unit density. This BD relates to class 3 of the attribute as shown in Table 5.4. The BD achieved is identical to the RDF used in some Egyptian cement kilns [41], but less than pellets made from other pulper rejects with BD between 400 to 450 kg/m^3 [20], [123]. The ash content of pellets was tested in a muffle furnace instead of through proximate analysis because the use of larger particles is expected to provide a more representative sample. The ash content was determined as 8.65 ± 0.01 wt.% and fell under class 1 for the ash content attribute as seen in Table 5.4, and significantly low for a non-biomass SRF product [42]. The chlorine (Cl) content was not tested, but assumed as 0.3 wt.% based off a similar SRF called "Cement-pellets" produced by Indaver [42]. This SRF, made from C&IW, had an HHV of 25 MJ/kg, ash content of 11 wt.% and moisture content of 6.9 wt.% [42]. Cl is mainly from PVC, a major component of construction and demolition waste [74], and unexpected in packaging or single-use plastics found in pulper rejects. Hence, it is unlikely the Cl content will exceed the maximum content for RDF in cement kilns at 1 wt.% [42].

Table 5.4: The attributes that make up the technical factor of the solid-recovered fuel

Attribute	Measure	Unit	Class				
			1	2	3	4	5
Bulk density	Mean	kg/m^3 (a.r)	> 650	≥ 450	≥ 350 ✓	≥ 250	≥ 100
Cl content	Mean	wt.% (d)	≤ 0.2	≤ 0.6 ✓	≤ 1.0	≤ 1.5	≤ 3.0
Ash content	Mean	wt.% (d)	≤ 10 ✓	≤ 20	≤ 30	≤ 40	≤ 50

5.2.2.3. Environmental attributes of SRF

The specific concentration (mg/MJ) of 3 environmental attributes were calculated from the absolute concentration (mg/kg) and the LHV of the SRF determined as 29.7 MJ/kg. The difference between the absolute and specific concentration for the different statistical measures of the different environmental attributes are shown in Table 5.5. The class codes for each attribute are shown in Table 5.6 according to the median and 80th percentile. The median and 80th percentile for the Hg attribute were 0.0137 and 0.0536 mg/MJ, respectively and hence in class code 2 due the 80th percentile being greater than 0.04 mg/MJ, but less than 0.06 mg/MJ. Likewise, the Cd content values were both in class code 2 as shown in Table 5.6 and the heavy metals (HM) content was in class code 2 due to both median and 80th percentile being 6.45 and 7.11 mg/MJ, respectively.

Table 5.5: Mass concentration in mg/kg and mg/MJ of the different environmental attributes, based off 5 replicates

Statistic*	Mean		Median		80th perc.	
Attribute	mg/kg	mg/MJ	mg/kg	mg/MJ	mg/kg	mg/MJ
Mercury (Hg)	0.712	0.0239	0.406	0.0137	1.59	0.0536
Cadmium (Cd)	4.45	0.150	3.85	0.130	8.87	0.298
Sum of heavy metals (HM)	184	6.20	192	6.45	212	7.11

Table 5.6: The attributes that make up the environmental factor of the SRF classification

Attribute	Measure	Unit	Class				
			1	2	3	4	5
Mercury (Hg) (d)	Median	mg/MJ (ar)	≤ 0.02 ✓	≤ 0.03	≤ 0.08	≤ 0.15	≤ 0.50
	80th perc.	mg/MJ (ar)	≤ 0.04	≤ 0.06 ✓	≤ 0.16	≤ 0.30	≤ 1.00
Cadmium (Cd) (d)	Median	mg/MJ (ar)	≤ 0.1	≤ 0.3 ✓	≤ 1.0	≤ 5.0	≤ 7.5
	80th perc.	mg/MJ (ar)	≤ 0.2	≤ 0.6 ✓	≤ 2.0	≤ 10	≤ 15
Sum of heavy metals (HM) (d)	Median	mg/MJ (ar)	≤ 15 ✓	≤ 30	≤ 50	≤ 100	≤ 190
	80th perc.	mg/MJ (ar)	≤ 30 ✓	≤ 60	≤ 100	≤ 200	≤ 380

*(ar) – "as received"; (d) – "dry"; 80th perc. – 80th percentile

5.2.3. End use of SRF

5.2.3.1. Adherence to Air Quality Act

The last check for the SRF should be its adherence of the environmental attributes to the South African Air Quality Act 39 of 2004 [38]. The ranges of the experimentally determined specific gas concentration (mg/MJ) are compared against the permissible concentrations in Table 5.7 to determine whether the cofiring of the SRF would adhere to the Air Quality Act for the cement and power industry in South Africa. The calculations for the permissible concentrations in Table 5.7 are explained in section 4.3.3.3. In Table 5.7, the experimentally determined permissible specific gas concentration (C_s) for all three environmental attributes of the SRF are lower than permissible specific gas concentration. Incidentally, the maximum value for the permissible gas concentration of Hg is the same as permissible specific gas concentration for use in the cement kiln.

Table 5.7: Comparison of permissible specific gas concentration to the range determined experimentally.

Attribute	Symbol	Permissible specific gas conc. [C_S] (mg/MJ)		Range of C_S (mg/MJ)
		Power	Cement	
Mercury	Hg	0.563	0.0574	0.00402 – 0.0574
Cadmium	Cd	5.63	1.50	0.00967 – 0.321
Sum of HM	HM	56.3	56.3	5.27 – 7.23

*The permissible C_s value was based off the assumption of burning with 11% excess O_2 and pressure of 101 kPa.

5.2.3.2. SRF classification

Figure 5.6 shows a radar plot for the different classes for the attributes of each factor. The yellow triangles, red squares and green circles are representative of the economic factors, technical factors, and environmental factors, respectively. The SRF with its high LHV, low ash and permissible heavy metals content will favour its use as an alternative fuel in the primary burner of a cement kiln, as shown in Table 2.4 [42], [144], [145]. The substitution rate of coal with SRF can be determined according to the fuel requirement and the SRF available. SRF that is shown to be appropriate for

firing in cement kilns, like the current fuel, is capable of substitution rates higher than 50% with coal, provided that the burner is appropriately retrofitted for handling SRF [42].
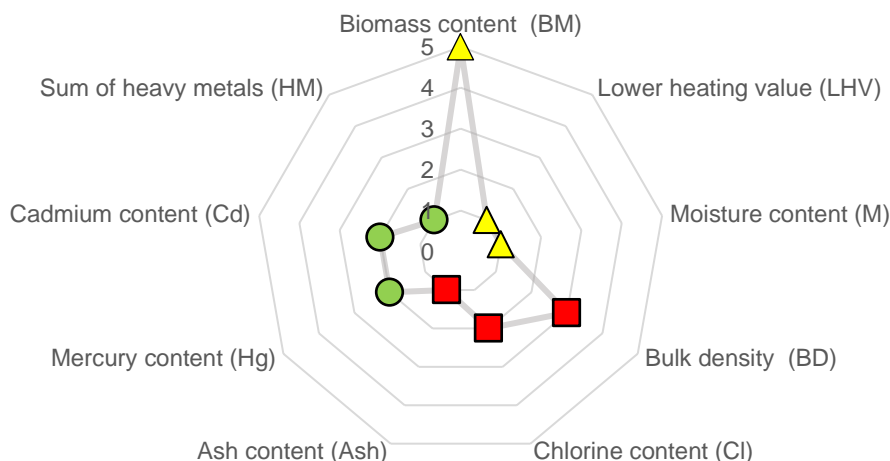
Figure 5.6: Radar plot for the classification of pre-treated pulper rejects as SRF according to their class code

5.3. Bench-scale pyrolysis conversion to fuel oil

In order to assess the pyrolysis route, the conversion of reject pellets was tested on a batch, bench-scale unit as shown in Figure 4.2 and results were compared with observations of other researchers for the batch pyrolysis of pulper rejects [24], [25].

5.3.1. Condensable product yield

The conversion of pulper rejects to condensable product was tested on a bench-scale pyrolysis setup at temperatures of 350, 450, 500 and 550 °C and the product yields are detailed in Figure 5.7. These runs were performed prior to pilot-scale experiments to select an appropriate temperature range for maximizing condensable product yield.

The condensable product collected in the second pot (see Figure 4.2) looked like an oil. In Figure 5.7, it is seen that the oil yield increases with an increase in temperature, whereby the mean oil yield at 350 °C was 1.9 wt.% and 10.7 wt.% at 550 °C. However, statistical analysis proved that there was no significant difference between the oil yield at different temperatures. This was evident by the F value of 3.08, which was less than the F_{crit} of 5.41. This result is probably due to the heterogeneity of the feedstock. The condensable product from the first pot in Figure 4.2 was wax. Unlike the oil yield, there was a significant difference between the wax yields at different pyrolysis temperatures. Whereby five of the six pairwise comparisons were shown to be statistically significant following the Tukey-Kramer test. The only comparison which was not different in wax yield was between 450 and 500 °C, which incidentally had the same mean yield of 53.2 wt.%, as seen in Figure 5.7. The most pronounced wax yield difference was between 350 and 450 °C, whereby at 350 °C the mean wax yield was 13.4 wt.% which increased to the maximum of 53.2 wt.% for 450 °C, as shown in Figure 5.7. Similarly, the increase in temperature from 500 to 550 °C resulted in a significantly decreased

71

wax yield from 53.2 wt.% to 28.6 wt.%, as seen in Figure 5.7, proving how at higher temperatures, wax is converted via secondary, cracking reactions to low molecular weight compounds (LMWC) that enrich the non-condensable gas (NCG) phase [271].

The condensable product yield was the summation of the oil and wax yield. It can be seen in Figure 5.7, that the wax yield comprises most of the condensable product and hence, pyrolysis temperature does have a statistically significant effect on the condensable product yield. Similarly, to the wax, the difference between 450 and 500 °C is not statistically significant despite 500 °C displaying a higher condensable product of 62.4 wt.% compared to 58.7 wt.% as shown in Figure 5.7. The maximized condensable product yields was found to be fractionally higher than that attained by another researcher for the fast pyrolysis of rejects from another source [25], as shown in Figure 5.7. However, this article [25] reported the condensable product yield to be maximized at 550 °C (500 °C was not tested). The increased temperature for maximizing condensable product yield can be attributed to the higher N_2 flowrate (for the same batch reactor) of 2.5 L/min compared to 0.5 L/min used for the current study [25]. At the temperature of 550 °C, the flowrate of 0.5 L/min results in a longer residence time for volatiles in the reactor, leading to more secondary reactions and significant cracking of primary products into NCG. The lower flow rate for the current study was selected to allow better condensation of the volatiles and to better simulate the conditions in the pilot reactor.
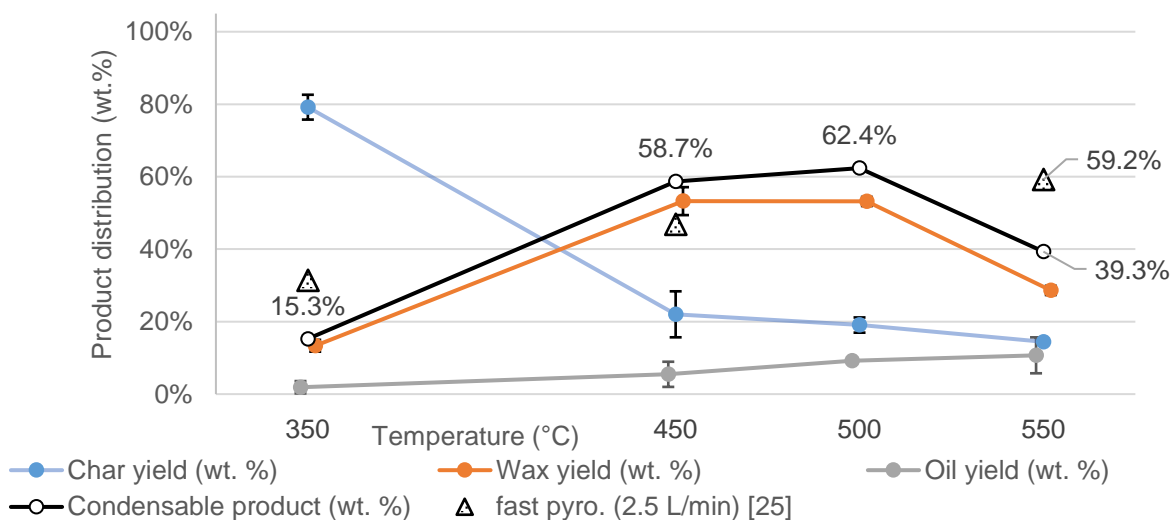
Figure 5.7: The char, wax, and oil product yields from the bench-scale experiments

5.3.2. Char product yield and energy content

As shown in Figure 5.7, at the lowest tested temperature of 350 °C, most of the product was concentrated in the solid phase as either unconverted rejects or partially converted char, whereby 79.2 wt.% of the rejects remains in the solid phase at 350 °C. This solid phase consisted of melted rejects and some char product. The melted rejects in the solid phase are attributed to the fraction of plastics which tend to melt and only partially volatize at temperatures less than 400 °C [192]. The HHV of the solid phase at 350 °C was 37.6 ± 0.45 MJ/kg, being *ca.* 6 MJ/kg higher than the feedstock

composition. The increase in HHV of the solid phase compared to the feedstock is attributed to deoxygenation occurring from dehydration of the sample specifically for the fibre fraction and then subsequent recombination reactions converting the feed into aromatic char compounds of higher energy content [83], [100]. It was observed that there was statistical significance between the char yields at different pyrolysis temperatures. However, from the post-hoc analysis, it was seen that statistical significance was seen only for the conversion at 350 °C. At the maximum condensable product yield from 450 and 500 °C, the char yield has a mean value between 19.1 and 22 wt.% as shown in Figure 5.7. The drastic decrease of char within this range indicates that a large fraction of material degrades between 350 °C and 450 °C, but not significantly thereafter. Hence, it can be deduced that a temperature of 450 °C is enough to convert most of the feedstock. The char produced at 450 °C was viscous, probably due to the presence of remaining melted plastic, and had a lower HHV of 24.8 MJ/kg but high variability, with a SD of 4.5 MJ/kg as shown in Table 5.8. Additionally, at 500 °C, the char became ashier and the HHV decreased to 19.8 ± 1.2 MJ/kg, which remained constant for char at 550 °C with an HHV of 19.7 ± 1.1 MJ/kg.

5.3.3. Gross-energy conversion evaluation

The gross-energy conversion (GEC) is the ratio of the energy content of the pyrolysis products to the feedstock [24], [25], [328]–[330]. The GEC for each temperature is shown in Figure 5.8 and represents the energy contained in the liquid and char product compared to the feedstock (HHV of 31.5 MJ/kg). The NCG is not collected and hence is not included for the GEC. The energy of the products are given as an equivalent energy reading in relation to the mass fed [25]. Table 5.8 provides the HHV of the different products from the pyrolysis of rejects at the tested temperatures.

Table 5.8: The HHV (MJ/kg) of the wax and oil from the bench-scale experiments

Temperature	350 °C	450 °C	500 °C	550 °C
Wax	-	39.6 ± 0.3	40.7 ± 1.0	24.8 ± 2.8
Oil	-	-	20.6 ± 5.4	-

In Table 5.8, the produced wax has an HHV of 39.6 and 40.7 MJ/kg at 450 and 500 °C, respectively and at 550 °C, the HHV of wax decreases to 24.8 MJ/kg, due to secondary cracking of waxes into NCG. In Table 5.8 only the experiments at 500 °C produced enough oil where the HHV could be determined. This oil produced at 500 °C had a mean HHV of 20.6 MJ/kg with a highly variable SD of 5.37 MJ/kg and as shown in Figure 5.8, had an energy equivalent of only 1.89 MJ/(kg feedstock) due to the small oil yield.

In Figure 5.8, at 350 °C almost all the energy was concentrated in the solid product, comprised of some char, and melted plastic. The energy in the condensable product at this temperature could not be determined, because not enough product was collected to perform the HHV experiments. Despite

this, from the high energy content of the solid phase alone, the GEC was 94.5% as shown in Figure 5.8. Similarly, the slow pyrolysis of rejects from another source at 300 °C yielded the highest GEC at 300 °C with a value of 83.8% [24]. Post-hoc analysis showed that the GEC did not significantly change for the temperatures from 350 to 500 °C, but the GEC at 550 ° was significantly different from the rest at 32.3% instead of between 85% to 95%, as for 350 to 500 °C, as seen in Figure 5.8. Despite the similar GEC from the 350 to 500 °C, the contribution of the char to the GEC is significantly different at 350 °C compared to the other temperatures – whereby solid char had an energy equivalent as high as 29.8 MJ/(kg feedstock) for 350 °C as seen in Figure 5.8. The contribution of the char to total GEC was much lower for the temperatures between 450 to 550 °C and not significantly different from one another, contributing to between 17.3 (at 450 °C) to 9.0% (at 550 °C) of the total GEC. The char produced from 450 to 550 °C was shown in Figure 5.8 to have an energy equivalent between 6 and 2 MJ/(kg feedstock) indicating major energy conversion to other products. As seen in Figure 5.8, at the temperatures from 450 to 550 °C, most of the energy is contained in the wax. The difference in the wax contribution to the GEC for 450 °C and 500 °C is not significantly different because they have similar yields (Figure 5.7) and HHV (Table 5.8). Consequently, both waxes produced at 450 and 500 °C have an energy equivalent of 21 to 22 MJ/(kg feedstock).
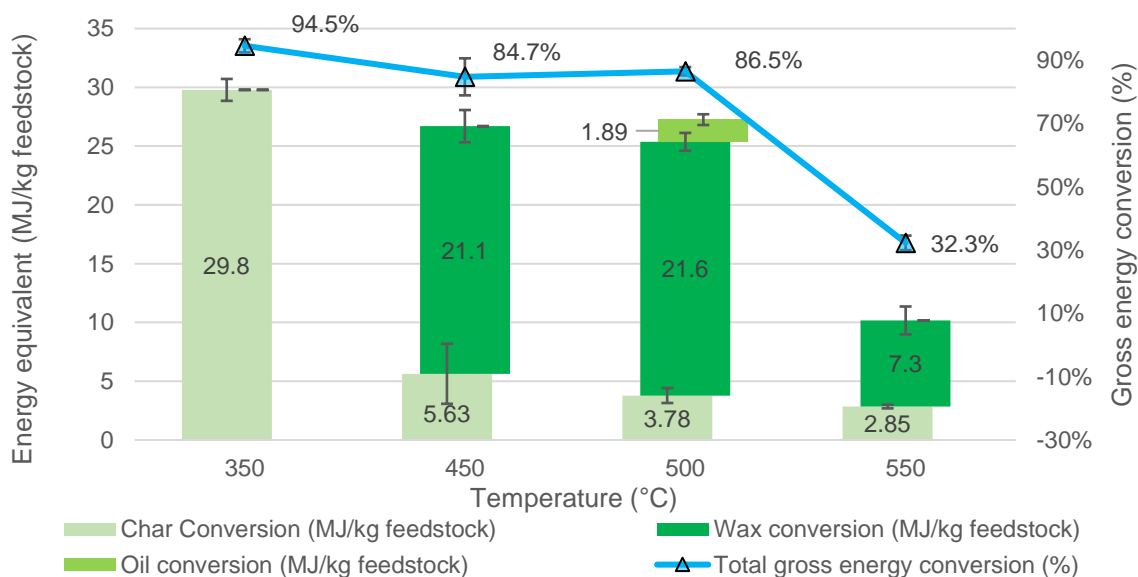
Figure 5.8: Gross energy conversion from bench-scale results

The energy equivalent with respect to the rejects from another source [25] were compared against the current study and it was seen that the GEC was also maximized at the lowest temperature of 350 °C due to the high yield and HHV of char, with char having a lower energy equivalent of 20.3 MJ/(kg feedstock) [25], than that observed in the current study. The energy equivalent of wax produced at 550 °C from the study was identical to the current with a value of 22 MJ/(kg feedstock) [25]. This was because although the wax yield was slightly lower (Figure 5.7), the HHV of the wax was fractionally higher than for the current study at 41.7 ± 0.2 MJ/kg [25].

5.4. Pilot-scale conversion to fuel oil

5.4.1. Improvements to mass balance closure

The pilot-scale runs were performed on the apparatus shown in Figure 4.3. The temperatures of 450, 500 and 550 °C were tested on pilot-scale because maximum condensable product yield was achieved for temperatures from 450 to 500 °C on the bench-scale setup.

The summation of the product masses in different forms should be equal to the feed mass according to the conservation of mass. It is difficult to identify all the product masses for each run and typically about 10 wt.% of mass is unaccounted for. For the same pilot-scale setup, the pyrolysis of PS attained a mean mass balance (MB) closure of 85 wt.% [192], the pyrolysis of biomass achieved 89 to 92 wt.% MB closure [331] and the MB closure from the pyrolysis of PP ranged from 80 to 88 wt.% [274]. Two modifications were performed to improve the MB closure and included the following.

- When the setup was cleaned it was evident that a significant fraction of the char did not effectively deliver to the char-pot. Instead, some of the char accumulated in the reactor kiln or screw conveyor. Therefore, after each run, a vacuum cleaner with a manufactured, extended nozzle was used to extract the char from inside the reactor and screw conveyor. Both the vacuum and charpot char were used for HHV analysis and proximate analysis.
- A Liebig condenser using chilled water was attached above the fourth and final condenser to maximize the condensable product yield. The decision to include the condenser was made after wax and oil were seen condensing in the Tedlar bags that were previously sampled after the fourth condenser indicating a deficient condensation train [241]. The condensation occurring in the condenser was considerable, especially at 550 °C.

Only experiments which attained between 88 and 112 wt.% MB closure were considered for further analysis. These adjustments improved the MB closure, with only two of the ten experiments being discarded due to not attaining mass balance closure within the limits.

5.4.2. Overall product distribution in the pilot-setup

The product distribution yield for the pilot setup is shown in Figure 5.9. Although it looks like the condensable product yield is maximized at 500 °C with a yield of 51.9 ± 7.21 wt.%, ANOVA testing determined that there was no significant difference between the condensable product yield for the three tested temperatures – 450, 500 and 550 °C. The mean condensable product yields at 450 and 550 °C in Figure 5.9 were shown to be 44.8 and 43.6 wt.%, respectively, while the apparent maximum yield is at 500 °C with a value of 51.9 ± 7.2 wt.%. The lack of significance within the yields of condensable product for the different temperatures is attributed to large variation between results. The results for the condensable product yield at 500 °C were 45.3, 50.9 and 59.6 wt.% (Appendix D.2), indicating large variation due to the heterogenous composition of feedstock. The variability

might also be attributed to the fluctuating ambient temperature during the summer months where the experiments were conducted (20 to 40 °C), which might influence condensation of the product.
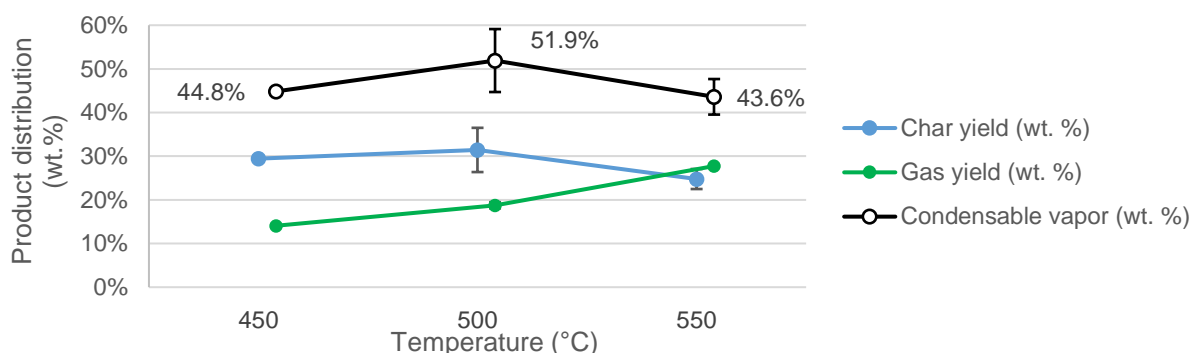
Figure 5.9: Product distribution yield for the different temperatures of the pilot-scale experiments

The char yield between the three temperatures is not significantly different either. As shown in Figure 5.9, the mean char yield produced at 450 and 500 °C is similar with a yield of 29.4 and 31.4 wt.%, respectively. Although the char yield is observed to decrease to 24.8 wt.% at 550 °C as seen in Figure 5.9, post-hoc analysis proved that the statistical significance was not enough to deem the changes in char yields as significantly different. Conversely, the NCG yield was shown in Figure 5.9 to decrease with significant difference for increasing temperatures according to the ANOVA testing. The significance between the NCG yield of all the temperatures was attributed to increase in NCG yield and the small variance within groups of results at different temperatures. As seen in Figure 5.9, for temperature increase from 450 to 500 °C, the NCG yield was shown to increase from 14.1 to 18.8 wt.% and with small SD of 0.29 and 0.70 wt.%, respectively. Additionally, increasing the temperature to 550 °C increased the NCG yield to 27.7 ± 0.21 wt.% as seen in Figure 5.9.

The significantly different NCG yield but insignificantly different condensable product and char yield can be attributed to the losses of masses when collecting the product, which is evident from the significant difference in MB closure at the different temperatures. As mentioned, the MB closure was improved from the two modifications, but low MB closures were still observed at 450 °C (88.3 ± 0.6 wt.%). Conversely, the mean MB closure was increased to 102 ± 11.7 wt.% and 96.1 ± 4.01 wt.% at 500 °C and 550 °C, respectively.

5.4.3. Condensable product yield and characterization

5.4.3.1. Distribution of condensable product

The condensable product is the product residing in the condensation train post run. For all three temperatures, the condensable product yield ranged from 40 to 60 wt.% with an apparent maximum at 500 °C. The temperature of 500 °C has been reported by several researchers to maximize the condensable product yield for biomass-plastic feedstocks [23], [100], [290], [332]. Figure 5.10 shows the mass distribution (wt.%) of condensable products within the four condensers at the tested temperatures and for all temperatures, most of the condensable product resided in condenser 1.
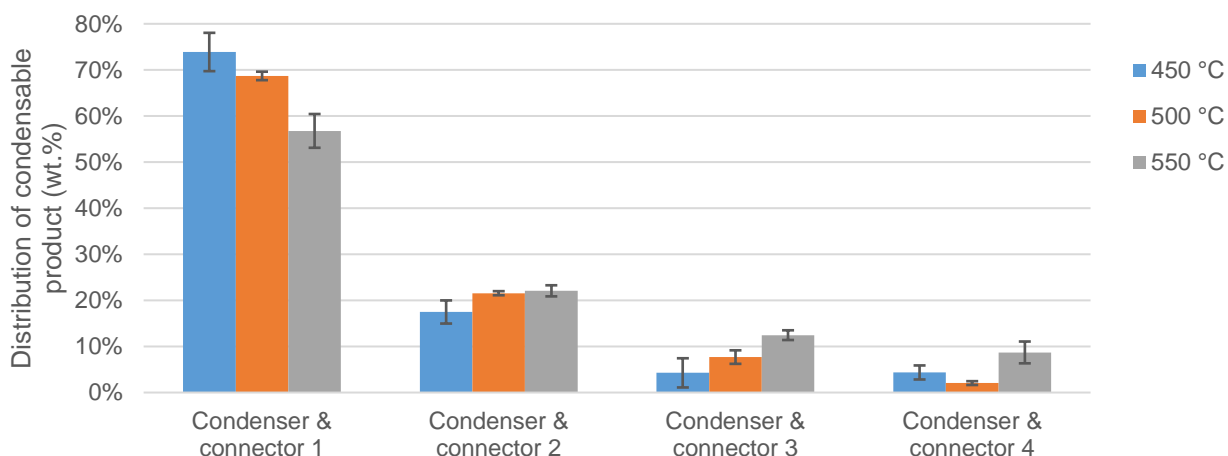
Figure 5.10: The liquid distribution in the condensation train

The two runs tested at 450 °C achieved 44.3% and 45.4% conversion to condensable product or on average, 44.8% conversion. Of this condensable product, 73.9 ± 4.2% resided in the first condenser and 17.5 ± 2.5% in the second condenser as shown in Figure 5.10. The third and fourth condensers held only 4.3 ± 3.2% and 4.4 ± 1.5% of the condensable product, respectively. Although the condensable product yields identified at 500 °C had a large range (Figure 5.9), the range for the product distribution between the condensers was narrow. At 500 °C, the yield of vapours that condensed in the first and second condensers was 68.7 ± 0.9% and 21.6 ± 0.4%, respectively. In Figure 5.10, the third and fourth condenser contained 7.6 ± 1.5% and 2.1 ± 0.4% of the total condensed vapour, respectively. The experiments at 550 °C were very similar to the results gathered at 450 °C where the condensable product yield had a mean yield of 43.6 wt.%, but at the higher tested temperature, it was evident that the vapours condensed more readily in the third and fourth condensers than at lower temperatures. It was seen in Figure 5.10, that at 550 °C, the first and second condenser contained 56.9 ± 3.7% and 22 ± 1.2% of the total condensable product, respectively. Whilst the third and fourth condenser contained 12.4 ± 1.1% and 8.7 ± 2.4% of the condensable product, respectively.

Therefore, the first two condensers held more than 90 wt.% of the product at 450 °C while the first two condensers for the experiments at 550 °C held 78.9 wt.% of the total condensable product in the first two condensers. This could be attributed to the higher temperatures that are associated with more secondary and cracking reactions forming lighter compounds (lighter molecular weight and lower condensation temperature) from the heavier waxes produced at the lower temperatures. These lighter compounds are more likely to be swept with the inert gas to condense further downstream.

5.4.3.2. Appearance of condensable product

Figure 5.11 shows pictures of condenser 1 and 2 and an example of the appearance of the liquid product contained within. As shown in Figure 5.11, the material from the first condenser (C1) consists of a large fraction of viscous wax with low flowing capabilities, being unable to pour through a funnel

as seen in picture 2. Liquid from C1 also consisted of a colloidal mixture with wax, organic and aqueous phase oil, and had a powerful odour. The mixture from the second condenser (C2) was like the first but had less liquid product, but a higher wax yield and lower aqueous phase yield.
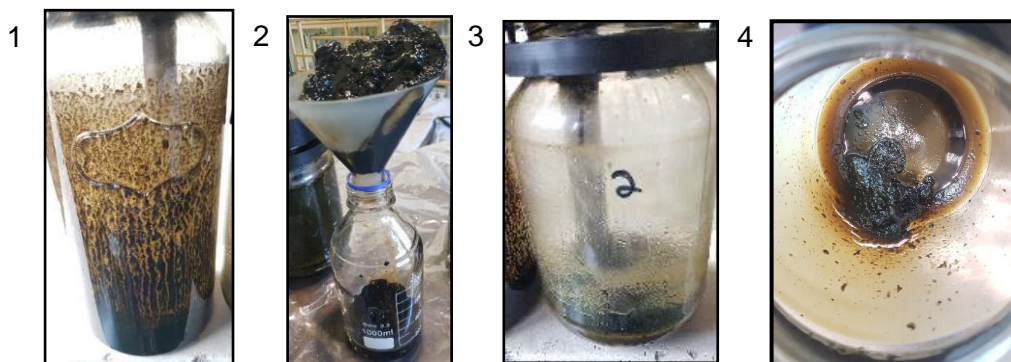
Figure 5.11: Condensable product collected in C1 (Picture 1 and 2) and C2 (Picture 3 and 4)

Conversely the third (C3) and fourth condensers (C4) contained far less material than the first two condensers for all runs, as seen in Figure 5.10. In addition, it was observed that the condensable product from the last two condensers was a wax with higher viscosity, as shown in Figure 5.12. The wax in C3 and C4 is shown in Figure 5.12 and due to these problems, the third and fourth condenser were not used in the physical separations and assumed as 100 wt.% wax.
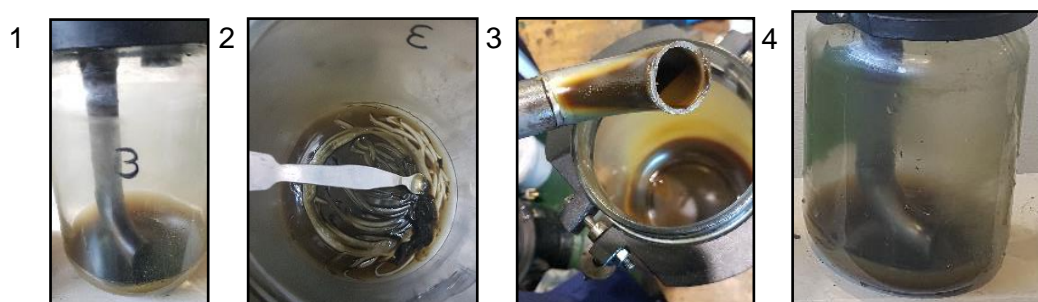
Figure 5.12: Condensable product collected in C3 (Picture 1 and 2) and C4 (Picture 3 and 4)

5.4.3.3. Fractionation of condensable product

Despite a goal of pyrolysis being the conversion of "heterogenous waste into a homogenous, energy-dense product," the homogeneity of the condensable product is difficult to control, especially for non-uniform waste streams which is increasingly evident for pilot-scale [285]. Different fuel oil grades must remain uniform in storage and not separate by gravity into light and heavy oil components [286], therefore it was necessary to separate out some of the condensable product to improve the energy content or HHV of the fuel oil and extract some of the condensable product of lower energy content, like aqueous phase oil which could contain as much as 70 wt.% water according to some literature sources [102], [190], [240], [241].

Although not clearly seen in Figure 5.11, the condensable product was heterogenous and consisted of 3 distinct phases, *viz.,* wax, organic phase oil, and aqueous phase oil. Generally researchers

separate condensable product as two phases, but the separation into three phases for plastic-fibre streams has been observed [102], [280]. The composition of the condensable product w.r.t the 3 fractions is shown in Figure 5.13. The secondary (right) axis of Figure 5.13 represents the HHV of the organic phase oil and wax phase. Statistical testing proved the composition of the condensable product to not significantly change for the tested temperature range. This was attributed to high variability within the results, evident from the error bars (1 SD) in Figure 5.13 and small changes between the mean phase yields, of 13 wt.% and less, between all phases at their temperatures.

In Figure 5.13, it is seen that the wax phase has the highest composition of the condensable product phases. Whereby the wax phase was recorded to be between 35 to 60 wt.% of the condensable product and was not significantly different for the different temperatures despite the apparent increase of wax phase from 37.2 ± 2.7 wt.% to 50.7 ± 14 wt.% for the temperature increase from 450 to 550 °C, as shown in Figure 5.13. It is generally expected that higher temperatures will be associated with more severe cracking and conversion of wax to shorter carbon compounds, like oil [275]. Conversely, the opposite has been observed to occur for the pyrolysis of pulper rejects [25], Tetra Pak [102], and even HDPE [264], whereby higher temperatures increased the wax content. This was attributed to some high molecular weight compounds (HMWC), for instance the C_{35} alkane which has a boiling point of 490 °C [275], to volatize but not undergo significant cracking reactions [275]. Hence at 500 °C, the C_{35} alkane will volatize but not undergo major secondary cracking and will condense as wax [275].

The aqueous phase yield in the condensable product did not prove to be significantly different according to statistical analysis. In Figure 5.13, the aqueous phase of condensable product at 450 and 500 °C, had mean values of 30.1% and 31.8%, respectively. Although less obvious is the change in aqueous phase yield at 550 °C, which was observed to decrease in Figure 5.13 to 18.9% but not be significantly different to other temperatures due to its high SD (7.3 wt.%). The small (yet insignificant) decrease in aqueous phase yield at 550 °C is attributed to some components of the aqueous phase being held in the wax at 550 °C. This would explain why the HHV of the wax is lowered to 32.8 MJ/kg for 550 °C and significantly different to the HHV of the wax at 500 °C of 38.9 MJ/kg, as shown in Figure 5.13.

The water gas-shift reactions (WGSR) that convert H_2O and CO into CO_2 and H_2 are associated with gasification and higher temperatures of *ca.* 700 °C and above. However, catalytic pyrolysis of biomass with 30 wt.% calcium oxide (CaO) was shown to favour WGSR for the same reactor at temperatures between 500 and 550 °C [241] and on bench-scale [190]. CaO is present as filler in the paper fraction and aluminium is observed in the char product (Figure 5.15). Despite it being unlikely that the small concentration of inorganics will have significant catalytic effect causing the water content to decrease from 500 to 550 °C, the possibility of WGRS occurring is not impossible.

The possibility of WGSR occurring can explain why there is a significant increase in the mass of H_2 and CO_2 in the NCG phase from 500 to 550 °C, as shown in Table B-3 of Appendix B.5.

The organic oil phase, as seen in Figure 5.13, has a higher HHV than wax, with a mean HHV of 45.0, 43.6 and 43.2 MJ/kg for oil produced at 450, 500 and 550 °C, respectively. Unlike the HHV of wax, the HHV of organic phase oil is not significantly different for the tested temperatures and its HHV between 42 to 45 MJ/kg is similar to the HHV of oil produced from a study on the slow pyrolysis of rejects at 425 °C (43 MJ/kg), but higher than the oil produced at 550 °C (40 MJ/kg) [24]. The HHV of wax was significantly lower than the organic oil fraction and had higher variability within the results, whereby the wax at 500 °C had the highest HHV of 38.9 ± 1.04 MJ/kg as shown in Figure 5.13.
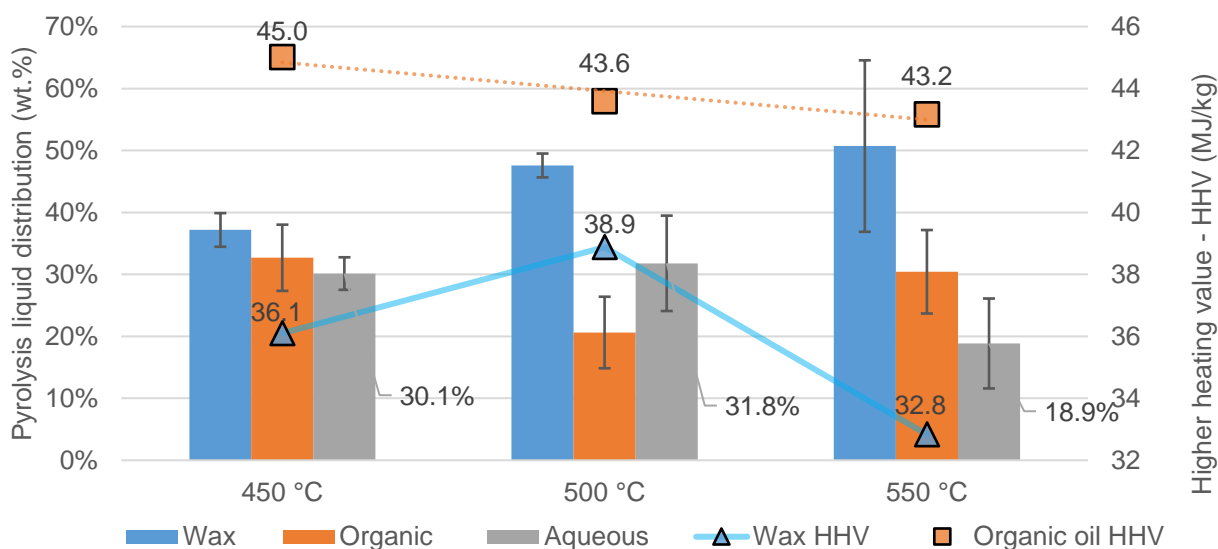
Figure 5.13: The distribution of wax, organic and aqueous phase oil in the four condensers and their HHV (MJ/kg)

5.4.3.4. Characterization of the main fraction of condensable product - wax

Elemental analysis of the largest condensable product fraction, wax, was performed and the results of the elemental analysis are shown in Figure 5.14. Most of the wax is carbon (C) with C content between 64 and 66 wt.% for the three temperatures, as shown in Figure 5.14. This content is lower than the C content for gasoline and diesel, being *ca.* 86.5% [333], [334]. The hydrogen (H) content was between 11.1 and 12.1 wt.%, as shown in Figure 5.14, for the three temperatures and like the C content it remained largely unchanged for the wax from the three temperatures. The H content of the wax was similar to the H content for gasoline and diesel fractions which is *ca.* 13.5 wt.% [333].

The nitrogen (N) and sulphur (S) content is negligible for the wax with both tests showing results below the detection limit. Lastly the oxygen (O) content for the wax was assumed as the balance of the elemental analysis and shown to range, without significance, from 21.5 wt.% (at 450 °C) to 24.4 wt.% (at 500 °C) as shown in Figure 5.14. These results indicate the presence of oxygenated organic compounds in the wax which causes the O content to increase and be potentially too high for gasoline, with a limit of 2 wt.% [333], but still have other possible uses as fuel oil.
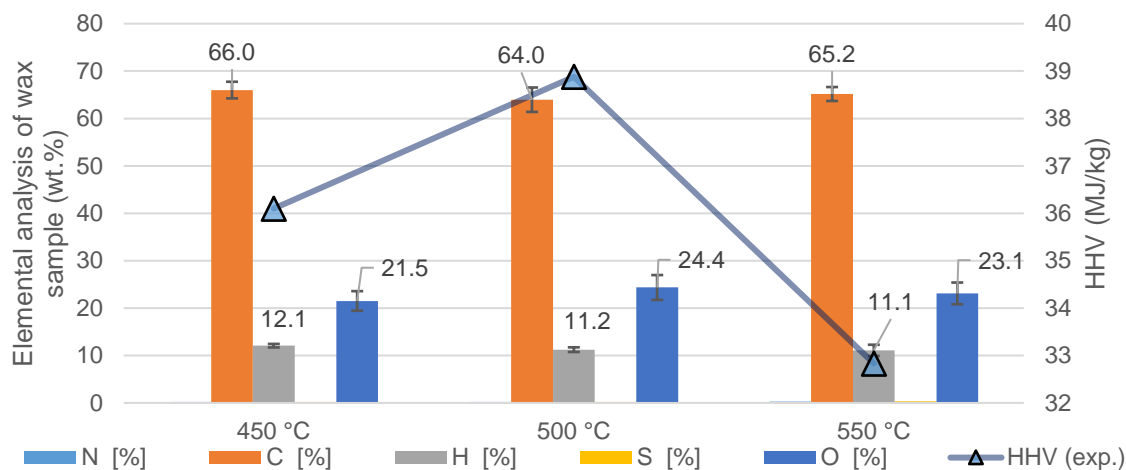
Figure 5.14: Elemental analysis of the wax produced from pyrolysis of rejects

5.4.4. Char product yield and characterization

5.4.4.1. Distribution of char product

Char was divided into vacuum char and charpot char. The charpot char consisted mainly of heavy wax, with an HHV between 35 and 43 MJ/kg. The same phenomenon was described by researchers who pyrolyzed pure plastic in the setup [192], [274] and it has been stipulated that the wax is agglomerated wax from the condensation of volatiles in the charpot. The charpot was designed to maintain a temperature of 300 °C throughout the experiment by acting as a quench zone to minimize undesirable secondary or ternary reactions but prevent condensation of volatiles. Although, 300 °C is generally successful for preventing the condensation of LMWC from depolymerizing biomass, the condensation of heavier waxes from depolymerizing plastic is inevitable. Longer chain alkanes with a carbon length of 17 or greater (C_{17+}) have a boiling point greater than 300 °C [335] and hence may have the tendency to condense in the charpot. Figure 5.15 shows how the consistency of charpot char can change for each run and temperature. The two leftmost pictures (photo 1 and 2) of Figure 5.15, is when wax (C_{17+}) is deposited on the lid, typically seen for runs at 450 °C. Photo 3 shows the deposited char to be less waxy, but grainer and ashier and is seen for runs at 500 and 550 °C. Photo 4 is aluminium from the foil plastics that is concentrated in the char product. Photo 5 is an example of the successful deposition of char into the charpot via the screw conveyer, because less char was needed to be extracted from the reactor via the vacuum.
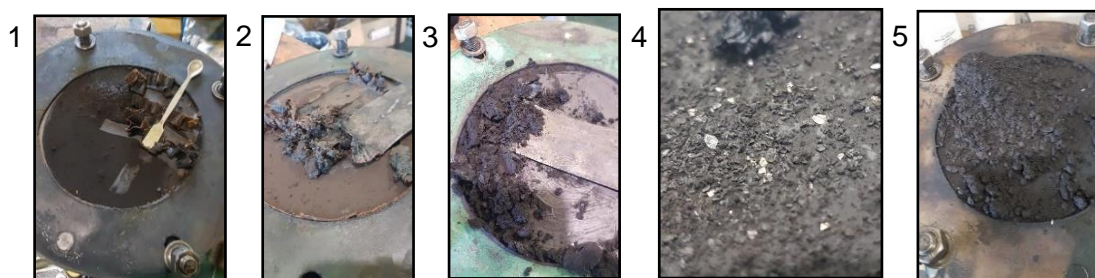
Figure 5.15: Pictures of material deposited on charpot lid, being wax (leftmost) to char (rightmost), similar to vacuum char

Figure 5.16 shows how temperature affects yield of the char types. It also shows the HHV of the combined char as a function of the individual yields and their HHV. This figure contains two datasets, being a stacked bar graph for the yield of the two char types and the second, a line graph with a secondary axis to elucidate the HHV of the char produced. The vacuum char yields were not significantly different at tested temperatures according to ANOVA analysis. Whereby in Figure 5.16, the vacuum char yield at 450 °C was 25.9 wt.%, which decreased to 23.7 and 22.9 wt.% for the increase in temperature to 500 °C and 550 °C, respectively.

Likewise, the results for the charpot yield from 450 to 550 °C were also not significantly different. This was attributed to the low yields being less than 11 wt.% and the high SD between results - for example in Figure 5.16, the charpot yield is maximized at 500 °C with an apparent mean yield of 7.7 wt.% and SD of 4.8%, due to two of the three runs having a yield of 9.8% and 11.2%. These two runs at 500 °C with high yield were attributed to successful transportation of char from inside the reactor to the charpot with a screw conveyor, like that seen in picture 5 (Figure 5.15). Reasons for lower charpot yields observed for some experiments could be due to blockages.

The addition of the charpot and vacuum char yield is the total char yield which is not significantly different between temperatures and has a char yield of around 30 wt.%. The HHV of the total char is the summation of the char yields and their HHV calculated as a weighted average. The HHV of the two char types is provided in section 5.4.4.2. The HHV of the combined char is not significantly different for the tested temperatures according to the ANOVA testing. Whereby as seen in Figure 5.16, the HHV is 28.2, 27.6 and 22.7 MJ/kg for the temperatures of 450, 500 and 550 °C, respectively. Hence, the char produced from these experiments with a combined HHV between 22 and 29 MJ/kg could be within the HHV range of high-quality coals like bituminous and anthracite coals with an HHV of 24 to 33 MJ/kg [133], [336], [337].
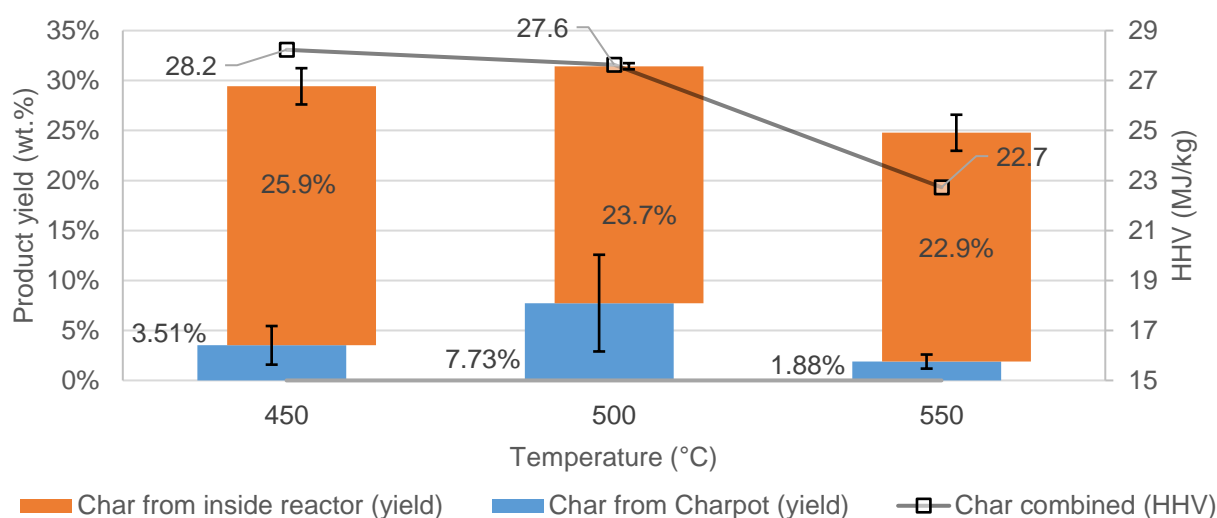
Figure 5.16: The effect of temperature on char yields and HHV of the char

5.4.4.2. Proximate analysis of char products

The proximate analysis of both char types on a moisture-free basis is provided in Figure 5.17. This graph indicates the relationship between the volatile matter (VM), fixed carbon (FC) and ash content of the char to its energy content (HHV). From Figure 5.17, it is seen at 450 °C that vacuum char is a combination of ash, FC and VM content in similar proportions whereby, the VM content and ash content each comprise 35 wt.% of the total char and the remaining 30 wt.% is FC. ANOVA testing proved the proximate analysis of the char to vary significantly for the tested temperatures and post-hoc analysis proved for which pairwise comparisons, significance was observed. It was observed in Figure 5.17, that increasing the temperature to 500 °C significantly decreased the VM content to 26.4 wt.% and significantly increased the FC content to 36.6 wt.% while no significant change to ash content was observed. As shown in Figure 5.17, increasing the temperature to 550 °C caused the VM content to further decrease significantly to 18.6 wt.%, at the expense of FC and ash. The difference of the ash content, FC and VM content of the char produced at 550 °C was significantly different to the char produced at 450 °C. As observed in Figure 5.17, the char produced at 550 °C had a mean ash content of 41.2 wt.% and a FC content of 40.2 wt.%. As seen in Figure 5.17, the HHV of the vacuum char was shown to decrease linearly (R^2=0.988), but without significance, from 26.3 MJ/kg at 450 °C to 21.8 MJ/kg at 550 °C. This evolution is characteristic of what is usually observed for lignocellulosic char.

The results of the proximate analysis of the charpot char were not significantly different for the tested temperatures according to the statistical analysis. It was seen in Figure 5.17, that the mean VM content of char from the charpot was 74.5 and 72.1 wt.% at 450 and 550 °C, respectively. This was higher, although not significantly higher, than the VM content of char at 500 °C with a value of 62.7 wt.% as shown in Figure 5.17. Likewise, in Figure 5.17 it can be observed that the ash content was between 7.2 to 12.4 wt.% for all three temperatures while the FC content was between 16.4 and 24.9 wt.%. Despite these insignificant differences, the energy content of the charpot char at 450 °C is 42.8 MJ/kg while at 550 °C, it is 34.4 MJ/kg (see Figure 5.17) and also significantly different to each other according to post-hoc analysis. The change in HHV for the charpot char also follows a linear trend with temperature (R^2=0.974), like the vacuum char.

The results from the proximate analysis and HHV of the vacuum char correlate closely to that observed for lignocellulosic char. This was established due to the increasing FC and ash content at increasing temperature, resulting in decreased HHV with similar values to char from the pyrolysis of biomass [241], [328] and RDF [221]. Contrarily, char from the charpot contains mainly plastic-derived compounds in the form of heavy volatiles. This is evident from its high volatile matter content, coupled with relatively low ash and FC content. In addition, the high HHV of the charpot char elucidates that the components were derived from plastics, instead of biomass. The phenomenon of charpot char being characteristic of heavy volatiles (or waxes derived from plastic) and vacuum char being similar

83

to char derived from fibres or RDF has not been previously observed in the pilot-scale unit. Therefore, this study adds to the understanding of the pilot-scale pyrolysis unit and how setting the temperature of the charpot to 300 °C might be deficient for maximizing condensable product yield.
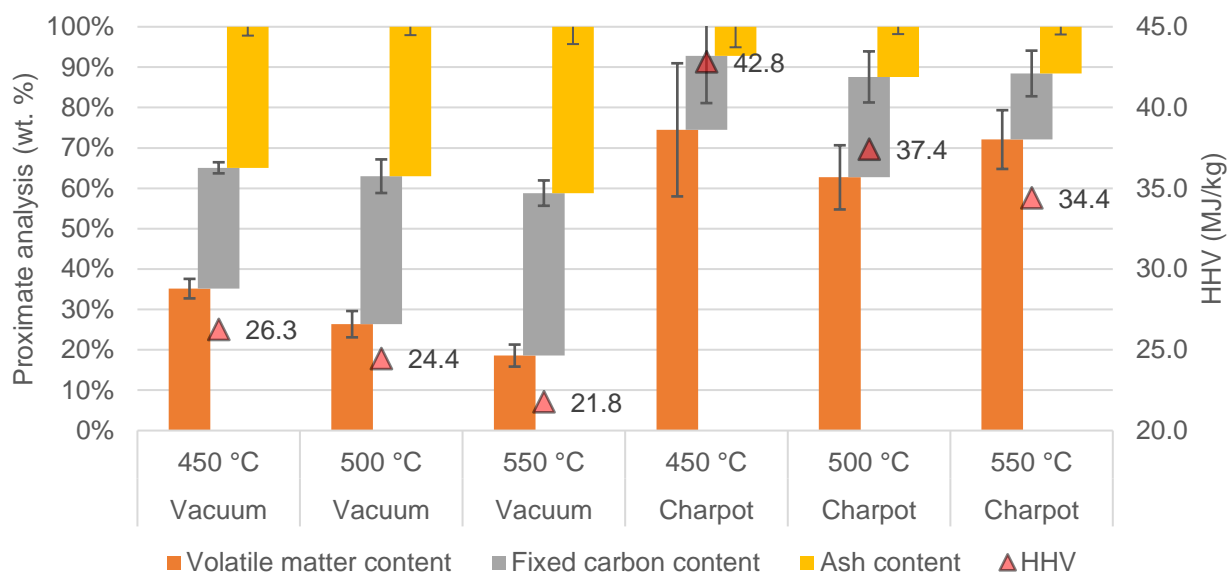
Figure 5.17: The proximate analysis of the two char types and their HHVs

5.4.5. NCG product yield and characterization

5.4.5.1. Composition of NCG

For this section, the NCG composition is provided w.r.t the gases analysed from Compact GC 4.0 machine and the temperature at which the NCG is produced. Nine gas compounds were identified in the sample. The mean mass composition (wt.%) of the nine components in the NCG for the three temperatures are used in Figure 5.18 with error bars indicating one SD from the mean. The percentages of CO and C_4H_{10} were observed to not change significantly for the tested temperatures according to ANOVA testing. CO was the third most abundant component and comprised between 9.3 to 10.4 wt.% of the NCG at the temperatures, likewise C_4H_{10} associated with the pyrolysis of plastics had a composition of around 9 wt.% as seen in Figure 5.18.

The main component of NCG was CO_2 which decreased from 44.9 wt.% at 450 °C to 32.7 wt.% at 550 °C. The large presence of CO_X gases is probably mostly from the degradation of fibres and has been reported to make up more than 60 wt.% of the NCG from MSW pyrolysis [221] or attributed to PET degradation [247], [248]. The only other gas which decreased its composition with increasing temperature was C_5H_{12} which was 5.93 and 4.27 wt.% at 450 and 500 °C, respectively with barely any signal seen for C_5H_{12} at 550 °C, as shown in Figure 5.18. This result could be from cracking of C_5H_{12}, resulting in increased production of smaller hydrocarbons as described below.

The other 5 components were all shown to significantly increase in percentage of the NCG for increasing temperature. As shown in Figure 5.18, the second largest component in NCG is the C_3H_8.

The percentage of C_3H_8 in NCG increased with temperature from 13.9 wt.% at 450 °C, to 16.0 wt.% at 500 °C and lastly to 20.0 wt.% at 550 °C. The large component of the C_3H_8 gas fraction, common in the NCG from plastic pyrolysis, is consequent of the high plastic fraction in the feedstock, [100]. CH_4 is the fifth most abundant gas in the NCG and was shown to significantly increase from 5.2 wt.% at 450 °C to 9.5% at 550 °C as seen in Figure 5.18. Two more gases which also increase in NCG composition at increasing temperature were C_2H_6 and C_2H_4 which are each around 4 to 6 wt.% at 450 and 500 °C and increased to 9 wt.% at 550 °C, as shown in Figure 5.18. The composition of H_2 in NCG increases from 0.2 wt.% at 450 °C to 0.4 and 0.8 wt.% at 500 and 550 °C, respectively. In Figure 5.18, the H_2 content is very small due to its molecular weight of 2 g/mol.

5.4.5.2. Energy content of NCG

The effect of mass composition on the energy content of the NCG is elucidated in the secondary (right) axis of Figure 5.18 whereby the energy content (LHV and HHV) of the gas are shown and the data labels are included for each temperature on Figure 5.18. ANOVA testing showed that the LHV and HHV of the NCG did significantly increase at increasing temperature. Subsequent post-hoc analysis showed that the difference between energy content at 450 to 500 °C was not significant, but the increasing the temperature to 550 °C showed significant increase. Naturally, the pairwise comparison between 450 and 550 °C also showed significance. The energy content of the gas was most dependent on the CO_2, CO and CH_4 content. The first and third most abundant compounds in NCG are CO_2 and CO, respectively. CO_2 is non-combustible and CO has a relatively low HHV, hence their presence highly affects the energy content of NCG. In addition, the hydrocarbons of longer carbon chains would also drastically increase energy content of the sample. Consequently, as seen in Figure 5.18, increasing the temperature from 500 to 550 °C yielded NCG with an increased mean HHV from 24.0 to 31.1 MJ/kg. The HHV of NCG at 550 °C was congruent to the NCG from a previous report about the fast pyrolysis of rejects at 550 °C with an HHV of 30.8 MJ/kg [25].The HHV was used for the calculation of the gross energy conversion (GEC) on pilot-scale.
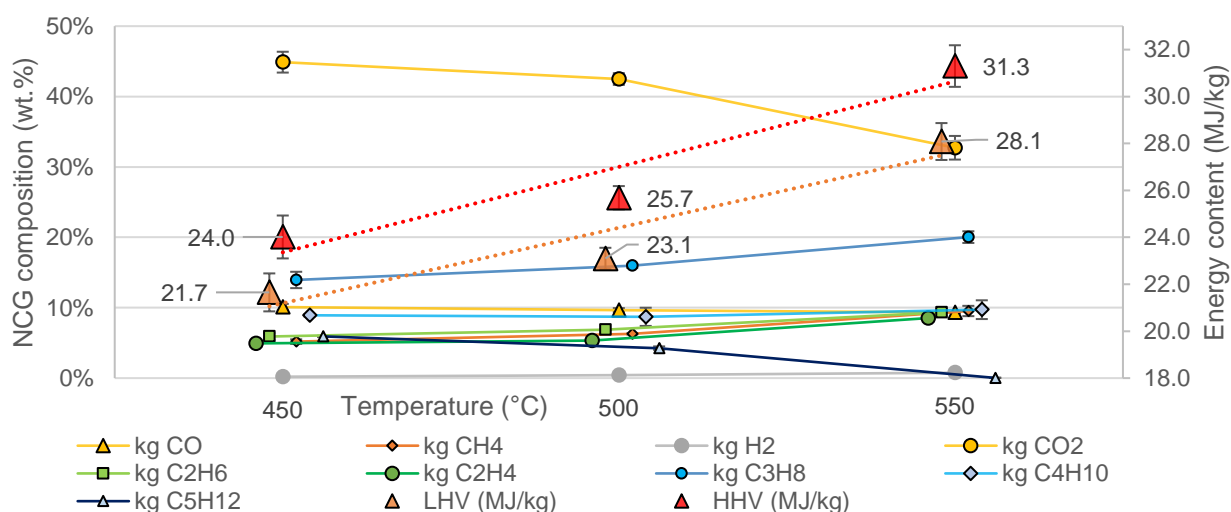
Figure 5.18: The mass composition and energy content of NCG produced at tested temperatures.

5.4.6. Energy evaluation

The net energy conversion (NEC) of each experiment was calculated from the GEC results and the energy expenditure of the pilot-scale pyrolysis setup that is recorded with an energy meter. Ancillary process units like the vacuum pump, feeding piston and valves (See Figure 4.3) also contributed to the reading on the energy meter. During each pyrolysis run, temperature control is used to maintain the set temperature by the reactor and therefore the various endothermic and exothermic reaction occurring in the reactor will probably have an influence on the energy required to maintain the pyrolysis heat, shown as $Q_{pyrolysis}$ in Table 5.9. Table 5.9 provides several values that were used for the calculation of the NEC. Thereafter, Figure 5.19 shows the NEC on a kg basis.

As seen in Table 5.9, the reactor was heated to the target temperature (450, 500 or 550 °C) at a rate of 152 ± 16.4 °C/h. The time required to heat the reactor ($t_{heating}$) was typically 3 to 4 hours depending on the temperature used, as seen in Table 5.9. The mean energy required per run for heating ($Q_{heating}$) as shown in Table 5.9, ranges between 33.7 to 50.5 MJ for 450 to 550 °C, is not used for the calculation of the NEC. This is because for a typical industrial process, the time for heating is usually only a few hours, which is followed by weeks of continuous operation. Conversely, the energy required per run to maintain the temperature ($Q_{pyrolysis}$) is used for the NEC. In Table 5.9, $Q_{pyrolysis}$ is shown to range from 20.3 and 23.8 MJ/run for the temperature of 450 °C and 500 °C, respectively and increasing the temperature to 550 °C further increased $Q_{pyrolysis}$ to 27.4 MJ/run. Lastly, the time for which pyrolysis was extended ($t_{pyrolysis}$) as shown in Table 5.9, was 3 to 4 h/run and included the time for feeding and allowing the volatiles to condense.

Table 5.9: Values used for the net energy conversion results on a per run basis

Property (units)	$t_{heating}$ (h)	$t_{pyrolysis}$ (h)	Heating rate (°C/h)	$Q_{heating}$ (MJ)	$Q_{pyrolysis}$ (MJ)
450 °C	2.98 ± 0.31	3.00 ± 0.90	151 ± 15.6	33.7 ± 2.8	20.3 ± 0.3
500 °C	3.30 ± 0.47	3.37 ± 0.82	153 ± 21.9	43.4 ± 1.8	23.8 ± 1.0
550 °C	3.62 ± 0.49	2.82 ± 0.21	154 ± 21.0	50.5 ± 7.1	27.4 ± 1.9

The typical mean NEC for each temperature is shown in Figure 5.19, where a column bar represents the mean equivalent energy per run (kg-basis) and a line graph (secondary-right axis) represents the NEC. The equivalent energy graph is analogous to the same graph for the bench-scale, shown as Figure 5.8. For Figure 5.19, it can be seen that inputs to the process like fed material and the heat for pyrolysis are indicated as negative values and products are represented as positive values. The heat required for heating was not included in the calculation of NEC, which assumes the continuous operation of the pyrolysis reactor. The feedstock has an equivalent energy of 31.5 MJ/kg for all temperatures, representing its HHV as seen in Figure 5.19. The heat for pyrolysis is equivalent to the energy required per run ($Q_{heating}$) in Table 5.9, but incorporates the 2 kg of fed material to the

process. As seen in Figure 5.19, the heat required at 450 and 500 °C is 10.1 and 11.9 MJ/(kg feedstock) respectively and not significantly different, while the heat for 550 °C is 13.6 MJ/(kg feedstock) and significantly different to that from 450 °C. This is significantly higher than the energy equivalent associated for laboratory scale pyrolysis of dry, biomass at around 500 °C which has been observed to range from 1.1 to 3.5 MJ/kg [338], [339], but up to 8 MJ/kg when feed has a high moisture content of 50 wt.% [339]. The higher energy demand is attributed to energy-intensive ancillary units like the vacuum pump, hydraulic feeding system and piston which are included in the energy meter reading. The equivalent energy of the char and condensable product is not significantly different for any of the temperatures and as seen in Figure 5.19, shown to be from 5.6 to 8.6 MJ/kg and 12.5 to 14.7 MJ/kg, respectively. The equivalent energy for char from another study on the pilot-scale energy recovery from corn stover at 550 °C was 7.7 MJ/(kg feedstock) and congruent with this study [328]. Conversely, for the same study a much lower energy equivalent of 5.8 MJ/(kg feedstock) was observed for bio-oil [328]. The same trend was seen for another pilot-scale study for the energy equivalent of char and bio-oil from pyrolysis at 500 °C of chicken litter and rice husk [330]. Whereby, the energy equivalent of 6.3 and 6.2 MJ/(kg feedstock) was observed for char and bio-oil from chicken litter, respectively [330]. Indicating the low energy equivalent of bio-oil from the pyrolysis of biomass. In Figure 5.19 it can be seen that NCG has the smallest energy equivalent for 450 and 500 °C with a mean equivalent of 3.4 and 4.8 MJ/kg which significantly increased to 8.7 MJ/kg for 550 °C, which was also greater than the energy equivalent of NCG from biomass [328], [330].
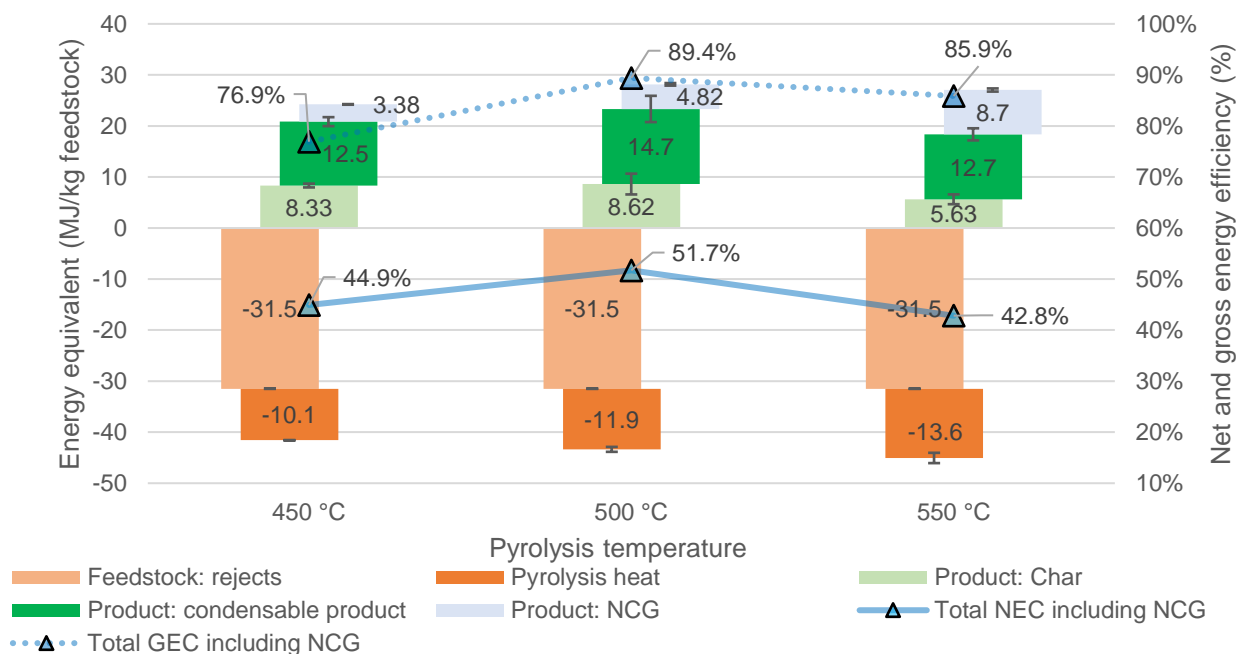
Figure 5.19: The equivalent energy, GEC, and NEC for the pilot-scale experiments

The results for the energy equivalent were then used for the calculation of the NEC as shown from the secondary axis in Figure 5.19. The comparison between the GEC and NEC is included in Figure 5.19 to show how the process heat affects the energy conversion. Although the apparent maximum

for the NEC including NCG is at 500 °C in Figure 5.19, statistical analysis showed no significant difference for the NEC between 450 to 550 °C. Post-hoc analysis showed that the difference of the NEC between 500 and 550 °C is very close to significance (q [4.2] < q $_{crit}$ [4.6]), but not enough to render significance. Likewise, the GEC was shown to also not be significantly different between the temperatures and hence has a mean GEC of 85.0 ± 8.8%, indicating that the process energy contributes to a loss of energy conversion of almost 40%, as shown in Figure 5.19. When NEC excludes the NCG product (for comparison against bench-scale pyrolysis), the NEC is decreased to 27.9 ± 13%. The NEC, when including NCG, was shown to be less than experiments from literature. The slow pyrolysis of corn stover showed to have a NEC of 82.1% at 550 °C [328], while pyrolysis of chicken litter and rice husk, had an NEC of 84% and 89%, respectively at 500 °C [330].

5.5. Comparison between bench and pilot-scale pyrolysis

5.5.1. Condensable product yield

As seen in Figure 5.7, the condensable product yield from the batch reactor at bench-scale was of 62.4 ± 1.1 wt.% for the temperature of 500 °C. Conversely, the yield of condensable product from the pilot-scale pyrolysis at 500 °C as seen in Figure 5.9 was 51.9 ± 7.2 wt.% and more than 10 wt.% less than that observed on bench-scale. The condensable product yield on pilot-scale is analogous to other studies on the pyrolysis using auger reactors; whereby the condensable product yield of 45 wt.% was reported for pyrolysis of rice straw at 500 °C [340]. Similarly, the lower condensable product yields of 39 wt.% and 46 wt.% were observed for the co-pyrolysis of HDPE and pine and PP and pine in 2 kg/h auger reactor at 450 °C, respectively [341]. The lowered condensable product yield from auger reactors might be attributed to their slow pyrolysis application. Similarly, both the bench and pilot-scale setups used the same carrier gas flowrate of 0.5 L N_2/min, despite being different sized reactors and consequently the bench-scale will have shorter vapor residence times associated with higher yields of condensable product [183], [186].

5.5.2. Char and NCG products yield

The average char yield from the batch pyrolysis of rejects at 500 °C on bench-scale was 19.1 ± 2.1 wt.%, as shown in Figure 5.7. Hence, the char yield from bench-scale is 12 wt.% less than that for pilot-scale experiments at 500 °C which can be seen in Figure 5.9 - shown to have a mean char yield of 31.4 ± 4.3 wt.% at 500 °C. The higher char yield on pilot-scale is attributed to the condensation of heavy waxes in the charpot which increases the char yield. Contrarily, the heavy waxes produced on bench-scale will have less difficulty exiting the batch-reactor and will more easily condense downstream as condensable product. The difference between the NCG yield at the different temperatures was smaller on pilot-scale than on bench-scale pyrolysis. Whereby, the NCG yield on bench-scale changed from 14.3 ± 7.7 wt.% at 450 °C to 48.0 ± 1.1 wt.% at 550 °C, indicating significant cracking in the batch reactor for the solid's residence time (30 minutes) at 550 °C.

Conversely, the NCG yield from pilot-scale increased from 14.1 ± 0.3 wt.% at 450 °C to 27.7 ± 0.2 wt.% at 550 °C. This indicates how on pilot-scale significantly less secondary cracking occurs to NCG when compared to a batch, bench-scale unit.

In addition, the HHV of the char produced between 450 to 550 °C on bench-scale is not significantly different, with a mean HHV of 19.8 ± 1.2 MJ/kg at 500 °C. This char has a lower HHV than the combined char from pilot-scale at 500 °C with an HHV of 27.2 ± 2.7 MJ/kg as shown in Figure 5.16, which was also not significantly different between 450 and 550 °C. Likewise, the VM content of the vacuum char from pilot-scale still contained 19 wt.% VM content indicating volatiles still present in the char after the experiment, while in bench-scale it is expected that the VM content will be less due to the lower HHV value. Bench-scale char will undergo more severe cracking due to the small sample size (30 g) that is held in the reactor for a considerable solid residence time (30 min). Although, the solids residence time is relatively long in the auger reactor, between 5 to 10 minutes, the large sample size (2 kg) causes thermal lag during heat penetration, aiding mass-transfer limitations, and preventing severe cracking of char. Hence, the lowered HHV for bench-scale char compared to pilot-scale char is attributed to the more severe cracking of the bench-scale char into secondary NCG.

5.5.3. Fractions of condensable product and their energy contents

The condensable product from bench-scale was shown to consist of two phases being a wax in the first pot and an oil phase in the second pot. The wax from bench-scale was shown to be at least 70 wt.% of the total condensable product and have a high HHV from 39 to 42 MJ/kg for 450 and 500 °C, but significantly reduced to 24.8 MJ/kg at 550 °C (Table 5.8). For the bench-scale pyrolysis, most of the energy can be seen to be transferred to the wax product as shown in Figure 5.8, whereby at 450 and 500 °C as much as 21 to 22 MJ per kilogram of feed was converted to wax, thereby increasing the GEC to 85% in Figure 5.8. The oil from bench-scale was shown to be largely negligible w.r.t to its energy equivalent due to its small yield. In Figure 5.8, it can be seen that only for the 500 °C experiment, was the HHV of the light-yellow oil recorded with a mean value of 20.6 ± 5.4 MJ/kg (Table 5.8). Conversely, the pilot-scale experiments could produce more than 1 kg of condensable product and hence would provide a better idea of what to expect for a commercial pyrolysis process. The condensable product was observed to be heterogenous and must be separated if it is to adhere to fuel oil standards [286]. The condensable product was separated into three fractions, *viz.* wax, aqueous phase oil (non-combustible) and organic phase oil. Like bench-scale, wax was the major fraction of the condensable product, whereby the wax fraction in condensable product from pilot-scale at 500 °C was 47.6 ± 1.9 wt.% as shown in Figure 5.13. In Figure 5.13, this wax had an HHV of 38.9 ± 1.7 MJ/kg which decreased to 32.8 ± 3.6 MJ/kg at 550 °C, contributing to the condensable product energy (product of highest energy) as shown in Figure 5.19. The HHV of organic phase oil did not change significantly for the different temperatures as seen in Figure 5.13, (43.2 to 45.0 MJ/kg)

and far higher than HHV of oil from bench-scale at 20.6 MJ/kg. The lowered HHV of oil on bench-scale was attributed to its mixing with aqueous phase.

5.5.4. Energy conversion

The GEC from the pilot-scale is shown in Figure 5.19, whereby no significant difference was observed for GEC between the temperatures. The mean GEC at 500 °C was 89.4% and 74.1 ± 12.8% when NCG was included and excluded, respectively. Comparatively, the GEC from bench-scale pyrolysis at 500 °C was 86.5 ± 1.8%, when NCG was excluded, as shown in Figure 5.8.

5.5.5. Effect on technoeconomic studies

Technoeconomic studies rely on experimental data for product yields and characterization. Oftentimes, results from bench-scale experiments can be overly optimistic and represent results that will have higher condensable product (primary product) yields than that expected for pilot- and commercial scale. In addition, the condensable product from bench-scale can be significantly different in composition to the condensable product produced on pilot-scale.

In the current study it has been seen that the condensable product yield on bench-scale was significantly different to pilot-scale. The condensable product from bench-scale was comprised of wax and oil, of which the condensable product was predominantly wax (70 wt.%). Comparatively, the condensable product from the pilot-scale experiments consisted of wax, organic phase oil and aqueous phase oil. The yield of wax was far less for the pilot-scale than the bench-scale, despite the more severe cracking experienced on the bench-scale, as evident from the higher NCG yields. This is attributed to the fact that condensable product from bench-scale pyrolysis could not be separated (like on pilot-scale) due to the small amount of condensable product collected and recovered in the pot. In addition, on pilot-scale the aqueous phase is considered a waste product due to its untestable HHV which could not be tested. Therefore, the product yield is less on pilot-scale compared to bench-scale and is the reason why the GEC is lower on pilot-scale than on bench-scale.

The pilot-scale data used in a technoeconomic study would include normalized product yields, composition, and energy content of the 3 main pyrolysis products. The mass, heat, and phase transfer limitations are more pronounced on pilot-scale experiments than bench-scale due to use of larger, more representative, feedstock and continuous operation for pilot-scale, instead of batch scale. Therefore, the use of pilot-scale data will benefit the technoeconomic study as the only previous technoeconomic study on the pyrolysis of pulper rejects used batch, bench-scale data [29]. Hence, the use of pilot-scale data will produce more appropriate results for the technoeconomic study. There are several technoeconomic studies in literature have been identified that use pilot-scale data to aid the simulation, but all identified studies focus on the pyrolysis of biomass [30], [302].

Chapter 6: Economic Analysis

Chapter 6 provides the economic results to address objective 3. **Chapter 6** first deals with the methodology for the economic analysis. Thereafter, the results for the economic analysis for the pelleting and pyrolysis lines are each explained and then compared w.r.t the profitability.

6.1. Economic analysis methodology

Section 6.1 to 6.3 describes the methodology followed for the economic analysis and the subsequent techno-economic analysis (TEA) development for both the pelleting and pyrolysis process.

6.1.1. Economic modelling strategy

The discounted cash flow (DCF) method has been followed to predict the long-term plant profitability for both conversion processes, assuming a plant life of 25 years. The DCF analysis considers the time value of money and therefore discounts future cash flows so that they can be represented with the present value of money [342]. The cash flow analysis of each business is summarized in Figure 6.1 where capital cost is shown in the bottom-left yellow box, calculations required for the annual cash flow in blue and calculations to predict financial success in green in the top right box.
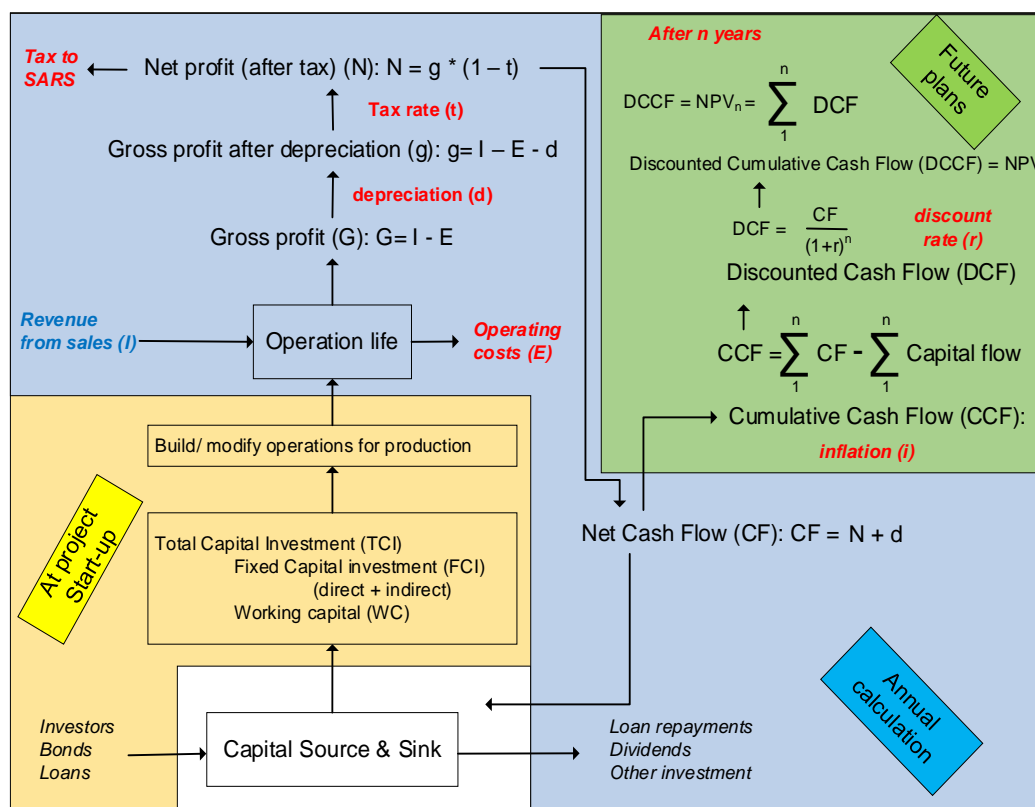
Figure 6.1: Cash flow analysis method for start up, operation and future costs. As adapted from Cohen & Deglon, 2009 [343]

Appendix E describes the calculations for the TEA with the following assumptions used:

- In the first and second year, 70% and 30% of the FCI is spent on the plant, respectively.

- All WC is used in the second year to fund the necessary purchases for start-up.
- Plant depreciation (1% scrap value) occurs over 5 years using the straight-line method.
- Operation phase of the project begins in the third year (generate revenue and incur OPEX).
- The escalation rate is assumed as 6.5% per year and company tax rate is 28% [344].
- A discount rate (m_{ar}) of 25% for both projects is assumed (attractive to investors) [291].

6.1.1.1. Key profitability indicators

There are several key profitability indicators (KPIs) used to establish the success of long-term projects. Indicators like the cumulative cash flow (CCF), payback-period (PB) or return on investment (ROI) do not consider the time value of money and are not as rigorous as the net-present value (NPV_n) or internal rate of return (IRR), which do [345], [346]. The minimum fuel selling price (MFSP) provides the selling price needed to attain an $NPV_{25}=0$, using a specific discount rate. Hence the profitability of each project will be determined according to MFSP of pellets and fuel oil to reach a target IRR of 25% (discount rate) to an attain $NPV_{25}=0$.

6.1.1.2. Annual capacity of pulper rejects

The annual capacity of pulper rejects was calculated according to the capacity of recovered paper fed to the secondary fibre mill and the percent of recovered paper fed that end up as rejects, to be disposed to landfill. As shown in Equation 6.1, 58 kilotons per annum (ktpa) of recovered paper is used by the secondary fibre mill. It is estimated that 6% of this recovered paper ends up as pulper rejects [51]. Hence, the annual capacity of pulper rejects for both the pelleting or pyrolysis facility is 3.48 ktpa and similar to another rejects stream, with an annual capacity of 4.32 ktpa [29].

$$10 \ \frac{\text{tonnes}}{\text{batch}} \times 11 \ \frac{\text{batches}}{\text{shift}} \times 2 \ \frac{\text{shifts}}{\text{day}} \times 22 \ \frac{\text{days}}{\text{month}} \times 12 \ \frac{\text{months}}{\text{year}} = \ 58 \frac{\text{Kt}}{\text{year}} \qquad \text{Equation 6.1}$$

6.1.2. Total capital investment (TCI)

Total capital investment (TCI) is split into fixed capital investment (FCI) and working capital (WC). The FCI is subdivided into direct and indirect capital, calculated from factors and the purchase cost of equipment (PCE). The TCI, FCI and PCE of the pelleting and pyrolysis conversion process are explained in more detail in Section 6.2.2 and 6.3.2, respectively.

6.1.2.1. Fixed capital investment (FCI) and working capital (WC)

The methods for determining the FCI of the pelleting and pyrolysis process are calculated differently. The pelleting process was calculated according to a modified Lang factorial method which used the purchase cost of equipment (PCE) and Lang factors to account for total physical plant cost (direct) and indirect capital cost [297]. Although the Lang factorial method has a solids-handling setting, a study appropriately modified the factors to suit an MSW-to-RDF pelleting line [31]. The Lang factors used for the calculation of the FCI for the pelleting process are shown in Table 6.7.

The FCI of pyrolysis processes is costed according to a modified Lang factorial method, for a biorefinery [301]. This method for TCI estimation has been used for several studies on the pyrolysis of biomass [302]–[304], and once for the pyrolysis of paper mill rejects [29]. This method separates process units of a plant into those that are 'inside battery limits' (ISBL) and 'outside battery limits' (OSBL). The ISBL refers to the area where direct production takes place, while units that are OSBL are where utility generation is required [295], [297]. The FCI is the summation of total direct capital (TDC) cost and total indirect capital (TIC). The TDC is the summation of the total PCE and the direct costs - calculated as a fraction of the summated PCE for units that are ISBL [296], [302]. The TIC costs are calculated as a fraction of the, then calculated, TDC [296], [302]. The factors used for the biorefinery method as used for the pyrolysis process are shown in Table 6.11.

The WC for the pelleting and pyrolysis process are both assumed as 5% of their calculated FCI due to their smaller demand raw materials, utilities, and start-up requirements (practically zero in a solids-handling process). Although the pyrolysis process uses liquid and gas process lines, the WC is also assumed as 5% of FCI as seen in literature [29], [296], [302], [305], [306].

6.1.2.2. Purchase cost of equipment (PCE)

Most of the units for the pelleting process are costed according to the historical shortcut method to provide a ballpark estimate (15 to 25%) for the PCE [295], [297]. Some units of the pelleting process like the direct and indirect dryer and their ancillary process units were sized [347] and costed [348] according to heuristics. The data used for the costing of the units for the pelleting process is explained in Section 6.2.2. The historical shortcut method involved costing a specific unit (C_2), according to the cost of the same unit from another project (C_1), while considering the inlet flowrate of the unit from that project (S_1) to this project (S_2) as scalable factor (S_2/S_1) to the power of an index (n), as shown in Equation 6.2 [297], [349]. The scaling factor (n) is taken as 0.8 for solids-handling equipment [295], [296], [350] and 0.6 for most chemical engineering equipment, hence the *six-tenths* rule [297], but can be different depending on the unit. The CEPCI indexes and location factors (LF) are included to account for the inflation (year) and location differences, respectively. The exchange rates (ER) should be added, so that the PCE is given in South African Rands (ZAR). The LF, CEPCI, and ER values are shown in Appendix F.

$$C_2 = C_1 \times \left(\frac{S_2}{S_1}\right)^n \times \frac{CEPCI_{2019}}{CEPCI_{ref}} \times \frac{LF_{S.A}}{LF_{ref}} \times \frac{ER_{S.A}}{ER_{ref}}$$ Equation 6.2

Most of the PCE for the pyrolysis process were based off heuristics from Couper, 2009 [348] or Seader et. al, 2009 [351]. The sizing factors used for the PCE was taken from Aspen Plus and a safety factor applied to account for inefficiency losses. Each costed unit was subject to an installation factor to attain the PCE. Only the decanter and steam drum were based off the historical costing method using the cost and capacity from Dutta et., al, 2015 [303]. The sample calculations for each unit are provided in Appendix G and H and all the units for pyrolysis are shown in Figure 6.4.

6.1.3. Total operating costs (OPEX)

OPEX are divided into variable and fixed costs. Variable OPEX vary with plant capacity and forms the cost for the feedstock, raw materials, utilities, and waste disposal. Conversely, fixed OPEX are constant (only influenced by inflation) and comprise of plant personnel salaries, plant maintenance and property insurance. The calculation of OPEX for both processes use the same method.

6.1.3.1. Variable operating costs (OPEX)

Variable OPEX are comprised of feedstock, raw material, utilities, disposal, and miscellaneous costs. The feedstock is a waste stream that would have be disposed to landfill, if not converted to a product. Hence the feedstock cost of the pulper rejects is assigned a negative value, or treated as income, due to the associated cost of avoiding the landfill [29]. The utilities used by each process include steam, electricity, process water and air. The price, specification, and reference for each utility is summarized in Table 6.1. A major difference between the pyrolysis and pelleting process is that the pyrolysis process produces its own thermal energy on-site and does not require any coal. Conversely due to the drying requirement for the pelleting process and the fact that it does not produce its own thermal energy – coal is required to produce steam on the boiler on-site.

Table 6.1: Variable operating costs

Parameter	Specification	Cost	Reference
Feedstock *"cost"*	Revenue due to circumnavigation	*R517.62/ton	[29]
Solid waste disposal	Includes collection & landfill	R517.62/ton	[4]
Air	16.5 °C & 59% RH	-	[352], [353].
Coal	HHV of 19 MJ/kg	R400/ton	[146], [354]
Electricity	Non-local authority, business rate	R0.9696/kWh	[355]
Cooling water	Supplied at 30 °C, 1 bara	R25.37/kL	[4], [356]

*Treated as revenue and not as a cost.

6.1.3.2. Fixed operating costs (OPEX)

The 'biorefinery' method for the fixed OPEX was chosen over the heuristics from Sinnott, 2005 [297]. This method subdivided fixed OPEX into four types as shown in Table 6.2 with heuristics related to the salaries and FCI to calculate the contribution of each [302], [304].

Table 6.2: Heuristics for the fixed operating costs

Parameter	Determined from	Reference
$f1$ Salaries	Shift basis and plant complexity	-
$f2$ Benefits and overheads	$f1 \times 0.90$	[302], [304]
$f3$ Maintenance costs	FCI $\times$ 0.03	
$f4$ Insurance and taxes	FCI $\times$ 0.007	

The labour (salaries) was costed according to number of shifts for both processes and necessary personnel. It is estimated that 1 maintenance supervisor, 1 production foreman and 2 production operators are needed per shift on either plant [357]. Salaries of personnel are shown in Table 6.3 and are based off annual median salaries from the paper - and waste recycling sector according to PayScale™. Labour costs are dependent on number of shifts performed per day whereby the pelleting process has only 1 shift per day while the pyrolysis process has 2. In Table 6.3, 9 personnel are required per pyrolysis shift which is comparable to a 200 kg/h plant [30].

Table 6.3: Annual median salaries of workers in the paper, plastic, and waste recycling sector

Job title	Number of operators per shift		Median annual salary (R/year)
	Pelleting	Pyrolysis	
Sorter/ laborers	*6	3	R52 000
Maintenance supervisor	1	1	R243 000
Production Foreman	1	1	R260 000
Production operators	2	2	R121 000
Shift operator	-	2	R86 500
Reference	[357]	[30]	PayScale™

*The inclusion of a hand-sorting line will require 6 sorters (Figure 6.2), otherwise no sorters/ laborers required.

6.2. The pelleting processes methodology

6.2.1. Pelleting line configuration

6.2.1.1. Composition of the pulper rejects

To calculate the ash and energy content of the produced SRF, the composition of the rejects must be provided. The composition of the pulper rejects was estimated according to experimental results. Whereby, the moisture (M) and ferrous metal content (Fe) for the rejects was described in section 5.1.1. Section 5.1.2 described how the organic fraction was separated into three fractions as fibres (PPC), plastics (P) or other organic residue (OOR). Lastly, the presence of non-ferrous metal and other inorganic residue (NFM & OIR), like aluminium (Al) was evident in the char product (Figure 5.15). The composition of NFM & OIR in the dry rejects was calculated by assuming 75 wt.% of the ash from vacuum char (VC) produced at highest pyrolysis temperature (550 °C) was NFM & OIR. This VC was used for the calculation because it represents material after significant devolatization. Whereby in section 5.4.4, the pyrolysis of rejects at 550 °C produced VC at a yield of 22.9 wt.% (Figure 5.16), containing 41.2 wt.% ash (Figure 5.17). Consequently, the NFM & OIR content was determined as 4.0 wt.% (Table 6.4). The wet and dry composition of the pulper rejects is provided in Table 6.4, whereby the rejects are split into the 6, above mentioned components.

In Table 6.4, each component is assigned a specific ash content (AC) and HHV [32], [162]. The ash content and HHV of SRF is calculated as a weighted average of its components. However, the moisture content will affect the HHV of the SRF, and Equation 6.3 provides a means of calculating

the HHV of the SRF (HHV_{wet}) from the HHV calculated as a weighted average (HHV_{dry}) and moisture content of the SRF (x_{H2O}) [35], [118]. The HHV and ash of the SRF from the model are compared against that determined experimentally and shown in the Economic Results (Section 6.4.1).

$$HHV_{wet} = HHV_{dry} \times (1 - x_{H2O}) - (0.02443 \times x_{H2O} \times 100)$$
<div align="right">Equation 6.3</div>

Table 6.4: The composition of the waste stream and ash and energy content of components

Fraction	Moisture	Ferrous metal	NFM & OIR	Paper	Plastics	OOR
Abbreviation	M	Fe	Al	PPC	P	OOR
Wet composition (wt.%)	46.40	7.23	4.00	4.69	30.20	7.48
Dry composition (wt.%)	5.90	12.70	7.07	8.23	53.00	13.10
Specific AC (wt.%)	-	100	100	10.7	2.4	10
Specific HHV (MJ/kg)	-	-	-	13.5	41.4	6.3
Reference				[60]	[100]	[32]

6.2.1.2. Process line configuration

The pelleting process consists of units configured in series. Each unit performs a binary separation of the incoming stream to produce a main output and secondary stream. The main output stream forms the incoming stream for the next unit and the secondary stream is a by-product, to be sent to landfill or be an additional revenue stream like scrap metal. The main output from the final process unit is the SRF product. A method of evaluating the composition of the main output stream after each unit in the process is the "recovery factor transform function (RFTF) matrix" [32], [39], [162], [358].

For this method, the waste stream is subdivided into various components and each assigned an HHV and ash content as described in section 6.2.1.1. The mass flowrate of each fraction in the incoming stream is represented by a vector, **U**. The RFTF of each process unit is a square, diagonal matrix, **R**, with the same number of columns and rows as fractions in the stream. Each element in **R** is a value between 0 and 1, representing a percentage of the corresponding fraction that is recovered in the main output stream. Hence the product of **U** and **R**, will form the mass flowrate of the fractions in the main output stream, **X**, i.e. **U. R=X**. Due to the conservation of mass, all the material not in the main output stream, must be in the secondary stream and therefore the diagonal matrix **R'** represents the fraction to secondary stream. The matrix, **R'** is the subtraction of R from the identity matrix, i.e. **R'=I-R** and consequently the multiplication of **R'** and **U** will form the mass flowrate vector in the secondary stream, **Y**. Therefore, **Y=R'. U=(1-R). U.**

The RFTF matrix used for the SRF conversion line is shown in Table 6.5, with most values taken from 3 sources [32], [90], [108]. The recovery factor of 0.3 was allocated for the direct dryer as seen in literature [32], and 0.2 was assumed for the indirect dryer due to its capability to reduce the

moisture content by 80 wt.% [359]. The RFTF matrix method was implemented with MS Excel and able to compare multiple lines w.r.t to SRF quality, process efficiency and economic feasibility.

Table 6.5: Recovery factor transfer function (RFTF) matrix used for the SRF conversion process

Key:	Equipment	Moisture	Fe	Al	PPC	Plastics	OOR
S	Shredder	0.8	1	1	1	1	1
M	Hammermill	0.7	1	1	1	1	1
T	Trommel screen	0.85	0.8	0.8	0.85	0.9	0.25
PT	Preliminary screen	0.69	0.41	0.37	0.69	0.62	0.11
MS $_{electromagnet}$	Magnetic separator	1	0.05	1	0.98	0.97	0.99
MS $_{permanent}$	Permanent overhead magnet	1	0.2	1	1	1	1
HS	Hand sorting	1	0.9	0.5	1	1	0.9
dD	Direct dryer	0.3	1	1	1	1	1
indD	Indirect dryer	0.2	1	1	1	1	1
DE	Densifier/ Baler	0.6	1	1	1	1	1
P	Pelletizer	1	1	1	1	1	1

6.2.1.3. Feedstock capacity and operating shifts

Solids-handling lines can and should be operated on a shift-basis because they do not have to undergo plant start-up like chemical plants and often require maintenance [32]. Solid lines are often operated with one to two 7-hour shifts per day [32], [162], [360], whereby a line processing less than 10 ktpa is liable for only one, 7 hour shift per day [360]. Consequently, as calculated in Equation 6.4, the SRF line will operate for *ca.* 1848 h/year which excludes the time for equipment maintenance, setup, and cleaning. At the annual operating hours of 1848, the incoming flowrate of pulper rejects is 1.89 t/h and nearer to unit capacities of other RDF conversion lines in Table 6.6.

$$7 \, \frac{\text{hours}}{\text{shift}} \times 1 \, \frac{\text{shifts}}{\text{day}} \times 22 \, \frac{\text{days}}{\text{month}} \times 12 \, \frac{\text{months}}{\text{year}} = \, 1848 \frac{\text{h}}{\text{year}} \qquad \text{Equation 6.4}$$

6.2.2. CAPEX and OPEX estimation

6.2.2.1. Purchase cost of equipment (PCE) and electrical power demand

The purchase cost of equipment (PCE) for the pelleting process was based off the unit cost and flowrate from other projects as provided in Table 6.6. All the units in Table 6.6 used a scaling factor of 0.8. The units used for each process configuration were costed and summated to attain the PCE. The only units that were not costed according to this method are the direct - and indirect dryer configurations, which were costed according to heuristics of Couper, 2009 [348] or Mujumdar, 1988 [361] as demonstrated in Appendix H. The indirect dryer configuration included a steam-tube dryer, a storage tank for steam condensate and a pump to transport the condensate back to the boiler. These ancillary units can be seen in the base-case example in Figure 6.2. Likewise, the direct dryer configuration, as seen in Figure 6.2, consisted of a direct rotary dryer, a blower, and an air heater to increase the inlet air temperature. The direct and indirect dryer were designed to decrease moisture

content by 70% and 80%, respectively (Table 6.5). The electrical power requirements used for the OPEX of each unit are included in Table 6.6. The units were provided with either a power rating (kW) or specific energy rating (kWh/ton) for electrical requirement, as shown in Table 6.6.

Table 6.6: Units used for the SRF conversion line

Equipment	Symbol	Unit cost	Capacity	Power	Energy	Reference	
(-)	(-)	(€ or $)	(t/h)	(kW)	(kW/ton)	Cost	Power
Densifier/ Baler	DE	€206 600	6	-	26.67	[32]	Quote
Hammermill	M	€129 100	2	200	-	[32]	[32]
*Hand-sorting line	HS	€5 000	-	0.6	-	[162]	[32]
Magnetic separator	MS electro	€36 150	5	8	-	[32]	[362]
Overhead magnet	MS perm	€7 300	4.3	-	-	[300]	-
Pelletizer	P	$530 000	5	-	45	[32]	[363]
Pre-trommel	PT	€35 300	15	-	1.33	[300]	[32]
Shredder	S	€11 700	0.4	-	20	[300]	[29]
Trommel	T	€103 300	15	-	1.33	[32]	[32]

*Capacity did not influence cost of Hand-sorting conveyor.

6.2.2.2. Fixed capital investment (FCI) of pelleting line

The modified Lang factors used for the FCI calculations are shown in Table 6.7 and based off the Lang factors in Sinnott, 2005 [297] and a waste-to-WDF line, which modified the solids-handling Lang factors [31]. The total physical plant cost (PPC) is the product of the PCE and the direct factors, $f1$ to $f6$, as shown in Table 6.7. The FCI was calculated from the product of indirect factors, $f7$ to $f9$, and the PPC as shown in Table 6.7. The Lang factors for utilities, storage, site development and ancillary buildings are ignored because it is an annexed facility [31], [297].

Table 6.7: Lang factors used for calculation of total capital investment of SRF conversion

Total capital investment (TCI) contributor	Heuristic	Reference
Major equipment cost, total purchase cost	PCE	
$f1$ Equipment installation	0.5 × PCE	[297]
$f2$ Services & site preparation	0.3 × PCE	[31]
$f3$ Piping	0.15 × PCE	[31]
$f4$ Buildings	0.1 × PCE	[297]
$f5$ Instrumentation	0.1 × PCE	[31]
$f6$ Electrical	0.1 × PCE	[31], [297]
Plant physical costs: PPC= PCE× (1+$f1$+…+$f6$) = PCE ×	2.30 × PCE	
$f7$ Overheads and contingency	0.15 × PPC	[31]
$f8$ Construction and contractor's fees	0.05 × PPC	[31], [297]
$f9$ Design and Engineering	0.1 × PPC	[31], [297]
Fixed capital investment: FCI = PPC×(1+$f7$+$f8$+$f9$) = PPC×	1.35 × PPC	

6.2.2.3. Variable operating costs (OPEX)

Although the process units described in section 6.2.2.1 used electricity, the direct and indirect dryer configurations required steam. Steam is produced in a pulverized coal boiler on-site and requires coal for heating and process water. The steam produced on-site is either medium pressure steam (MPS) at 5-bar for indirect drying in a steam-tube dryer [361] or low-pressure steam (LPS) at 2-bar for heating the drying air for direct drying [347]. The mass of coal required to produce LPS or MPS can be calculated according to the mass of steam required and the enthalpy difference between steam and feed water (H_{steam}-H_{water}), as shown in Equation 6.5. The HHV of bituminous coal in South Africa is 19 MJ/kg [323], [364] and a boiler efficiency taken as 70%, also influence the coal requirement. Appendix I provides sample calculations used for calculating the mass of steam and water required for the direct and indirect dryer requirements. The cost of coal and process water is taken as R400 per ton [354], [365] and R25.37 per Kl [4], respectively. Fixed OPEX is determined from labour costs and FCI as explained in section 6.1.3.2.

$$m_{coal}\,(kg/h) = m_{steam}(kg/h) \times \frac{H_{steam}-H_{feed\,water}(kJ/kg)}{HHV_{coal}(kJ/kg)\times\eta_{boiler}(\%)}$$

Equation 6.5

6.2.3. Evaluating the pelleting process

6.2.3.1. Base-case process line

The base-case scenario (BC) was a line meant to simulate the experimental process followed to convert as-received pulper rejects into Ø6 mm SRF pellets. The BC is shown in Figure 6.2 and it includes two magnetic separators in series (MS $_{perm}$). Followed by a hand-sorting line (HS) to extract glass or ballistics from the sample. The material was then dried in rotary-air dryer (tunnel greenhouse experimentally), followed by a steam-tube dryer (oven dryer experimentally) before being shredded to 4 mm, pelleted to 6 mm and lastly, weighed on a weighbridge before storage and resale.
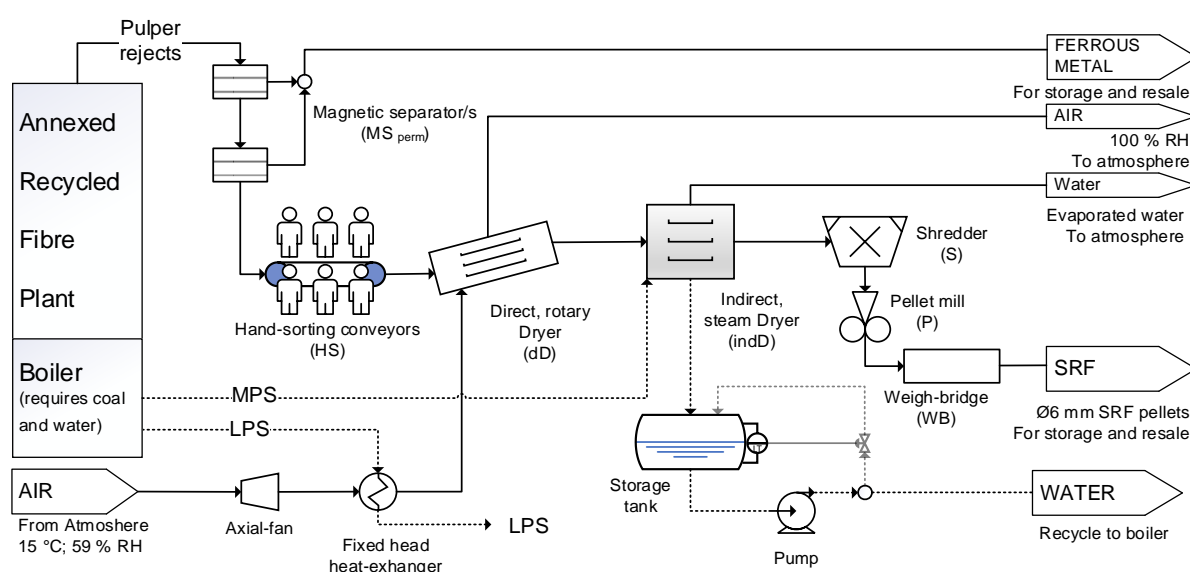
Figure 6.2: PFD of the base-case scenario (BC) for the pelleting process.

6.2.3.2. Comparable process lines

11 process lines that are similar to the base-case scenario were tested using the RFTF matrix method explained in Section 6.2.1.2. The 11 lines are shown in Table 6.8 and the main differences between the lines are given. As shown in Table 6.8, all the process lines consisted of a metal separator and a direct dryer (dD), indirect dryer (indD) or both. Magnetic separation was performed using a permanent magnet (MS $_{perm}$) or electromagnetic separator (MS $_{electro}$) and employed prior to shredding (S) to avoid equipment damage. The effect of using a hand-sorting conveyor (HS) was tested, whereby lines 1,2, 8 and 9 of Table 6.8 did not used as HS unit. In addition, HS was employed early in the process line and not on shredded material.

Table 6.8: The BC line and ten process lines used for comparison

Line #	Line configuration	Description
BC	MS $_{perm}$ – MS $_{perm}$ – HS – dD – indD – S - P - WB	Base case (BC) example
1	MS $_{perm}$- dD – indD – S – P - WB	One MS $_{perm}$ and no HS
2	T - MS $_{perm}$ – S – indD – P - WB	Begin with trommel (T) and no dD
3	MS $_{perm}$ – HS – S – dD – indD – P - WB	1 MS $_{perm}$ and S before dD
4	MS $_{perm}$ – HS – S – MS $_{electro}$ - dD – indD – P -WB	MS $_{electro}$ after shredding
5	HS - MS $_{perm}$ – MS $_{perm}$ – S – dD – indD - P - WB	HS to begin and S before drying
6	MS $_{perm}$ – MS $_{perm}$ – HS - S – dD – indD – P - WB	Same as BC but S before drying
7	HS - MS $_{perm}$ – S – dD – indD – P - WB	Same as line 3 but 1st 2 units swap
8	MS $_{perm}$ – S – dD -indD – P - WB	Same as line 2 but S before dD
9	MS $_{electro}$ - S – dD – indD – P - WB	Swap MS $_{electro}$ with MS $_{perm}$
10	MS $_{electro}$ – HS – S – dD – indD – P - WB	Like line 3 but MS$_{electro}$ with MS$_{perm}$
11	MS $_{perm}$ - MS $_{perm}$ – S – dD -indD – P - WB	Like lin 8, but two MS$_{perm}$ to begin

6.2.3.3. Process efficiency evaluation of SRF

The simplest means of comparison of solid waste lines is the mass efficiency of the process (MEC) [108]. It is a comparison of the mass of wet SRF (m_{fuel}) to wet waste feed ($m_{feedstock}$), as shown in Equation 6.6. The GEC and NEC were calculated similar to the experimental procedure, although the LHV was used instead of the HHV [108], [366]. The NEC includes energy for electricity and drying duty and both GEC and NEC are reported on a dry basis to avoid values over 100% [108].

$$MEC(\%) = \frac{m_{SRF}\ (kg/h)}{m_{feedstock}\ (kg/h)}$$

Equation 6.6

$$GEC\ (\%) = \frac{|m_{SRF}\ (kg/h) \times LHV_{SRF}\ (MJ/kg)|}{|m_{feedstock}\ (kg/h)\ \times LHV_{feedstock}(MJ/kg)|}$$

Equation 6.7

$$NEC_{SRF}\ (\%) = \frac{|m_{SRF}\ (kg/h) \times LHV_{SRF}\ (MJ/kg)| + E_{elec.power}(MJ/h) + H_{drying}(MJ/h)}{|m_{feedstock}\ (kg/h) \times LHV_{feedstock}\ (MJ/kg)|}$$

Equation 6.8

6.2.3.4. Selling price of SRF and ferrous metal

The Indian Ministry of Housing and Urban Affairs [40] gathered information from cement kilns in India and developed a correlation for determining selling price of RDF depending on its LHV. This correlation, when converted from INR per kcal/kg to ZAR per MJ/kg shows the minimum and maximum correlation cost of RDF to be R22.94 and R45.89 per MJ/kg, respectively [40]. The maximum correlation value for selling price was used as shown in Equation 6.9. This correlation was used because the WDF adhered to quality tests (SRF), had uniform particle size (pellets) and was similar to processed RDF used in Egyptian cement kilns costed at R1060 per ton ($64 per ton) [41]. According to Equation 6.9, SRF with an LHV of 25 MJ/kg would cost R1 150 per ton. The market value for the ferrous metal by-product is a constant value of R 2 per kg, but was only considered a product if it was at least 95 wt.% ferrous metal [31].

$$\text{Market value}_{\text{SRF}}\left(\frac{\text{R}}{\text{ton}}\right) = \left[\text{LHV}_{\text{SRF,wet}}\left(\frac{\text{MJ}}{\text{kg}}\right) \times 45.89\left(\frac{\text{R}}{\text{(MJ/kg).ton}}\right)\right] \qquad \text{Equation 6.9}$$

6.3. The pyrolysis processes methodology

6.3.1. Pyrolysis line configuration

The feedstock composition, product yields and HHV from pilot-scale experiments were input to an Aspen Plus model, based off that from Petersen [29]. The model design is explained in Appendix J and K. The mass and energy balance data from the model was then used for the economic analysis.

6.3.1.1. Composition and capacity of feedstock

Pyrolysis processes, as for most processes involving gas and liquid lines, must be run continuously. An annual operating time of 8000 h (91% availability) has been assumed for pyrolysis processes [29], [350]. This project is assumed annual operation of 7884 hours (90% availability). Hence, the hourly capacity of wet rejects is 442 kg as shown in Table 6.9, calculated from the annual capacity of 3.48 Kt and the operating hours. Treated, dried rejects have a capacity of 218 kg/h and generally considered small-scale according to case-studies of similar capacity [29], [30], [307], [367]. Table 6.9 provides the composition of the as-received rejects used for the Aspen Plus model, whereby the organic fraction are components; Al, P, PPC and OOR (Table 6.4) fed to the pyrolysis reactor.

Table 6.9: The flowrates for the incoming flowrates used for the model

Fraction	Organic (NC Solid)	Water (Mixed)	Metal (C Solid)	Total
Flowrate (kg/h)	205	205	32.0	442
Composition (wt.%)	46.4	46.4	7.2	100

6.3.1.2. Overview of process

The BFD of the pyrolysis process (Figure 6.3) consists of five areas. The pre-treatment, pyrolysis, combustion, and product recovery areas are ISBL and the steam and power generation area is OSBL

[302]. The PFD is provided (Figure 6.4) to show the units in each colour-coded area. The received pulper rejects are first milled, extracted of ferrous metal, dried, and pelleted in the **pre-treatment area** and sent to the **pyrolysis section.** Rejects, with inert gas enter the jacketed pyrolysis reactor (R-201) to be converted to condensable volatiles, NCG, and char. The reactor is heated from the combustion of recycled NCG (F-401) to maintain the reactor temperature at 450, 500 or 550 °C. The flue gas was assumed to be at the same temperature as the combustor, which was kept above 1100 °C, to degrade any chlorine (Cl) that might be present [46]. Char is separated from volatiles in a cyclone (S-201) and the hot volatiles enter the **product recovery** section. Here, the volatiles are quenched in two exchangers (E-301 and E-302) to lower their temperature to 260 and 100 °C, respectively using boiler feed water (BFW). The cooler vapours are sent through a fractionation condensation train (C-301 to C-304), imitating the pilot-scale setup. The first condenser is maintained at 56 °C and the next three condensers are at 20, 12 and 10 °C, respectively. The condensers use refrigerated water (RW) in a cascade system, with the fourth condenser first using RW. A decanter (D-301) separates the aqueous phase oil, leaving the mixture of wax and organic phase oil to be sold as heavy fuel oil (HFO).

The steam Rankine cycle of the **steam and power generation** area provided the cooling duty to quench the volatiles (E-301 and E-302), and to cool the flue gas (E-402). The heat would be transferred to the pressurized BFW to vaporize the stream so that it could generate electricity in a steam turbine (T-501), generate steam for the indirect dryer (I-101) and generate electricity in a subsequent steam turbine (T-502). Process integration included recycling chilled water from a refrigeration unit (E-303) to provide cooling duty for the condensers, recycling the NCG from the product recovery section to be used as inert gas in the pyrolysis reactor (R-201) or fuel for the pyrolysis furnace (F-401). Whereby, 4 to 5 kg/h of NCG (based off N_2 flowrate used experimentally) could be used as sweeping gas. The **combustion** area produced large quantities of CO_2 rich flue gas, which was used for drying in the **pre-treatment area** before being released to the atmosphere.
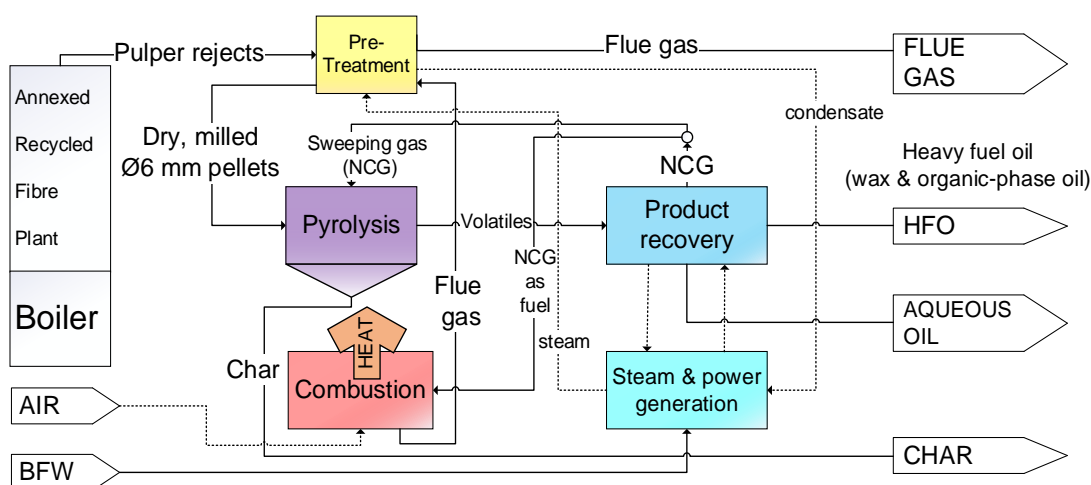
Figure 6.3: BFD of the pyrolysis plant, as adapted from Petersen, 2020 [29].

6.3.1.3. Process Flow diagram (PFD)
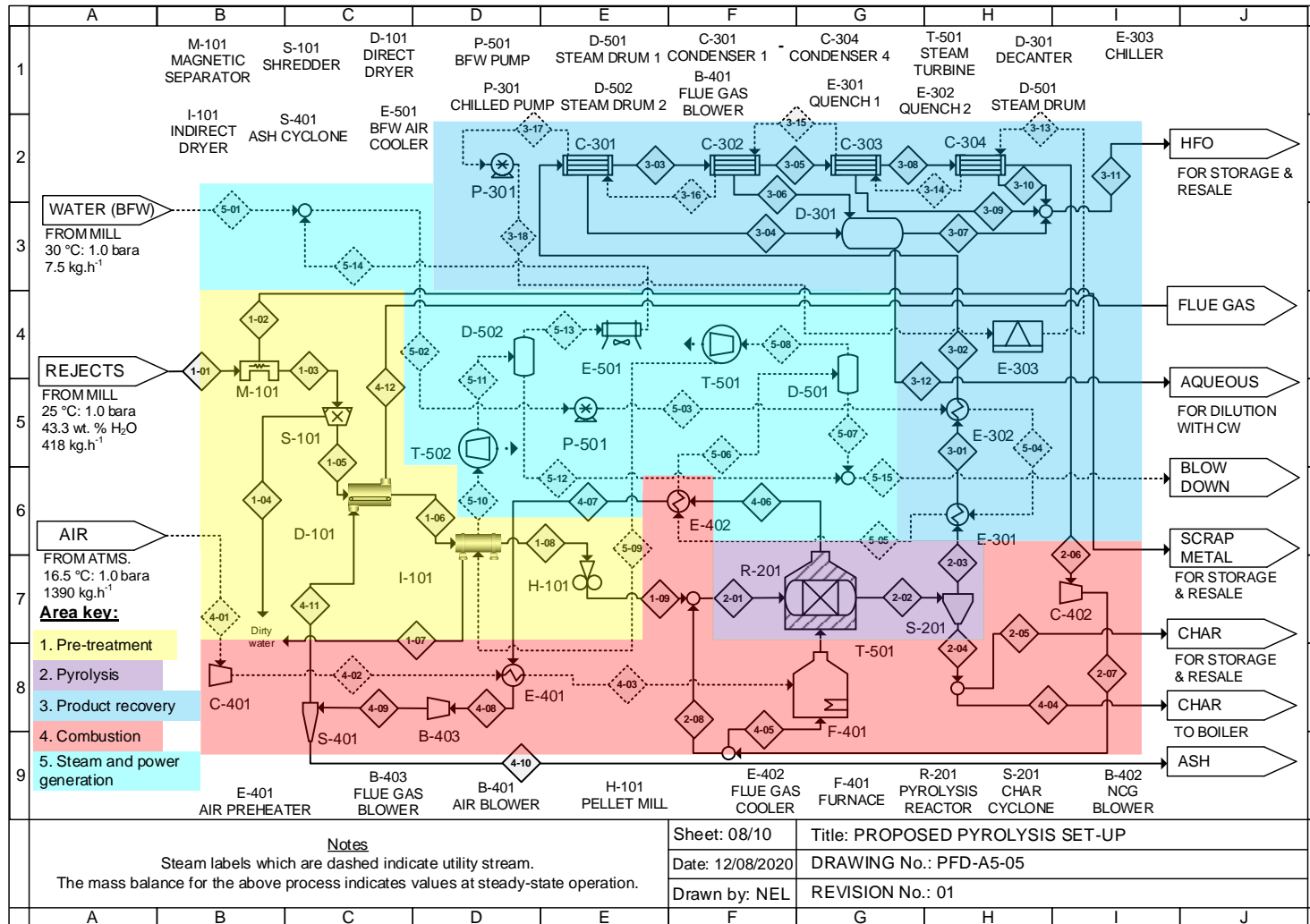
Figure 6.4: Process flow diagram (PFD) for the pyrolysis process

103

6.3.1.4. Product yields

For the Aspen Plus model, an *RYIELD* reactor was used to convert the rejects into the pyrolysis products. The product yield of the NCG, char and condensable product (including its three fractions) were taken from the pilot-scale experimental results. These yields were then normalized to avoid convergence issues in the model. The normalized yields used in the model are shown in Figure 6.5, with each phase colour coded according to the temperature from pilot-scale (450, 500 or 550 °C).
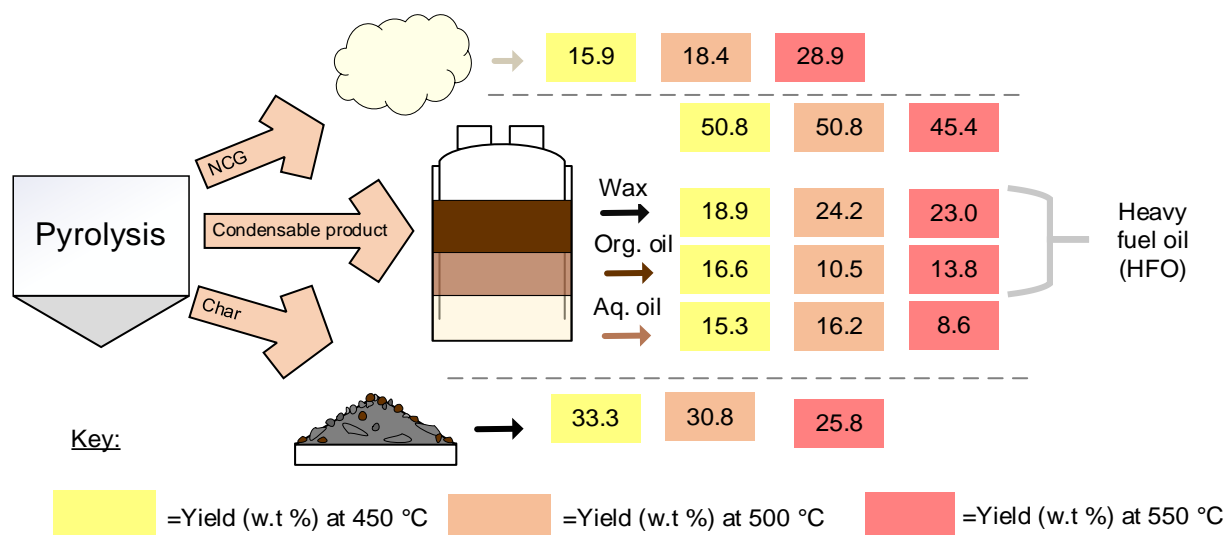
Figure 6.5: Normalized product yields of the main products of pyrolysis at the different temperatures

Due to the complex composition of the condensable product and char, model components were used to represent the contained compounds present. The yield for the model components used for each phase and temperature are shown in Figure 6.6. The alkanes produced from the pyrolysis of plastics were assumed to be either dissolved in the organic oil or wax phase. As shown in Figure 6.6, the 3 alkane compounds that dissolved in the organic phase oil were C_8H_{18}, $C_{12}H_{26}$ and $C_{16}H_{34}$ and three alkanes in the wax phase were $C_{18}H_{38}$, $C_{24}H_{50}$ and $C_{30}H_{62}$. The yield distribution of each alkane compounds at 450, 500 and 550 °C was based off condensable product from the pyrolysis of plastics and shown in Figure 6.6 [240], [283], [367], [368]. As shown in Figure 6.6, the organic phase is comprised of 13 compounds, of which 3 are from plastics and the rest from fibres. As shown in Figure 6.6, Levoglucasan (LGA) and 5-hydroxymethylfurfural (HMF) are the main components in the organic phase from fibres, with yields based off that from PWS, paper and biomass bio-oil [204], [239], [240]. The only other carbohydrate-derived compound in organic phase was 2-cyclopenten-1-one, which was also included in Figure 6.6 [204]. The other 6 components in the organic phase were lignin-derived components that were evident in the bio-oil from PWS [204] and biomass [240]. These components are shown with their total yield (almost negligible) in Figure 6.6. The aqueous phase oil is shown in Figure 6.6 to be 70 wt.% water for all the temperatures and 6 other components that were derived from carbohydrates. The carbohydrate derived components in the aqueous phase were based off compositions in bio-oil seen in the pyrolysis of PWS [204], fibre [239] and biomass [240].

The yields of the 6 components are shown in Figure 6.6. Appendix J.4 shows the composition of the trace amounts of carbohydrate and lignin-derived components in more detail.
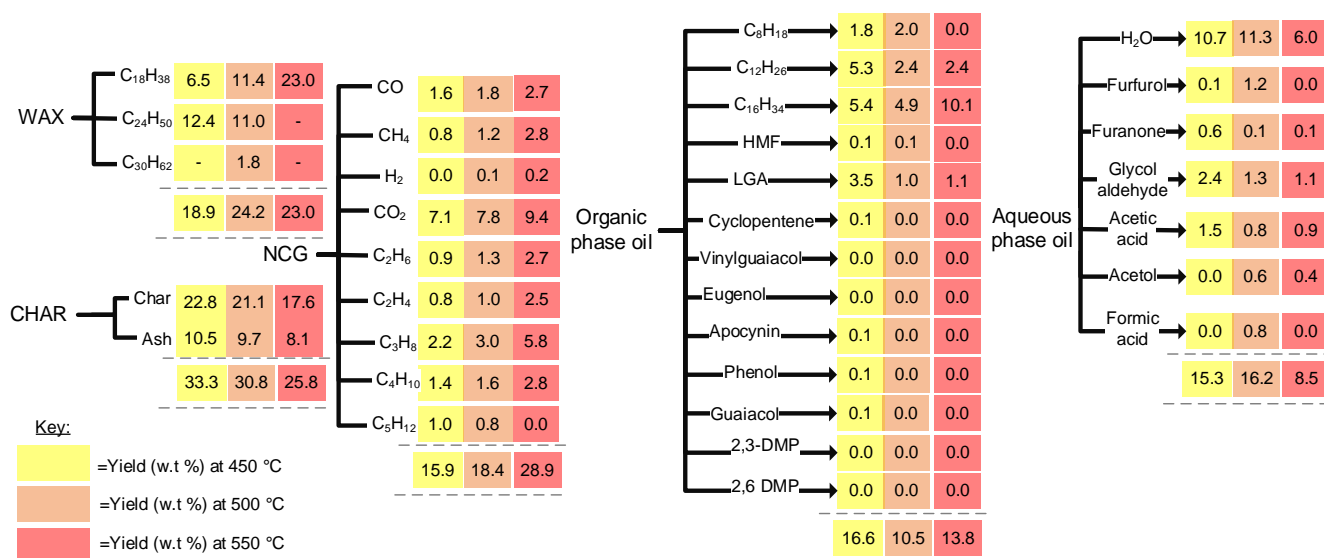
Figure 6.6: Normalized product yields of the fractions of the condensable product

6.3.2. CAPEX and OPEX estimation

6.3.2.1. Calculating the variable costs

The utilities used for the power, heating, and cooling requirements for the pyrolysis process are shown in Table 6.10. Table 6.10 includes the units from the PFD (Figure 6.4) that use each utility. Most of the process units for the pyrolysis process use electricity, as seen in Table 6.10. All pumps and compressors were assumed to use electricity, because none of the units had high power requirements, exceeding 150 kW, rendering for them to be driven by steam. The direct dryer (D-101) and reactor (R-201) both use electricity to rotate the shell and vessel. The air cooler, E-501, used fans with a power rating of 2.5 kW for blowing air [347].

Table 6.10: The utility requirements for the different process units

Energy	Utility	Process units
Power	Electricity	S-101; D-101; H-101; R-201; P-301; E-303; B-402; E-401; P-501; E-501
Heating	MPS	I-101
	NCG	F-401
Cooling	BFW	E-301; E-302; E-402
	RW	C-301; C-302; C-303; C-304
	Air	E-501;

Heating demand is needed for the furnace (F-401) to supply the energy for the reactor (R-201) and the indirect dryer (I-101). NCG supplies the furnace with fuel, with no additional char required like that previously observed for other case-studies [29]. The cooling demand is met with three utilities as shown in Table 6.10. BFW cools down the vapours exiting the reactor (E-301 and E-302) and flue

105

gas exiting the furnace (E-402). RW was recirculated through the 4 condensers to provide the low temperature cooling between 10 and 30 °C. The chiller, E-303 would cool down the refrigerated water back to 5 °C after condenser 4 using electricity, determined from duty and coefficient of performance (C.O.P) assumed as 4 [29]. All heat-exchanges are considered counter-current and most units use a minimum approach temperature (MAT) of 10°C, except for two cases; *viz.*, the air cooler (E-501) with a MAT of 22 °C and process units using refrigerated water with a MAT of 5 °C [347]. The air cooler assumed that an air inlet temperature of 30 °C. Fixed OPEX is determined from labour costs and FCI as explained in section 6.1.3.2.

6.3.2.2. Total capital investment (TCI) calculation

The units for the pyrolysis process were costed according to heuristics from Couper, 2009: Chapter 21 [348] or Seider et. al., 2009: Chapter 22 [351]. The units for sizing were taken from Couper 2009: Rules of thumbs [347]. Appendix G provides the sample calculations used for costing each process unit. The exchange rate, CEPCI indexes and location factors were included in the cost calculation. Table 6.11 provides the calculation for the total direct costs (TDC), indirect costs (IDC) and fixed capital investments (FCI) and their breakdown for the 'biorefinery method'. As seen in Table 6.11, the direct costs are a percentage of the PCE for the areas that are ISBL.

Table 6.11: Calculation of total direct cost, indirect cost, and fixed capital investment for the biorefinery method

Major Equipment PCE:	ISBL
$f1$: Warehouse	0.04
$f2$: Site development	0.09
$f3$: Additional piping	0.045
Total Direct Cost (TDC)	TDC = ISBL x (1 + 0.175)
$f4$: Prorate able expenses	0.1
$f5$: Field Expenses	0.1
$f6$: Home office & construction fees	0.2
$f7$: Project contingency fees	0.1
$f8$: Other costs	0.1
Indirect cost (IDC)	IDC = 0.6 x TDC
Fixed Capital Investment (FCI)	FCI = TDC + IDC

6.3.3. Evaluation of results from the pyrolysis process

6.3.3.1. Process lines for pyrolysis

The pyrolysis process is an altered Aspen Plus model designed by Petersen for a pulper rejects feedstock [29], with updates such a four-stage condensation train to imitate the pilot-scale setup and a steam-Rankine cycle to supply cooling for hot vapours, whilst generating electricity and steam on-site [302]. The pyrolysis product yields from each temperature tested on pilot-scale, i.e., 450, 500 and 550 °C were input to the model for comparison against each other on the mill capacity scale.

6.3.3.2. Process efficiency evaluation of pyrolysis

The products of the pyrolysis process were fuel oil and char. Fuel oil is a mixture of organic phase oil and wax, without aqueous phase oil and char is the solid residue post pyrolysis. The efficiency considers the energy of the fuel oil ($E_{fuel\ oil}$), NCG (E_{NCG}), char (E_{char}) and feedstock ($E_{feedstock}$), calculated from the product of mass and experimental HHV as shown in Equation 6.10 (for the example of char). This can then be used to attain the GEC, as shown in Equation 6.11 and then the NEC, as shown in Equation 6.12. The NEC is an extension to the GEC whereby the heating, cooling and power demand is included. The heating and cooling demand is the energy demand after heat exchange. The NEC is shown w.r.t including and excluding the NCG for comparison against the pilot-scale results. The overall NEC will include the NCG phase.

$$E_{char} = |m_{char}\ (kg/h) \times HHV_{char}\ (MJ/kg)| \qquad \text{Equation 6.10}$$

$$GEC(\%) = \frac{E_{char} + E_{fuel\ oil} + E_{NCG}}{E_{feedstock}} \qquad \text{Equation 6.10}$$

$$NEC(\%) = \frac{|E_{char}\ (MJ/h) + E_{fuel}\ (MJ/h) + E_{fuel}\ (MJ/h)| + E_{elec.}(MJ/h) + Q_{heat}(MJ/h) + Q_{cool}(MJ/h)}{|E_{feedstock}\ (MJ/h)|} \qquad \text{Equation 6.11}$$

6.3.3.3. Pricing of fuel oil

The fuel oil is made up of the waxy and organic phase oil, without the aqueous phase oil. This fuel oil can be priced as a fuel oil, if not further upgraded. The price of fuel oil depends on its HHV as identified by the World Bank Group [41] - the price of fuel oil for Egyptian cement kilns is equivalent to R0.127/MJ of fuel (converted from $7.65/GJ) as shown in Equation 6.12. Hence fuel oil with an HHV of 40.2 MJ/kg is priced at R5.1/kg, and this correlation is almost half that used for fuel oil from the pyrolysis of rejects ($15.9/GJ) [29]. Similarly the price of R5.1/kg is less than the average price of crude oil in 2019, at R6.4/L ($61/bbl.) [369]. Therefore, the price of fuel oil is not expected as over-valued according to the correlation.

$$\text{Market value}_{fuel\ oil} \left(\frac{R}{kg}\right) = \left[HHV_{fuel\ oil} \left(\frac{MJ}{kg}\right) \times 0.127 \left(\frac{R}{(MJ/kg)}\right) \right] \qquad \text{Equation 6.12}$$

6.3.3.4. Pricing of char

Char is costed by a corelation for petroleum coke (Petcoke) used by the World Bank Group for Egyptian cement kilns [41]. The correlation, shown for Equation 6.13, used for the cost of char is R0.078/MJ (converted from $4.73/GJ) and hence char produced at 500 °C, with an HHV of 27.6 MJ/kg will cost R2.2/kg [41]. This cost of Petcoke is comparable to the price stipulated in another article for the price in Jordan at $150/ton or R 2.5/kg [322].

$$\text{Market value}_{char} \left(\frac{R}{kg}\right) = \left[HHV_{fuel\ oil} \left(\frac{MJ}{kg}\right) \times 0.078 \left(\frac{R}{(MJ/kg)}\right) \right] \qquad \text{Equation 6.13}$$

6.4. Results for the pelleting processes

6.4.1. Model validation

6.4.1.1. Attributes of the SRF product

The moisture content, LHV and ash content of the SRF product from the model (BC line) was compared against the SRF produced experimentally. Table 6.12 provides the difference between the three attributes when determined experimentally and according to the RFTF model. In Table 6.12, it can be seen that the moisture content of the SRF from the model is 5.07 wt.% and 0.84% less than that determined experimentally, which is provided in section 5.1.1 and 5.2.2.1. The LHV of the SRF produced from the BC was 28.9 MJ/kg and only 0.8 MJ/kg less than that determined experimentally in Section 5.2.2.1. Lastly, the ash content from the SRF from the BC is 9.05 wt.% and more than 8.65 wt.% determined experimentally as explained in Section 5.2.2.2.

Table 6.12: Difference between the characteristics of SRF predicted from the model and experimentally

Attributes	Experimental		Model
Moisture content (wt.%)	5.90	Section 5.1.1 or 5.2.2.1	5.07
LHV (MJ/kg)	29.7	Section 5.2.2.1	28.9
Ash content (wt.%)	8.65	Section 5.2.2.2	9.05

6.4.1.2. Efficiency and energy characteristics of the pelleting model

Some qualities of the BC line and the 11 process lines are introduced in Table 6.13. The number for each line from Table 6.13, corresponds to the 11 process lines, and BC, described in Table 6.8. The first three columns for Table 6.13 correspond to the mass conversion (MC), gross energy conversion (GEC) and net energy conversion (NEC) described in section 6.2.3.3.

The MC for each line is provided on a wet-basis and hence most of the mass loss relates to water. The MC is shown to range between 43.2 to 50.1 wt.% with the lowest MC observed for the BC example. The GEC of Table 6.13 shows that all, but one process line, have a GEC higher than 97.5% while line 2 has a GEC of 87.5% due to the use of a trommel which loses some organic fraction. This result signifies that a trommel is not appropriate for SRF production, but better for "landfill mining" cases to produce several products [32], [39]. Most of the process units use electrical energy for running, which does not significantly affect the NEC, with a difference of only 1% to 3% between the NEC and GEC being observed for units running solely on electricity. Conversely, the incorporation of a direct and indirect dryer significantly increases the energy demand of the process and decreases the NEC from the GEC by about 10 to 15 % as seen for all the processes in Table 6.13. In Table 6.13 the NEC ranges from 80.2% to 88.3%, with the highest GEC of 88.3% observed for lines 8 and 11. The energy use of the direct and indirect dryer on a kilogram of entering feed basis is shown in Table 6.13. In Table 6.13, the direct dryer uses between 3.1 to 3.6 MJ/(kg wet feed), except for line

2 without a direct dryer (Table 6.8). Additionally, the energy consumption for the indirect dryer is lower due most of the water being driven removed in the direct dryer. However even for line 2, the indirect dryer is less energy intensive than the direct dryer, using 1.27 MJ/(kg wet feed). All the other indirect dryers can be shown to use within 0.62 to 0.77 MJ/(kg wet feed) as shown in Table 6.13. Lastly, the specific energy use for the process lines in Table 6.13 ranges from 135 to 250 kWh/ton of pellets produced and was lowest for stream 2 due to its exclusion of the direct dryer and lines 8, 9 and 11 all had values under 200 kWh/ton.

The results shown in Table 6.13 are congruent to values seen in literature for pelleting processes. The best conversion lines for an MSW conversion facility were shown to have MC that ranged from 38.6 to 62.8 wt.% for a line processing MSW [32]. The MC results from Table 6.13 are in the high range seen for MSW-to-WDF facility, because C&IW has fewer contaminants than MSW [32]. The GEC of a biomass pelleting process was recorded as 92% according to a biomass pelleting study [34]. The NEC for the same study and another for biomass pelleting process, was shown to range between 79% to 88% [34], [299]. The energy consumption of direct dryers has been observed to be between 2 to 3 MJ/(kg dry feedstock) [25], [370] and hence, the results in Table 6.13 indicate energy demand in the high range. Conversely, the energy demand for direct and indirect dryers is 4 to 6 and 2.8 to 3.6 MJ/(kg water), respectively [359] - indicating the lower energy demand for indirect dryers. The specific energy from 5 different biomass pelleting procedures was shown to range from 75 to 128 kWh per ton of pellets [361] for units containing one dryer, like that of line 2 in Table 6.13.

Table 6.13: Process efficiency and energy use data of the 12 tested lines

Line #	Process Efficiency			Energy use		
	MC	GEC	NEC	Direct Drying	Indirect drying	Specific energy
	(wt.%)	(%)	(%)	(MJ/kg $_{feed}$)	(MJ/kg $_{feed}$)	(kWh/ton $_{pellets}$)
BC	43.5	97.7	84.0	3.62	0.77	250
1	50.1	100	86.0	3.38	0.71	223
2	43.7	87.5	80.2	-	1.27	135
3	44.6	97.7	86.2	3.25	0.66	205
4	43.2	97.5	86.0	3.31	0.67	213
5	43.5	97.7	86.2	3.29	0.67	210
6	43.5	97.7	86.2	3.29	0.67	210
7	44.6	97.7	86.2	3.25	0.66	205
8	50.1	100	88.3	3.06	0.62	187
9	48.9	99.9	88.1	3.10	0.63	193
10	43.5	97.5	86.0	3.30	0.67	212
11	48.9	100	88.3	3.10	0.63	191

6.4.2. Economic comparison between the pelleting process lines

The CAPEX and OPEX (production cost) contributions of each of the 12 process lines is shown in Table 6.14. Table 6.14 includes the minimum fuel selling price (MFSP) data of each line for two

scenarios – when the discount rate is 10% (as used by authors testing pelleting economic feasibility) and 25% (a profitable investment). Similarly, the SRF price calculated according to Section 6.2.3.4 is included for comparison in Table 6.14.

As shown in Table 6.14, Line 2 had the lowest TCI of R31.9 mil, due to lack of a direct dryer, while all the other process lines had relatively the same TCI between R38.6 mil (line 4) to R40.4 mil (line 1) with slight variations of the TCI depending on the process units used. The use of an electromagnet can be seen to increase the total capital investment by R0.72 to R0.75 mil as the case for the differences between line 8 and 9, as well as line 3 and 10 in Table 6.14. Swapping the position of units, e.g., swapping the HS and MS as in line 7 and 3, had no change on TCI. In Table 6.14, the production cost for each line is provided on a mass and energy basis and w.r.t to the SRF product. The production cost was for OPEX alone, with no amortization included. In Table 6.14, the production cost can be grouped into two categories; lines with a cost between R1 431 and R1 704 per ton that do not include a hand-sorting unit (HS) and lines with a cost between R2 041 and R2 121 per ton that include HS. The lines without a HS unit being lines 1, 2, 8, 9 and 11 also generate the lowest production cost on an energy basis, except for line 2, which has a higher cost of R74.2/GJ because it uses only one dryer and the moisture of SRF reduces its energy content (Section 6.2.1.1). As shown in Table 6.14, the moisture of SRF from line 2 (14 wt.%) also lowers the cost of SRF to R1 050/ton compared all other lines which have SRF from R1 190 to R1 330 per ton.

Minimum fuel SRF selling price (MFSP $_{SRF}$) is provided in Table 6.14, which gives an indication the price that the SRF must be raised to before the project is profitable for a given discount rate. As shown in Table 6.14, none of the process lines had an SRF price that surpassed the MFSP, even for a 10% discount rate. The lowest MFSP $_{SRF}$ was R2 430 per ton (line 8), but when including the difference between the MFSP and the SRF price (see last column of Table 6.14) it should be noted that the ratio of MFSP to SRF price was lowest for line 11, at 2.02. This represents that the SRF price must be multiplied by 2.02 before it can be considered as viable investment for a 10% discount rate and similarly, multiplied by 5.2 times before it is profitable at a discount rate of 25% (R6 270/ton). Although none of the lines showed profitability for the used economic settings, Table 6.14 shows that line 11 is the most promising due to the minimized ratio of MFSP $_{SRF}$ to target SRF price.

Although RDF has been shown interest in the South African cement industry [146], it is unknown whether SRF at its current price (according to section 6.2.3.4) would be in demand. The current fuel used in South African cement kilns is coal [371] and the domestic price of coal used for the cement industry in 2016 was estimated at R400 to R450 per ton [146] and less than half the price of SRF in the study. Hence, unless cement kilns are incentivized to substitute coal or the landfill gate fees for waste are increased significantly, it is not viable for cement kilns to pursue SRF as fuel. Pelleting lines for biomass exist in Europe and America despite incurring similar production costs (mass and

energy basis) to the current study [299], and even when including a raw material cost [299]. This incentivized, overseas market for WDF is the reason why South Africa's only RDF producer (Interwaste) exports 3.6 – 4.8 ktpa [372], [373]. However, no product nor project data is available.

Table 6.14: CAPEX, OPEX, MFSP and current fuel selling price for the 12 tested process lines

Line #	CAPEX and OPEX				Minimum fuel selling price (MFSP)		
	TCI	Production costs		**SRF price	*10%	*25%	MFSP/price
	(R mil)	(R/ton)	(R/GJ)	(R/ton)	(R/ton)	(R/ton)	(-)
BC	39.70	2 111	73.1	1 330	3 290	7 610	2.47
1	40.39	1 452	56.1	1 190	2 500	6 320	2.10
2	31.87	1 704	74.2	1 050	2 590	6 050	2.47
3	38.74	2 041	72.3	1 300	3 190	7 310	2.45
4	39.60	2 121	73.1	1 330	3 290	7 630	2.47
5	38.79	2 095	72.6	1 330	3 260	7 490	2.45
6	38.78	2 087	72.3	1 330	3 220	7 440	2.42
7	38.75	2 048	72.5	1 300	3 230	7 360	2.48
8	39.46	1 431	55.3	1 190	2 430	6 170	2.04
9	40.28	1 481	56.0	1 210	2 500	6 400	2.07
10	39.58	2 106	73.0	1 320	3 270	7 590	2.48
11	39.48	1 463	55.3	1 210	2 440	6 270	2.02

*10% and 25% represent MFSP at respective discount rates; **P is the current price of SRF according to section 6.2.3.4

6.5. Breakdown of results for the best pelleting process

The results from section 6.4, prove the most profitable conversion line (line 11) to consist of seven process units. Line 11, as shown in Table 6.8, uses the following units in this order: 2 over-band ferrous magnets in series (MS $_{perm}$), a twin-blade shredder (S), rotary, direct dryer (dD) using hot air, a steam-tube, indirect dryer (indD), a single motor pelletizer (P) and a weighbridge (WB) for weighing the SRF product. The CAPEX breakdown, OPEX breakdown and optimization of most expensive units are included in this section. This information can be used to provide context to how the results for the optimal pelleting process were calculated (Section 6.4) and provide a summary of variables (purchase equipment cost, salaries, etc.) for comparison against appropriate data, when available.

6.5.1. Breakdown of CAPEX

The TCI for this process line is R 37.1 mil which is attained from the modified Lang factors and purchase cost of equipment (PCE). The purchase cost of equipment was demonstrated to be R 12.9 mil and the breakdown of the PCE is shown in Table 6.15.

Table 6.15: Capital cost of each process unit of the selected SRF conversion line (Line 11)

Unit	2 x MS $_{perm}$	S	dD	indD	P	WB
Cost (R)	175 000	756 000	4 860 000	3 920 000	3 130 000	11 000
Breakdown (%)	1.36	5.88	37.81	30.47	24.39	0.09

From Table 6.15, it can be seen that 68.29% of the total PCE is dedicated for drying alone amounting to a total of R8.78 mil. The pelleting mill contributes significantly to the PCE which was estimated to be R3.13 mil and 24.39% of the total PCE investment. The large PCE investment for those three units heavily outweighs the other three which are calculated to only contribute to 7.33% of the total PCE. Figure 6.7 provides a pie-of-a-pie chart for the PCE of the units of the pelleting process where the PCE of cheaper units (e.g., weighbridge, air-blowers, or each magnetic separator) is included as the secondary pie (right). The breakdown of the PCE of the direct and indirect dryer is shown in Figure 6.7. From Figure 6.7, the ancillary units of the direct dyer, *viz.*, the rotary dryer, air heat-exchanger and blower accounts for R3.51 mil, R1.25 mil, and R106 000, respectively. The PCE for indirect dryer is comprised of the steam-tube dryer, storage tank (holding steam condensate) and pump (transporting the condensate back to the boiler) with each unit costing R3.02 mil, R740 000 and R162 000, respectively (Figure 6.7). The PCE of the rotary direct dryer was observed to resemble the price estimated from an NREL report for biomass drying [374]. Whereby, the PCE of R3.46 mil was calculated for the direct dryer from the evaporative load correlation ($224/kg water evaporated) when considering the exchange rate and CEPCI index [374].
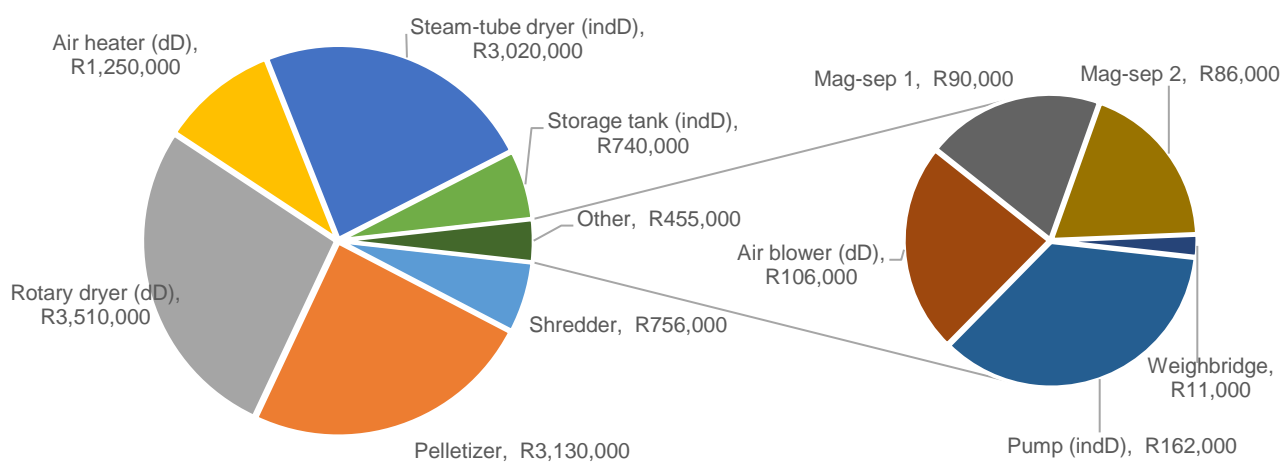
Figure 6.7: Breakdown of PCE of the various process units in the selected SRF conversion line (Line 11)

The cost of shredding was seen to be 2.39 times that of a local study that processed tires for shredding with similar capacity at R316 000 [307], but within the range of R217 000 to R1.93 mil when converted to from Euro to ZAR as specified by a Latvian study [107]. Likewise, the magnetic separator specified by the same local study for processing tires was only R61 000 [307], and fractionally less than the price of R89 700 and R85 500 specified for the first and second magnetic separator in this study, respectively. The range of the magnetic separators for the Latvian study, when converted to ZAR, was from R136 000 to R1.01 mil and probably for electromagnetic separators [107]. As shown in Table 6.15, the pelleting mill contributes significantly to the PCE and at R3.13 is congruent to a recent Italian study that recorded the PCE of a pelleting mill to be R7.8 mil when converted to ZAR, and account for around 50% of the total CAPEX investment [375].

6.5.2. Breakdown of Revenue

The generated revenue is from the main product (SRF), secondary product (scrap ferrous metal) and "income" from the waste that was diverted from landfill [29]. The production rate and market value of the main and secondary product is shown in Table 6.16. It is seen in Table 6.16 that if the SRF is sold for R1 210/ton and scrap metal at R2 000/ton, a revenue of R2.55 mil per year can be generated. The waste diversion factors refer to the dry waste that was used as either SRF or metal and therefore was not sent to landfill, as shown in Table 6.16 this income is R1.007 mil per year and is a function of the disposal cost (per ton). Hence the total revenue generated per year is R3.56 mil per year and 39.2% greater than the OPEX.

Table 6.16: Breakdown of generated revenue for Line 11

Product	Production rate (tpa)	Value (R/ton)	Revenue generated (R/year)	%
SRF	1 704	R 1 214	R 2 069 000	58.1
Scrap metal	242	R 2 000	R 484 000	13.6
Waste diversion	1 946	R 518	R 1 007 000	28.3

6.5.3. Breakdown of OPEX

The OPEX for line 11 and its breakdown is shown in Table 6.17. The fixed operating cost make up 85.4% of the total operating cost of which the three factors; salaries, benefits and overheads and maintenance costs all make up between 23 to 30% of the total operating cost. The estimated salaries are R745 000 per year for one operating shift per day and the benefits & overheads are estimated as 90% of the salaries. The maintenance costs and insurance and taxes are a function of the fixed capital investment and estimated to be R578 500 and R135 000 per year, respectively (Table 6.17).

Table 6.17: Operating cost per year and the breakdown of operating cost (Line 11)

Type of OPEX	Operating cost	Amount (R/year)	Breakdown (%)
Fixed costs	Salaries	R 745 000	29.9
	Benefits & overheads	R 670 500	26.9
	Maintenance costs	R 578 500	23.2
	Insurance & taxes	R 135 000	5.4
Total fixed costs		R 2 129 000	85.4
Variable costs	Coal	R 153 000	6.1
	Water	R 30	0.0
	Electricity	R 211 500	8.5
	Waste treatment	R -	-
Total variable costs		R 364 500	14.6

The variable operating costs make up 14.6% of the OPEX at R364 500 per year. The electricity cost is R211 500 per year and 8.5% of the OPEX as shown in Table 6.17. The coal is used to produce the steam on-site in the boiler and is R153 000 per year and makes up 6.1% of the total OPEX. The

cost of water is negligible for the operating and this process makes no waste as shown in the waste treatment cost of zero for the operating costs. The fact that this process produces no waste is partly why it is the most profitable of the process lines.

6.5.4. Key profitability indicators

Figure 6.8 shows the cash flow curves for different discount rates and SRF prices. As shown in Figure 6.8, the SRF selling price will change depending on the discount rate and yield a different net-present value after 25 years (NPV $_{25}$). The cumulative cash flow (CCF) curve of Figure 6.8 shows the example of when the SRF price is kept at R1 214 per ton and a discount rate of 0% is assumed, yielding a positive NPV_{25}. Conversely for the same SRF price, but at a discount rate of 0.83 %, the NPV_{25} will be 0 and therefore this discount rate represents the internal rate of return (IRR) for the project with the current selling price. In Figure 6.8, the MFSP to achieve a NPV_{25} at a discount rate of 10% and 25% is R2 443 and R6 269, respectively. As explained in section 6.4.2, the MFSP (10% discount rate) is 2.01 times greater than the current SRF selling price of R1 214 per ton. Naturally, increasing the discount rate to 25%, which is deemed acceptable to investors will result in the MFSP being increased R6 269 per ton before the project will have an NPV $_{25}$ of 0 as seen in Figure 6.8.
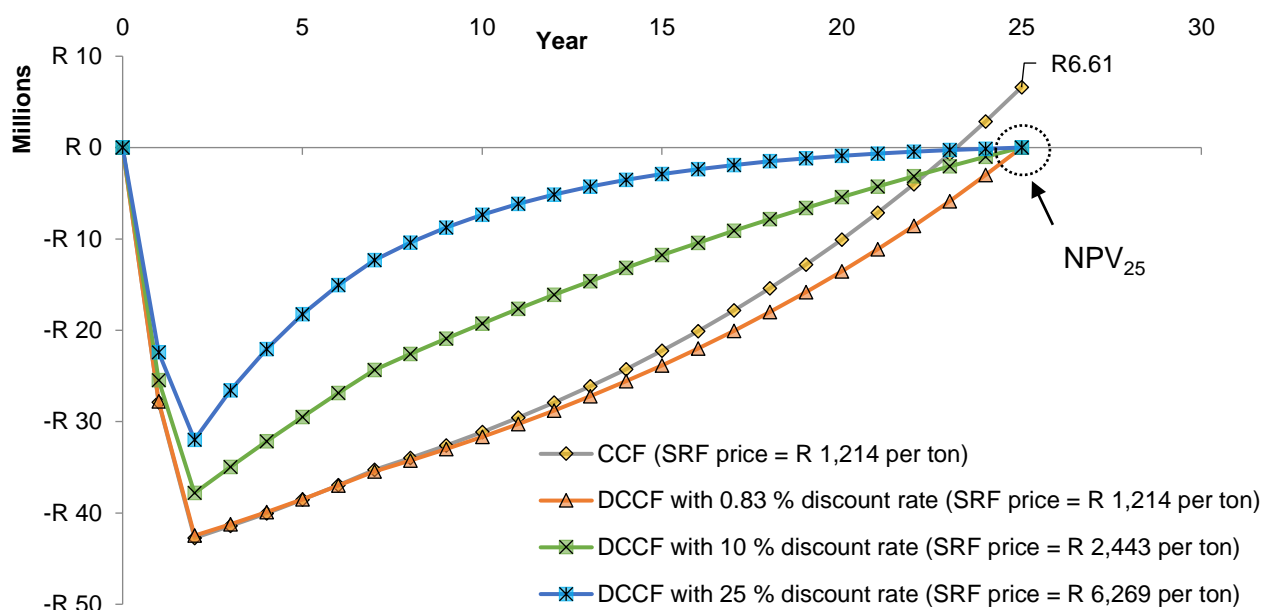
Figure 6.8: CCF curve and 3 DCCF curves for the pelleting process for various discount rates and MFSP

6.6. Sensitivity analysis of the pelleting process

The sensitivity analysis of the pelleting process has been provided in Figure 6.9 and provides a representation of the effect that adjusting a variable by 25% has on the MFSP $_{SRF}$ (25% discount rate). Figure 6.9 is represented as a tornado plot with sensitivity given as a percentage change from MFSP $_{SRF}$. In Figure 6.9, fixed CAPEX has the most significant effect on MFSP $_{SRF}$, and electricity cost (R0.97/kWh) has the least significant effect of the tested variables. The income tax rate (28%) was shown to have a higher sensitivity than OPEX on MFSP $_{SRF}$, as seen in Figure 6.9.

A variable which was further investigated in Section 6.6.1 was the effect of the scrap metal selling price on the MFSP $_{SRF}$. This variable was investigated because of the differences in scrap selling price seen in literature. A technoeconomic study based in South Africa used a scrap metal selling price of R2 500/ton [307]. Online sources have stated scrap metal prices from R1 000 to R6 000/ton [376]. In Figure 6.9, the MFSP $_{SRF}$ is shown to have a 1.1% decrease if the scrap metal price is increased by 25% (i.e., R2 500/ton). In Figure 6.9, it can be seen how the MFSP for the current air-drying temperature of 115 °C is lower than the MFSP if the drying air temperature was increased and decreased by 25%. Whereby, increasing the drying air temperature by 25% caused the MFSP to increase by 1.9% and decreasing the temperature by 25% also caused the MFSP to increase by 3.9%. Hence, how the optimal air-drying temperature for the direct dryer was selected is described in Section 6.6.2.
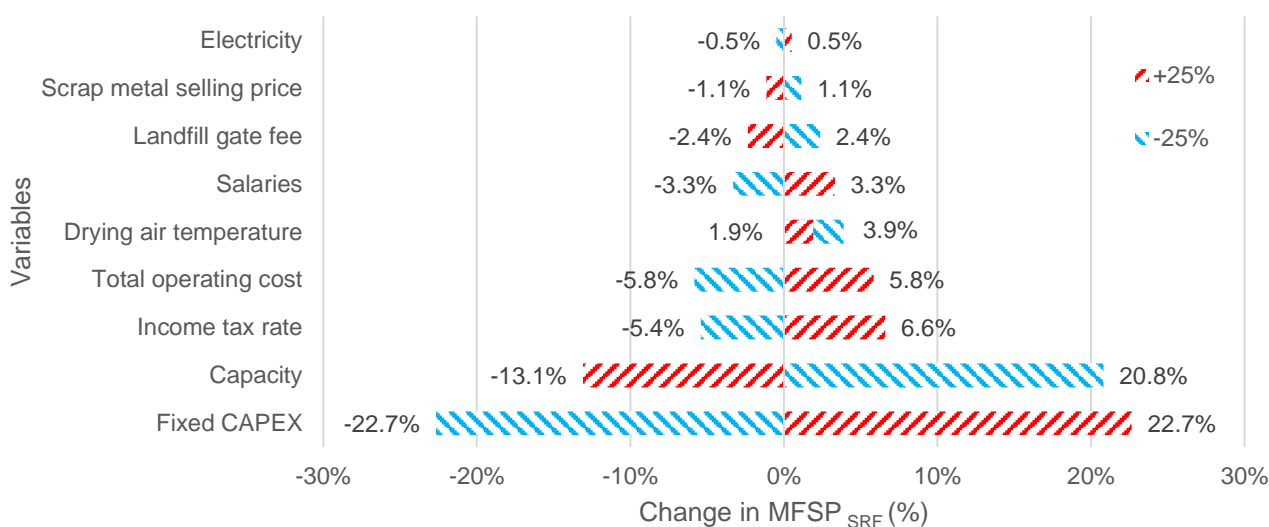
Figure 6.9: Sensitivity analysis for the pelleting process as a tornado plot

6.6.1. S1 - Effect of changing the scrap metal price on MFSP $_{SRF}$

Sensitivity analysis was performed on changing the market value of scrap metal to see the effect it had on MFSP $_{SRF}$. The results are shown in Figure 6.10 where values on the x-axis represent the scrap metal price, the primary y-axis represents the required MFSP $_{SRF}$, and secondary y-axis represents the percentage change in MFSP $_{SRF}$ from the MFSP $_{SRF}$ for the current scrap metal price. R2 000 is the current market value per ton of scrap metal. R1 000 and R1 500 is the case for when the current scrap metal price is decreased by 25% and 50%, respectively. The effect of increasing the scrap metal prices up to R6 000/ton was also investigated.

At the current scrap metal value of R2 000/ton, the MFSP $_{SRF}$ was R6 269/ton. This MFSP was indicated in Figure 6.10, and is the same MFSP $_{SRF}$ required for a 25% discount rate (Figure 6.8). Decreasing the scrap metal price to R1 500 and R1 000/ton caused the MFSP $_{SRF}$ to increase by 1.1% and 2.3%, respectively. Similarly increasing the scrap metal price by 25% to R2 500 caused the MFSP $_{SRF}$ to decrease by 1.1% to R6 198/ton. While further increasing the scrap metal to R3

000, R4 000, and R6 000 would cause the MFSP $_{SRF}$ to decrease to R6 127, R 5 985, and R5 701/ton. Hence, increasing scrap metal price to R6 000/ton would cause MFSP $_{SRF}$ to be decreased by 9.1% to R5 701, but still not less than the target SRF selling price of R1 214/ton, as shown in Table 6.16.
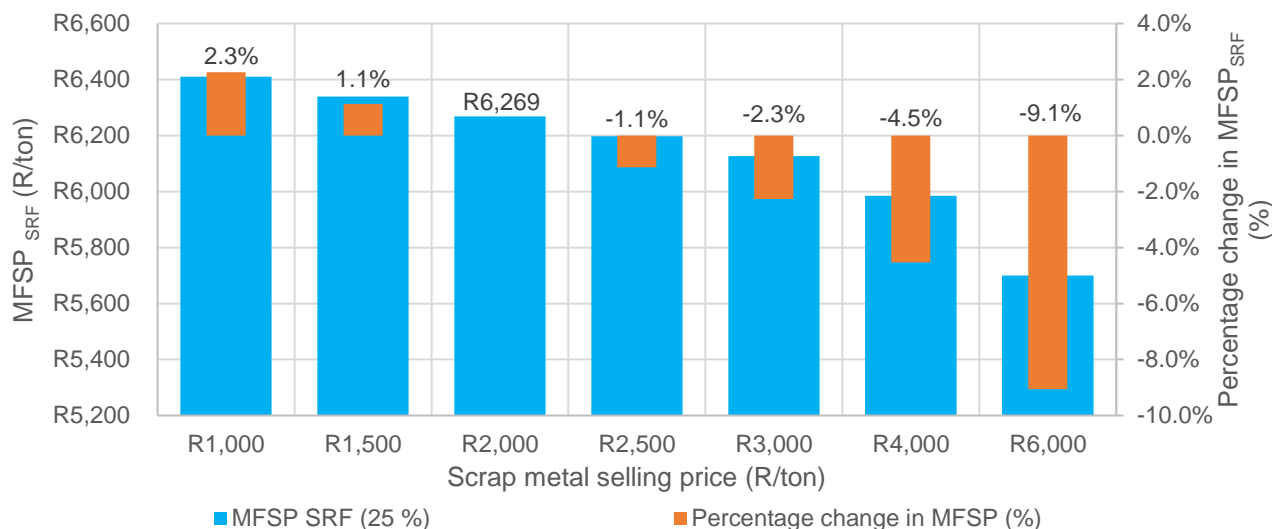
Figure 6.10: The effect of changing the scrap metal price on MFSP $_{SRF}$

6.6.2. S2 - Effect of changing the preheater air temperature

The direct dryer currently uses preheated air to uptake the moisture in the direct rotary dryer. The air is captured with an air blower and then heated in an exchanger. The air blower is sized according to the volumetric air flowrate and the heat exchanger is sized according to the heat transfer area that is a function of the duty, heat transfer coefficient and utility as explained in Appendix H. It is expected that changing the air temperature, will affect the necessary air flowrate which in turn will affect the CAPEX, OPEX and have an impact on MFSP $_{SRF}$. The effect of changing the temperature was shown to have significant effect on the amount of air needed to uptake the moisture whereby at 20 °C, over 100 kg of air was needed per kg of incoming wet feed, as shown in Figure 6.11. As seen in Figure 6.11, the amount of air required per kilogram of feed follows a negative exponential trend whereby as the temperature of air is increased to 50 °C, 27.6 kg air/(kg wet feed) is required and at 70 °C, 18.4 kg of air is required per kg of feed.

As seen in Figure 6.11, the required air continues to decrease, albeit slowly, to 5 kg of air required per kilogram of feed. Figure 6.11 also shows the energy consumption of the dryer on two bases, being MJ/(kg feedstock) and MJ/(kg water evaporated). After 50 °C when heating duty is required, the energy consumption per kg of water evaporated decreases steadily from 4.28 MJ per kg evaporated water at 60 °C to almost exactly 4 MJ per kg evaporated water at 200 °C. These results are congruent to literature stating energy consumption, within the range for direct dryers of 4 to 6 MJ/(kg water evaporated) [359]. Likewise, the energy consumption for a feed basis was increased from 2.86 MJ/kg at 50 °C to 3.25 MJ/kg at 200 °C.
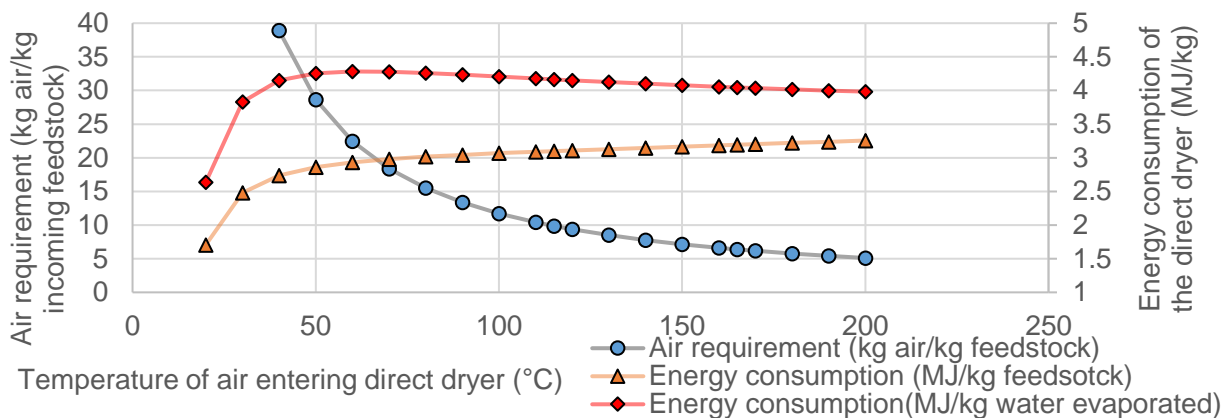
Figure 6.11: The effect of air temperature on the air requirement and energy consumption of the dryer.

It was noted that the rotary dryer worth R 3.51 mil would not be affected by the change in the drying air temperature and was kept constant. However, due to the amount of air that would be needed to uptake the moisture, the size of the blower and the air heater would change. The effect of changing the drying air temperature was shown to influence the MFSP $_{SRF}$, as shown in Figure 6.12. As shown in Figure 6.12, the MFSP $_{SRF}$ was minimized at 115 °C and 170 °C, to R6 269 and R6 182`ton, respectively. The percent change of MFSP from the MFSP using an air-drying temperature at 115 °C is included in Figure 6.12 and shown to maximizes at 110 °C, with a percentage change that is 9.9% greater than the MFSP for 115 °C case. The sudden change observed in the MFSP from 110 to 115 °C and again from 165 to 170 °C, as shown in Figure 6.12, is not due to changes in variable OPEX but fixed OPEX which changes w.r.t to the fixed capital investment (FCI) as explained in section 6.1.3.2. The variable OPEX did not significantly change because as temperature increases, more coal is required for steam production, but air requirement decreases (Figure 6.11), decreasing the electricity demand for blowing. Whereby at 110 °C and less, LPS with utility temperature of 120.2 °C, is used for heat exchange and as the process utility approaches this temperature the log mean temperature difference (LMTD) is decreased which negatively affects air heater CAPEX. Therefore from 115 to 165 °C, MPS is used and a similar trend is seen. For temperatures from 170 °C to 240 °C, HPS could be used but should not, because these temperatures would aid spontaneous combustion of the rejects. Hence, the drying air temperature of 115 °C is ideal for operation.
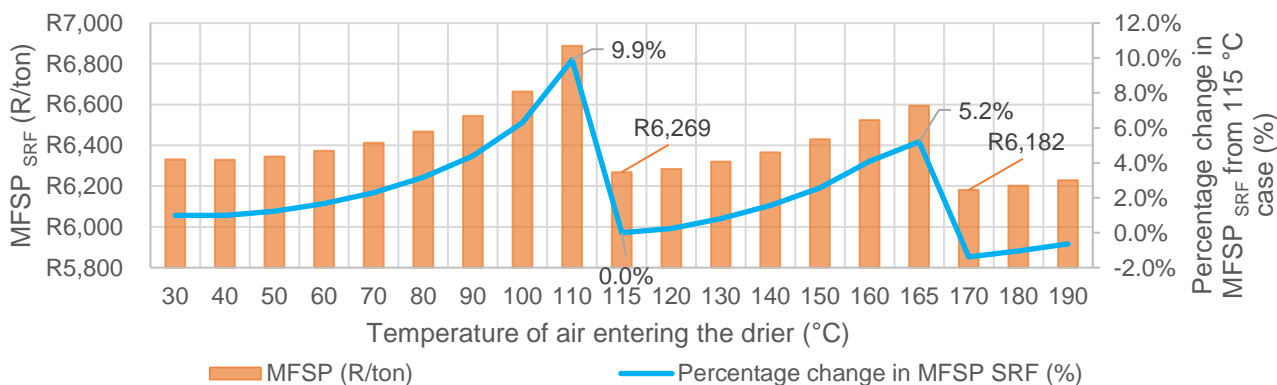
Figure 6.12: The effect of air drying on MFSP $_{SRF}$ at 25% discount rate

6.7. Results for the pyrolysis process

6.7.1. Model validation

6.7.1.1. Comparison of model product distribution yields to experimental yields

The product distribution yield from the Aspen Plus model was compared against the normalized yields from the pilot-scale experiments to see whether the model components acted appropriately within the model. For instance, did the C_5H_{12} component leave the unit as NCG, and not condense with the organic phase or aqueous phase oil streams? The yield of each phase for the model was according to the streams in the PFD (Figure 6.4), whereby the total condensable product was streams 3-11 and 3-12 combined, the fuel oil product (wax and organic phase oil) was stream 3-11, the aqueous phase oil was 3-12 and the NCG and char were streams 2-04 and 2-06, respectively.

As shown in Table 6.18, no difference in yield was observed between the simulation product yields and normalized experimental yields for the char and wax phases. The char was simulated as ash and carbon, both as conventional solids and were completely separated from the volatiles using the cyclone (S-201 of Figure 6.4). Similarly, the wax was simulated as alkanes of C_{18+} length and were completely condensed in the product recovery area to form stream 3-11. The remaining simulation yields of Table 6.18 were shown to have small errors (<0.5 wt.%) when compared to the experimental yields, except for the fuel oil yield for 450 °C. The fuel oil product relates to stream 3-11 alone (Figure 6.4) and is the main product. The difference of *ca.* 4% is seen in Table 6.18 for the simulation and experimental fuel oil yield at 450 °C. This is from the low recovery of 72.4% for the organic phase oil components in the fuel oil product, as seen in Table 6.19. Whereby, Table 6.19 includes the recoveries for the model component for the phases in each product stream.

Table 6.18: Comparison of simulation product yields to normalized experimental yields

Temperature	450 °C		500 °C		550 °C	
Sim. /exp. Yield (wt.%)	Sim.	Exp.	Sim.	Exp.	Sim.	Exp.
Char yield	33.3	33.3	30.8	30.8	25.8	25.8
Wax	18.9	18.9	24.2	24.2	23.0	23.0
Organic phase oil	16.3	16.6	10.1	10.5	13.8	13.8
Fuel oil product	31.4	35.5	34.4	34.7	36.0	36.8
Aqueous phase oil	15.1	15.3	16.0	16.2	8.29	8.55
Total liquid product	50.3	50.8	50.2	50.8	45.1	45.4
Non-condensable gas	15.9	15.9	18.7	18.4	28.9	28.9

6.7.1.2. Mass recovery of the model components into the aqueous and fuel oil phase

The model components used to describe the fuel oil product (wax and organic phase oil) and aqueous phase is explained in section 6.3.1.4. As shown in Table 6.19, the wax components were completely recovered in the fuel oil stream and water was well recovered in the aqueous phase product, being over 93 wt.% for all the temperatures. The water was separated from the aqueous

phase in Table 6.19 because water was assumed as 70 wt.% of the aqueous phase oil (section 6.3.1.4) for all the temperatures and hence the aqueous phase refers to the model components alone, *sans.* water. The lowest recoveries for organic components in the fuel oil product was 72.4% for 450 °C. This lower recovery is due to the high composition of levoglucasan (LGA) produced at 450 °C and that the UNIQUAC model used for Aspen Plus assigns LGA and 5-hydroxymethylfurfural (HMF) as aqueous phase products. Despite this caveat, the recoveries of organic phase components in the other temperatures were high being 84.7 and 90.9 wt.% for 500 and 550 °C, respectively.

The lowest recovery of aqueous phase in the aqueous phase stream was seen in Table 6.19 at 500 °C, with a recovery of 79.5 wt.%. This was because the yield of furanmethanol (furfurol) in the aqueous phase components was the highest at 500 °C compared to 450 and 550 °C, as shown in Figure 6.6. Furfurol is assigned to collect with fuel oil instead of the expected, aqueous phase according to the UNIQUAC model despite its high solubility in a polar solvent. Consequently 20.3% of the aqueous phase components (all furfurol) collects in the HFO stream, as shown in Table 6.19. Nevertheless, high recoveries of aqueous phase were seen for the other two temperatures. All the model components ended up as either fuel oil, aqueous phase oil or NCG and hence the recovery of the NCG fraction is included too in Table 6.19. In the NCG fraction, even for the worst case, at 500 °C, less than 6.2% of the components that should end up as liquid are recovered in the NCG phase. These results indicate that the chosen property method, *viz.,* UNIQUAC and the selection of model components for the organic, wax, and aqueous phase, depending on component polarity was satisfactory for modelling the pyrolysis products.

Table 6.19: Recovery of model components into HFO, aqueous phase stream and NCG stream

Stream recovery (%)	HFO stream			Aqueous stream			NCG stream		
Model component	450	500	550	450	500	550	450	500	550
Wax components	100	100	100	0	0	0	0	0	0
Organic phase	72.4	84.7	90.9	25.8	10.9	8.76	1.85	4.44	0.336
Water	0.568	0.630	2.32	98.0	97.8	93.2	1.45	1.59	4.44
Aqueous phase	2.53	20.3	4.07	97.1	79.5	95.2	0.324	0.187	0.710

6.7.1.3. Efficiency and energy characteristics of the pyrolysis model

The pyrolysis process required heating, cooling, and electrical power as explained in Section 6.3.2.1. The equivalent energy w.r.t the wet feedstock [MJ/(kg wet feedstock)] for the duties and products is shown in Figure 6.13. Additionally, the sum of the equivalent energies equated to the NEC, which is shown in Figure 6.13 (the GEC is also shown in Figure 6.13). This figure is analogous to the pilot-scale figure (Figure 5.19), but because the wet feedstock is used as a basis instead of dry feedstock, the equivalent energies of the products (and duties) are decreased in comparison to the pilot-scale.

The electrical power demand ranges between 0.45 to 0.01 MJ/kg for the three temperatures, as shown in Figure 6.13. This is due to 0.73, 0.81 and 1.11 MJ/kg of electricity being generated for the 450, 500 and 550 °C process, respectively. Similarly, the heating and cooling duties for the temperatures are not significantly high, due to the amount of heat that was exchanged in the steam and power generation area. Whereby, an equivalent energy of 5.59, 6.08 and 7.85 MJ/kg of duty was exchanged for the 450, 500 and 550 °C processes, respectively. This resulted in the heating duties ranging from 2.16 to 2.68 MJ/kg for 550 to 450 °C as shown in Figure 6.13. The heating duty is shown to decrease at higher temperatures, which is probably due to the selection of the specified model components at 550 °C. It is possible that the specified model components at 550 °C have lower enthalpies of formation and hence, require less heat to maintain temperature of the *RYIELD* reactor (R-201), despite a higher temperature setting. The cooling duty is shown to increase from 3.40 MJ/kg at 450 °C to 5.17 MJ/kg to 550 °C, as shown in Figure 6.13.

The equivalent energy of the three products (fuel oil, char and NCG) are shown in Figure 6.13, where they cumulatively make up 13.2, 14.3 and 14.6 MJ/kg for 450, 500 and 550 °C, respectively. The GEC for the 3 temperatures is shown to be highest for 550 °C in Figure 6.13 due to the high equivalent energy of the NCG (4.98 MJ/kg) at this temperature. Although when considering the electrical, heating, and cooling duties for each temperature, it can be seen in Figure 6.13 that the NEC is apparently highest for 500 °C, with a value of 45.1%.
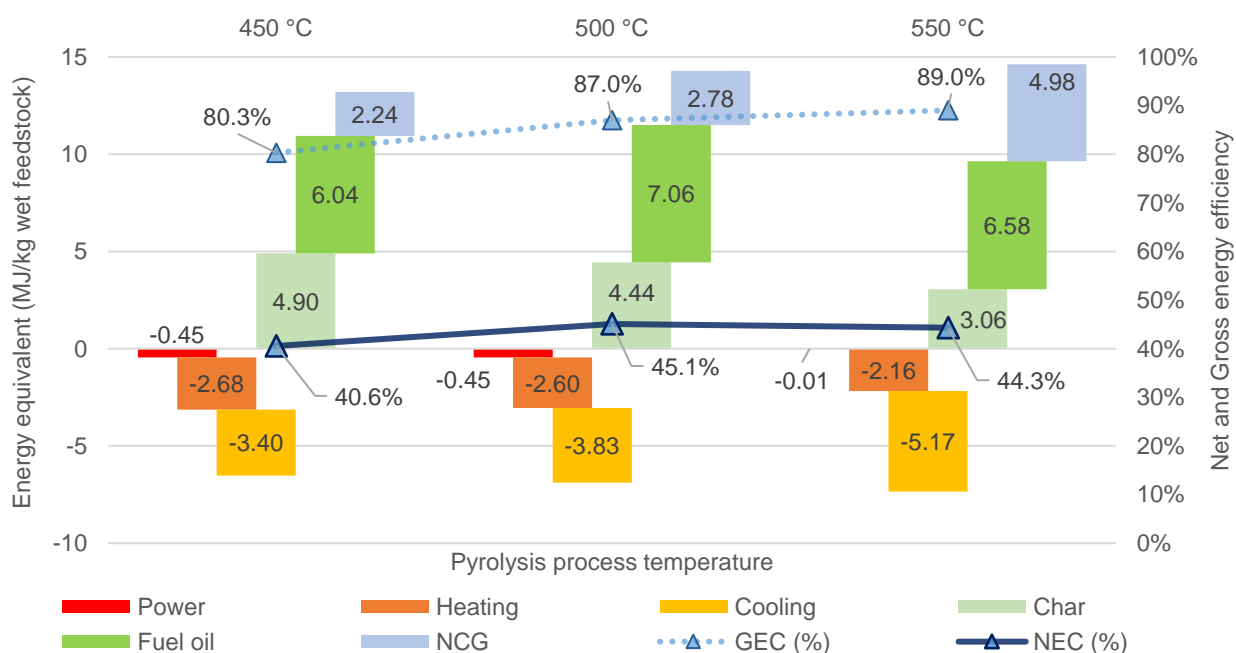
Figure 6.13: The equivalent energy, GEC, and NEC for the 3 pyrolysis temperatures (°C)

6.7.2. Economic comparison between pyrolysis lines

Table 6.20 provides a summary of the TCI, production costs and current fuel price compared to the MFSP for the fuel oil product. The production cost is provided on a product mass and energy basis,

which incorporates all 3 products - NCG, char and fuel oil. The selling price of fuel oil and char is provided according to the calculation in Section 6.3.3.3 and 6.3.3.4, respectively. The fuel oil is then compared against the MFSP of the fuel oil required to attain a discount rate of 10% and 25%.

In Table 6.20, the TCI ranges from R60.6 mil to R65.3 mil, whereby the process at 550 °C was shown to have the highest TCI. This higher TCI was due to the increased size of the three blowers needed for the higher NCG yield in the combustion area, as well as the larger air cooler (E-501) needed in the steam and power generation area. The production costs on a mass and energy basis (of all products) is shown to be lowest for the process at 550 °C because as much as 98.8% of the of electricity required could be generated at 550 °C, as shown by the small electrical demand of 0.01 MJ/(kg wet feed) from Figure 6.13. Conversely, the 450 and 500 °C processes could generate 62.2 and 64.5% of the electrical requirement, respectively. The production cost was shown in Table 6.20, to range from R3 196 at 550 °C to R3 686 and R3 817 for 500 and 450 °C, respectively. The reason why the temperature of 500 °C had a similar production cost to 450 °C was due to the higher electrical requirement from increased chilling demand (E-303) to condense more liquid product to attain the designated yield. The production costs on a mass basis can be seen to be 2.5 times greater than the production costs of the most economical pelleting lines (*ca.* R1 450/ton in Table 6.14). The production costs on an energy basis are shown in Table 6.20, to range between R106 to R125/GJ of products. The production costs on an energy basis for pyrolysis are less than double the production costs for the most economical pelleting process (R55 to R56/GJ in Table 6.14).

Table 6.20: CAPEX, OPEX, MFSP and current fuel selling price for the three pyrolysis temperatures

Line #	CAPEX & OPEX			Fuel price		MFSP for fuel oil		
	TCI	Production costs		Fuel oil	Char	*10%	*25%	SP/ MFSP
	(R mil)	(R/ton)	(R/GJ)	(R/ton)	(R/ton)	(R/ton)	(R/ton)	(-)
450 °C	60.58	3 817	124.9	4 665	2 210	13 897	32 430	2.98
500 °C	61.60	3 686	115.7	4 978	2 164	13 053	30 247	2.62
550 °C	65.34	3 196	105.8	4 431	1 798	12 954	30 378	2.92

*referring to discount rate used for calculating minimum fuel selling price (MFSP)

The selling price of the fuel oil and char product is shown in Table 6.20 and calculated from the HHV. The fuel oil, comprised of wax and organic phase oil, produced at 500 °C had the highest HHV (as shown in Figure 5.13) and consequently the selling price was R4 978/ton. In addition, the char product can be seen to range from R1 798/ton at 550 °C to R2 210/ton at 450 °C. The MFSP provides a comparison of the selling price of fuel oil to the price required to attain profitability for a discount rate of 10% and 25%. Although, a discount rate of 25% is required for an investment to be profitable, a discount rate of 10% was included as a comparison due to several researchers using this discount rate for pyrolysis processes [29], [377]. As shown in the last column of Table 6.20, the fuel oil price at 500 °C would need to increase by at least 2.62 times before it would equal the MFSP required for

a 10% discount rate. Therefore, at the current economic settings, the pyrolysis process for all three temperatures are unprofitable. In addition, as shown in Table 6.20, the fuel oil selling price must increase to R30.2/kg before the project is attractive for investment.

6.8. Breakdown of results for the best pyrolysis process

The breakdown of the 500 °C pyrolysis process is explained in this section. This temperature was used because the fuel oil selling price was closest to MFSP $_{fuel\ oil}$ at 10% and 25% discount rates.

6.8.1. Energy demand

The pyrolysis process used three main types of energy: Cooling, heating, and power. The duties for each of the energy sources in kW is provided in Table 6.21, where cooling duties are provided as a negative value to differentiate from the heating duty. The total heating and cooling demand for the 500 °C plant is shown in Table 6.21 as 1,007 kW and 1,150 kW, respectively. In Table 6.21, it can be seen that 302 kW of heating duty was required for the pyrolysis reactor which equated to 4.98 MJ/(kg dry rejects) and almost double the energy reported by a study for pyrolysis, which ranged from 1.5 to 2.5 MJ/(kg dry feedstock) [25], although this range was from a plant with 40 times greater capacity than this plant [370]. The difference between the process with no heat-exchange (No HX) to the process with HX, as shown in Table 6.21, refers to the difference in energy demand after exchanging heat. In Table 6.21, this difference is observed to be the same for the heating and cooling demand at 706 kW (i.e., 1,007–302 kW). The heat exchange was achieved through cooling with BFW, generating steam in the steam Rankine cycle and exchanging heat in the air-preheater (E-401 of Figure 6.4). This exchanged energy equated to 70.1% and 61.3% of the total heating and cooling duty, respectively. The total electrical power requirement for the plant was 146.4 kW and power generation could satisfy 64.5% of the total power requirement as 94.4 kW as shown in Table 6.21. Hence, the power requirement after generation is 52.0 kW.

Table 6.21: The electrical demand, heating, and cooling duty for each area of the pyrolysis process at 500 °C

Duty (kW)	Electricity (Power)		Heating duty		Cooling duty	
Area:	Required	Generated	No HX	with HX	No HX	with HX
Pre-treatment	20.2	-	67.6	-	-	-
Pyrolysis reactor	1.5	-	301.7	301.7	-	-
Product recovery	92.7	-	-	-	-92.4	-46.4
Combustion	27.3	-	67.1	-	-592.0	-
Steam and power generation	4.7	94.4	571.0	-	-466.0	-398.4
Total	146.4	94.4	1007.4	301.7	-1150.4	-444.7

6.8.2. Revenue

The revenue of the plant is shown in Table 6.22, where the main product is fuel oil, generating 52.6% of the total revenue equating to R2.94 mil per year. Char and scrap metal are secondary products

that combined, make up 29.4% of the total revenue, as shown in Table 6.22. The selling price of the products is shown in Table 6.22, where scrap metal, char and fuel oil are assumed as R2/kg, R2.16/kg, and R4.98/kg, respectively. The fuel oil and char were priced according to their experimental HHVs of 39.3 and 27.6 MJ/kg, respectively. Like the SRF process, the waste diversion fee is provided (Table 6.16). The total revenue for the 500 °C process is R5.6 mil per year.

Table 6.22: Breakdown of generated revenue for the 500 °C pyrolysis process

Product	Production rate (tpa)	Value (R/ton)	Revenue generated (R/year)	%
Fuel oil	591	4 978	2 944 000	52.6
Char	529	2 164	1 145 000	20.4
Scrap metal	252	2 000	504 000	9.0
Waste diversion	1 946	518	1 007 000	18.0

6.8.3. Breakdown of CAPEX

The purchase cost of equipment (PCE) for the 500 °C pyrolysis process is R32.2 mil, and the total capital investment (TCI) is R61.6 mil. The breakdown of the different areas is shown in Figure 6.14, according to the colours of the PFD (Figure 6.4). It is seen that the majority of the PCE is from the pre-treatment area mainly due to the cost of the two dryers, followed by the combustion area containing 3 blowers and a furnace.
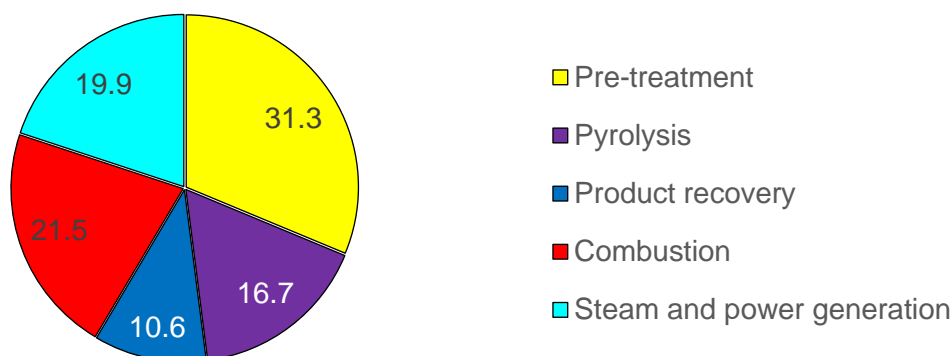
Figure 6.14: The percentage breakdown of the PCE in different areas of the 500 °C pyrolysis process

6.8.4. Breakdown of OPEX

The breakdown of the OPEX is shown in Figure 6.15, where the left figure describes the total OPEX with the values for each OPEX type given in Rands per year. The fixed costs are shown to make up most of the OPEX, with variable costs being R412 200 per year. The breakdown of the variable costs is shown on the right pie-chart in thousand Rands per year. The salaries and benefits and overheads make up 74.9% of the OPEX, whilst the variable costs make up only 7.6% of the OPEX. The variable costs labelled "other" in Figure 6.15, were comprised of electricity (R397 500 per year) and process water for steam and heat generation at R14 700 per year. The disposal fee (waste treatment) was reduced to nothing by recycling the aqueous phase to make up the water requirement. Whereby aqueous phase, containing 68.7 wt.% water, was mixed with process water to satisfy some process

water requirement. The aqueous phase could satisfy 15.7% of the total water requirement on the plant and thereby lower the process water requirement from 1.74 kt per year to 1.46 kt per year - also lowering the OPEX. In addition, the blowdown from the steam was recycled and the process produced no ash despite an ash cyclone existing for the flue gas (S-401).
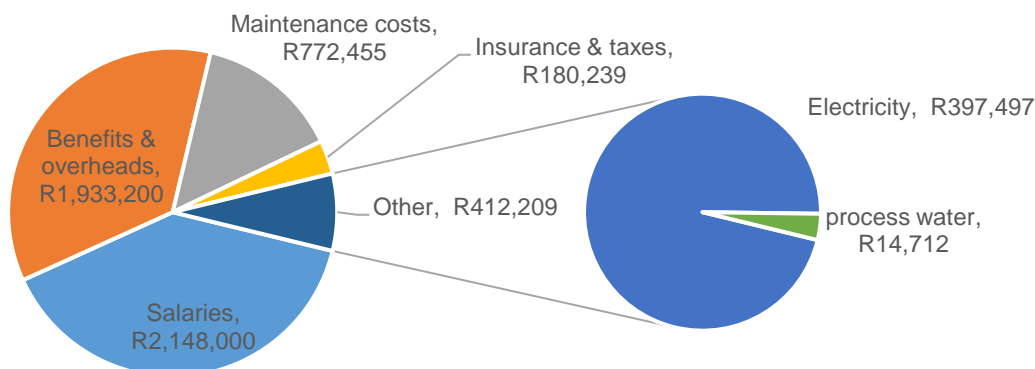
Figure 6.15: Breakdown of total pyrolysis OPEX, left (R per year), and breakdown of variable costs, right (R per year)

6.8.5. Key Performance Indicators (KPIs)

Figure 6.16 represents 1 cumulative cash flow (CCF) curve and 3 discounted cash flow (DCCF) curves, whereby it can be seen that for cumulative cash flow curve, after 25 years the net-present value (NPV $_{25}$) is negative at R-60 mil. Hence, although the revenue is greater than the OPEX for the pyrolysis process at 500 °C the amount is not great enough to eventually pay itself back even when the value is non-discounted. Hence, a negative IRR indicates a project where the non-discounted cash flow is less than the initial investment [378] and hence the discount rate would need to equal the IRR, at -12.3% before the project would have an NPV$_{25}$ of 0, as shown in Figure 6.16. The MFSP of the fuel oil at R13 053/ton for a discount rate (M_{ar}) of 10% would eventually pay back the investment as shown in Figure 6.16. Likewise, the MFSP of fuel oil for a discount rate of 25% (attractive to investors) will be R30 247 per ton, as shown in Figure 6.16.
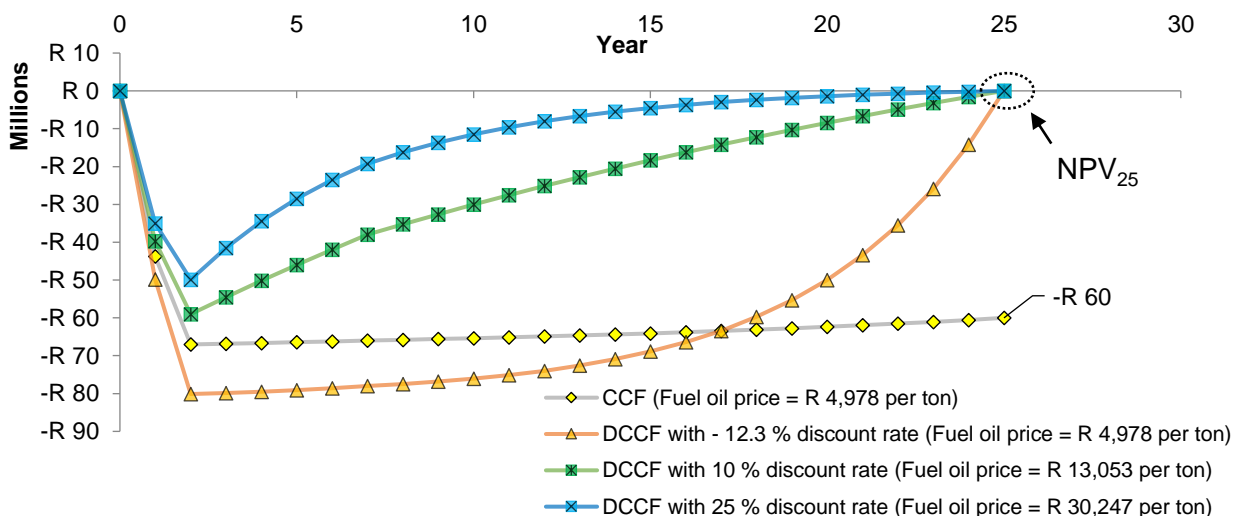
Figure 6.16: CCF curve and 3 DCCF curves for different discount rates and MFSP for the fuel oil product

6.9. Sensitivity analysis of the pyrolysis process

The effect of increasing and decreasing 9 variables by 25% on the MFSP of the pyrolysis process (MFSP $_{fuel\ oil}$) is shown in Figure 6.17. The drying air temperature variable for the sensitivity analysis of the pelleting process (Figure 6.9) was substituted for char selling price in the sensitivity analysis for the pyrolysis process (Figure 6.17). In Figure 6.17, the MFSP $_{fuel\ oil}$ is observed to be most sensitive to changes in Fixed CAPEX and the least sensitive to changes in electricity – just like the pelleting process (Figure 6.9). However, MFSP $_{fuel\ oil}$ was less sensitive to Fixed CAPEX and capacity than the MFSP for the pelleting process (MFSP $_{SRF}$) due to the smaller percentages observed. Additionally, the sensitivity of the OPEX, salaries, and electricity was higher for the pyrolysis process than the pelleting process.

In Figure 6.17, increasing and decreasing the char selling price by 25% caused the MFSP fuel oil to decrease and increase by 1.7%, respectively. Comparatively, the MFSP $_{fuel\ oil}$ was less sensitive to changes in the scrap metal selling price as seen by 0.7% in Figure 6.17. The effect of changing the market value of char was investigated w.r.t the MFSP $_{fuel\ oil}$ in section 6.9.1. The char could be sold as Petcoke and it is believed its price could be variable due to lack of available market research. Another variable which was further investigated is the salaries variable in Figure 6.17. Section 6.9.2 provides a comparison of different labour requirements per shift on MFSP $_{fuel\ oil}$. Labour requirement was tested because of the uncertainty of labour requirements for small scale facilities and the large effect that labour has on OPEX of the pelleting process, as shown in Figure 6.15.
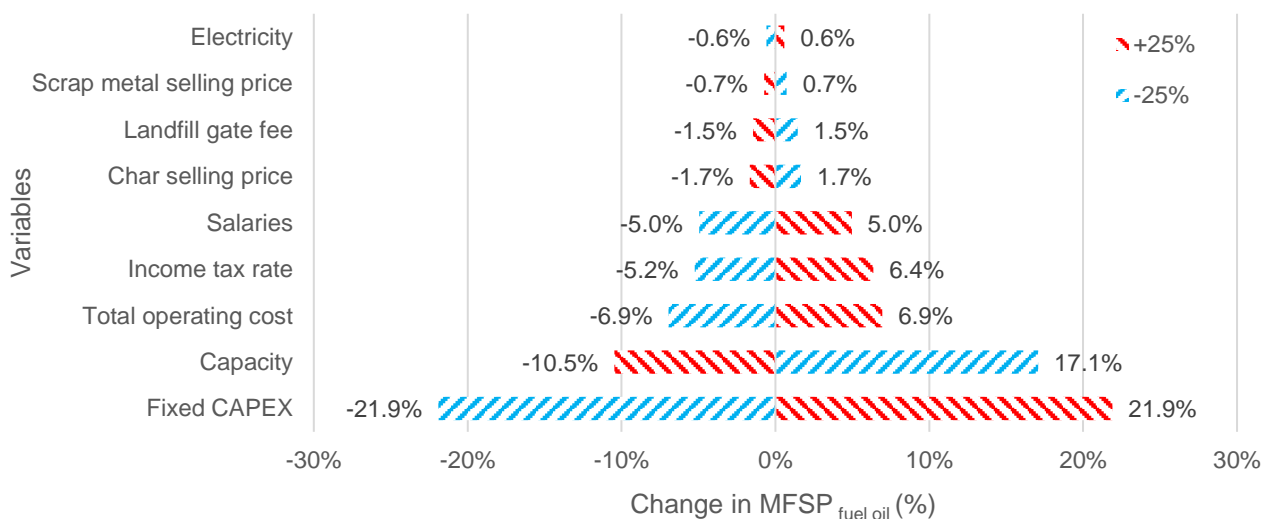
Figure 6.17: Sensitivity analysis for the pyrolysis process as a tornado plot

6.9.1. S1 - Effect of changing the market value of char on MFSP $_{fuel\ oil}$

Like the SRF process, sensitivity analysis was performed on changing the market value of a product, *viz.,* char to see the effect it had on project MFSP $_{fuel\ oil}$. In Figure 6.18, the values on the x-axis represent the market value of char whereby R2 164/ton is the current value, which can be seen to

have yield a process with a MFSP $_{\text{fuel oil}}$ of R30 266/ton. In Figure 6.18, R1 623/ton and R1 082/ton is the case for when the current char price is decreased by 25% and 50%, respectively. Four more cases were used, being char costing R2 705, R3 246, R4 328, and R6 492/ton which are 25, 50, 100 and 200% greater than the current market price, respectively.

The results indicated that when the char was at the current value of R2 164/ton, the MFSP $_{\text{fuel oil}}$ was R30 247/ton, and identical to the MFSP fuel oil for a 25% discount rate in Figure 6.16. From Figure 6.18, when the char price is increased by 25%, to R2 705/ton, the MFSP of fuel oil is reduced to R29 745, correlating to a mere 1.7% decrease (Figure 6.17). Likewise, increasing the char price by 100% to R4 328/ton caused the MFSP $_{\text{fuel oil}}$ to decrease to R28 190 correlating to a 6.8% decrease in MFSP. Lastly, increasing the char price by 200% so that the char price becomes R6 492/ton, causes the MFSP to decrease to R26 134 or a 13.6% decrease. The price of char, as shown in Figure 6.18 is tested to range from R1 082 to R6 492 and not yet competitive against the price of domestic coal, at *ca.* R400 to R450/ton [354]. However, if the char is priced as Petcoke, the current char price would need to increase by *ca.* 15% before it would cost the same as Petcoke supplied in Jordan at $150/ton or R2.5/kg [322].
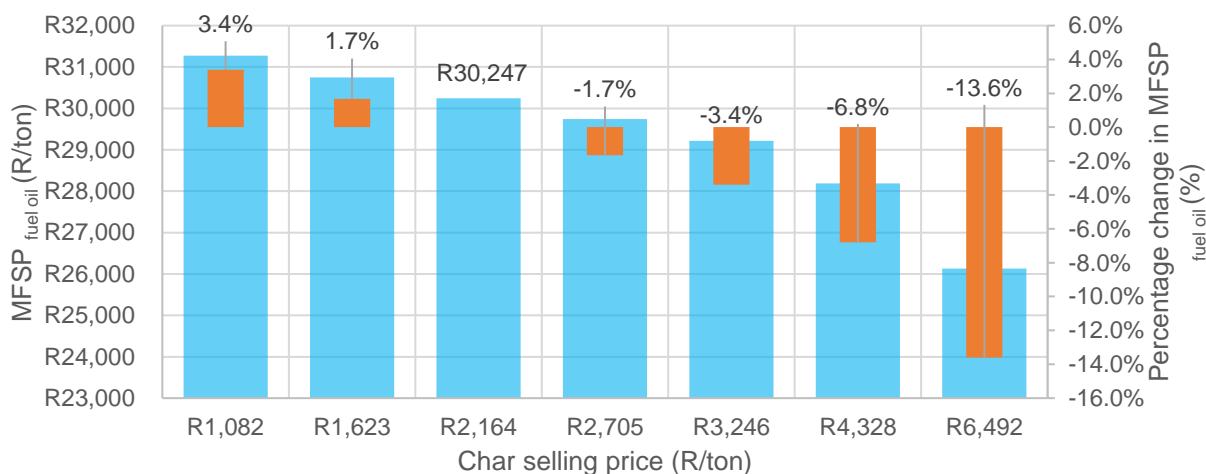
Figure 6.18: The effect of changing the market price of char on MFSP $_{\text{fuel oil}}$ to attain profitability

6.9.2. S2 - Effect of changing the labour requirements on MFSP $_{\text{fuel oil}}$ and IRR

The fixed operating costs were shown to heavily outweigh the variable operating costs, as explained in Section 6.8.4. Therefore, the effect of changing the labour per shift was analysed with accordance to the MFSP $_{\text{fuel oil}}$ required to attain profitability. The base-case (BC) example shows that for each of the 2 shifts, the line requires 3 sorters/ laborers (S), no chemical engineers (CE), 1 maintenance supervisor (MS), 1 production foreman (PF), 2 shift operators (SO) and 2 production operators (PO). Hence 9 people are needed per shift on the plant and the MFSP $_{\text{fuel oil}}$ for 25% discount rate remains R30 247 per ton, respectively, as shown in Table 6.23. The number of people required per shift and the effect of changing the number of sorters/ labourers, production operators, etc. can be seen in Table 6.23. Only 2 tested lines in Table 6.23 (0 S and -1 S & -1 PO) had less than 8 persons per

shift. Additionally, only 1 tested line in Table 6.23 (-1 S & -1 PO) did not use 2 production operators (PO) that is recommended for waste-management facilities [357]. Although, line "-1 S & -1 PO" still used 1 maintenance supervisor (MS) and 1 production foreman (PF) [357].

The effect of subtracting one of the staff members of the nine, for the BC, is shown in 3 of the 8 tested lines in Table 6.23 (-S, -1 PO, -1 SO). One line dismisses all three sorters/ labourers (0 S). One line dismisses two personnel (-1 S & -1 PO), and another substitutes 1 production operator for a chemical engineer (+1 CE & -1 PO). The last line adds a SO but dismisses a S and the second PO (-S +1 SO & -PO). All, but one tested scenario, had a positive effect on profitability resulting in increased IRR and decreased MFSP $_{fuel oil}$ from the BC as shown in Table 6.23. As shown in Table 6.23, the line (+ CE & -1 PO) which required 1 chemical engineer per shift at R318 000 per year according to PayScale™ made OPEX higher than the revenue, therefore this line had no IRR and higher MFSP than the other lines. Conversely, as seen in Table 6.23, the most profitable case was when a S and PO was dismissed (- S & -1 PO), which lowered the MFSP $_{fuel oil}$ to R29 137 per ton, but still yielded a negative IRR of 3.7% rendering it unprofitable at the current settings. In Table 6.23, it can be seen that the changes to the labour requirement cause the $_{MFSP fuel oil}$ to decrease by 3.7% for the "-1 S & -1 PO" line and increase by 3.1% for the "+1 CE & -1 PO" line. The percentage change in MFSP in Table 6.23 is w.r.t to the change in MFSP from the BC labour requirement.

It has been recommended to change the labour requirements from BC line to the "- 1S & -1 PO" line to reduce production costs. The decreased labour is expected to not have significant strain on the plant as when the two shifts per day are included, there are 14 personnel for the line. 14 Personnel adheres to the heuristic of two persons per area and contains the same number of personnel used for a technoeconomic pyrolysis study that was developed to process 600 kg/h of dry biomass [30].

Table 6.23: 8 Scenarios with different labour requirements per shift and impact on MFSP $_{fuel oil}$ and IRR

Labor per shift	BC	-S1	-1 PO	0 S	-1 SO	-1 S & -1 PO	+1 CE & -1 PO	- S + 1 SO & -PO
S	3	2	3	0	3	2	2	2
CE	0	0	0	0	0	0	1	0
MS	1	1	1	1	1	1	1	1
PF	1	1	1	1	1	1	1	1
SO	2	2	2	2	1	2	2	3
PO	2	2	1	2	2	1	1	1
Total	9	8	8	6	8	7	8	8
MFSP: 25% M_{ar} (R/ton)	30 247	29 913	29 471	29 246	29 693	29 137	31 179	29 693
% change in MFSP (%)	0	- 1.1	- 2.6	- 3.3	- 1.8	- 3.7	3.1	- 1.8
IRR (%)	-12.3	-8.3	-5.3	-4.2	-6.6	-3.7	N/A	-6.6

*S-sorter; CE–chemical engineer; MS–maintenance supervisor; PF-production foreman; SO-shift operator; PO-production operator

6.10. Comparison of best conversion processes

The two selected conversion processes, *viz.,* line 11 of the pelleting lines and the 500 °C pyrolysis process were compared to each other w.r.t to a comparison of current market price to MFSP to attain 10% and 25% discount rates. The best-case scenario of each was taken from the result after the second sensitivity (S2). Whereby, pelleting line 11 heated air to a temperature of 115 °C for use in the direct dryer, as explained in Section 6.6.2, and the 500 °C pyrolysis process, used 1 less production operator and 1 less sorter/ labourer as explained in Section 6.9.2 to improve profitability.

In Table 6.24, the current fuel oil is priced at R4.98 per kg and the price of SRF is R1.21 per kg. Whereby, the price of fuel oil was lower than the average price of crude oil in 2019 at R6.4 per L (61 $/bbl.) [369], indicating that this price of fuel oil represents a pessimistic case and the price of the fuel oil might be capable of increasing depending on its application, with its use not only restricted to cement kilns [41]. The price of SRF will depend on the user too as it is not yet competitive against the cheap price of coal in South African at *ca.* R400 per ton [146], [354]. In the current South African market, SRF might be more profitable if sold to international markets, like that current being done by Interwaste [372], [373].

Table 6.24 provided a comparison of the profitability, where IRR and MFSP of the main product of both processes is shown. Neither process is profitable because the current market value is less than the MFSP for both discount rates, as shown in Table 6.24. The current market value for SRF would need to be multiplied by 2.012 and 5.163 times before the MFSP at 10% and 25% discount rate would be achieved, respectively. Similarly, as shown in Table 6.24, the selling price of fuel oil would need to be multiplied by 2.399 and 5.853 times before the MFSP $_{fuel\,oil}$ at 10% and 25% discount rate would be achieved, respectively.

Hence, in comparison to the pyrolysis process, the pelleting process would require a smaller relative increase to the current market value before the MFSP of the main product would be attained. Additionally, as seen in Table 6.24, the IRR for the pelleting process is positive, and the IRR for the pyrolysis process is negative suggesting further proof that for the current economic settings and mill capacity (3.48 ktpa wet feed), the pelleting process might have a higher likelihood of profitability than the pyrolysis process.

The CAPEX, OPEX and efficiency data is included in Table 6.24, whereby production costs on a mass and energy basis for the pyrolysis process were 1.84 and 2.22 times greater than the pelleting process, respectively and within the range specified in a preliminary comparison for biomass pelleting and pyrolysis [34]. Similarly, the energy efficiency of the pyrolysis process is far lower than the pelleting process due to the exclusion of the aqueous phase and higher heating and cooling demands. In Table 6.24, the difference between GEC and NEC for the pelleting process is 11.7% and less than that for the pyrolysis process at 41.9%. This is contentious to the study by Uslu, Faaji

and Bergman, 2008, which reported a smaller difference between the GEC and NEC for the pyrolysis process when compared to the pelleting process for a biomass feedstock [34].

Table 6.24: Comparison of factors for the optimized processes as shown in the simulation of each conversion process

Type	Process	Pelleting	Pyrolysis
Profitability	IRR – Current market value	0.83%	-3.74%
	Current market value	R1 214 per ton SRF	R4 978 per ton fuel oil
	MFSP – 10% discount rate	R2 443 per ton SRF	R11 942 per ton fuel oil
	MFSP – 25% discount rate	R6 269 per ton SRF	R29 137 per ton fuel oil
MFSP/ market value (10% & 25% M_{ar})		2.012 & 5.163	2.399 & 5.853
CAPEX & OPEX	TCI (R mil)	R39.5 mil	R61.6 mil
	Personnel required	4/ shift (1 shift/day)	8/ shift (2 shift/day)
	Production cost (R /ton)	R1 463 per ton SRF	R3 241 per ton products
	Production cost (R /GJ)	R55.3 per GJ $_{SRF}$	R101.8 per GJ $_{products}$
Efficiency	GEC (%)	100.0%	86.95%
	NEC (%)	88.3%	45.1%

The sensitivity analysis for both processes involved adjusting (increasing or decreasing) nine variables by 25% to test the effect this had on MFSP for a 25% discount rate. Sensitivity was measured as a percentage change of the MFSP as a result of adjusting one of nine variables. The sensitivity analyses of the pelleting and pyrolysis process were represented as Figure 6.9 and Figure 6.17, respectively. For both processes, the fixed CAPEX had the most significant effect on MFSP, followed by capacity. For both the fixed CAPEX and capacity, a smaller percentage change from MFSP was expressed for the pyrolysis process (Figure 6.17) than the pelleting process (Figure 6.9). Hence, the MFSP of the pyrolysis process is less sensitive to changes in Fixed CAPEX and capacity than the pelleting process. Conversely, the total OPEX, salaries and electricity were 3 variables which had a greater effect on the MFSP for the pyrolysis process than the pelleting process. This was evident by the greater percentage change in MFSP shown in the pyrolysis process (Figure 6.17) when compared to the pelleting process (Figure 6.9).

Chapter 7: Conclusions

Chapter 7 deals with the main findings for each objective, its contribution to literature and some assumptions or noteworthy points made for each objective. The recommendations for the work going forward are included thereafter.

7.1. Addressing the objectives

7.1.1. To evaluate the suitability of solid-recovered fuel (SRF) derived from pulper rejects for use as alternative fuel in South African cement kilns

The conversion of rejects into waste-derived fuel (WDF) included pre-treatment in the form of drying, extraction of ferrous metals, milling and pelleting to uniform the particle size. No South African standards were found in literature for any WDF and hence a British standard was instead adopted for classification. This standard, known as the Waste Resources and Action Program (WRAP) classification scheme was an improvement to the current European standard for SRF (BS EN 15359, 2011), because it consisted of 3 attributes for each of the 3 factors instead of 1 (as reported for BS EN 15359) and it was suitable for producers of SRF with production rates less than 100 kilotons per annum (ktpa). The environmental attributes were then compared against the permissible emissions specified in the National Air Quality Act 39 of 2004 for South African cement kilns.

The pre-treatment was necessary for the rejects due to the high as-received moisture and ferrous metal content of 46.4 and 7.2 wt.%, respectively. Pre-treatment could reduce the moisture to 5.9 wt.%, extract the ferrous metals and increase the lower heating value (LHV) to 29.7 MJ/kg. The results from the classification of dried, Ø6 mm pellets according to the WRAP classification scheme is shown below. The classes for the 3 factors (economical, technical, and environmental) are each represented by 3 attributes where class 5 indicates the worst possible class and class 1, the best.

- Economical: Biomass content: 5 – LHV: 1 – Moisture content: 1
- Technical: Bulk density: 3 – Chlorine content: 2 – Ash content 1
- Environmental: Mercury content: 2 – Cadmium content: 2 – Heavy metals content: 1

The biomass content attribute was in the worst class for the economic factors because in European markets, companies processing biomass wastes are eligible for receiving government incentives and dried, pulper rejects are mainly plastics. However, no such incentives were observed to exist in the South African market and the high plastic content *ipso facto* increases the LHV and decreases the ash content. Additionally, the calculated specific gas concentrations of the heavy metals were shown to be lower than the maximum permissible concentration in the National Air Quality Act and permissible as alternative fuel for cement kilns (and lignite boilers).

Although South African cement kilns have shown interest in accepting refuse-derived fuel for substituting coal, it is unknown whether international standards are appropriate for the South African market due to lack of national legislature regarding WDF. Similarly, this method for evaluating the permissibility of firing SRF in South African cement kilns should be exercised with caution because the variables used in the calculations vary depending on the cement kiln technology – whereby, the targeted use for this SRF is only for primary burners in cement kilns. However, this research provides a means of comparing the environmental attributes of SRF according to the WRAP classification scheme to the permissible emissions specified according to the National Air Quality Act.

7.1.2. Assess the product yield and energy distribution from the pilot-scale pyrolysis of pulper rejects and how these variables differ from the bench-scale pyrolysis

The pyrolysis of the Ø6 mm pulper rejects that were classified as SRF were also converted to condensable product through pyrolysis on bench and pilot-scale. Pyrolysis experiments from 350 to 550 °C were performed on a bench-scale, batch reactor to identify the best temperature for conversion to condensable product. It was shown that the temperature of 500 °C had highest condensable product yield of 62.4 wt.%, of which over 70 wt.% was wax, and the rest, oil. The higher heating value (HHV) of wax and oil at 500 °C was 40.0 and 20.6 MJ/kg, respectively. The lowered HHV of the oil was attributed to it containing some water. The product of the HHV and yield was the gross energy conversion (GEC), where it was seen that at 500 °C, 86.5% of the feedstock energy was transferred to wax, oil, and char. The product distribution and GEC results attained for the bench-scale pyrolysis were congruent to the results reported from a previous study which tested three reject streams of varying plastic to fibre content. The results were most congruent to that attained for the rejects of highest plastic content.

The high GEC and yield of condensable product at 500 °C for bench-scale, motivated why the temperatures from 450 to 550 °C were tested on pilot-scale. Pyrolysis with the pilot-scale, rotary-kiln reactor showed that at 500 °C, 51.9 wt.% of the reject pellets were converted to a condensable product. The large amount of condensable product from pilot-scale (>1 kg), allowed the separation of the product into the 3 fractions: wax, organic phase oil and aqueous phase oil. The HHV of the wax ranged from 33 to 39 MJ/kg and the HHV of the organic phase oil ranged from 43 to 45 MJ/kg, being comparable to the HHV of gasoline or diesel. Typically, the condensable phase consisted of 35 to 60 wt.% wax, 21 to 33 wt.% organic phase oil and the rest, water-rich aqueous phase. The char product yield was 30 wt.% and higher than bench-scale because plastics tended to condense as heavy waxes in the charpot. The gas produced from the pilot-scale at 550 °C had an HHV of 31.3 MJ/kg and comparable to the comparative study, described in the previous paragraph at bench-scale. Using the product yields from pilot-scale and the HHV of the respective products, the GEC and net-energy conversion (NEC) of the pilot-scale could be determined. The GEC at 500 °C was

89% when the gas phase was also included, and 51.9% for the NEC - representing that almost 40% of the feedstock energy is required for the operation of the pilot-scale reactor.

These results contribute to literature because the availability of research regarding the pilot-scale pyrolysis of pulper rejects are in short supply. Although there are several published articles for the batch pyrolysis and energy conversion efficiencies of rejects on bench-scale, to the best of the author's knowledge there have been no studies regarding the pilot-scale pyrolysis of plastic-rich rejects or the differences in product distribution and energy conversion between bench-scale and pilot-scale. Similarly, through the separation of the undesirable component (aqueous phase oil) of the condensable product, a better representation of the energy-rich fraction of the condensable product was attained. Hence, when using this pilot-scale data for a techno-economic analysis (TEA), the results will provide a better (and more reliable) representation of commercial scale.

7.1.3. Evaluate which conversion process is more profitable at the mill capacity

A TEA was performed for both processes according to the discount cash flow method for a project lifetime of 25 years and mill capacity of 3.48 ktpa of wet rejects. Profitability was tested by comparing the current fuel selling price to the minimum fuel selling price (MFSP) for both processes to attain an internal rate of return (IRR) equal to the discount rate. The MFSP required for a 25% discount rate was used, as required by investors for a profitable venture. If this MFSP was not met, the MFSP for 10% discount rate was used for comparison - as seen in literature for pelleting and pyrolysis lines.

The recovery factor transform function (RFTF) method was used to compare multiple pelleting lines. For the RFTF method, a composition of the as-received rejects was required. Hence, a significant assumption of the pelleting TEA includes estimating the composition of the organic fraction through the area under the thermal degradation curves. The most profitable pelleting line had an SRF selling price of R1 214 per ton. This price was 5.16 times less than the MFSP of the SRF required to attain the 25% discount rate (R6 269 per ton) and still 2.01 times less than the MFSP required to attain a 10% discount rate (R2 443 per ton). The pyrolysis process was modelled through the Aspen Plus tool. Whereby, the product yields were taken from the pilot-scale experiments and model components used to represent the wax, organic phase oil, and aqueous phase oil streams. The main product, fuel oil, was taken as the sum of the wax and organic phase oil and its HHV was calculated as a weighted average. The price of char and fuel oil product was based off its HHV from pilot-scale and a pricing correlation for Pet coke and heavy fuel oil, respectively. The selling price of fuel oil produced from the 500 °C pyrolysis process was R4 978 per ton. This price was 5.85 times less than the MFSP needed to attain a 25% discount rate (R29 137 per ton) and still 2.85 times less the MFSP for a 10% discount rate (R11 942 per ton).

These results, with both conversion process experiencing fuel selling prices less than the MFSP for 25% and 10% discount rates, proves that neither process is profitable using the assumptions used

for the TEA. For both processes to become profitable, either the fixed capital cost would need to be subsidized or the capacity of rejects would need to increase significantly so that the production costs are reduced. Despite not fulfilling the aim of testing which process is most profitable, this study still contributes to the current literature by providing, to the best of the author's knowledge, the first TEA to compare the pelleting and pyrolysis processes for pulper rejects, or any plastic-rich waste stream.

7.2. Recommendations

The recommendations for the experimental and economic analysis sections are described below.

7.2.1. Experimental work

- Continued quality tests on a monthly or seasonal basis should be performed to test the consistency of the SRF. These tests would validify the class code of the SRF.
- The specific technology in which the SRF will be cofired in will result in different environmental results due to the transfer factor. Hence, depending on the firing technology specified by the customer, these results should be recalculated for the appropriate environmental factor.
- Incineration tests could be performed to determine the effectiveness of firing and control of emissions of each alternative fuel (SRF, fuel oil and char) in the cement industry or boilers.
- The effect of other variable such as vapor residence time was not tested for the pilot-scale pyrolysis. Vapor residence time can be manipulated by changing the inert sweeping gas flowrate and might be capable of increasing the condensable product yield.

7.2.2. Simulation work

- Waste diversion plants operating at a similar capacity of around 3.48 ktpa should be approached to see their labour requirements on-site. With very little literature relating to the labour requirements, it is difficult to predict the labour required for small-scale plants.
- More appropriate costing data is necessary for accurate estimation of CAPEX and OPEX demand. All units used in the pyrolysis and pelleting line are based off American heuristics or European costing data. The conversion of these lines with exchange rates might cause the price of the units to significantly inflate in comparison to local costs.
- Interest has been garnered by South African cement kilns to substitute coal with refuse-derive fuel (RDF) (as shown in literature), but without accessible market research regarding the use of fuel oil, SRF and char in South African cement kilns, it is difficult to attain a reasonable market value estimation. Questionnaires could be sent to cement producers near to the paper mill to determine realistic cost estimations.
- The export of the SRF or fuel oil to European or American markets might show higher market prices that could make the process profitable. For this, an international supply chain analysis would need to be performed.
- Use of alternative fuels in other coal intensive industries (e.g., mining) could be investigated.

References

[1]   PAMSA, "Industry Progress Report: Paper in Perspective," Pretoria, South Africa, 2016.

[2]   PAMSA, "Summary finding on 2017 production, import and export statistics: South African Pulp and Paper industry," 2017.

[3]   Green Cape, "Waste: Market Intelligence Report 2019," *Waste*, pp. 1–64, 2019.

[4]   City of Ekurhuleni, "Ekurhuleni Budget: Annexure C - Final tariffs schedules," Ekurhuleni Muncipality, 2019.

[5]   Green Cape, "Waste: Market Intelligence Report 2020," *Waste*, pp. 1–64, 2020.

[6]   Department of Environmental Affairs, "National Environmental management: Waste act, 2008 (Act no. 59 of 2008)," Pretoria, South Africa, 2017.

[7]   T. S. Andritz, "State-of-the-Art Reject Treatment Systems for Recycled Fiber Lines," Ljubljana, Slovenia, 2013.

[8]   World Bank Group, "Increasing the Use of Alternative Fuels at Cement Plants," Washington, D.C., 2017.

[9]   H. von Blottnitz, "Waste management reform and the green economy: When will they meet?," in *Greening the South African Economy: Scoping the Issues, Challenges and Opportunities*, 2016, pp. 252–267.

[10]   BS EN 15359, "Solid recovered fuels - Specification and classes," in *British Standard*, 2011.

[11]   T. Randall Curlee and S. Das, "Viability of Recycling Plastics by Tertiary Processes," *SOLID WASTE Technol.*, no. March/April, pp. 49–58, 1998.

[12]   VNP, "Overview of the reject streams applications," Amsterdam, Netherlands, 2014.

[13]   M. Marsidi, A. Westenbroek, and J. Ringman-Beck, "Maximum value from paper for recycling. Towards a multi-product paper mill," 2011.

[14]   S. Bousios, "Novel bio-based products from side streams of paper and board production," 2016.

[15]   M. Nasrullah, P. Vainikka, J. Hannula, and M. Hurme, "Elemental balance of SRF production process: Solid recovered fuel produced from commercial and industrial waste," *Fuel*, vol. 145, pp. 1–11, 2015.

[16]   M. Nasrullah, P. Vainikka, J. Hannula, M. Hurme, and P. Oinas, "Elemental balance of SRF

production process: Solid recovered fuel produced from municipal solid waste," *Waste Manag. Res.*, vol. 34, no. 1, pp. 38–46, 2016.

[17] M. Nasrullah, P. Vainikka, J. Hannula, M. Hurme, and J. Kärki, "Mass, energy and material balances of SRF production process. Part 2: SRF produced from construction and demolition waste," *Waste Manag.*, vol. 34, no. 11, pp. 2163–2170, 2014.

[18] M. Otten and H. Croezen, "Climate analysis of Subcoal® in coal-fired power plants," no. April, 2015.

[19] M. Otten, A. Van Grinsven, and H. Croezen, "Climate analysis Subcoal ® Subcoal ® from coarse rejects of the paper industry as fuel for limekilns," no. June, 2011.

[20] L. Jennissen and R. Koekoek, "Method for firing an industrial furnace using coal or cokes with a secondary fuel," US 2017/0130958 A1, 2017.

[21] BS EN 15357, "Solid recoverd fuels - Terminology, definitions and descriptions," in *British Standard*, 2011.

[22] J. Hopewell, R. Dvorak, and E. Kosior, "Plastics recycling: Challenges and opportunities," *Philos. Trans. R. Soc. B Biol. Sci.*, vol. 364, no. 1526, pp. 2115–2126, 2009.

[23] T. Salan, M. H. Alma, and E. Altuntaş, "The fuel properties of pyrolytic oils obtained from catalytic pyrolysis of non-recyclable pulper rejects using activated natural minerals," *Energy Sources, Part A Recover. Util. Environ. Eff.*, vol. 41, no. 12, pp. 1460–1473, 2019.

[24] L. J. Brown, F. X. Collard, and J. Görgens, "Pyrolysis of fibre residues with plastic contamination from a paper recycling mill: Energy recoveries," *Energy Convers. Manag.*, vol. 133, pp. 110–117, 2017.

[25] L. J. Brown, F. X. Collard, and J. Görgens, "Fast pyrolysis of fibre waste contaminated with plastic for use as fuel products," *J. Anal. Appl. Pyrolysis*, vol. 138, no. January, pp. 261–269, 2019.

[26] M. Ouadi, C. Greenhalf, N. Jaeger, L. G. Speranza, and A. Hornung, "Thermo-catalytic reforming of pulper rejects from a secondary fibre mill," *Reinf. Plast.*, vol. 26, no. 00, pp. 39–45, 2018.

[27] N. Sophonrat, L. Sandström, I. N. Zaini, and W. Yang, "Stepwise pyrolysis of mixed plastics and paper for separation of oxygenated and hydrocarbon condensates," *Appl. Energy*, vol. 229, no. May, pp. 314–325, 2018.

[28] A. Johansson, L. Sandström, O. G. W. Öhrman, and H. Jilvero, "Co-pyrolysis of woody biomass and plastic waste in both analytical and pilot scale," *J. Anal. Appl. Pyrolysis*, vol. 134,

no. May, pp. 102–113, 2018.

[29] A. M. Petersen, L. J. Brown, F. X. Collard, and J. F. Görgens, "Flowsheet Analysis of Valourising Mixed Lignocellulose and Plastic Wastes via Fast Pyrolysis at a Paper Mill," *Waste and Biomass Valorization*, no. 0123456789, 2020.

[30] Y. Yang, J. G. Brammer, D. G. Wright, J. A. Scott, C. Serrano, and A. V. Bridgwater, "Combined heat and power from the intermediate pyrolysis of biomass materials: performance, economics and environmental impact," *Appl. Energy*, vol. 191, pp. 639–652, 2017.

[31] A. C. Caputo and P. M. Pelagagge, "RDF production plants: II. Economics and profitability," *Appl. Therm. Eng.*, vol. 22, no. 4, pp. 439–448, 2002.

[32] A. C. Caputo and P. M. Pelagagge, "RDF production plants: I. Design and costs," *Appl. Therm. Eng.*, vol. 22, no. 4, pp. 423–437, 2002.

[33] P. Vounatsos, M. Agraniotis, P. Grammelis, E. Kakaras, O. Skiadi, and T. Zarmpoutis, "Refuse-derived fuel classification in a mechanical–biological treatment plant and its valorization with techno-economic criteria," *Int. J. Environ. Sci. Technol.*, vol. 12, no. 3, pp. 1137–1146, 2015.

[34] A. Uslu, A. P. C. Faaij, and P. C. A. Bergman, "Pre-treatment technologies, and their effect on international bioenergy supply chain logistics. Techno-economic evaluation of torrefaction, fast pyrolysis and pelletisation," *Energy*, vol. 33, no. 8, pp. 1206–1223, 2008.

[35] The Waste and Resources Action Programme (WRAP), "A classification scheme to define the quality of waste derive fuels," Banbury, Oxfordshire, United Kingdom, 2012.

[36] R. Sarc, I. M. Seidler, L. Kandlbauer, K. E. Lorber, and R. Pomberger, "Design, quality and quality assurance of solid recovered fuels for the substitution of fossil feedstock in the cement industry – Update 2019," *Waste Manag. Res.*, vol. 37, no. 9, pp. 885–897, 2019.

[37] R. Sarc, K. E. Lorber, R. Pomberger, M. Rogetzer, and E. M. Sipple, "Design, quality, and quality assurance of solid recovered fuels for the substitution of fossil feedstock in the cement industry," *Waste Manag. Res.*, vol. 32, no. 7, pp. 565–585, 2014.

[38] Department of Environmental Affairs, "National Environmental Management: Air Quality Act, 2004(Act No.39 of 2004).," 2010.

[39] S. J. Lee and H. C. Cho, "Optimum design of RDF processing system using RFTF method," *Geosystem Eng.*, vol. 9, no. 1, pp. 15–20, 2006.

[40] The Indian Ministry of Housing and Urban Affairs (MoHUA), "Guidelines on Usage of Refuse

Derived Fuel in Various Industries," New Dehli, India, 2018.

[41] World Bank Group, "Unlocking Value: Alternative Fuels for Egypt's Cement Industry," Washington, D.C., 2016.

[42] CEN/TR 15508, "Key properties on solid recovered fuels to be used for establishing a classification system," in *European committee for standardization*, Brussels, Belgium, 2006.

[43] M. Ouadi, "Sustainable energy from paper industry wastes," Aston University, 2012.

[44] A. Villanueva and H. Wenzel, "Paper waste – Recycling , incineration or landfilling ? A review of existing life cycle assessments q," vol. 27, 2007.

[45] D. Czajczyńska *et al.*, "Potentials of pyrolysis processes in the waste management sector," in *Energy Procedia*, 2017, vol. 123, pp. 387–394.

[46] M. C. Monte, E. Fuente, A. Blanco, and C. Negro, "Waste management from pulp and paper production in the European Union," *Waste Manag.*, vol. 29, no. 1, pp. 293–308, 2009.

[47] M. Ouadi, A. Fivga, H. Jahangiri, M. Saghir, and A. Hornung, "A Review of the Valorization of Paper Industry Wastes by Thermochemical Conversion," *Ind. Eng. Chem. Res.*, vol. 58, no. 35, pp. 15914–15929, 2019.

[48] L. D. Gottumukkala, K. Haigh, F. X. Collard, E. van Rensburg, and J. Görgens, "Opportunities and prospects of biorefinery-based valorisation of pulp and paper sludge," *Bioresour. Technol.*, vol. 215, pp. 37–49, 2016.

[49] PRASA, "Design for Recycling for packaging and paper in South Africa," Bryanston, Johannesburg, South Africa, 2017.

[50] K. Durai-Swamy, D. W. Warren, and M. N. Mansour, "Indirect steam gasification of paper mill sludge waste," *TAPPI*, vol. 74, no. 10, pp. 137–143, 1991.

[51] F. Hansen, "Personal communication," 2018.

[52] J. Arenales Rivera, V. Pérez López, R. Ramos Casado, and J. M. Sánchez Hervás, "Thermal degradation of paper industry wastes from a recovered paper mill using TGA. Characterization and gasification test," *Waste Manag.*, vol. 47, pp. 225–235, 2016.

[53] M. Séverin, C. A. Velis, P. J. Longhurst, and S. J. T. Pollard, "The biogenic content of process streams from mechanical-biological treatment plants producing solid recovered fuel. Do the manual sorting and selective dissolution determination methods correlate?," *Waste Manag.*, vol. 30, no. 7, pp. 1171–1182, 2010.

[54] I. B. Adefeso, "Techn-economic analysis of a gasification system using refuse-derived fuel

from municipal solid waste," Cape Peninsula University of Technology, 2017.

[55] H. Zhou, A. Meng, Y. Long, Q. Li, and Y. Zhang, "Classification and comparison of municipal solid waste based on thermochemical characteristics," *J. Air Waste Manag. Assoc.*, vol. 64, no. 5, pp. 597–616, 2014.

[56] B. Asamoah, J. Nikiema, S. Gebrezgabher, E. Odonkor, and M. Njenga, "A review on Production, Marketing and Use of Fuel Briquettes," in *Resource Recovery and Reuse. Series 7.*, 2016.

[57] D. A. Tillman, *Wood as an energy resource*, 1st ed. New York: Harcourt Brace Jovanovich, 1978.

[58] A. Demirbas, "Combustion characteristics of different biomass fuels," *Progress in Energy and Combustion Science*, vol. 30, no. 2. pp. 219–230, 2004.

[59] R. Wermuth, "The Impact of Coal Quality on Combustion efficiency," 2012.

[60] H. Zhou, Y. Long, A. Meng, Q. Li, and Y. Zhang, "Classification of municipal solid waste components for thermal conversion in waste-to-energy research," *Fuel*, vol. 145, pp. 151–157, 2015.

[61] M. Garcìa-Pérez, A. Chaala, H. Pakdel, D. Kretschmer, and C. Roy, "Vacuum pyrolysis of softwood and hardwood biomass. Comparison between product yields and bio-oil properties," *J. Anal. Appl. Pyrolysis*, vol. 78, no. 1, pp. 104–116, 2007.

[62] P. T. Williams, "6.2 Pyrolysis," in *Waste Treatment and Disposal*, Second., West Sussex, England: John Wiley & Sons Ltd., 2005, pp. 326–337.

[63] E. R. Kaiser, "Chemical Analyses of Refuse Components," *Proc. 1966 Natl. Incin. Conf.*, pp. 84–88, 1966.

[64] R. Geyer, J. R. Jambeck, and K. L. Law, "Production, uses, and fate of all plastics ever made," *Sci. Adv.*, vol. 3, no. 7, p. 5, 2017.

[65] Iupac, "International , Union of Pure Glossary of Basic Terms in Polymer," *Pure Appl. Chem.*, vol. 68, no. 12, pp. 2287–2311, 1996.

[66] K. S. Whiteley, "Polyethylene," in *Ullmann's Encyclopedia of Industrial Chemistry*, 6th ed., Welwyn Garden City, United Kingdom: Wiley-VCH Verlag GmbH & Co. KGaA, Weinheim, 2012, pp. 603–611.

[67] J. M. Heikkinen, J. C. Hordijk, W. De Jong, and H. Spliethoff, "Thermogravimetry as a tool to classify waste components to be used for energy generation," *J. Anal. Appl. Pyrolysis*, vol. 71,

pp. 883–900, 2004.

[68] J. Chattopadhyay, T. S. Pathak, R. Srivastava, and A. C. Singh, "Catalytic co-pyrolysis of paper biomass and plastic mixtures (HDPE (high density polyethylene), PP (polypropylene) and PET (polyethylene terephthalate)) and product analysis," *Energy*, vol. 103, pp. 513–521, 2016.

[69] S. S. Park, D. K. Seo, S. H. Lee, T. Yu, and J. Hwang, "Journal of Analytical and Applied Pyrolysis Study on pyrolysis characteristics of refuse plastic fuel using lab-scale tube furnace and thermogravimetric analysis reactor," *J. Anal. Appl. Pyrolysis*, vol. 97, pp. 29–38, 2012.

[70] A. Aboulkas, K. El, and A. El Bouadili, "Thermal degradation behaviors of polyethylene and polypropylene . Part I : Pyrolysis kinetics and mechanisms," *Energy Convers. Manag.*, vol. 51, no. 7, pp. 1363–1369, 2010.

[71] S. Jung, M. Cho, B. Kang, and J. Kim, "Pyrolysis of a fraction of waste polypropylene and polyethylene for the recovery of BTX aromatics using a fl uidized bed reactor," *Fuel Process. Technol.*, vol. 91, no. 3, pp. 277–284, 2010.

[72] F. Abnisa, W. M. A. W. Daud, and J. N. Sahu, "Pyrolysis of Mixtures of Palm Shell and Polystyrene : An Optional Method to Produce a High-Grade of Pyrolysis Oil," vol. 00, no. 00, pp. 1–8, 2013.

[73] R. H. Perry, D. W. Green, and J. O. Maloney, *Perry's Chemical Engineers' Handbook*. 1997.

[74] S. M. D. Prestes, S. D. Mancini, A. Rodolfo, and R. C. Keiroglo, "Construction and demolition waste as a source of PVC for recycling," *Waste Manag. Res.*, vol. 30, no. 2, pp. 115–121, 2012.

[75] L. J. Gibson, "The hierarchical structure and mechanics of plant materials," *J. R. Soc. Interface*, vol. 9, no. 76, p. pp 2749-2766, 2012.

[76] B. Betts, R. K. Dart, A. S. Ball, and S. L. Pedlar, "Biosynthesis and Structure of Lignocellulose," 1991.

[77] R. Joshi, G. R. Kale, and A. N. Vaidya, "Applications of pyrolysis for carbonaceous wastes in solid waste management – A mini-review," vol. 1, no. 1, pp. 10–25, 2018.

[78] C. H. Wu, C. Y. Chang, and C. H. Tseng, "Pyrolysis products of uncoated printing and writing paper of MSW," *Fuel*, vol. 81, no. 6, pp. 719–725, 2002.

[79] N. Miskolczi, F. Ateş, and N. Borsodi, "Comparison of real waste (MSW and MPW) pyrolysis in batch reactor over different catalysts. Part II: Contaminants, char and pyrolysis oil properties," *Bioresour. Technol.*, vol. 144, pp. 370–379, 2013.

[80] A. Demirbaş and A. Şahin, "Evaluation of biomass residue 1. Briquetting waste paper and wheat straw mixtures," *Fuel Process. Technol.*, vol. 55, no. 2, pp. 175–183, 1998.

[81] C. H. Wu, C. Y. Chang, C. H. Tseng, and J. P. Lin, "Pyrolysis product distribution of waste newspaper in MSW," *J. Anal. Appl. Pyrolysis*, vol. 67, no. 1, pp. 41–53, 2003.

[82] H. Chen, *Biotechnology of lignocellulose: Theory and practice*. 2014.

[83] F. Collard and J. Blin, "A review on pyrolysis of biomass constituents : Mechanisms and composition of the products obtained from the conversion of cellulose , hemicelluloses and lignin," *Renew. Sustain. Energy Rev.*, vol. 38, pp. 594–608, 2014.

[84] H. Yang, R. Yan, T. Chin, D. T. Liang, H. Chen, and C. Zheng, "Thermogravimetric Analysis−Fourier Transform Infrared Analysis of Palm Oil Waste Pyrolysis," *Energy & Fuels*, vol. 18, no. 6, pp. 1814–1821, 2004.

[85] N. Lavoine, I. Desloges, A. Dufresne, and J. Bras, "Microfibrillated cellulose - Its barrier properties and applications in cellulosic materials: A review," *Carbohydr. Polym.*, vol. 90, no. 2, pp. 735–764, 2012.

[86] M. A. Hubbe and O. J. Rojas, "Colloidal stability and aggregation of Lignocellulosic materials in aqueous suspension: A review," *BioResources*, vol. 3, no. 4, pp. 1419–1491, 2008.

[87] G. O. Aspinall, "Chemistry of Carbohydrates," *Annu. Rev. Biochem.*, vol. 31, no. July, pp. 79–102, 1961.

[88] R. E. Sommerlad, W. R. Seeker, A. Finkelstein, and J. D. Kilgroe, "Environmental characterization of refuse derived fuel incinerator technology," *AIChE Symp. Ser.*, vol. 84, no. 265, pp. 115–126, 1988.

[89] S. Kerdsuwan, P. Meenaroch, and T. Chalermcharoenrat, "The Novel Design and Manufacturing Technology of Densified RDF from Reclaimed Landfill without a Mixing Binding Agent Using a Hydraulic Hot Pressing Machine," *MATEC Web Conf.*, vol. 70, pp. 5–8, 2016.

[90] C. A. Velis, P. J. Longhurst, G. H. Drew, R. Smith, and S. J. T. Pollard, "Production and quality assurance of solid recovered fuels using mechanical-biological treatment (MBT) of waste: A comprehensive assessment," *Crit. Rev. Environ. Sci. Technol.*, vol. 40, no. 12, pp. 979–1105, 2010.

[91] S. T. Wagland *et al.*, "Comparison of coal/solid recovered fuel (SRF) with coal/refuse derived fuel (RDF) in a fluidised bed reactor," *Waste Manag.*, vol. 31, no. 6, pp. 1176–1183, 2011.

[92] S. Flamme and J. Geiping, "Quality standards and requirements for solid recovered fuels: A review," *Waste Manag. Res.*, vol. 30, no. 4, pp. 335–353, 2012.

[93]   S. A. Viczek, A. Aldrian, R. Pomberger, and R. Sarc, "Determination of the material-recyclable share of SRF during co-processing in the cement industry," *Resour. Conserv. Recycl.*, vol. 156, no. October 2019, p. 104696, 2020.

[94]   K. Isaac, "The Co-Combustion Performance of South African Coal and Refuse Derived Fuel," no. November, 2019.

[95]   M. Kara, E. E. GÜNAY, Y. Y. TABAK, Ş. YILDIZ, and V. ENC, "The Usage of Refuse Derived Fuel From Urban Solid Waste in Cement Industry As an Alternative Fuel," *6th IASME/WSEAS Int. Conf. HEAT Transf.*, pp. 172–177, 2008.

[96]   M. N. Pedersen, "Co-firing of alternative fuels in cement kiln burners," Technical University of Denmark, 2018.

[97]   S. Sadaka and A. A. Boateng, "Pyrolysis and Bio Oil," *Agric. Nat. Resour.*, no. Figure 1, pp. 1–25, 2017.

[98]   Y. Yang *et al.*, "Characterisation of waste derived intermediate pyrolysis oils for use as diesel engine fuels," vol. 103, pp. 247–257, 2013.

[99]   L. Quesada, M. Calero, M. A. Martín-Lara, A. Pérez, and G. Blázquez, "Characterization of fuel produced by pyrolysis of plastic film obtained of municipal solid waste," *Energy*, vol. 186, no. 2019, 2019.

[100] A. López, I. de Marco, B. M. Caballero, M. F. Laresgoiti, and A. Adrados, "Pyrolysis of municipal plastic wastes: Influence of raw material composition," *Waste Manag.*, vol. 30, no. 4, pp. 620–627, 2010.

[101] M. Ouadi, C. Greenhalf, N. Jaeger, L. G. Speranza, and A. Hornung, "Thermo-catalytic reforming of co-form® rejects (waste cleansing wipes)," *J. Anal. Appl. Pyrolysis*, vol. 132, no. March, pp. 33–39, 2018.

[102] A. Korkmaz, J. Yanik, M. Brebu, and C. Vasile, "Pyrolysis of the tetra pak," *Waste Manag.*, vol. 29, no. 11, pp. 2836–2841, 2009.

[103] SASOL™, "Safety Data Sheet: Waxy Oil 30," Johannesburg, South Africa, 2018.

[104] SASOL™, "Safety Data Sheet: Waxy oil 12," Johannesburg, South Africa, 2018.

[105] SASOL™, "Safety Data Sheet: Fuel Oil 6," Johannesburg, South Africa, 2018.

[106] SASOL™, "Safety data sheet: Fuel oil 150," Johannesburg, South Africa, 2017.

[107] D. Āriņa, K. Kļavenieks, and J. Burlakovs, "The Cost-estimation of Mechanical Pre-treatment Lines of Municipal Solid Waste in Latvia," *Proc. Latv. Univ. Agric.*, vol. 32, no. 1, pp. 17–28,

2015.

[108] V. S. Rotter, T. Kost, J. Winkler, and B. Bilitewski, "Material flow analysis of RDF-production processes," *Waste Manag.*, vol. 24, no. 10, pp. 1005–1021, 2004.

[109] L. Del Zotto, A. Tallini, G. Di Simone, G. Molinari, and L. Cedola, "Energy enhancement of Solid Recovered Fuel within systems of conventional thermal power generation," *Energy Procedia*, vol. 81, pp. 319–338, 2015.

[110] D. Garcés, E. Díaz, H. Sastre, S. Ordóñez, and J. M. González-LaFuente, "Evaluation of the potential of different high calorific waste fractions for the preparation of solid recovered fuels," *Waste Manag.*, vol. 47, no. August, pp. 164–173, 2016.

[111] G. Habert, C. Billard, P. Rossi, C. Chen, and N. Roussel, "Cement production technology improvement compared to factor 4 objectives," *Cem. Concr. Res.*, vol. 40, no. 5, pp. 820–826, 2010.

[112] Parliament of the Republic of South Africa, *Carbon Tax Bill (As introduced in the National Assembly (proposed section 77)).* 2018.

[113] Department Environmental Affairs, "National Waste Management Strategy," Pretoria, South Africa, 2011.

[114] J. Doraiswamy, N. J. Sell, J. Norman, G. Massey, K. Nelson, and M. Doshi, "Use of secondary-fiber rejects as fuel for a coal-fired stoker boiler," 1996.

[115] H. Manninen, K. Peltola, and J. Ruuskanen, "Co-combustion of refuse-derived and packaging-derived fuels (RDF and PDF) with conventional fuels," *Waste Manag. Res.*, vol. 15, no. 2, pp. 137–147, 1997.

[116] I. Barnes, "Operating experience of low grade fuels in circulating fluidised bed combustion," no. June, 2015.

[117] C. Ibbetson, K. Wengenroth, R. Fuels, and T. U. Gmbh, "Optimisation of Fuels from MBT Processes Drivers for the production of Waste Derived Fuels," pp. 372–384, 2007.

[118] BS EN 15296, "EN 15296. Solid biofuels. Conversion of analytical results from one basis to another," in *British Standards Institution (BSI)*, 2011.

[119] C. K. Öqvist, "Microbial Life and Deposits in Department of Applied Chemistry and Microbiology," University of Helsinki, 2008.

[120] P. Vainikka *et al.*, "Bromine as an ash forming element in a fluidised bed boiler combusting solid recovered fuel," *Fuel*, vol. 90, no. 3, pp. 1101–1112, 2011.

[121] Y. Setiawan and A. Surachman, "Reject waste pellets of paper mills as fuel and their Contribution to Greenhouse Gas (GHG)," *Int. J. Technol.*, vol. 6, no. 5, pp. 847–855, 2015.

[122] E. Iacovidou, J. Hahladakis, I. Deans, C. Velis, and P. Purnell, "Technical properties of biomass and solid recovered fuel (SRF) co-fired with coal: Impact on multi-dimensional resource recovery value," *Waste Manag.*, vol. 73, pp. 535–545, 2018.

[123] L. Jennisen and N. Roberts, "Subcoal ® Concept Paper," Nieuw-Bergen, The Netherlands, 2015.

[124] H. Wu, A. J. Pedersen, P. Glarborg, F. J. Frandsen, K. Dam-Johansen, and B. Sander, "Formation of fine particles in co-combustion of coal and solid recovered fuel in a pulverized coal-fired power station," *Proc. Combust. Inst.*, vol. 33, no. 2, pp. 2845–2852, 2011.

[125] T. Hilber, H. Thorwarth, V. Stack-Lara, M. Schneider, J. Maier, and G. Scheffknecht, "Fate of mercury and chlorine during SRF co-combustion," *Fuel*, vol. 86, no. 12–13, pp. 1935–1946, 2007.

[126] J. Kers and P. Krizan, "Mechanical Recycling of Compounded Plastic Waste for Material Valorization by Briquetting," vol. 21, pp. 39–44, 2010.

[127] J. Kers, P. Kulu, A. Aruniit, V. Laurmaa, and P. Križan, "Determination of physical , mechanical and burning characteristics of polymeric waste material briquettes," pp. 307–316, 2010.

[128] J. S. Tumuluru, "Effect of pellet die diameter on density and durability of pellets made from high moisture woody and herbaceous biomass," *Carbon Resour. Convers.*, vol. 1, no. 1, pp. 44–54, 2018.

[129] W. Stelte, J. K. Holm, A. R. Sanadi, S. Barsberg, J. Ahrenfeldt, and U. B. Henriksen, "Fuel pellets from biomass : The importance of the pelletizing pressure and its dependency on the processing conditions," *Fuel*, vol. 90, no. 11, pp. 3285–3290, 2011.

[130] W. Stelte, A. R. Sanadi, L. Shang, and J. K. Holm, "Recent developments in biomass pelletization – a review," *BioResources*, vol. 7, no. 3, pp. 4451–4490, 2012.

[131] C. Schilling, J. S. Lee, B. Ghiasi, M. Tajilrou, and M. Wöhler, "Towards manufacturing the ' ideal pellet .'"

[132] O. Williams, S. Taylor, E. Lester, S. Kingman, D. Giddings, and C. Eastwick, "Applicability of Mechanical Tests for Biomass Pellet Characterisation for Bioenergy Applications," *Materials (Basel).*, vol. 11, no. 8, p. 1329, 2018.

[133] S. özge Gönen, "Briquetting of coal - Biomass Blends," Istanbul Technical University, 2010.

[134] N. Kaliyan and R. Vance Morey, "Factors affecting strength and durability of densified biomass products," *Biomass and Bioenergy*, vol. 33, no. 3, pp. 337–359, 2009.

[135] S. Yaman and S. Kuc, "Yaman et. al. - 2000 - Production of fuel briquettes from olive refuse and paper mill waste.pdf," pp. 23–31, 2000.

[136] S. K. Jha, A. Singh, and A. Kumar, "Physical characteristics of compressed cotton stalks," *Biosyst. Eng.*, vol. 99, no. 2, pp. 205–210, 2008.

[137] Y. Li, H. Liu, and O. Zhang, "High-pressure compaction of municipal solid waste to form densified fuel," pp. 81–91, 2001.

[138] P. D. Grover and S. K. Mishra, "Biomass briquetting: Technology and Practices," in *Regional Wood Energy Development Programme in Asia*, 1996, no. 46.

[139] ISO 17225-1, "Solid biofuels — Fuel specifications and classes," in *Annual Book of ISO Standards*, vol. 2014, 2014.

[140] L. Jennissen, "Subcoal® Production FRM," *N+P*, 2017. [Online]. Available: https://www.subcoal-international.com/locaties/subcoal(r)-subcoal-production-frm. [Accessed: 27-Mar-2019].

[141] A. Rahman, M. G. Rasul, M. M. K. Khan, and S. Sharma, "Recent development on the uses of alternative fuels in cement manufacturing process," *Fuel*, vol. 145, no. December, pp. 84–99, 2015.

[142] World Bank Group, "South Africa Energy Situation," *Energypedia*, 2014. [Online]. Available: https://energypedia.info/wiki/South_Africa_Energy_Situation. [Accessed: 27-May-2020].

[143] R. Sarc and K. E. Lorber, "Production, quality and quality assurance of Refuse Derived Fuels (RDFs)," *Waste Manag.*, vol. 33, no. 9, pp. 1825–1834, 2013.

[144] United Nations Environment Programme, "Feasibility study to use waste as fuel for cement factories Reference number : 2015-036 / MOZ-01 Output 1 : Report on the technical feasibility study for RDF production and its use as fuel in cement factories," pp. 1–64, 2015.

[145] R. Pomberger and R. Sarc, "Use of Solid Recovered Fuels in the Cement Industry," *Waste Manag.*, vol. 4, no. January, pp. 471–488, 2014.

[146] KfW Bankengruppe, "Feasibility study for an Advanced Integrated Solid Waste Management System for Rustenburg Local Municipality (RLM)," Rustenburg, South Africa, 2016.

[147] M. Mersmann, "Burning alternative fuels in cement kilns," *ZKG International*, 2014. [Online]. Available:

https://www.zkg.de/en/artikel/zkg_Burning_alternative_fuels_in_cement_kilns_2018848.html . [Accessed: 13-Nov-2020].

[148] K. H. Karstensen, "National Policy on High Temperature Thermal Waste Treatment and Cement Kiln Alternative Fuel Use," Pretoria, South Africa, 2007.

[149] Y. Xue, "Thermochemical Conversion of Organic and Plastic Waste Materials through Pyrolysis," p. 157, 2017.

[150] P. Capros, N. Kouvaritakis, and L. Mantzos, "Economic Evaluation of Sectoral Emission Reduction Objectives for Climate Change - Top-down Analysis of Greenhouse Gas Emission Reduction Possibilities in the EU," *Analysis*, no. May 2014, p. 120, 2001.

[151] G. M. Stefanović, G. D. Vučković, M. M. Stojiljković, and M. B. Trifunović, "CO2 reduction options in cement industry - The Novi Popovac case," *Therm. Sci.*, vol. 14, no. 3, pp. 671–679, 2010.

[152] H. Winkler, "Renewable energy policy in South Africa: Policy options for renewable electricity," *Energy Policy*, vol. 33, no. 1, pp. 27–38, 2005.

[153] A. Hlaba, A. Rabiu, and O. A. Osibote, "Refuse Derived Fuel Pellets as a Renewable Energy Source," in *International Proceedings of Chemical, Biological and Environmental Engineering*, 2017, vol. 32, no. 1, pp. 12–16.

[154] J. Lauridsen, "National Policy on High Temperature Thermal Waste Treatment and Cement Kiln Alternative Fuel Use:," Svendborg, Denmark, 2008.

[155] E. Mokrzycki and A. Uliasz- Bocheńczyk, "Alternative fuels for the cement industry," *Appl. Energy*, vol. 74, no. 1–2, pp. 95–100, 2003.

[156] W. R. Podolski, S. A. Miller, D. K. Schnialzer, and A. G. Fonseca, "Energy Resources, Conversion, and Utilization," in *PERRY'S CHEMICAL ENGINEERS' HANDBOOK*, Seventh., I. The McGraw-Hill Companies, Ed. The McGraw-Hill Companies, Inc., 1997.

[157] H. Von Blottnitz, A. Pehlken, and T. Pretz, "The description of solid wastes by particle mass instead of particle size distributions," *Resour. Conserv. Recycl.*, vol. 34, no. 3, pp. 193–207, 2002.

[158] P. E. Mason, L. I. Darvell, J. M. Jones, M. Pourkashanian, and A. Williams, "Single particle flame-combustion studies on solid biomass fuels," *Fuel*, vol. 151, pp. 21–30, 2015.

[159] C. R. Rhyner, L. J. Schwartz, R. B. Wenger, and M. G. Kohrell, "Chapter 5: Processing Solid Waste and Recyclable Materials," in *Waste Management and Resource Recovery*, vol. 53, no. 9, Boca Raton, Florida: Taylor & Francis Group, 1995, pp. 153–179.

[160] Andritz, "Industrial Pelleting Technologies," 2019. [Online]. Available: https://www.andritz.com/resource/blob/333840/b46c95da02e0edf67911082ba0abc497/fb-industrial-pelleting-technologies-data.pdf. [Accessed: 07-Jul-2020].

[161] N.-B. Chang and Y. H. Chang, "Benefit/Cost Analysis of RDF Process in Taiwan," *Fifth North Am. WastetoEnergy Conf. Res. Triangle Park NC April 2125 1997*, pp. 1007–1023, 1997.

[162] T. Wolfsberger, M. Pinkel, S. Polansek, R. Sarc, R. Hermann, and R. Pomberger, "Landfill mining: Development of a cost simulation model," *Waste Manag. Res.*, vol. 34, no. 4, pp. 356–367, 2016.

[163] Department of Labor, "Government Gazette Staatskoerant," *Gov. Gaz.*, vol. 583, no. 37230, pp. 1–4, 2020.

[164] M. Nafid and R. Koekoek, "Method for processing a mixture of cellulose/ plastic waste particles to form a fuel," 2017.

[165] R. Conti, N. Jäger, J. Neumann, A. Apfelbacher, R. Daschner, and A. Hornung, "Thermocatalytic Reforming of Biomass Waste Streams," *Energy Technol.*, vol. 5, no. 1, pp. 104–110, 2017.

[166] M. Hoeft and W. Emhofer, "Report on market research, national incidents, problems and lacks within national guidelines," 2013.

[167] S. Zafar, "Fuel Pellets from Solid Wastes," *BioEnergy Consult*, 2009. [Online]. Available: https://www.solidwastemag.com/feature/waste-pelletization/.

[168] A. Pirraglia, R. Gonzalez, and D. Saloni, "Techno-economical analysis of wood pellets production for U.S. manufacturers," *BioResources*, vol. 5, no. 4, pp. 2374–2390, 2010.

[169] B. Dudenhoefer, "Is Tramp Metal Wreaking Havoc in Your Pulp or Paper Mill?," *Eriez*, no. March, Mar-2012.

[170] J. S. Tumuluru, "Effect of process variables on the density and durability of the pellets made from high moisture corn stover," *Biosyst. Eng.*, vol. 119, pp. 44–57, 2014.

[171] L. Shang *et al.*, "Lab and Bench-Scale Pelletization of Torrefied Wood Chips-Process Optimization and Pellet Quality," *Bioenergy Res.*, vol. 7, no. 1, pp. 87–94, 2014.

[172] L. Axelsson, M. Franzén, M. Ostwald, G. Berndes, G. Lakshmi, and N. H. Ravindranath, "Perspective: Jatropha cultivation in southern India: Assessing farmers' experiences," *Biofuels, Bioprod. Biorefining*, vol. 6, no. 3, pp. 246–256, 2012.

[173] N. P. K. Nielsen, D. J. Gardner, T. Poulsen, and C. Felby, "Importance of temperature,

moisture content, and species for the conversion process of wood residues into fuel pellets," *Wood Fiber Sci.*, vol. 41, no. 4, pp. 414–425, 2009.

[174] M. Thomas, D. J. Van Zuilichem, and A. F. B. Van Der Poel, "Physical quality of pelleted animal feed. 2. Contribution of processes and its conditions," *Anim. Feed Sci. Technol.*, vol. 64, no. 2–4, pp. 173–192, 1997.

[175] C. J. Sprenger, "Classification and densification of municipal solid waste for biofuels applica," University of Saskatchewan, Saskatoon, 2017.

[176] N. P. K. Nielsen, J. K. Holm, and C. Felby, "Effect of fiber orientation on compression and frictional properties of sawdust particles in fuel pellet production," *Energy and Fuels*, vol. 23, no. 6, pp. 3211–3216, 2009.

[177] C. Serrano, E. Monedero, M. Lapuerta, and H. Portero, "Effect of moisture content , particle size and pine addition on quality parameters of barley straw pellets," *Fuel Process. Technol.*, vol. 92, no. 3, pp. 699–706, 2011.

[178] M. Jewiarz, K. Mudryk, M. Wróbel, J. Fraczek, and K. Dziedzic, "Parameters affecting RDF-based pellet quality," *Energies*, vol. 13, no. 4, 2020.

[179] C. J. Sprenger, L. G. Tabil, M. Soleimani, J. Agnew, and A. Harrison, "Pelletization of refuse-derived fuel fluff to produce high quality feedstock," *J. Energy Resour. Technol. Trans. ASME*, vol. 140, no. 4, 2018.

[180] D. A. Vallero, "Thermal Waste Treatment," in *Waste: A handbook for Managment*, First., T. M. Letcher and D. A. Vallero, Eds. Durham, N. Carolina, USA: Elsevier, 2011, pp. 219–231.

[181] S. M. Al-Salem, A. Antelava, A. Constantinou, G. Manos, and A. Dutta, "A review on thermal and catalytic pyrolysis of plastic solid waste (PSW)," *J. Environ. Manage.*, vol. 197, no. 1408, pp. 177–198, 2017.

[182] A. Buekens, *Introduction to Feedstock Recycling of Plastics*. 2006.

[183] R. W. J. Westerhout, J. A. M. Kuipers, and W. P. M. Van Swaaij, "Experimental Determination of the Yield of Pyrolysis Products of Polyethene and Polypropene. Influence of Reaction Conditions," *Ind. Eng. Chem. Res.*, vol. 37, no. 3, pp. 841–847, 1998.

[184] N. N. Kasim *et al.*, "Optimization of pyrolysis process parameters of torrefied demineralized palm empty fruit bunch (TDEFB) by response surface methodology," *Proceeding Int. Conf. Math. Eng. Ind. Appl.*, vol. 2013, no. October, 2018.

[185] E. Menya, P. W. Olupot, H. Storz, M. Lubwama, Y. Kiros, and M. J. John, "Optimization of pyrolysis conditions for char production from rice husks and its characterization as a precursor

for production of activated carbon," *Biomass Convers. Biorefinery*, vol. 10, no. 1, pp. 57–72, 2020.

[186] L. Quesada, A. Pérez, V. Godoy, F. J. Peula, M. Calero, and G. Blázquez, "Optimization of the pyrolysis process of a plastic waste to obtain a liquid fuel using different mathematical models," *Energy Convers. Manag.*, vol. 188, no. January, pp. 19–26, 2019.

[187] A. S. Abbas and S. D. A. Shubar, "Pyrolysis of High-density Polyethylene for the Production of Fuel-like Liquid Hydrocarbon," *IJCPE Iraqi J. Chem. Pet. Eng.*, vol. 99, no. 231, pp. 23–29, 2008.

[188] J. Walendziewski, "Engine fuel derived from waste plastics by thermal treatment," *Fuel*, vol. 81, no. 4, pp. 473–481, 2002.

[189] J. J. Park, K. Park, J. W. Park, and D. C. Kim, "Characteristics of LDPE pyrolysis," *Korean J. Chem. Eng.*, vol. 19, no. 4, pp. 658–662, 2002.

[190] F. Chireshe, F. X. Collard, and J. F. Görgens, "Production of an upgraded bio-oil with minimal water content by catalytic pyrolysis: Optimisation and comparison of CaO and MgO performances," *J. Anal. Appl. Pyrolysis*, vol. 146, no. December 2019, p. 104751, 2020.

[191] M. D. R. Hernández, Á. N. García, A. Gómez, J. Agulló, and A. Marcilla, "Effect of residence time on volatile products obtained in the HDPE pyrolysis in the presence and absence of HZSM-5," *Ind. Eng. Chem. Res.*, vol. 45, no. 26, pp. 8770–8778, 2006.

[192] S. van der Westhuizen, "Pyrolysis of contaminated PS single-layer and LDPE / PET multi-layer waste plastic packaging to optimise the production of oil for fuel applications," Stellenbosch University, 2020.

[193] B. Zhu and Y. Sun, "Co-pyrolysis Polystyrene / Fir : Pyrolysis Characteristics and Pyrolysis Kinetic Studies," in *2011 Third International Conference on Measuring Technology and Mechatronics Automation Co-pyrolysis*, 2011.

[194] M. J. Antal, "Cellulose Pyrolysis Kinetics: The Current State of Knowledge," pp. 703–717, 1995.

[195] L. Zajec, "Slow pyrolysis in a rotary kiln reactor: Optimization and experiment," *Sch. Renew. Energy Sci.*, pp. 1–78, 2009.

[196] C. G. Jung and A. Fontana, "Production of Gaseous and Liquid Fuels by Pyrolysis and Gasification of Plastics : Technological," in *Feedstock Recycling and Pyrolys is of Waste Plastics: Converting Waste Plastics into Diesel and Other Fuels*, J. Scheirs., L. John Wiley & Sons, Ed. 2006.

[197] A. Demirbas, "Biorefineries: Current activities and future developments," *Energy Convers. Manag.*, vol. 50, no. 11, pp. 2782–2801, 2009.

[198] A. V. Bridgwater, "Renewable fuels and chemicals by thermal processing of biomass," *Chem. Eng. J.*, vol. 91, no. 2–3, pp. 87–102, 2003.

[199] D. Mohan, C. U. Pittman, and P. H. Steele, "Pyrolysis of wood/biomass for bio-oil: A critical review," *Energy and Fuels*, vol. 20, no. 3, pp. 848–889, 2006.

[200] A. Demirbaş and G. Arin, "An overview of biomass pyrolysis," *Energy Sources*, vol. 24, no. 5, pp. 471–482, 2002.

[201] A. V. Bridgwater, "Review of fast pyrolysis of biomass and product upgrading," *Biomass and Bioenergy*, vol. 38, pp. 68–94, 2012.

[202] A. V. Bridgwater, "Review: Biomass for energy," *J. Sci. Food Agric.*, vol. 1243, no. December 2005, pp. 1237–1243, 2007.

[203] D. A. Bulushev and J. R. H. Ross, "Catalysis for conversion of biomass to fuels via pyrolysis and gasification: A review," *Catal. Today*, vol. 171, no. 1, pp. 1–13, 2011.

[204] A. M. C. J. J. Ridout, "Chapter 6: Chemicals and biomaterials production from vacuum, slow and fast pyrolysis processes for low and high ash paper waste sludge," in *Valorisation of paper waste sludge using pyrolysis processing*, no. March, 2016.

[205] F. Shafizadeh and W. F. DeGroot, *Combustion Characteristics of Cellulosic Fuels*. ACADEMIC PRESS, INC., 1976.

[206] G. Zattini *et al.*, "Pyrolysis of Low-Density Polyethylene," in *Sustainable Design and Manufacturing 2017 Selected papers on Sustainable Design and Manufacturing*, vol. 68, 2017, pp. 480–492.

[207] R. Miranda, J. Yang, C. Roy, and C. Vasile, "Vacuum pyrolysis of PVC I. Kinetic study," *Polym. Degrad. Stab.*, vol. 64, no. 1, pp. 127–144, 1999.

[208] B. Saha and A. K. Ghoshal, "Thermal degradation kinetics of poly(ethylene terephthalate) from waste soft drinks bottles," *Chem. Eng. J.*, vol. 111, no. 1, pp. 39–43, 2005.

[209] L. Sorum, M. G. Gronli, and J. E. Hustad, "Pyrolysis characteristics and kinetics of municipal solid wastes," *Fuel*, vol. 80, no. 9, pp. 1217–1227, 2001.

[210] A. Marongiu, T. Faravelli, G. Bozzano, M. Dente, and E. Ranzi, "Thermal degradation of poly(vinyl chloride)," *J. Anal. Appl. Pyrolysis*, vol. 70, no. 2, pp. 519–553, 2003.

[211] A. Aboulkas, K. El Harfi, and A. El Bouadili, "Pyrolysis of olive residue/low density polyethylene

mixture: Part I Thermogravimetric kinetics," *J. Fuel Chem. Technol.*, vol. 36, no. 6, pp. 672–678, 2008.

[212] B. Lai *et al.*, "Kinetic studies of co-pyrolysis of rubber seed shell with high density polyethylene," *ENERGY Convers. Manag.*, vol. 87, pp. 746–753, 2014.

[213] X. Jing, G. Yan, Y. Zhao, H. Wen, and Z. Xu, "Cocracking Kinetics of PE / PP and PE / Hydrocarbon Mixtures (I) PE / PP Mixtures," no. I, 2014.

[214] J. K. Modh, S. a Namjoshi, and S. a Channiwala, "Kinetics and Pyrolysis of Glossy Paper Waste," vol. 2, no. 2, pp. 1067–1074, 2012.

[215] J. Chattopadhyay, C. Kim, R. Kim, and D. Pak, "Thermogravimetric characteristics and kinetic study of biomass co-pyrolysis with plastics," *Korean J. Chem. Eng.*, vol. 25, no. 5, pp. 1047–1053, 2008.

[216] Y. Matsuzawa, M. Ayabe, and J. Nishino, "Acceleration of cellulose co-pyrolysis with polymer," vol. 71, pp. 435–444, 2001.

[217] H. Yang, R. Yan, H. Chen, D. H. Lee, and C. Zheng, "Characteristics of hemicellulose, cellulose and lignin pyrolysis," *Fuel*, vol. 86, no. 12–13, pp. 1781–1788, 2007.

[218] S. Wang, B. Ru, H. Lin, and W. Sun, "Pyrolysis behaviors of four O-acetyl-preserved hemicelluloses isolated from hardwoods and softwoods," *Fuel*, vol. 150, pp. 243–251, 2015.

[219] S. Soares, G. Camino, and S. Levchik, "Comparative study of the thermal decomposition of pure cellulose and pulp paper," *Polym. Degrad. Stab.*, vol. 49, no. 2, pp. 275–283, 1995.

[220] D. Zhao, Y. Dai, K. Chen, Y. Sun, F. Yang, and K. Chen, "Effect of potassium inorganic and organic salts on the pyrolysis kinetics of cigarette paper," *J. Anal. Appl. Pyrolysis*, vol. 102, pp. 114–123, 2013.

[221] W. K. Buah, A. M. Cunliffe, and P. T. Williams, "Characterization of products from the pyrolysis of municipal solid waste," *Process Saf. Environ. Prot.*, vol. 85, no. 5 B, pp. 450–457, 2007.

[222] A. Anca-Couce, *Reaction mechanisms and multi-scale modelling of lignocellulosic biomass pyrolysis*, vol. 53, no. March 2016. 2016.

[223] I. P. Boukis, "Fast Pyrolysis of Biomass in a Circulaing Fluidised Bed Reactor," pp. 56–57, 1997.

[224] F. J. Kilzer and A. Broido, "Speculations on the Nature of Cellulose Pyrolysis," *Pyrodynamics*, vol. 2, no. April 1964, pp. 151–163, 1965.

[225] F. Shafizadeh and A. G. W. Bradbury, "Thermal degradation of cellulose in air and nitrogen

at low temperatures," *J. Appl. Polym. Sci.*, vol. 23, no. 5, pp. 1431–1442, 1979.

[226] J. L. Banyasz, S. Li, J. Lyons-Hart, and K. H. Shafer, "Gas evolution and the mechanism of cellulose pyrolysis," *Fuel*, vol. 80, no. 12, pp. 1757–1763, 2001.

[227] G. N. Richards, "Glycolaldehyde from pyrolysis of cellulose," *J. Anal. Appl. Pyrolysis*, vol. 10, no. 3, pp. 251–255, 1987.

[228] J. Piskorz, D. S. A. G. Radlein, D. S. Scott, and S. Czernik, "Pretreatment of wood and cellulose for production of sugars by fast pyrolysis," *J. Anal. Appl. Pyrolysis*, vol. 16, no. 2, pp. 127–142, 1989.

[229] Y. Chhiti and M. Kemiha, "Thermal Conversion of Biomass, Pyrolysis and Gasification: A Review," *Int. J. Eng. Sci.*, vol. 2, no. 3, pp. 75–85, 2013.

[230] A. N. Phan, C. Ryu, V. N. Sharifi, and J. Swithenbank, "Characterisation of slow pyrolysis products from segregated wastes for energy production," *J. Anal. Appl. Pyrolysis*, vol. 81, no. 1, pp. 65–71, 2008.

[231] P. T. Williams, C. Efica, P. B. Sanchez, L. Myers, C. Wu, and J. a Onwudili, "Hydrogen and syngas production from pyrolysis-gasification of RDF and wood pellets in a continuous screw kiln reactor," *19th Eur. Biomass Conf. Exhib.*, no. June, pp. 1134–1136, 2011.

[232] R. K. Singh and B. Ruj, "Time and temperature depended fuel gas generation from pyrolysis of real world municipal plastic waste," *Fuel*, vol. 174, pp. 164–171, 2016.

[233] A. Adrados, I. de Marco, B. M. Caballero, A. López, M. F. Laresgoiti, and A. Torres, "Pyrolysis of plastic packaging waste: A comparison of plastic residuals from material recovery facilities with simulated plastic waste," *Waste Manag.*, vol. 32, no. 5, pp. 826–832, 2012.

[234] L. Li, H. Zhang, and X. Zhuang, "Pyrolysis of waste paper: Characterization and composition of pyrolysis oil," *Energy Sources*, vol. 27, no. 9, pp. 867–873, 2005.

[235] B. Biswal, S. Kumar, and R. K. Singh, "Production of Hydrocarbon Liquid by Thermal Pyrolysis of Paper Cup Waste," *J. Waste Manag.*, vol. 2013, pp. 1–7, 2013.

[236] D. S. Scott and J. A. N. Plskorz, "The Continuous Flash Pyrolysis of Biomass," vol. 62, no. June, 1984.

[237] ASTM D1742-6, "Standard Test Method for Oil Separation from Lubricating Grease During Storage," in *ASTM Book of Standards*, 2010, pp. 1–5.

[238] V. Strezov and T. J. Evans, "Thermal processing of paper sludge and characterisation of its pyrolysis products," *Waste Manag.*, vol. 29, no. 5, pp. 1644–1648, 2009.

[239] S. S. Kolapkar, "Pyrolysis of Fiber-Plastic Waste Blends," Michigan Technological University, 2018.

[240] Y. Xue, S. Zhou, R. C. Brown, A. Kelkar, and X. Bai, "Fast pyrolysis of biomass and waste plastic in a fluidized bed reactor," *Fuel*, vol. 156, pp. 40–46, 2015.

[241] F. Chireshe, F. X. Collard, and J. F. Görgens, "Production of low oxygen bio-oil via catalytic pyrolysis of forest residues in a kilogram-scale rotary kiln reactor," *J. Clean. Prod.*, vol. 260, 2020.

[242] M. Radovanovic, R. H. Venderbosch, W. Prins, and W. P. M. Van Swaaij, "Some remarks on the viscosity measurement of pyrolysis liquids," *Biomass and Bioenergy*, vol. 18, no. 3, pp. 209–222, 2000.

[243] F. Nsaful, F. X. Collard, M. Carrier, J. F. Görgens, and J. H. Knoetze, "Lignocellulose pyrolysis with condensable volatiles quantification by thermogravimetric analysis - Thermal desorption/gas chromatography-mass spectrometry method," *J. Anal. Appl. Pyrolysis*, vol. 116, pp. 86–95, 2015.

[244] S. D. Stefanidis, K. G. Kalogiannis, E. F. Iliopoulou, C. M. Michailof, P. A. Pilavachi, and A. A. Lappas, "A study of lignocellulosic biomass pyrolysis via the pyrolysis of cellulose, hemicellulose and lignin," *J. Anal. Appl. Pyrolysis*, vol. 105, pp. 143–150, 2014.

[245] P. R. Patwardhan, J. A. Satrio, R. C. Brown, and B. H. Shanks, "Influence of inorganic salts on the primary pyrolysis products of cellulose," *Bioresour. Technol.*, vol. 101, no. 12, pp. 4646–4655, 2010.

[246] E. A. Williams and P. T. Williams, "The Pyrolysis of Individual Plastics and a Plastic Mixture in a Fixed Bed Reactor *," *Chem. Technol. Biotechnol.*, vol. 70, no. 1, pp. 9–20, 1997.

[247] T. Yoshioka, G. Grause, and C. Eger, "Pyrolysis of poly (ethylene terephthalate) in a fluidised bed plant," *Polym. Degrad. Stab.*, vol. 86, pp. 499–504, 2004.

[248] M. Artetxe, G. Lopez, M. Amutio, G. Elordi, M. Olazar, and J. Bilbao, "Operating conditions for the pyrolysis of poly-(ethylene terephthalate) in a conical spouted-bed reactor," *Ind. Eng. Chem. Res.*, vol. 49, no. 5, pp. 2064–2069, 2010.

[249] O. Cepeliogullar and A. E. Putun, "Utilization of Two Different Types of Plastic Wastes from Daily and Industrial Life," *J. Selcuk Univ. Nat. Appl. Sci.*, pp. 694–706, 2000.

[250] A. K. Panda, R. K. Singh, and D. K. Mishra, "Thermolysis of waste plastics to liquid fuel. A suitable method for plastic waste management and manufacture of value added products-A world prospective," *Renew. Sustain. Energy Rev.*, vol. 14, no. 1, pp. 233–248, 2010.

[251] S. Kumagai, G. Grause, T. Kameda, T. Takano, H. Horiuchi, and T. Yoshioka, "Decomposition of gaseous terephthalic acid in the presence of CaO," *Ind. Eng. Chem. Res.*, vol. 50, no. 4, pp. 1831–1836, 2011.

[252] L. Zhang, Z. Bao, S. Xia, Q. Lu, and K. Walters, "Catalytic Pyrolysis of Biomass and Polymer Wastes," *Catalysts*, vol. 8, no. 12, p. 659, 2018.

[253] J. Yu, L. Sun, C. Ma, Y. Qiao, and H. Yao, "Thermal degradation of PVC: A review," *Waste Manag.*, vol. 48, pp. 300–314, 2016.

[254] B. Dietrich, *Simple Methods for Identification of Plastics. With the Plastics Identification Table /by Hansjürgen Saechtling.* Darmstadt, Germany: Carl Hanser Verlag München 1982, 1982.

[255] S. D. Anuar Sharuddin, F. Abnisa, W. M. A. Wan Daud, and M. K. Aroua, "A review on pyrolysis of plastic wastes," *Energy Convers. Manag.*, vol. 115, pp. 308–326, 2016.

[256] R. W. J. Westerhout, J. Waanders, J. A. M. Kuipers, and W. P. M. Van Swaaij, "Recycling of polyethene and polypropene in a novel bench-scale rotating cone reactor by high-temperature pyrolysis," *Ind. Eng. Chem. Res.*, vol. 37, no. 6, pp. 2293–2300, 1998.

[257] G. Elordi, G. Lopez, M. Olazar, R. Aguado, and J. Bilbao, "Product distribution modelling in the thermal pyrolysis of high density polyethylene," *J. Hazard. Mater.*, vol. 144, no. 3, pp. 708–714, 2007.

[258] R. W. J. Westerhout, J. Waanders, J. A. M. Kuipers, and W. P. M. Van Swaaij, "Development of a continuous rotating cone reactor pilot plant for the pyrolysis of polyethene and polypropane," *Ind. Eng. Chem. Res.*, vol. 37, no. 6, pp. 2316–2322, 1998.

[259] G. Lopez, M. Artetxe, M. Amutio, J. Bilbao, and M. Olazar, "Thermochemical routes for the valorization of waste polyolefinic plastics to produce fuels and chemicals. A review," *Renewable and Sustainable Energy Reviews*, vol. 73, no. January. Elsevier Ltd, pp. 346–368, 2017.

[260] P. T. Williams and J. M. Nazzal, "Polycyclic aromatic compounds in oils derived from the fluidised bed pyrolysis of oil shale," *J. Anal. Appl. Pyrolysis*, vol. 35, no. 2, pp. 181–197, 1995.

[261] F. Pinto, P. Costa, I. Gulyurtlu, and I. Cabrita, "Pyrolysis of plastic wastes. 1. Effect of plastic waste composition on product yield," *J. Anal. Appl. Pyrolysis*, vol. 51, no. 1, pp. 39–55, 1999.

[262] J. A. Onwudili, N. Insura, and P. T. Williams, "Composition of products from the pyrolysis of polyethylene and polystyrene in a closed batch reactor: Effects of temperature and residence time," *J. Anal. Appl. Pyrolysis*, vol. 86, no. 2, pp. 293–303, 2009.

[263] S. M. FakhrHoseini and M. Dastanian, "Predicting Pyrolysis Products of PE, PP, and PET

Using NRTL Activity Coefficient Model," *J. Chem.*, vol. 2013, pp. 1–5, 2013.

[264] S. . Al-Salem and P. Lettieri, "Chemical Engineering Research and Design Kinetic study of high density polyethylene (HDPE) pyrolysis," *Chem. Eng. Res. Des.*, vol. 88, no. 12, pp. 1599–1606, 2010.

[265] B. Purevsuren *et al.*, "Pyrolysis of waste polypropylene and characterisation of tar," *Eur. J. Mass Spectrom.*, vol. 15, no. 1, pp. 23–33, 2009.

[266] R. Miandad, M. A. Barakat, A. S. Aburiazaiza, M. Rehan, I. M. I. Ismail, and A. S. Nizami, "Effect of plastic waste types on pyrolysis liquid oil," *Int. Biodeterior. Biodegrad.*, vol. 119, pp. 239–252, 2017.

[267] P. T. Williams and E. Slaney, "Analysis of products from the pyrolysis and liquefaction of single plastics and waste plastic mixtures," *Resour. Conserv. Recycl.*, vol. 51, no. 4, pp. 754–769, 2007.

[268] E. Hájeková, L. Špodová, M. Bajus, and B. Mlynková, "Separation and characterization of products from thermal cracking of individual and mixed polyalkenes," *Chem. Pap.*, vol. 61, no. 4, pp. 262–270, 2007.

[269] M. Predel and W. Kaminsky, "Pyrolysis of mixed polyolefins in a fluidized-bed reactor and on a pyro-GC/MS to yield aliphatic waxes," *Polym. Degrad. Stab.*, vol. 70, no. 3, pp. 373–385, 2000.

[270] N. K. Ciliz, E. Ekinci, and C. E. Snape, "Pyrolysis of virgin and waste polypropylene and its mixtures with waste polyethylene and polystyrene," *Waste Manag.*, vol. 24, no. 2, pp. 173–181, 2004.

[271] M. Arabiourrutia, G. Elordi, G. Lopez, E. Borsella, J. Bilbao, and M. Olazar, "Characterization of the waxes obtained by the pyrolysis of polyolefin plastics in a conical spouted bed reactor," *J. Anal. Appl. Pyrolysis*, vol. 94, pp. 230–237, 2012.

[272] N. Miskolczi, L. Bartha, G. Deák, B. Jóver, and D. Kalló, "Thermal and thermo-catalytic degradation of high-density polyethylene waste," *J. Anal. Appl. Pyrolysis*, vol. 72, no. 2, pp. 235–242, 2004.

[273] S. Kumar and R. K. Singh, "Recovery of hydrocarbon liquid from waste high density polyethylene by thermal pyrolysis," *Brazilian J. Chem. Eng.*, vol. 28, no. 4, pp. 659–667, 2011.

[274] G. K. Parku, "Pyrolysis of waste polypropylene plastics for energy recovery : Optimisation of the conversion and process development at pilot scale by MASTER OF ENGINEERING in the Faculty of Engineering," no. March, 2019.

[275] G. K. Parku, F. Collard, and J. F. Görgens, "Pyrolysis of waste polypropylene plastics for energy recovery : In fl uence of heating rate and vacuum conditions on composition of fuel product," *Fuel Process. Technol.*, vol. 209, no. May, pp. 36–38, 2020.

[276] H. J. Park *et al.*, "Thermal degradation of plywood with block polypropylene in TG and batch reactor system," *J. Ind. Eng. Chem.*, vol. 17, no. 3, pp. 549–553, 2011.

[277] M. Artetxe *et al.*, "Styrene recovery from polystyrene by flash pyrolysis in a conical spouted bed reactor," *Waste Manag.*, vol. 45, pp. 126–133, 2015.

[278] W. C. Mccaffrey, M. J. Brues, D. G. Cooper, and M. R. Kamal, "Thermolysis of polyethylene/polystyrene mixtures," *J. Appl. Polym. Sci.*, vol. 60, no. 12, pp. 2133–2140, 1996.

[279] W. Kaminsky, M. Predel, and A. Sadiki, "Feedstock recycling of polymers by pyrolysis in a fluidised bed," *Polym. Degrad. Stab.*, vol. 85, no. 3 SPEC. ISS., pp. 1045–1050, 2004.

[280] I. Velghe, R. Carleer, J. Yperman, and S. Schreurs, "Study of the pyrolysis of municipal solid waste for the production of valuable products," *J. Anal. Appl. Pyrolysis*, vol. 92, no. 2, pp. 366–375, 2011.

[281] J. Scheirs, *Overview of Commercial Pyrolysis Processes for Waste Plastics*. 2006.

[282] D. D. . Strode K, "Advanced Recycling of Plastics.pdf." 1995.

[283] D. R. S. S. Rahman, K. Hawboldt, R. Helleur, and S. Macquarrie, "Pyrolysis of waste plastic fish bags (polyethylene and polypropylene) to useable fuel oil," 2018.

[284] E. Ansah, "Experimental Investigation And Aspen Plus Simulation Of The Msw Pyrolysis Process," North Carolina Agricultural and Technical State University, 2013.

[285] A. N. Rollinson and J. M. Oladejo, "'Patented blunderings' efficiency awareness, and self-sustainability claims in the pyrolysis energy from waste sector," *Resour. Conserv. Recycl.*, vol. 141, no. October 2018, pp. 233–242, 2019.

[286] ASTM D396 - 14a, "Standard Specification for Fuel Oils," in *ASTM Book of Standards*, 2002, pp. 1–6.

[287] C. A. Zaror, I. S. Hutchings, D. L. Pyle, H. N. Stiles, and R. Kandiyoti, "Secondary char formation in the catalytic pyrolysis of biomass," *Fuel*, vol. 64, no. 7, pp. 990–994, 1985.

[288] A. Demirbas, "Pyrolysis of municipal plastic wastes for recovery of gasoline-range hydrocarbons," *J. Anal. Appl. Pyrolysis*, vol. 72, no. 1, pp. 97–102, 2004.

[289] L. Quesada, M. Calero, M. A. Martín-Lara, A. Pérez, and G. Blázquez, "Characterization of fuel produced by pyrolysis of plastic film obtained of municipal solid waste," *Energy*, 2019.

[290] E. Önal, B. Uzun, and E. Pütün, "Bio-oil production via co-pyrolysis of almond shell as biomass and high density polyethylene," vol. 78, pp. 704–710, 2014.

[291] L. D. Smith, "Discounted cash flow analysis - methodology and discount rates," *CIM Bull.*, vol. 95, no. 1062, pp. 101–108, 2002.

[292] C. Patel, P. Lettieri, and A. Germanà, "Techno-economic performance analysis and environmental impact assessment of small to medium scale SRF combustion plants for energy production in the UK," *Process Saf. Environ. Prot.*, vol. 90, no. 3, pp. 255–262, 2012.

[293] J. G. Rogers and J. G. Brammer, "Estimation of the production cost of fast pyrolysis bio-oil," *Biomass and Bioenergy*, vol. 36, no. 0, pp. 208–217, 2012.

[294] C. Cimpan, A. Maul, H. Wenzel, and T. Pretz, "Techno-economic assessment of central sorting at material recovery facilities - The case of lightweight packaging waste," *J. Clean. Prod.*, vol. 112, pp. 4387–4397, 2016.

[295] M. Tsagkari, J. L. Couturier, A. Kokossis, and J. L. Dubois, "Early-Stage Capital Cost Estimation of Biorefinery Processes: A Comparative Study of Heuristic Techniques," *ChemSusChem*, vol. 9, no. 17, pp. 2284–2297, 2016.

[296] M. Mandegari, "Slides: Economic Analysis of Biorefineries," Stellenbosch, Cape Town, 2019.

[297] R. K. Sinnott, "Chapter 6:Costing and Project Evaluation," in *Coulson & Richardson's Chemical Engineering*, vol. 6, 2005, pp. 7, 43, 253.

[298] P. N. Pressley, J. W. Levis, A. Damgaard, M. A. Barlaz, and J. F. DeCarolis, "Analysis of material recovery facilities for use in life-cycle assessment," *Waste Manag.*, vol. 35, p. 18, 2015.

[299] H. Yun, R. Clift, and X. Bi, "Process simulation, techno-economic evaluation and market analysis of supply chains for torrefied wood pellets from British Columbia: Impacts of plant configuration and distance to market," *Renew. Sustain. Energy Rev.*, vol. 127, no. January, p. 109745, 2020.

[300] K. Tsilemou and D. Panagiotakopoulos, "Economic Assessment of Mechanical-Biological Treatment Facilities," *Engineering*, vol. 1, no. 1, pp. 55–63, 2007.

[301] S. N. Naik, V. V. Goud, P. K. Rout, and A. K. Dalai, "Production of first and second generation biofuels: A comprehensive review," *Renew. Sustain. Energy Rev.*, vol. 14, no. 2, pp. 578–597, 2010.

[302] D. L. van Schalkwyk, M. Mandegari, S. Farzad, and J. F. Görgens, "Techno-economic and environmental analysis of bio-oil production from forest residues via non-catalytic and catalytic

pyrolysis processes," *Energy Convers. Manag.*, vol. 213, no. April, p. 112815, 2020.

[303] A. Dutta *et al.*, "Process Design and Economics for the Conversion of Lignocellulosic Biomass to Hydrocarbon Fuels. NREL/TP-5100-62455 and PNNL-23823," *Nrel*, no. March, 2015.

[304] S. Jones *et al.*, "Process design and economics for the conversion of lignocellulosic biomass to hydrocarbon fuels: Fast pyrolysis and hydrotreating bio-oil pathway," *Energy*, no. November, p. 97, 2013.

[305] O. K. K. Bedzo, M. Mandegari, and J. F. Görgens, "Techno-economic analysis of inulooligosaccharides, protein, and biofuel co-production from Jerusalem artichoke tubers: A biorefinery approach," *Biofuels, Bioprod. Biorefining*, pp. 1–18, 2020.

[306] M. Mandegari, S. Farzad, and J. F. Görgens, "A new insight into sugarcane biorefineries with fossil fuel co-combustion: Techno-economic analysis and life cycle assessment," *Energy Convers. Manag.*, vol. 165, no. March, pp. 76–91, 2018.

[307] N. Nkosi, E. Muzenda, T. A. Mamvura, M. Belaid, and B. Patel, "The development of a waste tyre pyrolysis production plant business model for the gauteng region, South Africa," *Processes*, vol. 8, no. 7, 2020.

[308] S. Jirka and T. Tomlinson, "State of the Biochar Industry 2013 - A Survey of Commercial Activity in the Biochar Field," *Int. Biochar Initiat.*, no. March, pp. 1–61, 2014.

[309] M. Carrier *et al.*, "Thermogravimetric analysis as a new method to determine the lignocellulosic composition of biomass," *Biomass and Bioenergy*, vol. 35, no. 1, pp. 298–307, 2011.

[310] S. McAllister, J.-Y. Chen, and A. C. Fernandez-Pello, *Fundamentals of Combustion Processes.* 2011.

[311] T. Waldheim, L. Nilsson, "Heating value of gases from biomass gasification," *IEA Bioenergy Agreement, Task 20 - Therm. Gasif. Biomass*, no. May, p. 61, 2001.

[312] CEN/TS 15400, "CEN/TS 15400: Solid recovered fuels - Methods for the determination of calorific value," Brussels, Belgium, 2005.

[313] Z. Xu *et al.*, "Properties of Torrefied U.S. Waste Blends," *Front. Energy Res.*, vol. 6, no. July, pp. 1–13, 2018.

[314] A. Sluiter, B. Hames, R. Ruiz, C. Scarlata, J. Sluiter, and D. Templeton, "NREL/TP-510-42622: Determination of Ash in Biomass," in *National Renewable Energy Laboratory*, vol. 36, no. 4, 2005, pp. 302–305.

[315] G. Genon and E. Brizio, "Perspectives and limits for cement kilns as a destination for RDF," *Waste Manag.*, vol. 28, no. 11, pp. 2375–2385, 2008.

[316] S. Lee and D. K. Lee, "What is the proper way to apply the multiple comparison test?," *Korean J. Anesthesiol.*, vol. 71, no. 5, pp. 353–360, 2018.

[317] M. L. McHugh, "Multiple comparison analysis testing in ANOVA," *Biochem. Medica*, vol. 21, no. 3, pp. 203–209, 2011.

[318] H.-Y. Kim, " Statistical notes for clinical researchers: post-hoc multiple comparisons ," *Restor. Dent. Endod.*, vol. 40, no. 2, p. 172, 2015.

[319] C. Zaiontz, "Tukey-Kramer Test," *Real Statistics Using Excel*, 2020. [Online]. Available: https://www.real-statistics.com/one-way-analysis-of-variance-anova/unplanned-comparisons/tukey-kramer-test/. [Accessed: 26-Sep-2020].

[320] S. Glen, "Tukey Test / Tukey Procedure / Honest Significant Difference," *StatisticsHowTo.com*, 2016. [Online]. Available: https://www.statisticshowto.com/tukey-test-honest-significant-difference/. [Accessed: 26-Sep-2020].

[321] S. Glen, "Studentized Range Distribution," *StatisticHowTo.com*, 2017. [Online]. Available: https://www.statisticshowto.com/studentized-range-distribution/#qtable. [Accessed: 26-Sep-2020].

[322] S. Hemidat, M. Saidan, S. Al-Zu'bi, M. Irshidat, A. Nassour, and M. Nelles, "Potential utilization of RDF as an alternative fuel to be used in cement industry in Jordan," *Sustain.*, vol. 11, no. 20, 2019.

[323] K. Isaac and S. O. Bada, "The co-combustion performance and reaction kinetics of refuse derived fuels with South African high ash coal," *Heliyon*, vol. 6, no. 1, p. e03309, 2020.

[324] M. Ouadi, J. G. Brammer, M. Kay, and A. Hornung, "Fixed bed downdraft gasification of paper industry wastes," *Appl. Energy*, vol. 103, pp. 692–699, 2013.

[325] L. J. Brown, P. J. Görgens, and F.-X. Collard, "Pyrolysis of Fibre Residues with Plastic Contamination from a Paper Recycling Mill: Energy Recoveries," Stellenbosch University, 2018.

[326] L. Zhao *et al.*, "Characterization of Singapore RDF resources and analysis of their heating value," *Sustain. Environ. Res.*, vol. 26, no. 1, pp. 51–54, 2016.

[327] M. Iqbal, A. Nadeem, and M. Butt, "Impact of process parameters on refused derived fuel pellets," *Bangladesh J. Sci. Ind. Res.*, vol. 55, no. 1, pp. 73–82, 2020.

[328] H. Cong *et al.*, "Slow Pyrolysis Performance and Energy Balance of Corn Stover in Continuous Pyrolysis-Based Poly-Generation Systems," *Energy and Fuels*, vol. 32, no. 3, pp. 3743–3750, 2018.

[329] N. Tröger, D. Richter, and R. Stahl, "Journal of Analytical and Applied Pyrolysis Effect of feedstock composition on product yields and energy recovery rates of fast pyrolysis products from different straw types," *J. Anal. Appl. Pyrolysis*, vol. 100, pp. 158–165, 2013.

[330] H. Weldekidan *et al.*, "Energy Conversion Efficiency of Pyrolysis of Chicken Litter and Rice Husk Biomass," *Energy and Fuels*, vol. 33, no. 7, pp. 6509–6514, 2019.

[331] F. Chireshe, "Production of an upgraded bio-oil by catalytic pyrolysis of forest residues," no. April, 2019.

[332] M. Brebu, S. Ucar, C. Vasile, and J. Yanik, "Co-pyrolysis of pine cone with synthetic polymers," *Fuel*, vol. 89, no. 8, pp. 1911–1918, 2010.

[333] Advanced Motor Fuels: Technology Collaboration Programme, "Diesel and Gasoline Fuel Types," *International Energy Agency*. [Online]. Available: https://iea-amf.org/content/fuel_information/diesel_gasoline. [Accessed: 10-Sep-2020].

[334] J. Bacha *et al.*, "Diesel Fuels Technical Review," *Chevron Glob. Mark.*, pp. 1–116, 2007.

[335] PubChem Database, "Heptadecane, CID=12398," *National Center for Biotechnology Information.* [Online]. Available: https://pubchem.ncbi.nlm.nih.gov/compound/12398#x291. [Accessed: 21-Jul-2020].

[336] ASTM D388-15, "Standard Classification of Coals by Rank," in *ASTM Book of Standards*, 2015, pp. 1–7.

[337] L. R. Radovic and H. H. Schobert, "Chapter 7. Coal," in *Energy and Fuels in Society: Analysis of Bills and Media Reports*, no. Chapter 7, New York : McGraw-Hill : Primis Custom Pub, 1997, pp. 113–136.

[338] H. Yang *et al.,* "Estimation of enthalpy of bio-oil vapor and heat required for pyrolysis of biomass," *Energy and Fuels*, vol. 27, no. 5, pp. 2675–2686, 2013.

[339] T. B. Reed and S. Gaur, "The High Heat of Fast Pyrolysis for Large Particles," *Dev. Thermochem. Biomass Convers.*, pp. 97–103, 1997.

[340] H. Nam, S. C. Capareda, N. Ashwath, and J. Kongkasawan, "Experimental investigation of pyrolysis of rice straw using bench-scale auger, batch and fluidized bed reactors," *Energy*, vol. 93, pp. 2384–2394, 2015.

[341] P. Bhattacharya, P. H. Steele, E. B. M. Hassan, B. Mitchell, L. Ingram, and C. U. Pittman, "Wood/plastic copyrolysis in an auger reactor: Chemical and physical analysis of the products," *Fuel*, vol. 88, no. 7, pp. 1251–1260, 2009.

[342] D. W. Edwards, "Comparison of the Technical and Economic Feasibility of Devulcanisation Processes for Recycling Waste Tyres in South Africa by in the Faculty of Engineering," no. March, 2016.

[343] B. Cohen and D. Deglon, "CHE4048F: Engineering Economic Analysis," Cape Town, South Africa, 2009.

[344] SARS, "Icome tax of Companies, Trusts and Small Business Corporations (SBC)," 2020. [Online]. Available: https://www.sars.gov.za/Tax-Rates/Income-Tax/Pages/Companies-Trusts-and-Small-Business-Corporations.aspx. [Accessed: 04-Aug-2020].

[345] D. Deglon, "CHE4048F: Engineering Economic Analysis," 2016.

[346] M. S. Peters and K. D. Timmerhaus, *Plant Design and Economics for Chemical Engineers*, Fourth., vol. 2, no. 4. 1994.

[347] J. R. Couper, W. R. Penney, J. R. Fair, and S. M. Walas, "Chapter 0: Rules of Thumb: Summary," in *Chemical Process Equipment: Selection and Design*, Third., U.S.A, 2010.

[348] J. R. Couper, W. R. Penney, J. R. Fair, and S. M. Walas, "Chapter 21: Costs of Individual Equipment," in *Chemical Process Equipment: Selection and Design*, 2012, pp. 1–755.

[349] D. R. Woods, *Rules of Thumb in Engineering Practice*. Ontario, Canada: Wiley-VCH Verlag GmbH & Co. KGaA, Weinheim, 2007.

[350] D. L. Van Schalkwyk, "Techno-economic and Environmental Analysis of Bio-oil Production from Forest Residues via Non-catalytic and Catalytic Pyrolysis Processes by," Stellenbosch University, 2019.

[351] W. D. Seider, J. D. Seader, D. R. Lewin, and S. Widagdo, "Cost accounting and Capital Cost Estimation," in *Product and Process Design Principles*, Third., J. Welter, S. Dumas, and L. Sapira, Eds. New Jersey, USA: John Wiley & Sons, 2009.

[352] Weather & Climate, "Average Humidity In Johannesburg (Gauteng)," *Weather-and-climate*, 2019. [Online]. Available: https://weather-and-climate.com/average-monthly-Humidity-perc,johannesburg,South-Africa. [Accessed: 30-Mar-2020].

[353] Climate Data.Org, "Johannesburg Climate," *Climate-Data.org*, 2020. [Online]. Available: https://en.climate-data.org/africa/south-africa/gauteng/johannesburg-3221/. [Accessed: 30-Mar-2020].

[354] T. Jika and S. Skiti, "The high price of coal connections," *Mail & Guardian*, 11-Oct-2019.

[355] Eskom, "General purchase schedule of standard prices for non-local authority supplies," vol. 20, pp. 1–10, 2020.

[356] J. Reddick and R. Kruger, "GreenCape 2019 Market Intelligence report," *Greencape*, 2019.

[357] L. F. Diaz *et al.*, *Solid waste management, Volume 1*. 2005.

[358] L. F. Diaz, G. M. Savage, and C. G. Golueke, "Chapter 3: Planning, Designing, and Modeling the Resource Recovery Facility," in *Resource Recovery From Municipal Solid Wastes: Volume I: Primary Processing*, 1984.

[359] J. Havlík and T. Dlouhý, "Indirect Dryers for Biomass Drying—Comparison of Experimental Characteristics for Drum and Rotary Configurations," *ChemEngineering*, vol. 4, no. 1, p. 18, 2020.

[360] R. Dvorak, R. Evans, and E. Kosior, "Commercial scale mixed plastics recycling: A report on the technical viability of recycling mixed plastic packaging waste from domestic sources on a commercial scale in the UK.," 2009.

[361] A. S. Mujumdar, "Chapter 6: Indirect drying," in *Handbook on Industrial Drying*, Third., vol. 6, no. 3, Taylor & Francis Group, LLC, 1988, pp. 571–573.

[362] Kanetec, "Magnetic Separators," 2013. [Online]. Available: http://kanetec.co.jp/en/pdf/120_138.pdf. [Accessed: 07-Jul-2020].

[363] Andritz, "Designed to Maximize Reliability and Efficiency," 2018. [Online]. Available: https://www.andritz.com/resource/blob/19104/e07b978e53eedb2ba2f9feac17f1375d/fb-paladin-pellet-mill-en-data.pdf. [Accessed: 07-Jul-2020].

[364] A. Eberhard, "Market, investment, and policy challenges for South African coal," *Glob. Coal Mark. Supplying Major Fuel Emerg. Econ.*, no. January, pp. 164–203, 2015.

[365] P. Venter and N. Naude, "Evaluation of some optimum moisture and binder conditions for coal fines briquetting," *J. South. African Inst. Min. Metall.*, vol. 115, no. 4, pp. 329–333, 2015.

[366] G. W. Diederichs, M. Ali Mandegari, S. Farzad, and J. F. Görgens, "Techno-economic comparison of biojet fuel production from lignocellulose, vegetable oil and sugar cane juice," *Bioresour. Technol.*, vol. 216, pp. 331–339, 2016.

[367] A. Fivga and I. Dimitriou, "Pyrolysis of plastic waste for production of heavy fuel substitute: A techno-economic assessment," *Energy*, vol. 149, pp. 865–874, 2018.

[368] R. Krzywda and B. Wrzesińska, "Simulation of the Condensation and Fractionation Unit in

Waste Plastics Pyrolysis Plant," *Waste and Biomass Valorization*, no. 0123456789, 2020.

[369] M. Gusev, "Monthly Crude Oil Prices," *South Africa Data Portal*, 2019. [Online]. Available: https://southafrica.opendataforafrica.org/iaeapfb/monthly-crude-oil-prices. [Accessed: 07-Nov-2020].

[370] K. Onarheim, Y. Solantausta, and J. Lehto, "Process simulation development of fast pyrolysis of wood using aspen plus," *Energy and Fuels*, vol. 29, no. 1, pp. 205–217, 2015.

[371] R. Arp, T. Bole-Rental, M. Gulati, N. Nkume, and L. Scholtz, "Cement sector : Life Cycle Optimisation Service," 2018.

[372] Interwaste Holdings Limited and A. Report, "Integrated Annual Report 2016," Johannesburg, South Africa, 2016.

[373] Interwaste Holdings Limited and M. Honda, "Integrated Annual Report 2017," Johannesburg, South Africa, 2017.

[374] N. Haque and M. Somerville, "Techno-economic and environmental evaluation of biomass dryer," *Procedia Eng.*, vol. 56, pp. 650–655, 2013.

[375] A. Pantaleo, M. Villarini, A. Colantoni, M. Carlini, F. Santoro, and S. R. Hamedani, "Techno-economic modeling of biomass pellet routes: Feasibility in Italy," *Energies*, vol. 13, no. 7, pp. 1–15, 2020.

[376] www.priceofscrapmetals.com, "Scrap Metal Prices - South Africa," 2020. [Online]. Available: https://www.priceofscrapmetals.com/south-africa/. [Accessed: 12-Nov-2020].

[377] M. Ghodrat, J. Abascall Alonso, D. Hagare, R. Yang, and B. Samali, "Economic feasibility of energy recovery from waste plastic using pyrolysis technology: an Australian perspective," *Int. J. Environ. Sci. Technol.*, no. 0123456789, 2019.

[378] N. Jawaid, "The Curious Case of Negative IRR," *Feasibility.pro*, 2016. [Online]. Available: https://feasibility.pro/negative-irr/. [Accessed: 04-Sep-2020].

[379] J. Anderson and A. Fennell, "Calculate financial indicators to guide investments," *Chem. Eng. Prog.*, vol. 109, no. 9, pp. 34–40, 2013.

[380] Richardson Products & Cost Data On Line Inc. and Richardson Engineering, "Richardson International Construction Factors Manual," *Richardson books*, p. 20, 2008.

[381] K. K. Humphreys, "Sources of International Cost Data," *Nord. '97 Conf. "Quality Proj. Manag.*, vol. 4, no. September 1997, pp. 1–23, 1997.

[382] T. Gebreegziabher, A. O. Oyedun, and C. W. Hui, "Optimum biomass drying for combustion

- A modeling approach," *Energy*, vol. 53, pp. 67–73, 2013.

[383] W. L. McCabe, S. C. Smith, and P. Harriott, "Chapter 24: Drying of Solids," in *Unit Operation of Chemical Engineering*, Fifth., McGraw-Hill Book Co., 1993, p. 767.

[384] H. T. Luk, T. Y. G. Lam, A. O. Oyedun, T. Gebreegziabher, and C. W. Hui, "Drying of biomass for power generation: A case study on power generation from empty fruit bunch," *Energy*, vol. 63, pp. 205–215, 2013.

[385] S. T. Mrus and C. A. Prendergast, "Heating Value of Refuse Derived Fuel.," pp. 365–372, 1978.

[386] K. Brown, "Psych: An Open Source Psychrometric Plug-in for Microsoft Excel." Western Cooling Efficiency Centre, Davis, California, 2012.

[387] I. C. Kemp, "Humidity effects in solids drying processes," *Meas. Control*, vol. 40, no. 9, pp. 268–271, 2007.

[388] R. Turton, R. C. Bailie, W. B. Whiting, J. A. Shaeiwitz, and D. Bhattacharyya, *Analysis, Synthesis, and Design of Chemical Processes*, Fourth. New Jersey, USA: Pearson Education, Inc., 2012.

[389] Aspen Technology Inc., *Aspen Plus User Guide*, no. 1. 2000.

[390] P. Waterson, S. Weibelzahl, and D. Pfahl, "Software Process Modelling," *Softw. Process Model.*, vol. 44, no. 0, pp. 111–139, 2005.

[391] R. Schefflan, "Physical Property Methods and Models," *Teach Yours. Basics Aspen Plus^{TM}*, pp. 1–21, 1–30, 2011.

[392] ASTM D7582-15, "Standard Test Methods for Proximate Analysis of Coal and Coke by Macro Thermogravimetric Analysis," in *ASTM Book of Standards*, 2015, pp. 1–9.

[393] P. Bio-oil, F. G. Fonseca, A. Funke, and N. Dahmen, "27th European Biomass Conference and Exhibition, EUBCE 2019," *Eur. Biomass Conf. Exhib. Proc.*, no. May, pp. 27–30, 2019.

[394] F. G. Fonseca, A. Funke, and N. Dahmen, "Aspen plus^{TM} modeling of fractional condensation schemes for production of fast pyrolysis bio-oil," *Eur. Biomass Conf. Exhib. Proc.*, no. July, pp. 1227–1233, 2019.

[395] J. Haydary, "Chapter 14: Process with Nonconventional Solids," in *Chemical Process Design and Simulation: Aspen Plus and Aspen HYSYS Applications*, 2019, pp. 321–346.

[396] H. Chu and P. Basu, "Stoichiometric Calculations," in *Combustion and Gasification in Fluidized Beds*, 2006, pp. 445–451.

Appendices

Appendix A. Characterization and SRF

A.1. MATLAB code for calculating area under dTG peaks

```matlab
%thermal degradation of the pulper rejects (1st sample)/ column 2 = TG curve
TGcurve1 = xlsread('Thermal Stability.xlsx','2','A5:E33103');
x1 = TGcurve1(:,2);
y1 = TGcurve1(:,4);

dy1 = diff(y1);
dx1 = diff(x1);
dydx1=abs(dy1./dx1);
xd1=x1(2:end);
numberMovMean=200;
meandydx1=movmean(dydx1,numberMovMean);

figure(1)
plot(xd1,meandydx1,'r-','LineWidth',1.5), hold on
xlabel('Temperature (°C)'), ylabel('Rate of mass loss (wt. % / °C)'), ylim([0
2.3]), grid, hold on

gausfnc = @(b,xd1)b(1).*exp(-((xd1-b(2)).^2)./b(3));        % Gaussian Function
SSECF = @(b,xd1,meandydx1) sum((meandydx1-gausfnc(b,xd1)).^2);         % Sum-
Squared-Error Cost Function

[pks,locs] = findpeaks(meandydx1, 'MinPeakDist',4500, 'MinPeakHeight',0.05);
% Find Centres, change "MinPeakDist" for adjusting peaks
q = xd1(locs);
lims=1500;                                                % To make tighter fit

for k1=1:size(pks,1)
    idxrng = locs(k1)-lims : locs(k1)+lims;
    [Parms(:,k1),                            SSE(k1)]                          =
fminsearch(@(b)SSECF(b,xd1(idxrng),meandydx1(idxrng)),[pks(k1);   xd1(locs(k1));
1]);
    AUC1(k1) = trapz(xd1, gausfnc(Parms(:,k1),xd1));
end
figure(1)
plot(xd1(locs), pks, '^r')

for k1 = 1:size(pks,1)
    plot(xd1, gausfnc(Parms(:,k1),xd1), 'LineWidth',1)
end

 xd1New=xd1(~isnan(xd1));
idx=find(~isnan(xd1));
meandydx1New=meandydx1(idx);
if(isnan(meandydx1New)==false)
    I1=trapz(xd1New,meandydx1New);
else
    heightNew1=meandydx1New(~isnan(meandydx1New));
    idx1=find(~isnan(meandydx1New));
    dataNew1=xd1New(idx1);
    I1=trapz(dataNew1,heightNew1);
```

```matlab
end
figure(1)
legend(num2str(I1,'total area pellet 1 = %5.2f ; '),num2str(AUC1,'AUC = %5.3f
;'),'Location','NorthWest')

%% Thermal degradation of pulper rejects (2nd sample)
TGcurve2 = xlsread('Thermal Stability.xlsx','2','H5:L33101');
x2 = TGcurve2(:,2);
y2 = TGcurve2(:,4);

figure(2)
dy2 = diff(y2);
dx2 = diff(x2);
dydx2=abs(dy2./dx2);
xd2=x2(2:end);
numberMovMean2=600;
meandydx2=movmean(dydx2,numberMovMean2);
plot(xd2,meandydx2,'b-','LineWidth',1.5)
xlabel('Temperature (°C)'), ylabel('Rate of mass loss (wt. % / °C)'), ylim([0
1.6]), grid, hold on

gausfnc2 = @(a,xd2)a(1).*exp(-((xd2-a(2)).^2)./a(3));         % Gaussian Function
SSECF2 = @(a,xd2,meandydx2) sum((meandydx2-gausfnc2(a,xd2)).^2);        % Sum-
Squared-Error Cost Function

[pks2,locs2] = findpeaks(meandydx2, 'MinPeakDist',5500, 'MinPeakHeight',0.1); %
Find Centres, change "MinPeakDist" for adjusting peaks
q = xd2(locs2);
lims2=1500;                                    % To make tighter fit

for j1=1:size(pks2,1)
    idxrng2 = locs2(j1)-lims2 : locs2(j1)+lims2;
    [Parms2(:,j1),                          SSE(j1)]                         =
fminsearch(@(a)SSECF2(a,xd2(idxrng2),meandydx2(idxrng2)),[pks2(j1);
xd2(locs2(j1)); 1]);
    AUC2(j1) = trapz(xd2, gausfnc2(Parms2(:,j1),xd2));
end

%plot(xd1, meandydx1, 'LineWidth',1.5)

plot(xd2(locs2), pks2, '^b')

for j1 = 1:size(pks2,1)
    plot(xd2, gausfnc2(Parms2(:,j1),xd2),'LineWidth',1)
end

xd2New=xd2(~isnan(xd2));
idx2=find(~isnan(xd2));
meandydx2New=meandydx2(idx2);
if(isnan(meandydx2New)==false)
    I2=trapz(xd2New,meandydx2New);
else
    heightNew2=meandydx2New(~isnan(meandydx2New));
    idx2=find(~isnan(meandydx2New));
    dataNew2=xd2New(idx2);
    I2=trapz(dataNew2,heightNew2);
end
hold off

legend(num2str(I2,'total area pellet 2 = %5.2f ; '),num2str(AUC2,'AUC_2 = %5.3f
;'),'Location','NorthWest')
```

A.2. Treatment of the pulper rejects into SRF

Figure A-1: Materials in pulper rejects, *viz.* LDPE (left), agglomerated fibres (middle), PET bottles and HDPE lids (right)

Calculations for geometric mean for particle size analysis

$$\frac{d_{80} - 4733\ \mu m}{80\ \% - 69.69\ \%} = \frac{6693\ \mu m - 4733\ \mu m}{82\ \% - 69.69\%}$$

$$\frac{d_{50} - 3347\ \mu m}{50\ \% - 39.5\ \%} = \frac{4733\ \mu m - 3347\ \mu m}{69.69\ \% - 39.5\ \%}$$

A.3. Heavy metal analysis results from ICP (C.A.F department)

Table A-1: Raw data for heavy metal, cadmium and mercury content (µg/kg) from ICP analysis (August 2020)

		LOQ (limit of quantification)	% Accuracy on Internal QC	% Recovery on Certified Reference Material	1000 µm Joshua 1	1000 µm Joshua 1	1000 µm Joshua 1	1000 µm Joshua 1	1000 µm Joshua 1
B	µg/kg	1531	102	104	14202	15065	23225	16038	12587
Al	µg/kg	409	103	71	9253532	2598429	2790324	4541834	3601579
V	µg/kg	5	100	88	2846	1953	1888	2844	2097
Cr	µg/kg	147	101	91	57260	55728	46487	60426	44781
Mn	µg/kg	81	99	99	26070	44332	24234	29862	21364
Fe	µg/kg	858	99	90	1845952	7558475	1562919	2207292	1636902
Co	µg/kg	6	100	94	1111	2306	1851	1241	896
Ni	µg/kg	74	100	95	20592	20243	18081	20374	16940
Cu	µg/kg	264	102	100	82116	71117	66778	98104	68160
Zn	µg/kg	133	111	97	208599	164240	92448	193351	74580
As	µg/kg	10	96	113	518	422	439	490	428
Se	µg/kg	23	100	126	71	BDL	29	51	28
Sr	µg/kg	14	97	97	41564	52904	773339	62915	38245
Mo	µg/kg	7	100	98	1198	1828	743	1444	2210
Cd	µg/kg	2	100	96	9559	6126	288	2444	3854
Sn	µg/kg	9	102	-	28611	15847	26655	15339	49356
Sb	µg/kg	3	91	99	1452	1931	721	1633	2156
Ba	µg/kg	6	98	97	61436	26296	152877	39407	35980
Hg	µg/kg	15	-	101	1144	1706	120	406	184
Pb	µg/kg	6	92	-	135793	76386	112636	160674	96497

*BDL- Below detection limit

Table A-2: The mercury content from ICP analysis (January 2020)

(Lower Limit of Detection)	Hg ug/kg
LOD	14.7
Joshua 1400µm 1	134
Joshua 1400µm 2	148
Joshua 1400µm 3	108
Joshua 1400µm 4	83
Joshua 1400µm 5	112
Joshua 1400µm 6	71
Joshua 1400µm 7	82
Joshua 1400µm 8	112
Joshua 1400µm 9	76
Joshua 1400µm 10	72

Appendix B. Pyrolysis experiments

B.1. Karl Fischer titration results on pyrolysis liquid from bench-scale

Table B-1: Results from Karl-Fischer Titration

31 January 2020

RESULTS: WATER CONTENT

Method: Karl Fischer titration

Sample	Water (%m/m)
4.1 (1) [Wax sample] – condenser 1	57.2835
	3.6191
4.1(2) [Wax sample] – condenser 2	10.1021
	8.1931
4.2(3) [Oil sample] – condenser 1	73.8828
	66.9058
	65.7539
4.2(4) [Oil sample] – condenser 2	0.2812
	1.9745
	52.7130
	68.7400

Regards

Levine Simmers

Junior Technical Officer

B.2. Photographs from bench-scale pyrolysis

Figure B-1: The bench-scale, fixed bed reactor set-up with first collection pot, two condensers & ESP

Figure B-2: The first collection pot with wax (left) and second collection pot with oil (right)

Figure B-3: The 30 g sample feed in the sample boat (left) and the char left post pyrolysis (right).

B.3. Photographs from pilot-scale pyrolysis

Figure B-4: The charpot (left), condensation train (middle) and condensers (right) of pilot-scale setup.

Figure B-5: New condenser set-up. For each run the condenser part is weighed and the part for extracting the non-condensable gas. Since changing there has been no sign of wax/ oil going into the bags
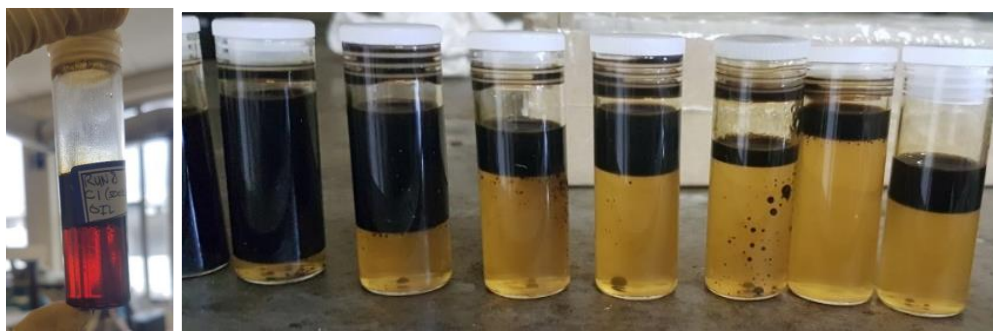
Figure B-6: The heterogeneity of the oil fraction, including the aqueous (bottom) and organic phase oil (top)..

B.4. Distribution of wax, organic –, and aqueous phase oil in C1 and C2
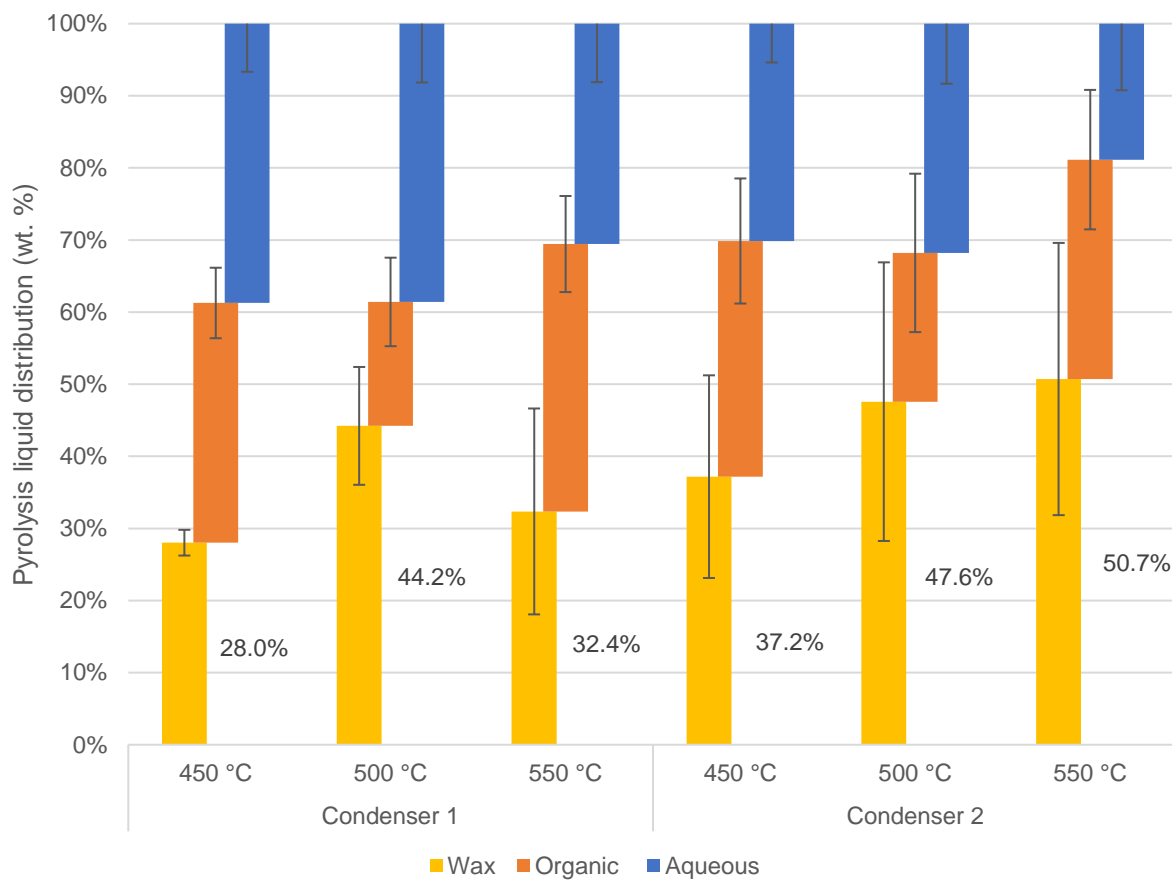
Figure B-7: The distribution of wax, organic and aqueous phase oil from condenser 1 and 2.

B.5. Gas analysis components

Table B-2: Average mass composition (wt. %) of NCG components at tested temperatures

Component	CO	CH_4	H_2	CO_2	C_2H_6	C_2H_4	C_3	C_4	C_5
450 °C	10.1	5.18	0.197	44.9	5.91	4.93	13.9	8.93	5.93
500 °C	9.67	6.27	0.424	42.5	6.87	5.35	16.0	8.71	4.27
550 °C	9.33	9.54	0.767	32.7	9.33	8.53	20.0	9.73	0.0283

Table B-3: Mass of components (g) in gas phase at respective temperatures

Compounds	CO	CO_2	H_2
450 °C	28.6 ± 1.61	127.4 ± 5.66	0.559 ± 0.113
500 °C	36.3 ± 1.37	159.6 ± 5.10	1.59 ± 0.0318
550 °C	52.2 ± 0.495	183.3 ± 8.78	4.30 ± 0.449

172

Appendix C. Bench-scale results (ANOVA and post-hoc analysis)

C.1. Char-yield results

Sample	350	450	500	550
1	81.6%	29.1%	20.5%	14.4%
2	76.8%	16.8%	17.6%	14.5%
3	-	20.1%	-	-

SUMMARY

Groups	Count	Sum	Average	Variance
350	2	1.583651	0.791825	0.001174773
450	3	0.660723	0.220241	0.004026459
500	2	0.381245	0.190623	0.000440373
550	2	0.288856	0.144428	1.646E-07

ANOVA

Source of Variation	SS	df	MS	F	P-value	F crit
Between Groups	0.57009	3	0.19003	98.27547151	7.27E-05	5.409451318
Within Groups	0.009668	5	0.001934			
Total	0.579758	8				

Table C-1: Pairwise-comparison for the char product yields

			x1	x2	difference	n1	n2	SE	q	q crit	q > q crit?	Therefore,
1	350	450	0.8	0.2	0.572	2	3	0.028	20.14	5.22	TRUE	Significant
2	450	500	0.2	0.2	0.030	3	2	0.028	1.04	5.22	FALSE	NO significance
3	500	550	0.2	0.1	0.046	2	2	0.031	1.49	5.22	FALSE	NO significance
4	550	350	0.1	0.8	0.647	2	2	0.031	20.82	5.22	TRUE	Significant
5	350	500	0.8	0.2	0.601	2	2	0.031	19.34	5.22	TRUE	Significant
6	450	550	0.2	0.1	0.076	3	2	0.028	2.67	5.22	FALSE	NO significance

C.2. Oil-yield results

Sample	350	450	500	550
1	0.7%	5.3%	9.3%	14.2%
2	3.1%	9.0%	9.1%	7.2%
3		2.1%		

SUMMARY

Groups	Count	Sum	Average	Variance
350	2	0.038008	0.019004	0.000288304
450	3	0.16403	0.054677	0.001205852
500	2	0.183967	0.091984	3.15744E-06
550	2	0.214168	0.107084	0.002458393

ANOVA

Source of Variation	SS	df	MS	F	P-value	F crit
Between Groups	0.009524	3	0.00317	3.075	0.129	5.409
Within Groups	0.005162	5	0.00103			
Total	0.014685	8				

Table C-2: Pairwise-comparison for the oil product yields

			x1	x2	difference	n1	n2	SE	q	q crit	q > q crit?	Therefore,
1	350	450	0.0	0.1	0.036	2	3	0.0207	1.72	5.22	FALSE	NO significance
2	450	500	0.1	0.1	0.037	3	2	0.0207	1.80	5.22	FALSE	NO significance
3	500	550	0.1	0.1	0.015	2	2	0.0227	0.66	5.22	FALSE	NO significance
4	550	350	0.1	0.0	0.088	2	2	0.0227	3.88	5.22	FALSE	NO significance
5	350	500	0.0	0.1	0.073	2	2	0.0227	3.21	5.22	FALSE	NO significance
6	450	550	0.1	0.1	0.052	3	2	0.0207	2.53	5.22	FALSE	NO significance

C.3. Wax-yield results

Sample	350	450	500	550
1	12.2%	52.7%	52.3%	27.7%
2	14.5%	49.7%	54.0%	29.5%
3		57.4%		

SUMMARY

Groups	Count	Sum	Average	Variance
350	2	0.267008	0.133504	0.000266551
450	3	1.597499	0.5325	0.001488617
500	2	1.063171	0.531585	0.000153996
550	2	0.572395	0.286198	0.000158445

ANOVA

Source of Variation	SS	df	MS	F	P-value	F crit
Between Groups	0.254	3	0.08471	119.101	0.000045	5.409
Within Groups	0.003556	5	0.000711			
Total	0.258	8				

Table C-3: Pairwise-comparison for the wax product yields

			x1	x2	difference	n1	n2	SE	q	q crit	q > q crit?	Therefore,
1	350	450	0.1	0.5	0.399	2	3	0.0172	23.2	5.22	TRUE	Significant
2	450	500	0.5	0.5	0.001	3	2	0.0172	0.1	5.22	FALSE	NO significance
3	500	550	0.5	0.3	0.245	2	2	0.0189	13.0	5.22	TRUE	Significant
4	550	350	0.3	0.1	0.153	2	2	0.0189	8.1	5.22	TRUE	Significant
5	350	500	0.1	0.5	0.398	2	2	0.0189	21.1	5.22	TRUE	Significant
6	450	550	0.5	0.3	0.246	3	2	0.0172	14.3	5.22	TRUE	Significant

C.4. NCG yield results

Sample	350	450	500	550
1	2.0%	6.5%	3.5%	47.2%
2	2.9%	22.0%	19.3%	48.8%
3		14.5%		

SUMMARY

Groups	Count	Sum	Average	Variance
350	2	0.048751	0.024376	4.48745E-05
450	3	0.430072	0.143357	0.005970369
500	2	0.228089	0.114045	0.012508607
550	2	0.960224	0.480112	0.000129629

ANOVA

Source of Variation	SS	df	MS	F	P-value	F crit
Between Groups	0.241054	3	0.080351	16.31573975	0.005147955	5.409451318
Within Groups	0.024624	5	0.004925			
Total	0.265678	8				

Table C-4: Pairwise-comparison for the NCG product yields

			x1	x2	difference	n1	n2	SE	q	q_{crit}	$q > q_{crit}$?	Therefore,
1	350	450	0.0	0.1	0.119	2	3	0.0453	2.63	5.22	FALSE	NO significance
2	450	500	0.1	0.1	0.029	3	2	0.0453	0.65	5.22	FALSE	NO significance
3	500	550	0.1	0.5	0.366	2	2	0.0496	7.38	5.22	TRUE	Significant
4	550	350	0.5	0.0	0.456	2	2	0.0496	9.18	5.22	TRUE	Significant
5	350	500	0.0	0.1	0.090	2	2	0.0496	1.81	5.22	FALSE	NO significance
6	450	550	0.1	0.5	0.337	3	2	0.0453	7.43	5.22	TRUE	Significant

C.5. Wax HHV results

Sample		350	450	500	550
	1	0.00	39.71	40.25	24.61
	2	0.00	39.77	40.03	22.18
	3		39.23	41.83	27.66

SUMMARY

Groups	Count	Sum	Average	Variance
350	2	0	0	0
450	3	118.7	39.6	0.09
500	3	122.1	40.7	0.97
550	3	74.4	24.8	7.54

ANOVA

Source of Variation	SS	df	MS	F	P-value	F crit
Between Groups	2479.5	3	826.5	336.7	0.000000063	4.35
Within Groups	17.2	7	2.5			
Total	2496.7	10				

Table C-5: Pairwise-comparison for the HHV of the wax product

	x1	x2		difference	n1	n2	SE	q	q crit	q > q crit?	Therefore,
1	350	450	0.0 39.6	39.571	2	3	1.011	39.13	5.22	TRUE	Significant
2	450	500	39.6 40.7	1.134	3	3	0.905	1.25	5.22	FALSE	NO significance
3	500	550	40.7 24.8	15.889	3	3	0.905	17.57	5.22	TRUE	Significant
4	550	350	24.8 0.0	24.816	3	2	1.011	24.54	5.22	TRUE	Significant
5	350	500	0.0 40.7	40.705	2	3	1.011	40.25	5.22	TRUE	Significant
6	450	550	39.6 24.8	14.755	3	3	0.905	16.31	5.22	TRUE	Significant

C.6. Gross-energy conversion (GEC) results

Sample	350	450	500	550
1	0.966	0.930	0.852	0.300
2	0.925	0.734	0.878	0.346
3		0.877		

SUMMARY

Groups		Count	Sum	Average	Variance
	350	2	1.891	0.945	0.0009
	450	3	2.542	0.847	0.0103
	500	2	1.730	0.865	0.0003
	550	2	0.646	0.323	0.0011

ANOVA

Source of Variation	SS	df	MS	F	P-value	F crit
Between Groups	0.496	3	0.165	36.2	0.000815	5.409
Within Groups	0.023	5	0.00457			
Total	0.519	8				

Table C-6: Pairwise-comparison for the gross-energy conversion (GEC)

	x1	x2		difference	n1	n2	SE	q	q crit	q > q crit?	Therefore,
1	350	450	0.9 0.8	0.098	2	3	0.0436	2.25	5.22	FALSE	NO significance
2	450	500	0.8 0.9	0.018	3	2	0.0436	0.40	5.22	FALSE	NO significance
3	500	550	0.9 0.3	0.542	2	2	0.0478	11.35	5.22	TRUE	Significant
4	550	350	0.3 0.9	0.623	2	2	0.0478	13.03	5.22	TRUE	Significant
5	350	500	0.9 0.9	0.080	2	2	0.0478	1.68	5.22	FALSE	NO significance
6	450	550	0.8 0.3	0.525	3	2	0.0436	12.03	5.22	TRUE	Significant

C.7. Wax conversion (MJ/kg feedstock)

Sample	350	450	500	550
1	0.00	20.91	21.04	6.49
2	0.00	19.77	22.12	8.16
3		22.51		

SUMMARY

Groups	Count	Sum	Average	Variance
350	2	0.0	0.0	0.00
450	3	63.2	21.1	1.89
500	2	43.2	21.6	0.58
550	2	14.6	7.3	1.40

ANOVA

Source of Variation	SS	df	MS	F	P-value	F crit
Between Groups	743.0	3	247.7	215.4	0.000010	5.409
Within Groups	5.748	5	1.150			
Total	748.7	8				

Table C-7: Pairwise-comparison for the wax conversion (MJ/kg feedstock)

	x1	x2	difference	n1	n2	SE	q	q crit	q > q crit?	Therefore,
1	350 450	0.0 21.1	21.06	2	3	0.692	30.43	5.22	TRUE	Significant
2	450 500	21.1 21.6	0.52	3	2	0.692	0.75	5.22	FALSE	NO significance
3	500 550	21.6 7.3	14.26	2	2	0.758	18.80	5.22	TRUE	Significant
4	550 350	7.3 0.0	7.32	2	2	0.758	9.66	5.22	TRUE	Significant
5	350 500	0.0 21.6	21.58	2	2	0.758	28.46	5.22	TRUE	Significant
6	450 550	21.1 7.3	13.74	3	2	0.692	19.85	5.22	TRUE	Significant

C.8. Oil conversion (MJ/kg feedstock)

Sample	350	450	500	550
1	0	0	1.564	0
2	0	0	2.211	0
3		0		

SUMMARY

Groups	Count	Sum	Average	Variance
350	2	0	0	0
450	3	0	0	0
500	2	3.77	1.89	0.21
550	2	0	0	0

ANOVA

Source of Variation	SS	df	MS	F	P-value	F crit
Between Groups	5.54	3	1.85	44.2	0.00051	5.409
Within Groups	0.209	5	0.042			
Total	5.75	8				

177

Table C-8: Pairwise-comparison for the oil conversion (MJ/kg feedstock)

	x1	x2	difference	n1	n2	SE	q	q crit	q > q crit?	Therefore,
1	350	450	0.0	0.0	0.000	2	3	0.132	0	5.22	FALSE	NO significance
2	450	500	0.0	1.9	1.887	3	2	0.132	14.30	5.22	TRUE	Significant
3	500	550	1.9	0.0	1.887	2	2	0.145	13.06	5.22	TRUE	Significant
4	550	350	0.0	0.0	0.000	2	2	0.145	0	5.22	FALSE	NO significance
5	350	500	0.0	1.9	1.887	2	2	0.145	13.06	5.22	TRUE	Significant
6	450	550	0.0	0.0	0.000	3	2	0.132	0	5.22	FALSE	NO significance

C.9. Char conversion (MJ/kg feedstock)

Sample	350	450	500	550
1	30.44	8.40	4.23	2.96
2	29.12	3.36	3.33	2.74
3		5.13		

SUMMARY

Groups	Count	Sum	Average	Variance
350	2	59.6	29.8	0.87
450	3	16.9	5.63	6.52
500	2	7.56	3.78	0.41
550	2	5.69	2.85	0.02

ANOVA

Source of Variation	SS	df	MS	F	P-value	F crit
Between Groups	1019.5	3	339.8	118.6	0.000046	5.409
Within Groups	14.3	5	2.87			
Total	1033.8	8				

Table C-9: Pairwise-comparison for the char conversion (MJ/kg feedstock)

	x1	x2	difference	n1	n2	SE	q	q crit	q > q crit?	Therefore,
1	350	450	29.8	5.6	24.15	2	3	1.093	22.10	5.22	TRUE	Significant
2	450	500	5.6	3.8	1.85	3	2	1.093	1.69	5.22	FALSE	NO significance
3	500	550	3.8	2.8	0.94	2	2	1.197	0.78	5.22	FALSE	NO significance
4	550	350	2.8	29.8	26.93	2	2	1.197	22.50	5.22	TRUE	Significant
5	350	500	29.8	3.8	26.00	2	2	1.197	21.72	5.22	TRUE	Significant
6	450	550	5.6	2.8	2.78	3	2	1.093	2.55	5.22	FALSE	NO significance

Appendix D. Pilot-scale results (ANOVA and post-hoc analysis)

D.1. Char yield

Sample	450	500	550
1	29.5%	25.7%	26.6%
2	29.3%	35.3%	25.6%
3		33.4%	22.2%

SUMMARY

Groups	Count	Sum	Average	Variance
450	2	0.588	0.294	0.00000
500	3	0.943	0.314	0.00256
550	3	0.743	0.248	0.00052

ANOVA

Source of Variation	SS	df	MS	F	P-value	F crit
Between Groups	0.0069	2	0.0035	2.80	0.153	5.786
Within Groups	0.0062	5	0.0012			
Total	0.0131	7				

Table D-1: Pairwise-comparison for the char-yield results

	x1	x2	difference	n1	n2	SE	q	q crit	q > q crit?	Therefore,
1	450	500	0.3	0.3	0.020	2	3	0.0227	0.8863	4.6	FALSE	NO significance
2	500	550	0.3	0.2	0.067	3	3	0.0203	3.280578	4.6	FALSE	NO significance
3	550	450	0.2	0.3	0.046	3	2	0.0227	2.047939	4.6	FALSE	NO significance

D.2. Condensable product yield

Sample	450	500	550
1	45.4%	45.3%	39.5%
2	44.3%	50.9%	47.7%
3		59.6%	43.6%

SUMMARY

Groups	Count	Sum	Average	Variance
450	2	0.90	0.448	0.0001
500	3	1.56	0.519	0.0052
550	3	1.31	0.436	0.0017

ANOVA

Source of Variation	SS	df	MS	F	P-value	F crit
Between Groups	0.012	2	0.0058	2.11	0.217	5.79
Within Groups	0.014	5	0.0028			
Total	0.025	7				

Table D-2: Pairwise-comparison for the char-yield results

	x1	x2	difference	n1	n2	SE	q	q crit	q > q crit?	Therefore,
1	450	500	0.4	0.5	0.071	2	3	0.034	2.09	4.60	FALSE	NO significance
2	500	550	0.5	0.4	0.083	3	3	0.030	2.74	4.60	FALSE	NO significance
3	550	450	0.4	0.4	0.012	3	2	0.034	0.36	4.60	FALSE	NO significance

D.3. Non-condensable gas (NCG) yield

Sample	450	500	550
1	13.9%	18.1%	27.9%
2	14.3%	19.5%	27.5%
3		18.7%	27.8%

SUMMARY

Groups	Count	Sum	Average	Variance
450	2	0.281	0.141	0.000008
500	3	0.563	0.188	0.000049
550	3	0.832	0.277	0.000004

ANOVA

Source of Variation	SS	df	MS	F	P-value	F crit
Between Groups	0.0248	2	0.0124	541.16	0.0000014	5.79
Within Groups	0.0001	5	0.00002			
Total	0.0249	7				

Table D-3: Pairwise-comparison for the NCG yield results

	x1	x2	difference	n1	n2	SE	q	q crit	q > q crit?	Therefore,
1	450	500	0.1	0.2	0.047	2	3	0.0031	15.2	4.6	TRUE	Significant difference
2	500	550	0.2	0.3	0.090	3	3	0.0028	32.5	4.6	TRUE	Significant difference
3	550	450	0.3	0.1	0.137	3	2	0.0031	44.3	4.6	TRUE	Significant difference

D.4. Wax HHV (MJ/kg)

Sample	450 °C	500 °C	550 °C
1	34.8	38.1	35.0
2	36.5	38.2	35.8
3	36.4	40.4	35.7
4	37.1	38.8	28.8
5	36.0	39.9	27.7
6	35.8	37.8	34.0

SUMMARY

Groups	Count	Sum	Average	Variance
450	6	216.6	36.1	0.61
500	6	233.3	38.9	1.08
550	6	197.0	32.8	13.12

ANOVA

Source of Variation	SS	df	MS	F	P-value	F crit
Between Groups	109.9	2	54.94	11.13	0.0011	3.68
Within Groups	74.0	15	4.94			
Total	183.9	17				

Table D-4: Pairwise-comparison for the HHV of the wax phase

	x1	x2			difference	n1	n2	SE	q	q_{crit}	$q > q_{crit}$?	Therefore,
1	450	500	36.1	38.9	2.78	6	6	0.907	3.06	4.6	FALSE	NO significance
2	500	550	38.9	32.8	6.05	6	6	0.907	6.66	4.6	TRUE	Significant difference
3	550	450	32.8	36.1	3.27	6	6	0.907	3.60	4.6	FALSE	NO significance

D.5. Organic phase oil HHV (MJ/kg)

Sample	450 °C	500 °C	550 °C
1	43.5	42.7	43.6
2	43.7	44.7	39.3
3	43.3	43.9	43.8
4	44.2	44.7	45.2
5	50.4	43.8	42.6
6		41.7	44.4

SUMMARY

Groups	Count	Sum	Average	Variance
450	5	225.1	45.0	9.22
500	6	261.5	43.6	1.36
550	6	259.0	43.2	4.26

ANOVA

Source of Variation	SS	df	MS	F	P-value	F crit
Between Groups	10.0	2	5.01	1.08	0.367	3.74
Within Groups	65.0	14	4.64			
Total	75.0	16				

Table D-5: Pairwise-comparison for the HHV of the organic oil phase

	x1	x2			difference	n1	n2	SE	q	q_{crit}	$q > q_{crit}$?	Therefore,
1	450	500	45.0	43.6	1.432	5	6	0.923	1.55	4.60	FALSE	NO significance
2	500	550	43.6	43.2	0.417	6	6	0.880	0.47	4.60	FALSE	NO significance
3	550	450	43.2	45.0	1.849	6	5	0.923	2.00	4.60	FALSE	NO significance

Appendix E. Techno-economic strategy

E.1. Revenue, OPEX and the time value of money

The generated revenue from the project is shown in Equation E.1, where the revenue is the product of the production rate and market value.

$$\text{Revenue } [R/year] = \sum_{i=0}^{n}(\text{Prod. rate}_i [ton/year] \times \text{Market value}_i [R/ton]) \qquad \text{Equation E.1}$$

The operating cost or OPEX is calculated as the summation of the variable and fixed costs shown in equation E.2.

$$\text{OPEX } [R/year] = \text{Variable cost } [R/year] + \text{Fixed costs } [R/year] \qquad \text{Equation E.2}$$

The revenue, OPEX and CAPEX considers the time value of money and therefore the future value of money is calculated as shown in equation E.3.

$$FV = PV \times (1 + i)^n \qquad \text{Equation E.3}$$

Where:

- FV = future value of money (R/year) or (R)
- PV = present value of money (R/year) or (R)
- i = escalation rate (%)
- n = number of years since profitability analysis

E.2. Gross profit, net profit, and cash-flow

Gross profit is calculated by the difference between revenue and expenses, shown in equation E.4. It is calculated on an annual basis according to the discounted cash flow (DCF) method. According to the DCF method, the net profit is the gross profit remaining after company tax has been paid and the annual depreciation has been considered (See section E.3). The equation for calculating net profit from the gross profit, depreciation and tax rate can be seen in E.5. Tax is only paid if the annual net profit is greater than 0. The income tax rate of 28% is used to calculate the net profit as shown in Equation E.5. Lastly, the net cash flow shown in Equation E.6, is the money remaining after all revenue is received and expenses are paid [379], and hence it is the summation of the net profit and depreciation, which was subtracted from the gross profit to calculate the net profit after tax.

$$\text{Gross profit } \left(\frac{R}{year}\right) = \text{Generated revenue } \left(\frac{R}{year}\right) - \text{Operating cost } \left(\frac{R}{year}\right) \qquad \text{Equation E.4}$$

$$\text{Net profit } \left(\frac{R}{year}\right) = \left(\text{Gross profit } - \text{depreciation } \left(\frac{R}{year}\right)\right) \times (1 - \text{tax rate } (\%)) \qquad \text{Equation E.5}$$

$$\text{Cash flow } \left(\frac{R}{year}\right) = \text{Net profit } \left(\frac{R}{year}\right) + \text{depreciation } \left(\frac{R}{year}\right) \qquad \text{Equation E.6}$$

E.3. Depreciation tax and net profit

The depreciation of the assets/ fixed capital investments was calculated according to Equation E.7 whereby depreciation is taken over 5 years and the equipment has a 1% scrap value.

$$\text{Depreciation amount} = \frac{\text{Fixed capital investment (R)} \times (1 - \text{Scrap value (\%)})}{\text{Number of years that depreciation occurs (years)}}$$

Equation E.7

E.4. Discount rate determination and discounted cash flow

Discount rate, also known as the minimum acceptable rate of return (M_{ar}) is determined by the level of risk of the business and typically chosen as number within the ranges outlined in the table. The discounted cash flow (DCF) is calculated from cash flow and discount rate, shown in Equation E.8.

Table E-1: Indication of discount rate (m_{ar}) for processes of varying risks

Investment Type	Level of Risk	m_{ar} (%/year)
Basic, very safe investment	Safe	4 to 6
New capacity with established market position	Low	6 to 12
New product/ process technology entering established market	Medium	12 to 18
New product or process in a new application	High	18 to 30
Everything new, high R&D and marketing effort	Very high	30 +

$$\text{Discounted cash flow} \left(\frac{R}{\text{year}}\right) = \frac{\text{Cash flow (R/year)}}{(1 + \text{discount rate (\%)})^n}$$

Equation E.8

E.5. Key profitability indicators

The net-present value (NPV_n) is the discounted cumulative cash flow (DCCF), and if it is positive after a specified project lifespan (n years), the project is profitable. Likewise the larger the NPV, the more favourable the investment [346]. Comparison of the NPV value for projects must be compared at the same lifespan and are often compared at 15 years for short-term projects (NPV_{15}) or 25 years for longer term projects (NPV_{25}). The NPV_n after n years can be calculated provided the prior steps are taken and a discount rate (r) is selected as seen in Equation E.9.

$$NPV_{n \text{ (years)}}(\text{ZAR}) = \sum_{i=0}^{n} \frac{\text{Cash flow}}{(1+r)^n} - \sum_{i=0}^{n} \frac{\text{Capital flow}}{(1+r)^n}$$

Equation E.9

The DCF method to calculate the "present worth of future earnings" [297] is sensitive to the discount rate and by changing the discount rate it is possible, to select a rate where the NPV_n after n years is equal to zero. The more profitable a project, the higher IRR it can afford to pay [297]. The discount rate is often used as a 'hurdle' for the internal rate of return (IRR) to surpass before an investment is worth considering [343]. Consequently, changing the market value (R/ton) of the main product to a case where the IRR is equal to the discount rate will show a project that has a product (fuel) of minimum (fuel) selling price – MFSP - to make a project economically feasible and have a NPV of 0

by the end of the project lifespan, i.e., $NPV_{25} = 0$. The goal-seek function on MS Excel can be used to easily calculate this minimum fuel selling price (MFSP) when the $NPV_{25} = 0$ as seen in Equation E.10.

$$0 = \sum_{i=0}^{n} \frac{\text{Cash flow}}{(1+\text{IRR})^n} - \sum_{i=0}^{n} \frac{\text{Capital flow}}{(1+\text{IRR})^n}$$

Equation E.10

Appendix F. Total capital investment (TCI) methodology

F.1. CEPCI Indexes, location factors & Exchange rates

The CEPCI, LF indexes and exchange rates (ER) at time of computation are shown in Tables below.

The following assumptions were made for the location factors.

- The location factor of Latvia was assumed to be the same as Poland.
- The location factor of Greece was assumed to be the same as Italy.

Table F-1: The location factors used for study [380], [381]

Country	City	Value
South Africa	Johannesburg	1.09
Italy	Milan	1.20
Greece	-	1.20
Germany	Frankfurt	1.10
Austria	-	1.10
United States	-	1.00
Poland	Warsaw	0.96
Latvia	-	0.96

$$y = -5E\text{-}07x^6 + 0.0062x^5 - 30.644x^4 + 81069x^3 - 1E+08x^2 + 1E+11x - 3E+13$$
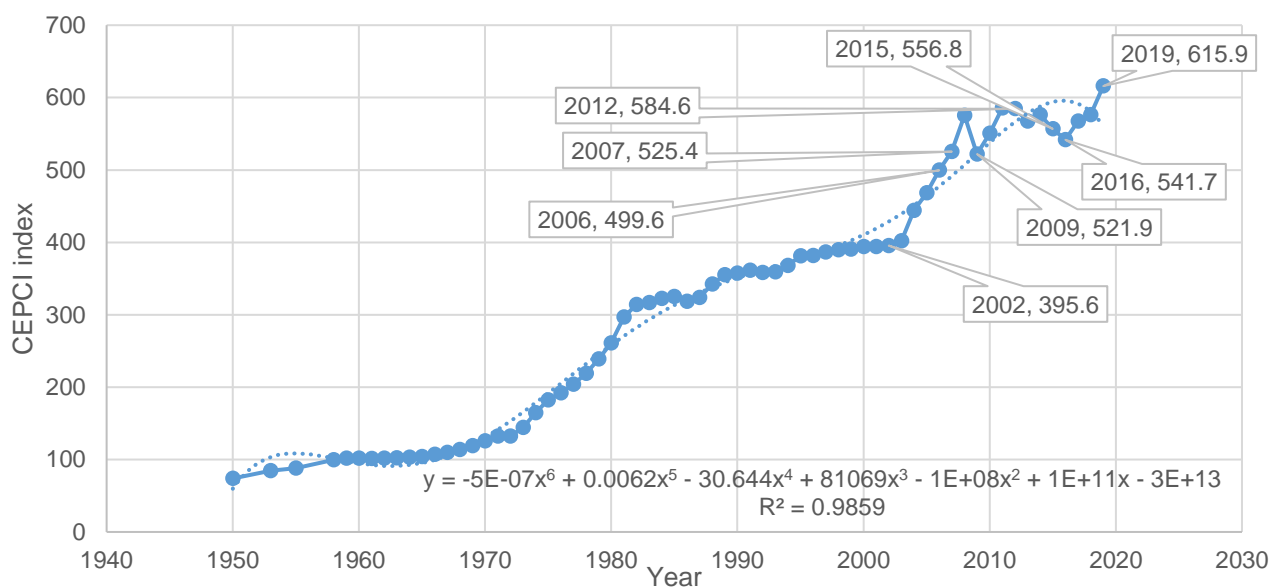$$R^2 = 0.9859$$

Figure F-1: Chemical Engineering Plant Cost Index from 1950 to 2019

Table F-2: Exchange rate for different currencies used for the CAPEX estimations

Date:	US ($)	=Yen (¥)	=ZAR (R)	=Euro (€)	=AUS ($)
Pre-COVID-19 (2020)	1	6.88	16.5451	0.89	0.72

Table F-3: Installation factors of process units

Unit	Type	Installation factor
Agitators	Carbon steel	1.3
	Stainless steel	1.2
Air heaters	All	1.5
Beaters		1.4
Blenders		1.3
Blowers		1.4
Boilers		1.5
Centrifuges	Carbon steel	1.3
	Stainless steel	1.2
Chimneys & stacks		1.2
Columns	Carbon steel, distillation	3
	Stainless steel, distillation	2.1
Compressors	motor driven	1.3
	steam or gas driven	1.5
Conveyors & elevators		1.4
Cooling towers	concrete	1.2
Crushers, classifiers & mills		1.3
Crystallizers		1.9
Cyclones		1.4
Dryers, spray, and air		1.6
	other	1.4
Ejectors		1.7
Evaporators	Calandria	1.5
	thin film, carbon steel	2.5
	thin film, stainless steel	1.9
Extruders	compounding	1.5
Fans		1.4
Filters	all types	1.4
Furnaces	direct fired	1.3
Gas holders		1.3
Granulators for plastic		1.5
Heat exchangers	air cooled, carbon steel	2.5
	coil in shell, stainless steel	1.7
	glass	2.2
	graphite	2
	plate, stainless steel	1.5
	plate, carbon steel	1.7
	shell and tube, stainless/ stainless steel	1.9
	shell and tube, carbon/ steel/ aluminium	2.2
	shell and tube, carbon steel/ copper	2
	shell and tube, carbon steel/ monal	1.8

186

	Shell and tube, monel/ monel	1.6
	shell and tube, carbon steel/ hastelloy	1.4
Instruments	all types	2.5
Miscellaneous	carbon steel	2
	stainless steel	1.5
Pumps	centrifugal, carbon steel	2.8
	centrifugal, stainless steel	2
	centrifugal, hastelloy trim	1.4
	centrifugal, nickel trim	1.7
	centrifugal, monel trim	1.7
	centrifugal, titanium trim	1.4
	all others, stainless steel	1.4
	all others, carbon steel	1.6
Reactor kettles	carbon steel	1.9
	kettles, glass lined	2.1
	kettles, carbon steel	1.9
Reactors	multitubular, stainless steel	1.9
	multitubular, copper	1.8
	multitubular, carbon steel	2.2
Refrigeration plant		1.5
Steam drums		2
Sum of equipment costs	stainless steel	1.8
	carbon steel	2
Tanks	process, stainless steel	1.8
Tanks	process,copper	1.9
Tanks	process, aluminium	2
Tanks	storage, stainless steel	1.5
Tanks	storage, carbon steel	2.3
Tanks	field erected, stainless steel	1.4
Tanks	field erected, carbon steel	1.5
Turbines		1.5
Vessels	pressure, stainless steel	1.7
Vessels	pressure, carbon steel	2.8

Appendix G. Sample calculations

G.1. Furnace sizing

The furnace was sized according to Couper, Chapter 0: Rules of Thumb [351]. The heating duty of the furnace was taken from the Aspen Plus model where a safety factor of 10% was assumed to attain the design duty

$$Q_{design} = Q_{design} \times (1 + \text{safety factor}) \qquad \text{Equation G.1}$$

The total exchange area for the fired heater was the summation of the convective and radiant areas. The radiant and convective rate of heat transfer was assumed as 37.6 and 12.5 kW/m^2, respectively [351]. It was assumed that there was equal heat transfer in either sections [351]. Hence, the convective and radiant areas were calculate according to equation G.2 and G.3, respectively [351].

$$A_{convective} (m^2) = 0.5 \times \frac{Q_{design} \text{ (kW)}}{\text{Convective rate } (12.5 \text{ kW/m}^2)} \qquad \text{Equation G.2}$$

$$A_{radiant}(m^2) = 0.5 \times \frac{Q_{design} \text{ (kW)}}{\text{Radiant rate } (37.6 \text{ kW/m}^2)} \qquad \text{Equation G.3}$$

$$A_{total}(m^2) = A_{convective} (m^2) + A_{radiant}(m^2)$$

The design pressure and temperature were calculated according to the operating pressure and temperature as shown in equation G.4 and G.5 below.

$$P_{design} \text{ (bara)} = P_{operating \, max} \text{ (bara)} \times (1 + 0.1) \qquad \text{Equation G.4}$$

$$P_{operating \, max} \text{ (bara)} = P_{operating} \text{ (bara)} + 1.7 \text{ bara} \qquad \text{Equation G.5}$$

$$T_{design} (°C) = T_{operating \, max} (°C) + 50 °C \qquad \text{Equation G.6}$$

G.2. Furnace costing

The cost was calculated according to an installed fired heater in Couper, 2009 [348]. For a box-type heater with a design heating duty between 20 and 200 million Btu/h, equation G.7 can be used [348]. A cylindrical type furnace can be costed when the design heating duty is between 2 and 30 million Btu/h [348]. The factors k, fd and fp are shown in Table G-1 and Table G-2.

$$C_{p,box-type}(\$) = 1000 \times (1.218 \times k \times (1 + f_d + f_p) \times Q^{0.86}) \qquad \text{Equation G.7}$$

$$C_{p,cylindrical-type}(\$) = 1000 \times (1.218 \times k \times (1 + f_d + f_p) \times Q^{0.82}) \qquad \text{Equation G.8}$$

Once the base cost (Cp ($)) has been calculated, the cost of the furnace can be calculated in South African Rands and for the current year according to the equation G.9 below.

$$C_{p,furnace} \text{ (ZAR)} = C_p(\$) \times \frac{CEPCI_{2019}}{CEPCI_{2006}} \times \frac{LF_{S.A}}{LF_{U.S}} \times \frac{\pm 16.5 \text{ ZAR}}{1 \text{ US\$}} \qquad \text{Equation G.9}$$

Table G-1: Parameters used for the two furnace types

Tube material	k (box-type)	K (cyl. type)	Design type	F_d (box-type)	F_d (cyl. type)
Carbon steel	25.5	27.3	Process heater	0	-
CrMo steel	33.8	40.2	Pyrolysis	0.10	-
Stainless	45.0	42	Reformer (no catalyst)	0.35	-
-			Cylinder-type	-	0
			Downtherm	-	0.33

Table G-2: Pressure parameters used for the costing equation

Design pressure (psi)	F_p (box-type)	F_p (cylinder-type)
>500	0	0
500 < x< 1000	0.10	0.15
1000 < x< 1500	0.15	0.2
1500 < x< 2000	0.25	-
2000 < x< 2500	0.40	-
2500 < x< 3000	0.60	-

G.3. Reactor sizing

The reactor was sized as a vessel. The diameter of the vessel depended on the solid's flowrate (kg/h), the solids residence time (h), density of the incoming feed (kg/m^3) and a constant of 0.45 - referred to as the cross-sectional area of the reactor that the solids occupy (%) [29]. The diameter of vessel was calculated as shown in Equation G.10. The density of the pelleted solids with water was 350 kg/m^3 and the constant were assumed to occupy 45% of the reactor [29].

$$D_{reactor}(m) = \frac{F_{solids}(kg/h)}{\rho\ (kg/m^3)} \times \tau_{solids}(h) \times \frac{1}{(0.45)} \qquad \text{Equation G.10}$$

Consequently, the length of the reactor could be calculated according to the equation G.11 below.

$$L_{reactor}(m) = 5 \times \sqrt[3]{\frac{D_{reactor}(m)}{1.25 \times \pi}} \qquad \text{Equation G.11}$$

G.4. Vessel costing

Once the diameter and the length of the diameter is calculated, the vessel can be costed according to its weight, dimensions and material as shown in equation G.12 for both horizontal & vertical vessels.

$$C\ (\$) = F_M C_B + C_A \qquad \text{Equation G.12}$$

The cost factor, CB, is calculated different according to whether the process vessel is horizontal or vertical. The horizontal and vertical factors are provided in Equations G-13 to G-16.

$$C_{B,\text{horizontal vessel}} = 1.672 \times \exp\left(8.571 - 0.2330 \times \ln(W(\text{lb})) + 0.0433 \times \ln(W(\text{lb}))^2\right) \quad \text{Equation G.13}$$

$$C_{A,\text{horizontal vessel}} = 2291 \times D^{0.2029}, \qquad 3 < D \text{ (ft)} < 12 \qquad\qquad \text{Equation G.14}$$

$$C_{B,\text{vertical vessel}} = 1.672 \times \exp\left(9.100 - 0.2889 \times \ln(W(\text{lb})) + 0.04576 \times \ln(W(\text{lb}))^2\right) \quad \text{Equation G.15}$$

$$C_{A,\text{vertical vessel}} = 480 \times D^{0.7396} \times L^{0.7066}, \qquad 6 < D \text{ (ft)} < 10, \ 12 < L \text{ (ft)} < 20 \qquad \text{Equation G.16}$$

The weight of the vessel is calculated according to the shell weight and the top and bottom section of the vessel. The top and bottom section of the vessel is constant at 148 kg (325 lb) according to Couper, 2009 [348]. The total weight is calculated according to Equation G-17.

$$W_{\text{total}} \text{ (lb)} = W_{\text{shell}} \text{ (lb)} + W_{\text{top-section}} \text{ (lb)} + W_{\text{bottom-section}} \text{ (lb)} \qquad\qquad \text{Equation G.17}$$

The shell part of the vessel can be calculated according to the diameter (m), length (m), thickness (m) and the density of the metal that is used for the function of the reactor [348]. The thickness and density for the metal can be found in Table G-4 and Table G-3, respectively.

$$W_{\text{shell}} \text{ (kg)} = \pi \times D \text{ (m)} \times L(m) \times \text{thickness (m)} \times \rho \left(\frac{\text{kg}}{\text{m}^3}\right) \qquad\qquad \text{Equation G.18}$$

Table G-3: The various metals used for vessels and their densities used to calculate vessel weight

Material	Cost factor	density
(-)	(F_M)	(ρ) kg/m^3
Stainless steel 304	1.7	7850
Stainless steel 316	2.1	7870
Carpenter 20CB-3	3.2	9010
Nickel-200	5.4	8890
Monel-400	3.6	8800
Inconel-600	3.9	8470
Incoloy-825	3.7	8470
Titanium	7.7	4500

Table G-4: Minimum wall thickness depending on the diameter of the vessel (pressure vessels)

Minimum wall thickness (mm)	Diameter (m)
6.4	0 < x < 1.07
8.1	1.07 < x < 1.52
9.7	1.52 < x

G.5. Heat exchanger sizing

The heat duty for the heat exchanger (Q) can be taken from the Aspen Flowsheet for the desired unit to be sized and costed. The design heat duty (Q_{design}) of the air heater adds a 10% safety factor to account for inefficiencies, as shown in Equation G.19.

$$Q_{design(kW)}=Q(kW)\times(1+10\ \%\ [safety\ factor])$$ Equation G.19

All units are assumed to be ideal counter current heat exchangers. The area of the heat exchange can be calculated according to the design heat duty (Q_{design}), the overall heat transfer coefficient (U) as shown in Table G-5 depending on the exchanger function, the factor (F) assumed as 1 and the log mean temperature difference (LMTD) calculated as Equation G.20 [382].

$$A\left(m^2\right)=\frac{Q_{design}(W)}{U(W/_{m^2.°C})\times F\times\Delta T_{LM}(°C)}$$ Equation G.20

Table G-5: Different heat transfer coefficient (U) used for various heat exchangers

Heat Exchange type	Heat transfer coefficient - U (W/m^2. °C)
Water to liquid	850
Condensers	850
Liquid to liquid	280
Liquid to gas	60
Gas to gas	30
Reboiler	1140

$$\Delta T_{LM}(°C)=\frac{\Delta T_1-\Delta T_2\ (°C)}{\ln\left(\Delta T_1/_{\Delta T_2}\right)}$$ Equation G.21

For the LMTD (ΔT_{LM}), the variables ΔT_1, and ΔT_1 for counter-current heat exchange is:

$$\Delta T_1 = T_{utility,OUT} - T_{process,IN}$$ Equation G.22

$$\Delta T_1 = T_{utility,IN} - T_{process,OUT}$$ Equation G.23

The design temperature and pressure is calculated by adding a factor to each variable.

$$T_{design}(°C) = T_{operating,MAX}(°C) + 25\ (°C) = T_{LPS}(°C) + 25\ (°C)$$ Equation G.24

$$P_{design}(bara) = P_{operating,MAX}(bara) + 1.7(bara) = P_{LPS}(bara) + 1.7(bara)$$ Equation G.25

The heat exchanger was calculated to be a shell and tube heat exchanger because the area was determined to be greater than 200 ft^2 as shown in Table G-6.

Table G-6: Selection of whether heat exchanger is shell and tube or double pipe exchanger

Area of heat exchanger	Type of heat exchanger
A > 200 ft^2	Shell-and-tube
A < 200 ft^2	Double pipe

G.6. Heat exchanger costing

The cost of shell-and-tube heat exchangers are determined from equation G.26 below. The pressure factor (F_p) based on the shell-side pressure and based on the design pressure (psig) as shown in Equation F.27. The tube-length correction factor (F_L) is based on the tube length, whereby typically a 20 ft tube length is provided to minimize costs as shown in Table G-7. The material construction factor (F_M) is calculated according to Equation G.28, whereby A is the contact area of the heat exchanger (A) in ft^2 and the values a & b are based off the materials which are assumed to be carbon steel on the tube side and stainless steel on the shell side (for steam).

$$\text{Cost(US\$)} = F_p \times F_l \times F_m \times C_B \times \left(\frac{\text{CEPCI}_{2005}}{\text{CEPCI}_{2018}}\right) \times \left(\frac{\text{LF}_{US}}{\text{LF}_{RSA}}\right) \times \frac{1\ \text{US\$}}{\pm 16.5\ \text{ZAR}}$$

Equation G.26

$$F_p = 0.9803 + 0.018\left(\frac{P\ (\text{psig})}{100}\right) + 0.0017\left(\frac{P(\text{psig})}{100}\right)^2$$

Equation G.27

$$F_m = a + \left(\left(\frac{A(\text{ft}^2)}{100}\right)^b\right)$$

Equation G.28

Table G-7: The tube-length correction factor (F_L)

Tube length (ft)	F_L
8	1.25
12	1.12
16	1.05
20	1.00

Table G-8: Materials of construction factors, F_M, for shell-and-tube Heat exchangers

Materials of construction Shell/ Tube	a	b
Carbon steel/ carbon steel	0	0
Carbon steel/ brass	1.08	0.05
carbon steel/ stainless steel	1.75	0.13
Carbon steel/ Monel	2.1	0.13
Carbon steel/ titanium	5.2	0.16
Carbon steel/ Cr-Mo steel	1.55	0.05
Cr-Mo steel/ Cr-Mo steel	1.7	0.07
Stainless steel/ stainless steel	2.7	0.07
Monel/ monel	3.3	0.08
Titanium/ titanium	9.6	0.06

In equation G.29, the value C_B is the base cost of the heat exchanger and it is calculated according to the type of shell-and-tube heat exchanger chosen. Shell-and-tube heat exchangers consist of four different types being kettle, floating head, U-tube, and Fixed head. The kettle shell-and-tube heat exchanger is used for reboilers in distillation columns. The floating head and U-tube heat exchangers are adjustable and usually more expensive than the fixed head type. Typically, the fixed head type is selected, and Equation G.29 is used to calculate the base cost where A is the contact area (ft^2).

$$C_B = \exp\{11.0545 - 0.9228[\ln(A)] + 0.09005[\ln(A)]^2\}$$
<div align="right">Equation G.29</div>

Appendix H. Equipment cost for SRF conversion line

Short-cut methods were used for most of the process units due to their simplicity and lack of utilities which in most cases, just used electrical power to drive motors.

H.1. Sample calculations for indirect dryer configuration

Instead of air, the indirect dryer uses steam for conduction drying. The dryer was assumed to be an indirect, steam-tube dryer. The steam used for the indirect dryer was from the boiler on-site and therefore no boiler was necessary. The steam used only latent heat to transfer the energy required for conduction drying and the steam condensate collected in a shop fabricated storage tank before being pumped back to the boiler to recycle the steam. Figure H-1 shows the process.
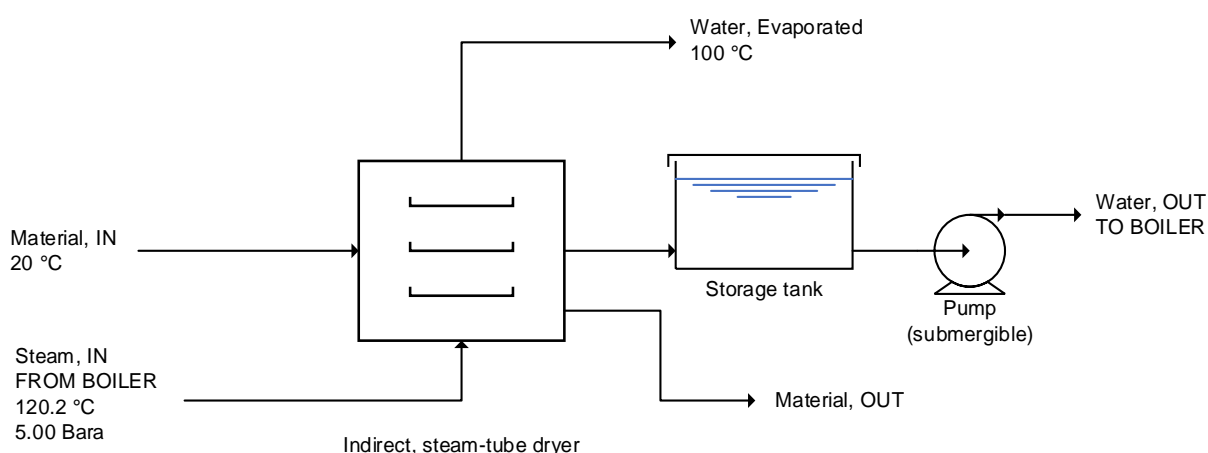

Figure H-1: Indirect dryer configuration using a storage tank to collect condensate and pump to recycle water to boiler.

H.2. Sizing and costing of the indirect dryer

The heat duty of the indirect dryer could be calculated from the heat duty to increase the solids heat duty, the duty to evaporate the water difference between inlet and outlet and the duty to increase the water in the sample from initial to final temperature [383], [384] as shown in Equation H.1.

$$Q_{min}(\tfrac{kJ}{h}) = Q_{solids\ temp.rise}\ (\tfrac{kJ}{h}) + \ Q_{moisture\ temp.rise}\ (\tfrac{kJ}{h}) + Q_{evaporation}\ (\tfrac{kJ}{h}) \qquad \text{Equation H.1}$$

$$Q_{solids\ temp.rise} = (\tfrac{kJ}{h}) = \dot{m}_{s,IN}\left(\tfrac{kg}{h}\right).(1\text{-}x_{w,IN}).C_{p,s}(\tfrac{kJ}{kg.°C}).\{T_{s,out}\text{-}T_{s,in}(°C)\} \qquad \text{Equation H.2}$$

$$Q_{w\ temp.rise}\ (\tfrac{kJ}{h}) = (\dot{m}_{s,IN}\left(\tfrac{kg}{h}\right).x_{w,IN} - \dot{m}_{s,OUT}\left(\tfrac{kg}{h}\right).x_{w,IN}).C_{p,L}\ (\tfrac{kJ}{kg.°C}).\{T_{s,out}\text{-}T_{S,in}(°C)\} \qquad \text{Equation H.3}$$

$$Q_{evp.}(\tfrac{kJ}{h}) = \lambda(\tfrac{kJ}{kg.°C}).\{X_{w,IN}.\dot{m}_{s,IN}\left(\tfrac{kg}{h}\right) - X_{w,OUT}.\dot{m}_{s,OUT}\left(\tfrac{kg}{h}\right)\} \qquad \text{Equation H.4}$$

The variables of heat capacities (C_p) and latent heat of vaporization of water at 20°C (λ_w) is provided in Figure H-1. The $C_{P,\ solid}$ was assumed to be 1.8 kJ/ (kg. °C) [385].

194

Table H-1: Physical constants used in Equations 1 to 4

Physical constants	$C_{p, air}$	$C_{p, sheet}$	$C_{p, liquid water}$	$C_{p, water vapor}$	λ_w	$C_{p, solid}$
Values	1	2.5	4.184	1.8	2256.1	1.8
Units	kJ/ (kg. °C)	kJ/ (kg. °C)	kJ/ (kg. °C)	kJ/ (kg. °C)	kJ/kg	kJ/ (kg. °C)

The thermal efficiency of indirect driers is 80% so a 20% heat loss is expected [361], and added to the minimum heat duty (Q_{min}) to account for inefficiencies for heat duty (Q) and the lateral surface area could be calculated according to Equation H.5.

$$A_{lateral} (m^2) = \left(\frac{Q\ (kJ/h)}{U\ (W/(m^2.K) \times (T_{s,out} - T_{S,in})\ (°C)} \right) \qquad \text{Equation H.5}$$

Usually he overall heat transfer coefficient is calculated according to Equation H.6 [361].

$$\frac{1}{U\ (W/(m^2.K)} = \frac{1}{h_h} + \frac{1}{h_w} + \frac{1}{h_f} + \frac{1}{h_m} + \frac{1}{h_r} \qquad \text{Equation H.6}$$

Table H-2: The constants and their ranges used for the calculation of overall heat transfer coefficient

Constant	h_h	h_w	h_f	h_m	h_r
Range	570 - 10,500	1050 – 13,650	2.8 – 280	4.5 – 1050	1050

The typical range of each of the values given in Equation H.6 is shown in Table H-2. Although these values were not used it was assumed that the heat transfer coefficient (U) was 90 W/(m².K) because the U values for steam-tube rotary dryers ranges from 30 to 90 W/(m².K) [361].

Once the lateral surface area (A) is converted from m² to ft², the following costing correlation shown on Equation H.7 was used to calculate the rotary steam tube dryer cost, provided 500 < A (ft²) < 18,000 [348]. The variable F, used in the Equation H.7 is shown in Table H-3 [348].

$$C\ (kUS\$) = 2.23 \times (F) \times A(ft^2)^{0.60} \times \frac{CEPCI_{2006}}{CEPCI_{2019}} \times \frac{LF_{U.S}}{LF_{S.A}} \times \frac{1\ US\$}{16.5\ ZAR} \qquad \text{Equation H.7}$$

Table H-3: The material factor values (F) used in Equation H.7 for the Rotary Dryer

Material	F	Selected?
Carbon steel	1.0	No
Stainless type 304	1.75	Yes

H.3. Sizing and costing the storage tank to collect steam condensate

The steam condensate collects in a tank that can hold one-months' capacity of condensate [347]. The capacity was calculated keeping in mind the operating hours of each shift, number of shifts per day, and the number of days operating per month.

- A freeboard of 10% was added to attain total volume of storage tank [347]
- A density of the once-cooled condensate (997 kg/m^3) was used.
- The length to diameter ratio of 3 was used.

The costing of the storage tank was calculated as seen in Equation H.8, according to the volume of the tank (according to 1 months' capacity) and the fact that the storage volume fell within the specifications of the "shop-fabricated" type and not "field-erected" type.

The volume was converted from m^3 to US gallon and the following costing correlation was used to calculate the storage tank, provided 1,300 < V (US gal) < 21,000 [348].

$$C \text{ (US\$)} = 1.218. F_m. \exp\{2.631 + 1.3676. (\ln(V)) - 0.06309. (\ln(V))^2\}$$

Equation H.8

- A material factor of 2.4 was used for Stainless Steel 304
- The cost of the unit was converted from US\$ to ZAR through equation H.9 below.

$$C \text{ (ZAR)} = C \text{ (US\$)} \times \frac{CEPCI_{2006}}{CEPCI_{2019}} \times \frac{LF_{U.S}}{LF_{S.A}} \times \frac{1 \text{ US\$}}{16.5 \text{ ZAR}}$$

Equation H.9

H.4. Sizing and power requirement of the pump

The pump required for transporting the water from the storage back to the boiler was sized according to the volumetric flowrate. A 10% safety factor was used for the design volumetric flowrate as shown in equation H.10 and the fluid pumping power was calculated according to the design volumetric flowrate, change in pressure, and shaft efficiency as seen in equation H.11 and H.12.

$$\dot{V}_{design}(m^3/min) = \dot{V}_{flow}(m^3/min) \times (1 + \text{safety factor} (\%))$$

Equation H.10

$$\dot{P}_{fluid}(kW) = 1.67 \times \dot{V}_{design}(m^3/min) \times \left(\frac{\Delta P \text{ (bar)}}{\varepsilon}\right)$$

Equation H.11

$$\Delta P \text{ (bara)} = P_{discharge}(bara) - P_{suction}(bara)$$

Equation H.12

A centrifugal, single stage pump was selected due to its availability. The following assumptions were made:

- The pump was on the same level as the storage tank and 10 m from the storage tank.
- The length of the pipeline from the pump to boiler was 60 m.

The suction pressure ($P_{suction}$) was calculated assuming that the storage tank and pump are on the same level and 10 m ($L_{suction}$) from the storage tank and is calculated according to Equation H.13

below. The discharge pressure is calculated according to Equation H.14 where the discharge pressure is the pressure required to attain height (z_{outlet}) and various pressure losses for the orifice (0.1 bar), control valve (0.69 bar), safety factor (0.3 bar) and line loss (0.271 bar). The line loss was determined from the product of the discharge line length (assumed to be 60 m) and $\Delta P_{line,suction}$ assumed to be 0.004524 bara/m for this line.

$$P_{suction}(bara) = P_{inlet}(bara) - (L_{suction}[m] \times \Delta P_{line,suction}\,[0.000905\ bara/m]) \qquad \text{Equation H.13}$$

$$P_{discharge}(bara) = P_{out}(bara) + \frac{\rho_{liq} \times g \times z_{outlet}}{100000} + \Delta P_{orifice} + \Delta P_{cntrl\ valve} + \Delta P_{safety} + \Delta P_{line,loss} \qquad \text{Equation H.14}$$

H.5. Sample calculations for direct dryer

The direct drying process uses air for convection to extract the water from the material. It is made up of three distinct sections, *viz.* the fan to direct the air to the dryer, the heat-exchanger to heat the air and the dryer which uses heated air to maximize the drying. Figure H-2 below shows the three process units and Table H-4 shows their utility and unit type.
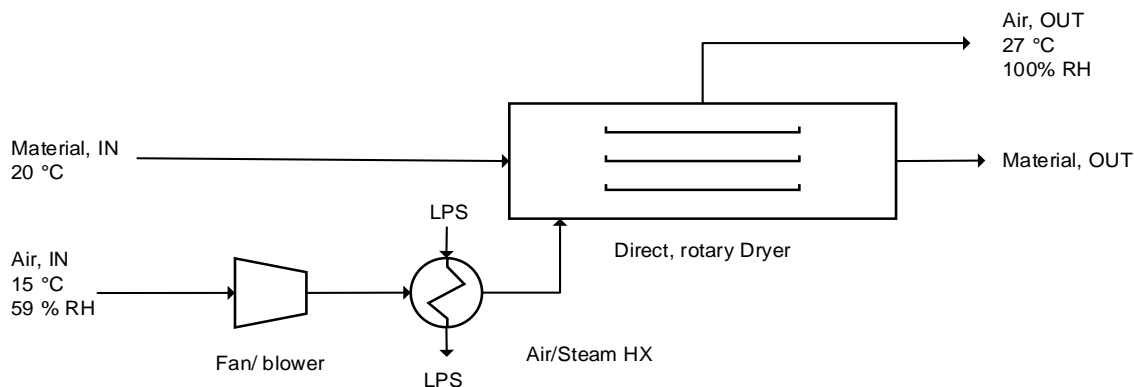
Figure H-2: The direct dryer configuration using a fan to direct the air, and heat exchanger to prepare the air

Table H-4: The process units, type, and utility of the dryer configuration

Unit	Type	Utility
Dryer	Rotary direct type	Air & Electricity
Air/ steam HX	Shell & Tube exchanger (fixed head)	Low-pressure steam/ LPS
Fan/ Blower	Axial fan (Vane-axial)	Electricity

Axial fans are designed to handle very high flowrates but low pressure changes [73]. The heat-exchanger was assumed to be shell & tube because it is assumed that the area will be too large for a double pipe exchanger [348].

197

H.6. Sizing and costing of the rotary dryer

The volume of the solid material (V_{solids}) in the dryer can be calculated according to the mass flowrate (m_{feed}) and density of material (ρ_{feed}) and its drying time in dryer (t_{dry}) as shown in Equation H.15 [382]. A drying time of 30 minutes (0.5 h) was used for the calculations.

$$V_{solids}(m^3) = \frac{m_{feed}(kg/h)}{\rho_{feed}\ (kg/m^3)} \times t_{drying}(h)$$
<div align="right">Equation H.15</div>

If the solids account for 7.5% of the cross-sectional area/ volume, the volume of the dryer can be calculated according to Equation H.16.

$$V_{dryer}(m^3) = \frac{V_{solids}(m^3)}{Solids\ area\ (\%)}$$
<div align="right">Equation H.16</div>

The diameter of the dryer can then be calculated assuming that the length to diameter ratio of the dryer is 6:1. Equation H.17 shows how the diameter can be subsequently calculated.

$$d_{dryer}(m) = \sqrt[3]{\frac{4 \times V_{dryer}(m^3)}{6 \times \pi}}$$
<div align="right">Equation H.17</div>

The lateral surface area of the dryer can be calculated according to Equation H.18, whereby the length of the dryer (l_{dryer}) is 6 times the dryer diameter.

$$SA_{dryer} = \pi \times d_{dryer}(m) \times l_{dryer}\ (m) = \pi \times 7 \times d_{dryer}(m)$$
<div align="right">Equation H.18</div>

The lateral surface area was then calculated from m^2 to ft^2 and the following costing correlation was used to calculate the rotary hot air heated dryer cost, provided 200 < A (ft^2) < 4000 [348].

$$C\ (kUS\$) = 2.90 \times (1 + f_g + f_m) \times A(ft^2)^{0.63} \times \frac{CEPCI_{2019}}{CEPCI_{2006}} \times \frac{LF_{S.A}}{LF_{U.S}}$$
<div align="right">Equation H.19</div>

The variables used in the Equation H.19 are shown in Table H-5 and Table H-6 [348].

Table H-5: The material factor values (f_m) used in Equation H.19 for the Rotary Dryer

Material	f_m	Selected?
Mild steel	1.0	Yes
Stainless type 304	1.4	No

Table H-6: The values for f_g used in Equation H.19

Drying gas	f_g	Selected?
Hot air	0.00	Yes
Combustion gas (direct contact)	0.12	No
Combustion gas (indirect contact)	0.35	No

The F.O.B cost of the dryer can be converted into South African rand using the location factor and exchange rate, shown below in Equation H.20.

$$C\ (ZAR) = C(kUS\$) \times (\pm 16.5\ ZAR/US\$) \times (1000\ US\$/kUS\$)$$ Equation H.20

H.7. Sizing and costing of the air heater for the dryer

The heat duty for the air heater (Q) can be calculated by the product of the volumetric flowrate ($\dot{V}$), Target temperature (T_{out}) and incoming temperature (T_{in}) of the process/ air stream, the density of air (ρ_{air}), and the heat capacity of air ($C_{p,air}$). The calculation is seen in Equation H.21.

$$Q\ (kW) = \dot{V}\left(\frac{m^3}{s}\right) \times [T_{out}\text{-}T_{in}](°C) \times C_{p,air}\left(\frac{kJ}{kg.°C}\right) \times \rho\left(\frac{kg}{m^3}\right)$$ Equation H.21

The design heat duty (Q_{design}) of the air heater adds a 10% safety factor to account for inefficiencies, as shown in Equation H.22.

$$Q_{design(kW)} = Q(kW) \times (1+10\ \%\ [safety\ factor])$$ Equation H.22

Assuming that the air heater is an ideal counter current heat exchanger [382], the area of heat exchange can be calculated by the design heat duty (Q_{design}), the overall heat transfer coefficient (U) assumed to be 10 W/(m².K), the factor assumed as 1 and the log mean temperature difference (LMTD) calculated as Equation H.23.

$$A(m^2) = \frac{Q_{design}(W)}{U(W/m^2.°C) \times F \times \Delta T_{LM}(°C)}$$ Equation H.23

Table H-7: Different heat transfer coefficient

Heat Exchange type	Heat transfer coefficient - U (W/m².°C)
Water to liquid	850
Condensers	850
Liquid to liquid	280
Liquid to gas	60
Gas to gas ✓	30
Reboiler	1140

$$\Delta T_{LM}(°C) = \frac{\Delta T_1 - \Delta T_2\ (°C)}{\ln\left(\Delta T_1/\Delta T_2\right)}$$ Equation H.24

For the LMTD (ΔT_{LM}), the variables ΔT_1, and ΔT_1 for counter-current heat exchange is:

$$\Delta T_1 = T_{utility,OUT} - T_{process,IN}$$ Equation H.25

$$\Delta T_1 = T_{utility,IN} - T_{process,OUT}$$ Equation H.26

The design temperature and pressure are calculated by adding a factor to each variable.

$$T_{design}(°C) = T_{operating,MAX}(°C) + 25\ (°C) = T_{LPS}(°C) + 25\ (°C)$$ Equation H.27

$$P_{design}(bara) = P_{operating,MAX}(bara) + 1.7(bara) = P_{LPS}(bara) + 1.7(bara)$$ Equation H.28

The heat exchanger was calculated to be a shell and tube heat exchanger because the area was determined to be greater than 200 ft^2 as shown in Table H-8.

Table H-8: Selection of whether heat exchanger is shell and tube or double pipe exchanger

Area of heat exchanger	Type of heat exchanger
A > 200 ft^2	Shell-and-tube
A < 200 ft^2	Double-pipe

The cost of shell-and-tube heat exchangers are determined from equation H.29 below.

$$Cost(US\$) = F_p \times F_l \times F_m \times C_B \times \left(\frac{CEPCI_{2005}}{CEPCI_{2018}}\right) \times \left(\frac{LF_{US}}{LF_{RSA}}\right) \times \frac{1\ US\$}{\pm 19\ ZAR}$$ Equation H.29

The pressure factor (F_p) based on the shell-side pressure and based on the design pressure (psig).

$$F_p = 0.9803 + 0.018\ \left(\frac{P\ (psig)}{100}\right) + 0.0017\left(\frac{P(psig)}{100}\right)^2$$ Equation H.29

The tube-length correction factor (F_L) is based on a 20 ft tube length shown in Table H-9.

Table H-9: The tube-length correction factor (F_L)

Tube length (ft)	F_L
8	1.25
12	1.12
16	1.05
20 ✓	1.00

The material construction factor (F_M) is calculated according to Equation H.30, whereby A is the contact area of the heat exchanger (A) in ft^2 and the values a & b are based off the materials which are assumed to be carbon steel on the tube side and stainless steel on the shell side (for steam).

$$F_m = a + \left(\left(\frac{A(ft^2)}{100}\right)^b\right)$$ Equation H.30

In equation H.31, the value C_B is the base cost of the heat exchanger and it is calculated according to the type of shell-and-tube heat exchanger chosen. Shell-and-tube heat exchangers consist of four different types being kettle, floating head, U-tube, and Fixed head. The kettle shell-and-tube heat

exchanger is used for reboilers in distillation columns. The floating head and U-tube heat exchangers are adjustable and usually more expensive than the fixed head type. The fixed head type was selected, and Equation H.31 is used to calculate the base cost where A is the contact area (ft^2).

Table H-10: Materials of construction factors, F_M, for shell-and-tube Heat exchangers

Materials of construction Shell/ Tube	a	b
Carbon steel/ carbon steel	0	0
Carbon steel/ brass	1.08	0.05
carbon steel/ stainless steel ✓	**1.75**	**0.13**
Carbon steel/ Monel	2.1	0.13
Carbon steel/ titanium	5.2	0.16
Carbon steel/ Cr-Mo steel	1.55	0.05
Cr-Mo steel/ Cr-Mo steel	1.7	0.07
Stainless steel/ stainless steel	2.7	0.07
Monel/ monel	3.3	0.08
Titanium/ titanium	9.6	0.06

$$C_B = \exp\{11.0545 - 0.9228[\ln(A)] + 0.09005[\ln(A)]^2\}$$

Equation H.31

H.8. Sizing and costing of the blower/ fan

An axial fan is used because of the high flowrate and low-pressure increase. The fan is also backward curved blade as it is cheaper and more efficient [351]. The costing of the unit is from pg. 566 of [351] and shown in Equation H.32

$$C_{P,fan} = F_H \times F_M \times C_B \times \frac{CEPCI_{2006}}{CEPCI_{2019}} \times \frac{LF_{U.S}}{LF_{S.A}} \times \frac{1\ US\$}{\pm16.5\ ZAR}$$

Equation H.32

The pressure difference between inlet and outlet pressure is 3% for fans [348] and due to the high altitude of Gauteng, the initial pressure of air was estimated at 0.984 bara. $k = \frac{C_P}{C_V} = 1.4$ for diatomic molecules and the difference in pressure, known as the head, is determined as 0.0295 bar or 11.86 in. H_2O and therefore a vane-axial is appropriate (Table H-12).

Table H-11: Inlet and outlet pressures (bara)

$P_{initial}$	0.98374	bara
P_{final}	1.01325	bara

Table H-12: The head factor values (f_H) used in Equation H.32 of the axial fan

Head [in. H$_2$O] / (bar)	Vane Axial	Tube axial
[5-8] / (0.0124 – 0.0199)	1.15	1.15
[9-15] / (0.02 – 0.0373)	1.30 ✓	-

Fiberglass is appropriate for non-corrosive gases such as air and is used as shown in Table H-13

Table H-13: The material factor (f_m) used in Equation H.32 for the axial fan

Head	f_m
Fibreglass	1.8 ✓
Stainless Steel	2.5
Nickel alloy	5.0

Therefore, adding the material factor and head factor values, Equation H.32 becomes Equation H.33.

$$C_{P,fan} = 1.3 \times 1.8 \ \times C_B \times \frac{CEPCI_{2019}}{CEPCI_{2006}} \times \frac{LF_{S.A}}{LF_{U.S}} \times \frac{\pm 16.5 \ ZAR}{1 \ US\$}$$

Equation H.33

The base cost for a vane axial fan with a capacity (Q) between 1,000 and 800,000 ACFM (actual cubic feet per minute) is calculated according to Equation H.34. The flowrate (Q) was calculated from the air requirement in mass flowrate and the density of the moist air. The density of the moist air was calculated from the "psych" function plugin [386]. This function is explained in the following section, Appendix I.2 and can calculate the moist air density considering the incoming air to have an average annual relative humidity of 59% and an annual average dry-bulb temperature of 15 °C.

$$C_B = \exp \{9.5229 - 0.97566[\ln(Q)] + 0.08532[\ln(Q)]^2\}$$

Equation H.34

Appendix I. OPEX requirements for the pelleting line

I.1. The quantity of LPS required to heat the air

Knowing the required heat duty, the quantity of 5-bar steam can be calculated according the latent heat of evaporation of the 5-bar steam ($\lambda_{5bar,Steam}$) and the required heat duty ($Q_{indirect\_dryer}$). The properties of the steam used for the indirect dryer are shown in Table I-1, where the enthalpy of evaporation is bold and Equation I.2 shows how to calculate the quantity of used for the dryer.

Table I-1: Steam used for the indirect dryer

Steam type	LPS properties		V (m^3/kg)		U (kJ/kg)		H (kJ/kg)		
	P(bar)	T (°C)	Water	Steam	Water	Steam	Water	Evaporation	Steam
5-bar	5	151.8	0.00109	0.375	639.6	2560.2	640.1	2107.4	2747.54

The utility and power requirement could be calculated. The heat duty, and consequent LPS required, can be calculated according to Equation I.1 where the product of the dry air flowrate ($\dot{m}_{in,DA}$) and the specific enthalpy difference between the outlet and inlet conditions $\left(\widehat{H}_{out,DA} - \widehat{H}_{in,DA}\right)$. A 20% safety factor is added to account for heat losses.

$$\dot{Q}(\,kJ/h\,) = \dot{m}_{in,DA}(kg\,DA/h) \times \left(\widehat{H}_{out,DA} - \widehat{H}_{in,DA}\right)(\,kJ/kg\,DA\,) \times (1 + 20\%) \qquad \text{Equation I.1}$$

Once the heat duty has been calculated, the steam requirement ($\dot{m}_{LPS,req.}$) can be determined knowing the specific enthalpy of evaporation of the steam ($\widehat{H}_{evp,LPS}$). It is assumed that low-pressure steam (LPS) is used to provide the heating duty $\dot{Q}(\,kJ/h\,)$.

$$\dot{m}_{LPS,req.}(\,kg\,LPS/h\,) = \frac{\dot{Q}(kJ/h)}{\widehat{H}_{evp,LPS}(kJ/kg\,LPS)} \qquad \text{Equation I.2}$$

I.2. Quantity of air required to dry the solids

The air required for the rotary dryer was calculated through an "open source Psychrometric Plug-In for Microsoft Excel" [386]. The plug-in used the psychrometric chart as a function that could calculate properties of moist air provided a few input properties are known.

The amount of water to be evaporated can be calculated according to Equation I.3, where the mass of water evaporated is calculated by the difference between mass of water entering & exiting.

$$\dot{m}_{w,evp}(\,kg\,H_2O/h\,) = \dot{m}_{in}(\,kg/h\,) \times x_{w,in}(wt.\%) - \dot{m}_{out}(\,kg/h\,) \times x_{w,out}(wt.\%) \qquad \text{Equation I.3}$$

The amount of air required to "uptake" the water can be calculated if the absolute humidity change between the inlet and outlet air is known [387]. Assuming that the drying air enters the dryer at 70 °C and because the drying air (DA) only underwent a sensible heat change to increase the

temperature from 15 °C (ambient) to 70 °C, the absolute humidity of the air was constant. Knowing the dry bulb temperature (70 °C) and the absolute humidity (0.00624 kg H2O/ (kg dry air)) of the entering air, the enthalpy of can be calculated using "psych" function designed as a Macro in Microsoft Excel by a chemical engineer [386], and the MS Excel goal-seek function was used to calculate the dry-bulb temperature of the exiting air.

The enthalpy was calculated as 86.83 kJ/ kg DA. When the air uptakes water during the drying process, the air follows the constant enthalpy line to 100% relative humidity (maximum water uptake). Therefore, the uptake of water will cause the dry bulb temperature to decrease but the enthalpy to remain constant at 86.83 kJ/kg DA. Once the relative humidity has achieved 100%, no more water can be transported by the air and therefore the difference between the inlet and outlet absolute humidity will provide the change in relative humidity which can be used to calculate the mass of dry air required to uptake the water according to Equation I.4 below.

$$\dot{m}_{DA,req.}(kg/h) = \frac{\dot{m}_{w,evp}(kg\ H_2O/h)}{x_{w,out}(kg\ H_2O/kg\ DA)\ \text{-}\ x_{w,in}(kg\ H_2O/kg\ DA)}$$ Equation I.4

I.3. The quantity of LPS required to heat the air

Knowing the DA required, the LPS utility and power requirement could be calculated. The heat duty, and consequent LPS required, can be calculated according to the product of the dry air flowrate ($\dot{m}_{in,DA}$) and the specific enthalpy difference between the outlet and inlet conditions $(\hat{H}_{out,DA} - \hat{H}_{in,DA})$. A 20% safety factor is added to account for heat losses, as in Equation I.5.

$$\dot{Q}(kJ/h) = \dot{m}_{in,DA}(kg\ DA/h) \times (\hat{H}_{out,DA} - \hat{H}_{in,DA})(kJ/kg\ DA) \times (1 + 20\%)$$ Equation I.5

Once the heat duty has been calculated, the steam requirement ($\dot{m}_{LPS,req.}$) can be determined knowing the specific enthalpy of evaporation of the steam ($\hat{H}_{evp,LPS}$). It is assumed that low-pressure steam (LPS) is used to provide the heating duty $\dot{Q}(kJ/h)$.

$$\dot{m}_{LPS,req.}(kg\ LPS/h) = \frac{\dot{Q}(kJ/h)}{\hat{H}_{evp,LPS}(kJ/kg\ LPS)}$$ Equation I.6

I.4. The power requirement of the fan

The adiabatic, non-reversible work of the tube-axial fan is calculated according to the molar flowrate ($\dot{n}_{air,IN}$), compressibility factor (z_1), gas constant (R), inlet air temperature (T_{in}), the inlet (P_{IN}) and outlet air pressure (P_{out}), inlet temperature (T_{in}) as in Equation I.7 [388]. The compressibility factor is not included because it is assumed to ideal, i.e. 1 and the "k" value of 1.4 is assumed for diatomic molecules [348], [388]. The molecular flowrate ($\dot{n}_{air,IN}$) is calculated knowing that the molecular weight is 28.84 kg/kmol. Equation I.8 and Equations I.9 to I.12 describes the variables used for Equation I.7.

$$\dot{W}_{rev,adiab} = \dot{n}_{air,IN} \times \dot{z}_1 \times R \times T_{in} \times [(P_{OUT}/P_{IN})^a - 1] \times \frac{1}{a}$$

Equation I.7

$$\dot{n}_{air,IN} \left(\frac{kmol}{s}\right) = \frac{\dot{m}_{air,IN} \ (kg/s)}{M_{W,air} \ (kg/kmol)} = \frac{m_{air,IN} \ (kg/s)}{(0.79 \times M_{W,N_2}) + (0.21 \times M_{W,O_2})}$$

Equation I.8

$$z_1 = 1$$

Equation I.9

$$k = \frac{C_P}{C_V} = 1.4$$

Equation I.10

$$a = \frac{(k-1)}{k} = 0.2856$$

Equation I.11

$$R = 8.314 \frac{J}{mol.K}$$

Equation I.12

The outlet temperature of the fan can be calculated according to Equation I.13 [388], and the actual shaft work can be calculated according the adiabatic, reversible work and its efficiency, which is assumed as 70% for fans as shown in Equation I.14 [348], [388].

$$T_{OUT}(K) = T_{IN}(K) \times (\frac{P_{OUT}}{P_{IN}})^a$$

Equation I.13

$$\dot{W}_{actual}(kW) = \dot{W}_{rev,adiab}(kW)/Efficiency \ (\%)$$

Equation I.14

I.5. The power requirement for rotating the dryer

The horsepower required to rotate the shell is based off several operating rotary dryers and the horsepower required can be calculated from the diameter D and length L in feet [348], as seen in Equation I.15

$$P(HP) = 5 + 0.11 \times D \ (ft) \times L \ (ft)$$

Equation I.15

Appendix J. Pyrolysis process development

The pyrolysis model on the Aspen Plus flow sheeting tool requires the use of a thermodynamic package, appropriate method of representing the feedstock and a way to represent the wax, organic and aqueous phase oil produced from pilot-scale into the model. The following section describes these three parts for the model components.

J.1. Physical Property method

The selection of the thermodynamic property method, referred to as the (physical) property method in Aspen, can be difficult due to the possible hundreds of components that are produced from pyrolysis of heterogenous material. Typically, the guidelines for choosing the thermodynamic property method depends on whether the associated compounds are polar or non-polar as outlined in the Aspen User guide [389] and whether high temperatures and pressures are involved. Property methods are typically categorized as either an equation of state (EOS) model or activity coefficient model [350], [390]

Equation of state (EOS) property methods are suitable for non-polar, real compounds as shown from the guidelines for choosing a property method package in the Aspen User Guide [389]. The EOS property methods are not suitable for polar compounds or long chain hydrocarbons [391], that are expected in the pyrolysis oil. Despite this caveat, researchers have used EOS property methods like the Peng-Robinson method with Boston-Mathias (PR-BS) EOS modifications for the for the pyrolysis of lignocellulosic biomass [303], [392] and for MSW [26]. The decision to choose this method could be due to the Aspen User guide recommending the use of EOS for the production of synthetic fuels from coal [389]. Popular EOS models include the PR-BS model, the BWR Lee-Starlings (BWR-LS) model or the Redlich-Kwong-Soave with Boston-Mathias alpha function (RKS-BM) model [389].

Conversely, the activity coefficient model has been identified as better suited for the pyrolysis process due to the non-ideal behaviour and interactions witnessed between bio-oil and polar components [350] [392]. Although there are examples of researchers using several activity coefficient models, like the NRTL physical property method with UNIFAC activity coefficients for the pyrolysis of a plastic-paper streams [29] and a biomass stream [389]. One activity coefficient model was shown to be the best because it could accurately predict behavioural interactions [393], [394] due to its ability to describe non ideal solutions by estimating the necessary transport and thermodynamic property parameters [370]. This is the UNIQUAC model, which has been used by several researchers for biomass [302], [370].

The UNIQUAC model is used for the product recovery section of this model and the pyrolysis process has been divided into different areas using hierarchy blocks so that different areas could be assigned different property methods as shown in Table J-1.

Table J-1: Different areas of the pyrolysis and the property methods used for each area

Area name & description	Description	Property method
A000: Pre-treatment	Shredder & magnetic separation	SOLIDS
A1000: Drying	Direct & indirect drying	SOLIDS
A2000: Pyrolysis	Reactor & char separation	UNIQUAC
A3000: Product recovery	Fuel oil & aqueous phase oil recovery	UNIQUAC
A4000: Combustion	Energy for pyrolysis	PR-BS
A5000: Heat generation	Steam for drying and cooling duty	IAPWS-95

J.2. Feedstock

All material streams in Aspen Plus are present as a MIXED, CI SOLID or NC SOLID sub stream which refers to normal components, conventional solids and non-conventional solids, respectively [395]. The stream class assigned for all areas of the flowsheet was the "MIXCINC" which is for when mixed streams, conventional streams and nonconventional solids are all present but no particle size distribution (PSD) is used for any of the calculations [395].

The pulper rejects for the pyrolysis process was made up of all three sub streams, *viz*., the moisture was present as water of the MIXED stream, the ferrous metal was modelled as Fe under the CI SOLID sub stream and the organics which are volatized in the reactor and condenser are modelled as NC SOLID according to its component attributes. The component attributes used for the NC SOLID characterization is the Proximate, Ultimate and Sulphur analysis and are gathered from the experimental results. The moisture was provided in the MIXED sub stream and hence the proximate analysis was shown to have moisture content of zero, consequently the other variables of the proximate analysis were provided on a moisture free basis. The NC SOLID sub stream also requires the input of "GENANAL" attributes, being the DCOALIGT and HCOALGEN which are used to estimate the density and enthalpy parameters, respectively [395]. All the variables used for the NC SOLID subs stream are shown in Table J-2.

Table J-2: Assigned component attributes of the nonconventional sub stream of pulper rejects

Attribute	Description	Element	Designation
ULTANAL	Ultimate analysis (wt.%)	1. Ash (dry basis)	8.11
		2. Carbon (dry basis)	58.4
		3. Hydrogen (dry basis)	8.38
		4. Nitrogen (dry basis)	0.31
		5. Chlorine (dry basis)	0.04
		6. Sulfur (dry basis)	0.08
		7. Oxygen (dry basis)	32.79
PROXANAL	Proximate analysis (wt.%)	1. Moisture (assume 0)	-
		2. Fixed carbon (dry basis)	4.29
		3. Volatile matter (dry basis)	87.6
		4. Ash (dry basis)	8.11
SULFANAL	Sulfur analysis forms (wt.%)	1. Pyritic (dry basis)	0
		2. Sulfate (dry basis)	0.08
		3. Organic (dry basis)	0
GENANAL	General analysis	HCOALGEN (enthalpy)	(6; 1; 1; 1)
		DCOALIFT (density)	
		DNSYGEN	

J.3. Model components for the condensable product

Pyrolysis liquid is comprised of hundreds of unknown components. Using the experimental results and from estimating the composition of wax, organic phase, and aqueous phase oil, it is possible to select components that should model the pyrolysis liquid accurately. Table J-3 provides the list of the model components used for each condensable product.

The pyrolysis of polyolefins like PE or PP yields aliphatic hydrocarbons with a carbon chain of length ranging from C_6 to C_{30} [240], [367]. Generally, these hydrocarbons are modelled as specific alkanes of a carbon chain length to represent a range, e.g. n-decane (C_{10}) would represent hydrocarbons of chain length of C_8 to C_{12}. Compounds with a carbon chain length of C_{18} and greater were assumed to be wax because C_{18} is the first alkane to be solid at room temperature. Hence the compounds with a carbon chain of C_{18} and greater, i.e. C_{24} and C_{30} were assumed to be the components of the wax phase [367]. Hence, wax was modelled by three compounds being C_{18}, C_{24} and C_{30} [240], [367].

The organic phase consisted of plastic-derived and lignocellulosic fibre-derived compounds. As mentioned, the components from C_6 to C_{18} would not form the wax phase due to their lower melting point and hence they comprise the organic phase instead. Typically, alkanes in the form of $C_8 – C_{10}$ and $C_{13} – C_{17}$ were significant in the fuel oil for pure plastic pyrolysis [283] and even when the plastic was low in feed composition [240]. Hence it was assumed that the organic phase from plastic

pyrolysis would consist of lower component alkanes and light waxes and would be represented by three model components, *viz.*, n-hexane, n-decane and n-hexadecane as shown from the pyrolysis of pure polyolefins [283]. The presence of aromatics is negligible and not included in the organic phase. The lignocellulosic fibre derived compounds of the organic phase include all the nonpolar compounds, soluble in solvents such as benzene or carbon tetrachloride as specified on PubChem. The organic phase oil is derived from both the plastic and lignin-derived compounds of the fibres. The components from the pyrolysis of plastic in the organic oil phase are n-hexane, n-decane and n-hexadecane. The components from the pyrolysis of fibres are derived from lignin and have been assigned as soluble within the organic phase due to their chemical properties showing their solubility within nonpolar medium.

Conversely the aqueous phase has been shown to be majorly water, but the presence of water-soluble compounds is present in the aqueous phase. Compounds that were soluble in polar solvents like water, alcohol, or methanol, etc. were assumed to be soluble in the aqueous phase. Carbohydrate-derived molecules such as formic acid, acetol and acetic acid are present from the pyrolysis of most biomass samples [243] and will most likely be present in the aqueous phase.

Table J-3: Compounds used to describe pyrolysis liquid product

Designation	In model?	Compounds	Formula	Designation
C18H38	✓	n-Octadecane	$C_{18}H_{38}$	Wax
C24H50	✓	n-Tetracosane	$C_{24}H_{50}$	
C30H62	✓	n-Triacontane	$C_{30}H_{62}$	
HEXANE	✓	n-Hexane	C_6H_{14}	Organic phase
DECANE	✓	n-decane	$C_{10}H_{22}$	
C16H34	✓	n-hexadecane	$C_{16}H_{34}$	
HMF	✓	5-Hydroxymethylfurfural (HMF)	$C_6H_6O_3$	
LEVOGL	✓	Levoglucasan	$C_6H_{10}O_5$	
3-MET-01	compromise	2-cyclopente-1-ene	C_5H_6O	
METHY-01	compromise	4-Vinylguaiacol	$C_9H_{10}O_2$	
ETHYL-01	compromise	Eugenol	$C_{10}H_{12}O_2$	
ACETOVANILLONE	✓	Apocynin	$C_9H_{10}O_3$	
PHENOL	✓	Phenol	C_6H_6O	
GUAIACOL	✓	Guaiacol	$C_7H_8O_2$	
2,3DMP	✓	2,3-dimethylphenol (DMP)	$C_8H_{10}O$	
2,6DMP	✓	2,6-dimethylphenol (DMP)	$C_8H_{10}O$	
H2O	✓	water	H_2O	Aqueous
FURFUROL	✓	2-furanmethanol \\ Furfurol	$C_5H_6O_2$	
DIKET-01	compromise	Furanone	$C_4H_4O_2$	
GLY-ALD	✓	Glycol aldehyde	$C_2H_4O_2$	
ACETICAC	✓	Acetic acid	$C_2H_4O_2$	
ACETOL	✓	Acetol	$C_3H_6O_2$	
FORMI-01	✓	Formic acid	CH_2O_2	

J.4. Product yields

The product yields from the pilot-scale experiments was used in the Aspen Plus mode. The normalized product yields for the components in each are shown in Table J-4. These product yields were input to the *RYield* reactor of the Aspen Plus model.

Table J-4: Normalized product yields for the model compoentns at the different pyrolysis temperaturtes

Compounds	Formula	Designation	450 °C	500 °C	550 °C
n-Octadecane	C18H38	**Wax**	0.065132335	0.113766059	0.230051532
n- Tetracosane	C24H50		0.123589041	0.10973823	0
n-Triacontane	C30H62		0	0.018370365	0
n-octane	C18H18	**Organic phase oil**	0.017773415	0.019737466	0
n-dodecane	C12H26		0.053110543	0.023508526	0.023923509
n-hexadecane	C16H34		0.054225795	0.049243881	0.100712179
5-Hydroxymethylfurfural (HMF)	C6H6O3		0.001329128	0.000672128	0.000411691
Levoglucasan	C6H10O5		0.035334735	0.010004489	0.01142878
2-cyclopente-1-ene	C5H6O		0.000902804	0.000496651	0.000390482
4-Vinylguaiacol	C9H10O2		0.000250779	0.000152296	0.000130161
Eugenol	C10H12O2		0.000275857	0.000167526	0.000143177
Apocynin	C9H10O3		0.000927882	0.000451663	0.000312386
Phenol	C6H6O		0.000727259	6.05951E-05	0.000226184
Guaiacol	C7H8O2		0.000777414	0.0002545	0.000240169
2,3-dimethylphenol (DMP)	C8H10O		0.000117866	3.63571E-05	5.16006E-05
2,6-dimethylphenol (DMP)	C8H10O		0.000160498	7.76837E-05	5.33659E-05
water	H2O	**Aqueous phase oil**	0.107090651	0.113121265	0.059868296
2-furanmethanol \\ Furfurol	C5H6O2		0.000902804	0.012293518	0.000442547
Furanone	C4H4O2		0.005742835	0.000757439	0.001228697
Glycol aldehyde	C2H4O2		0.023874143	0.013423277	0.010764296
Acetic acid	C2H4O2		0.015376211	0.008126652	0.009260342
Acetol	C3H6O2		0	0.005586872	0.00396196
Formic acid	CH2O2		0	0.008292784	0
Char (CISOLID)		**Char**	0.227790171	0.210511304	0.176258549
Ash (CISOLID)			0.105314561	0.097325998	0.081489872
kg CO		**NCG**	0.016074536	0.01777969	0.026922882
kg CH4			0.008255644	0.011534969	0.027525054
kg H2			0.000313624	0.000781072	0.002214434
kg CO2			0.071490694	0.078107395	0.09446189
kg C2H6			0.009413264	0.012631987	0.026942468
kg C2H4			0.007857425	0.00982831	0.024616413
C3H6			0.011105397	0.014662967	0.028909515
C3H8			0.011105397	0.014662967	0.028909515
C4H8			0.007108226	0.008002224	0.014033208
C4H10			0.007108226	0.008002224	0.014033208
C5H12			0.004720421	0.003914334	4.0819E-05
C5H10			0.004720421	0.003914334	4.0819E-05

Appendix K. Process model and development

As previously shown in Table J-1, different property methods were assigned for different areas of the pyrolysis process. Hierarchy blocks can be used to distinguish different areas of the process and to assign different property methods to different regions. The pyrolysis process is separated into seven areas or hierarchy blocks as shown in the Aspen Plus model, as shown in Figure K-1. The stream numbers and the process unit numbers are labelled according to the process-flow diagram (PFD of Figure 6.4). The minimum approach temperatures for heat exchangers is specified as 22 °C for air-coolers, 10 °C for exchangers using cooling water or process streams, 5 °C for exchangers using chilled water and 1 °C for reboilers [347].
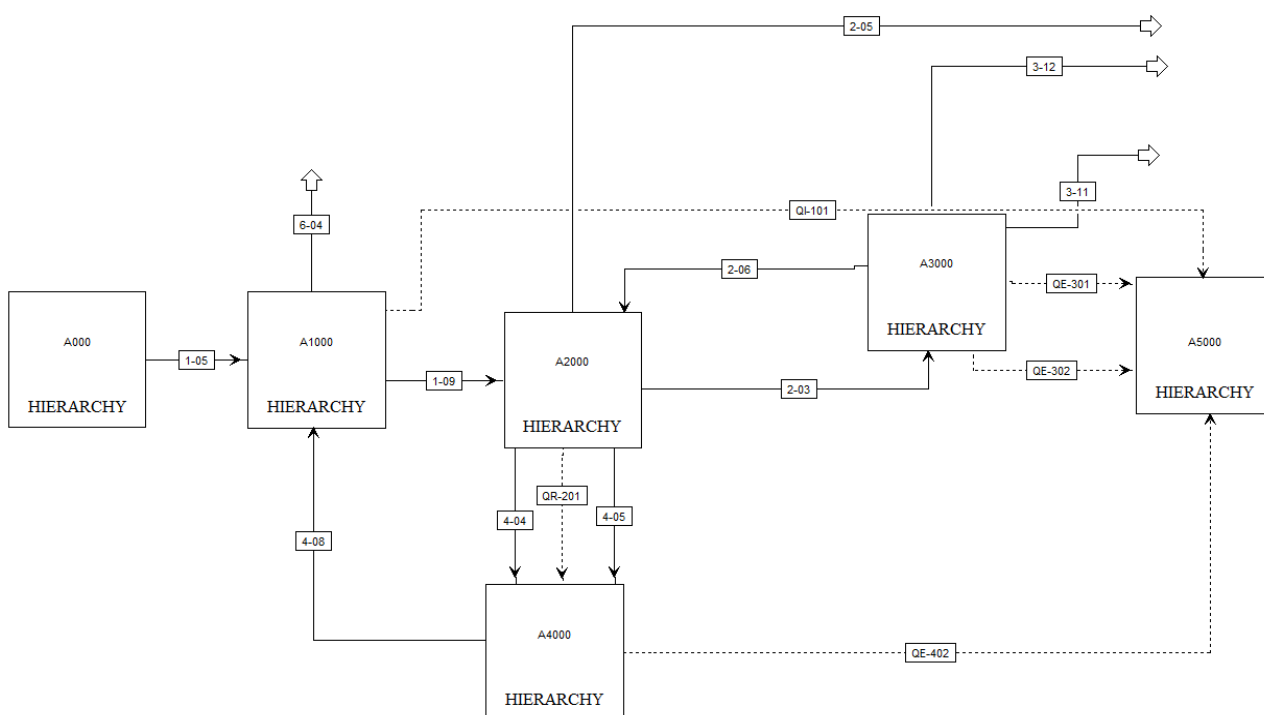

Figure K-1: The hierarchies of the Pyrolysis flowsheet on Aspen Plus

K.1. Section A0000: Magnetic separation and shredding

Figure K-2 shows the Area A000 where magnetic separation is performed, followed by shredding. The pulper rejects (1001) and water (1001M) are combined in a mixer (MIX1001) to attain a single stream. The mass flowrate of water (1001M) is calculated by the block (MCALC) according to the moisture content specified in the multiplier block (MOIST). The mixed stream (1-01) enters a SSplit unit (M-101) that completely separates the ferrous metal modelled as CI SOLID (1-02) from the rest of the material. The stream without the Fe fraction (1-03) enters the shredder (S-101) which is modelled as a hierarchy block. The block is used to calculate power requirement and the moisture removal. The calculator block (WORKMILL) calculates the power required to the shredded from stream WEMP1. It is assumed that the power requirement is 20 kWh/ton [29]. A pump named "MILLWORK" is used because mixer S1001A does not have an option for adding power. A filter in

211

series (S1001B) removes 20% of the water through shredding as stream 1-04. Thereby leaving the milled, moisture reduced stream as stream 4 in S-101 hierarchy and stream 1-05 in Area A000.
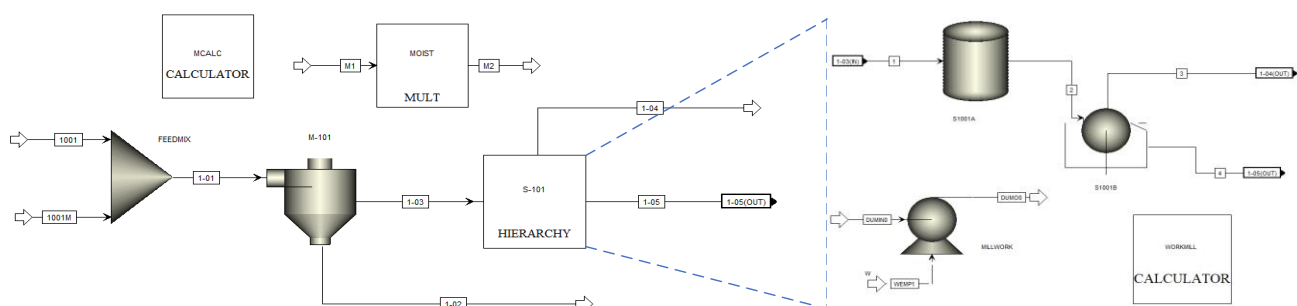

Figure K-2: Area A000: magnetic separation and shredding from the Aspen Plus tool.

K.2. Section A1000: Direct and indirect drying process

The direct and indirect drying hierarchy block from Aspen Plus is shown in Figure K-3. These units are used to decrease the moisture content of the sample entering the process, stream 1-05 from 43 wt.% (when containing metal) to the required equilibrium moisture content of 5.91 wt.%.

The reject stream (1-05) was dried in a direct dryer (D-101), modelled as an adiabatic flash tank at 1 atm. Flue gas, from the combustion chamber of A4000, was used as drying medium in the dryer. The flue gas, stream 4-08 was compressed to 1.3 bar (4-09) in unit B-401 before entering a cyclone modelled an SSplit unit labelled as S-401 on the diagram (Figure K-3). This cyclone would separate out the ash, a CISOLD (conventional solid), in the stream as waste to the process as stream 4-10. The hot compressed gas enters the direct dryer (D-101) and decreases the moisture content of the rejects according. The temperature of ash-free flue gas did not exceed 140 °C to prevent spontaneous combustion. The flue gas left the direct dryer as stream 6-04 to be released into the atmosphere.

The drier rejects (1-06) were then sent to the indirect dryer. The indirect dryer was composed of two parts, *viz.*, a heater (I-101A) and an adiabatic flash-tank (I-101B). A design spec named "DUTY" was built to deliver enough duty to the heater I-101A to evaporate water to attain the desired (equilibrium) moisture content of 5.91% for stream 1-08 or the dry reject stream. The removed water exits as vapor in stream 1-07 from the adiabatic flash tank. The pellet mill, H-101, is modelled as a mixer. The power requirement for the mill is calculated with a pump that uses a calculator block named "PLTMILL" to deliver the power from stream "W" to the pump at a rating of 45 kWh/ton. This was used because mills of 1 ton per hour used 2, 90 kW drives [363] but this unit is for *ca.* 250 kg/h.
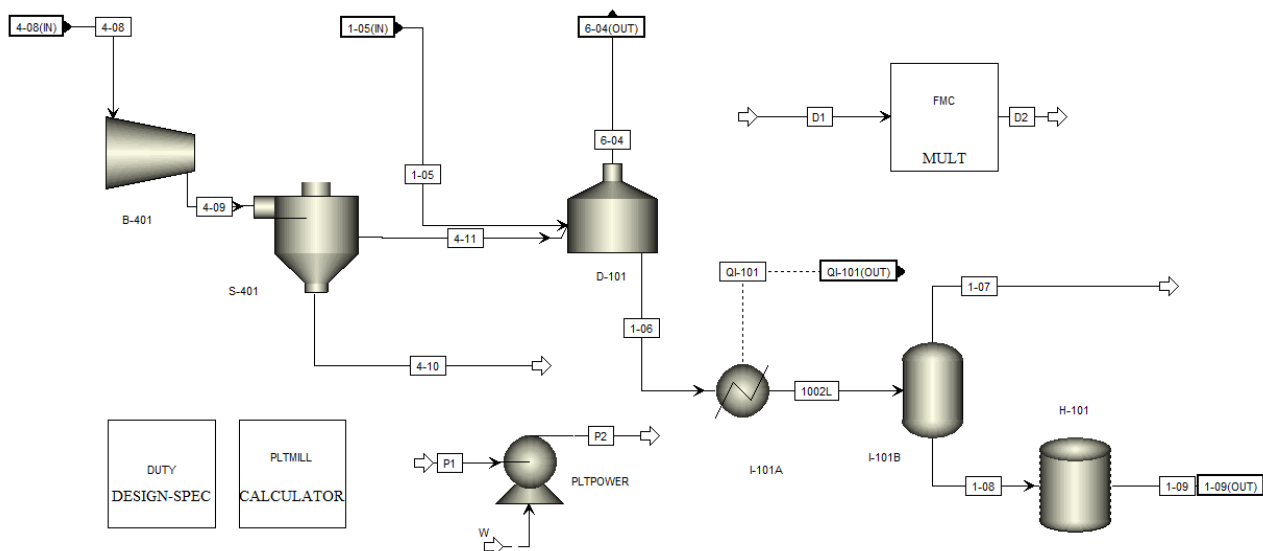
Figure K-3: The direct and indirect drying process of A1000

K.3. Section A2000: Pyrolysis and char separation

The pelleted, dry rejects present as stream 1-09 are now suitable for pyrolysis. Figure K-4 shows the hierarchy block in Aspen Plus whereby it can be seen that the rejects (2-01) enter the pyrolysis reactor (R-201A). The pyrolysis reactor is modelled as an *RYIELD* reactor to yield the NCG, char and liquid product. The condition of R-201A was set to 1 atmosphere pressure, and either 450, 500 or 550 °C and the mass yield of each component making up the liquid, NCG and char product was specified according to experimental results and model components explained in Appendix J. The recycled NCG is specified as 2-06 and is initially compressed to 1.3 bar in compressor C-402 before being split to go to the combustion reactor (4-05) or sent to the mixer (2-08) to be used as inert sweeping gas. The mass split specified by the splitter "SWEPSPLT" was determined according to the SWEEP Design-Spec. A split fraction was calculated that yielded 4.57 kg/h of NCG to stream 2-08. This flowrate was calculated knowing that the experimental results required 0.5 L/min of N_2 for 2 kg/h of feedstock. Hence because the stream is at least 100 times that of the experimental flowrate, i.e. 200 kg/h, 50 L/min of inert gas should yield a similar result. The average molecular weight of the NCG in stream 2-07 was 34.12 g/mol which equates to 4.57 kg/h.

The reactor products at reactor temperature and pressure are mixed with the 4.57 kg/h of inert gas in the mixer, MIXINERT, and heated back to reactor temperature in the heater, R-201B, and the heating requirement is sent to combustion area A4000. The PYTEMP calculator block maintains that the heater R-201B keeps ensures that heat of stream exiting the exchanger (2-02) is set to the reactor temperature. The inert gas and volatiles with the char exit the reactor as stream 2-02 and enter the cyclone modelled as SSplit unit, S-201, to perfectly separate the char and ash (from char) as stream 2-04 from the rest of volatiles stream, S-203. The char is split to be sent to either the hosting mill to be used as coal (2-05) or sent to the combustion area A4000 to supply the energetic

213

demand (4-04). The WORKPYRO calculator block determines the power requirement for the rotary kiln reactor, knowing that a 700 kg/h rotary kiln uses 5 kW of power [29].
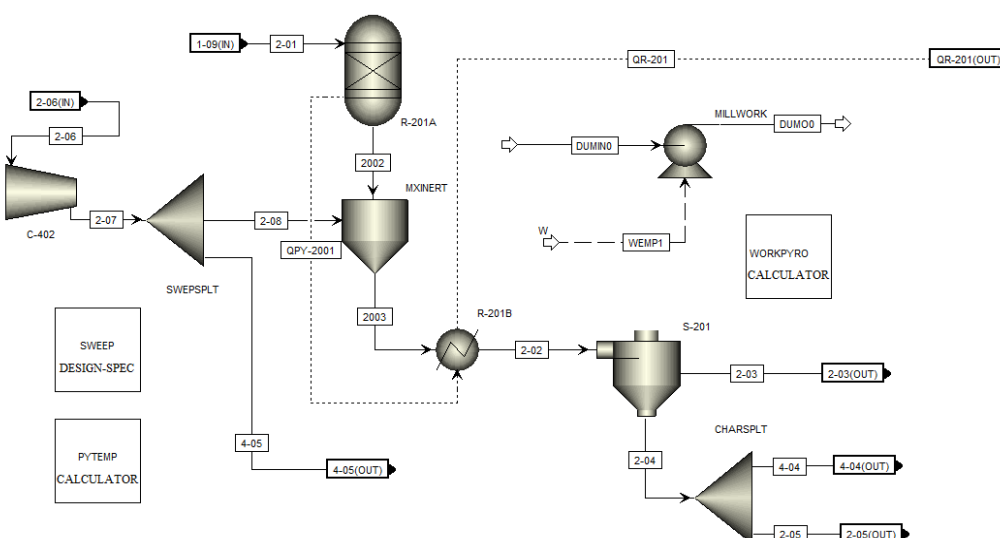

Figure K-4: The pyrolysis and char separation process in the hierachy block A2000

K.4. Section A3000: Product recovery

The product recovery section A3000, involved the isolation of the desirable components in the fuel oil from the undesirable components, is shown in Figure K-5. The hot gas from the reactor, 2-03, was initially quenched in two exchangers in series E-301 and E-302 to cool the stream from 500 °C to 260 and to 100 °C, respectively. The cooled stream 3-02 was then sent through a fractionation train consisting of four condensers like the pilot-scale setup on which the experiments were performed [302], [350].

Each heat exchanger was modelled as a cooler and adiabatic flash tank, for instance the first heat exchanger was a cooler (C-301A) followed by an adiabatic flash tank (C-301B). The temperature for each exchanger and flash was set at a cascading temperature whereby the first, second, third and fourth units were set to 60, 16, 12 and 5 °C, respectively. Each condenser used chilled water from the output of the next condenser as utility in a cascade-fashion. The chilled water exiting the first condenser (3-17) was the warmest with a temperature of 46 °C and was pumped to 1.3 bar in P-301 and then sent through the chiller unit E-303 to be chilled back to 5 °C and sent through condenser 4 again as stream 3-13. The C.O.P of the refrigerant unit is 4 [29]. The cycle remained open in the simulation to avoid convergence issues and 3-13A and 3-13B represent the same stream. All four condensers used utility approach temperature of 5 °C (condenser 2, 3 and 4) while the first condenser had a minimum approach temperature of 10 °C. Cross-over temperature was avoided by ensuring that each heat exchanger had counter-current configuration and the minimum amount of chilled water was determined by using the COOLING Design-spec block which made the utility exit temperature 45 °C for cooling water [347] and even 10 °C less than the exiting process stream.

The liquid product from the first and second condenser enter the atmospheric, adiabatic decanter (D-301) that split the fractions according to the liquids' fugacities determined from the property method. Both streams exited the decanter at 46.3 °C. The organic phase from D-301 mixes (PRDMIX) with the liquid product from condenser 3 and 4, streams 3-09 & 3-10. Stream 3-11 is the final product fuel oil stream consisting of the waxy and organic phase oil. Stream 3-12 from the decanter, D-301, is the aqueous phase oil which is a waste stream. Similarly to how Van Schalkwyk 2020 [302], [350] based their product yields off experimental results gathered from Chireshe 2020 [241], [331], the yields and temperature from the experimental study were input into this model.
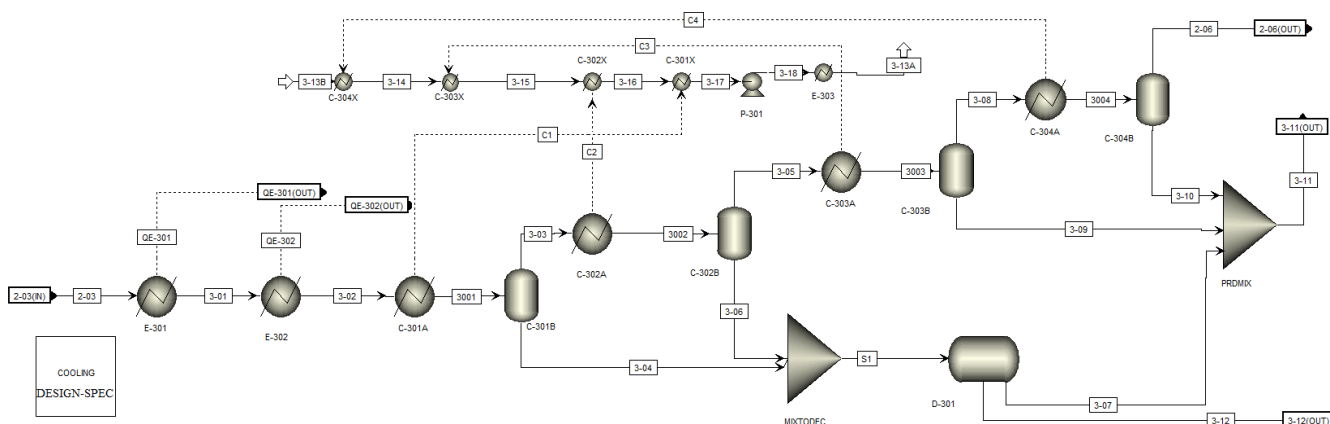

Figure K-5: Product recovery area in the hierachy block A3000

K.5. Section A4000: Combustion area

The combustion area (A4000) is used to calculate the fuel and air needed to sustain the pyrolysis reaction at the specified temperature and includes two forms of heat integration. The first is the cooling of the flue gas with BFW down to 250 °C, ensuring temperature crossover does not occur and the second is the subsequent preheating of air to further reduce flue gas temperature to 90 °C and increasing air temperature to 224 °C [325] in unit E-401. The flue gas is used as drying medium for the direct dryer in Area A1000. The Combustion area is shown in Figure K-6.

The combustion shell (F-401) was modelled as an atmospheric, RGIBBS reactor which only specified ash (CI SOLID) as an inert component. The predicted products were specified as H_2, H_2O, CO, CO_2, NO_2 in the mixed phase and Ash and char in pure solid phase. The RGIBBS reactor was also given the rigorous equilibrium calculations. 10% of the heat duty seen as stream QR-201 is initially split as heat loss while the rest of the heat, QR-201HT, is sent to the furnace F-401 to determine the outlet flue gas temperature and air requirement. All the NCG produced was either used as sweeping gas in the reactor or burnt in the reactor shell (F-401), whereby because the NCG needed for sweeping was so low, i.e. 4.57 kg/h, the NCG formed the main fuel in F-401. The NCG enters the furnace as stream 4-05 from the bottom of the shell. Only 10% of the char, seen as stream 4-04, was used as fuel in F-401. The stoichiometric air-to-fuel ratio (mass) of the solid char (C) and NCG gas (CH_4) is 11.4 and 17.1, respectively as calculated according to the combustion reactions

215

and molecular weights [396]. The stoichiometric air-to-fuel ratio (mass) of a multicomponent fuel such as NCG is harder to determine but has been given the same air-to-fuel ratio of 17.1 as seen for methane due to its similar HHV value and high composition thereof. This air requirement was calculated in 10% stoichiometric excess [325], as specified in the calculator block named AIR to remain the temperature under 1400 °C. The calculation is shown in Equation K.1 below.

$$m_{air} = 2.1 \times (11.4 \times m_{4-04} \left(\frac{\text{kg char}}{\text{h}} \right) + 17.1 \times m_{4-05} \left(\frac{\text{kg NCG}}{\text{h}} \right)) \qquad \text{Equation K.1}$$
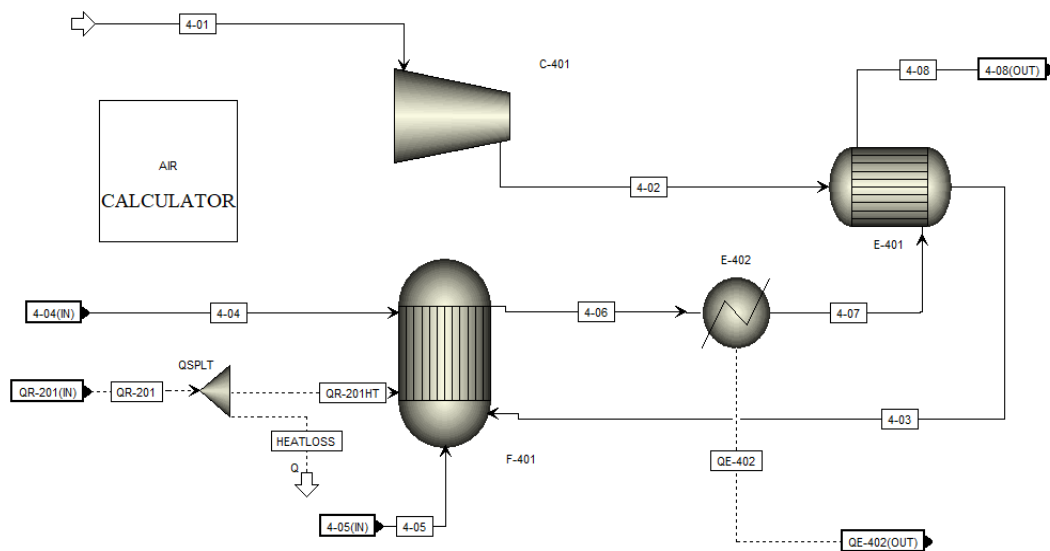

Figure K-6: Combustion area of the hierachy block A4000

K.6. Section A5000: Steam and Power generation area

Area A5000 is for generating steam from boiler feed water (BFD) to produce steam and electricity. 5-bar steam is used for the indirect dryer and the excess steam is used to produce more electricity. The liquid condensate is recycled back into the process. The electricity is generated in two turbines and can be used for all the compressors and pumps on-site. The area for steam and power generation is shown in Figure K-7.

The BFD as stream 5-02 is pumped from atmospheric pressure to 30 bar in a pump (P-501). The pressurized BFW was then used sent through heat exchangers from other areas to simulate using the BFW as cooling utility for their cooling. BFW was heated in E-302 and was checked so that the temperature did not cross over the process stream temperature of 260 to 100 °C. The BFW was further heated in E-301 and checked to see that temperature cross-over did not occur (for the process temperature of 500 to 260 °C). Lastly the BFW was heated in stream 5-05 in the flue gas cooler, E-402, to decrease the flue gas temperature from <1200 °C to 250 °C. The mass flowrate was determined by the "STEAM" calculator block whereby the mass flowrate of BFW designated in stream 5-02 was calculated according to the summation of the heat duties of E-302, E-301 and E-

216

402 divided by the summation of sensible and latent heat of the 5-bar water as shown in equation K.2 below.

$$m_{BFW}\left(\frac{kg}{h}\right) = \frac{Q_{E-302}+Q_{E-301}+Q_{E-402}}{C_{p,H2O}\times(T_S-T_0)+\Delta H_{vap,H2O}}$$
Equation K.2

The heated BFW at 30 bar and 234 °C, as stream 5-06, entered an adiabatic flash tank to ensure only vapor was sent to the turbine for power and steam generation. The liquid exited the steam, D-501, as blowdown (5-07) [302], [350] and the vapor, 5-08, was sent to a turbine set to exit pressure of 5 bar to produce steam at 152 °C for the indirect dryer [361]. WT-501 represents the work generated by the turbine. The 5-bar steam generated by the turbine shown as stream 5-09 can then be used in direct dryer modelled here as I-101 to condense the steam. All the excess steam was then sent through a second steam turbine (T-502) so that the exit pressure was ambient (1 atm). The liquid remaining was modelled as stream 5-12, as seen as the blowdown in the PFD (Figure 6.4). The condensate being stream 5-13 is recycled back to start of the run before being cooled in an air cooler to 55 °C using the minimum approach temperature of 22 °C for air cooler [347].

The condensate 5-12 can collect in condensate tank before being pumped back for recycle in the BFW recycle. The recycle loop remains open to avoid convergence issues and make-up water can be determined according to the water lost as blowdown.
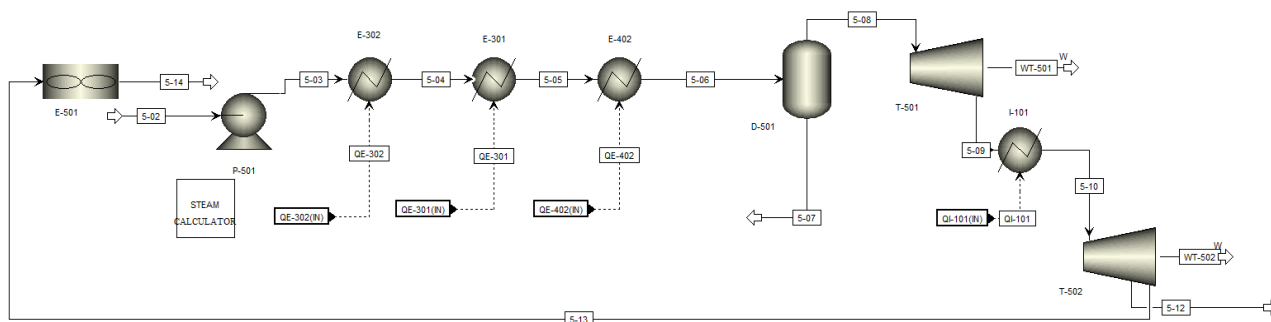

Figure K-7: Steam and power generation area of the hierachy block A5000

Appendix L. Comparison of pelleting lines

L.1. Technical comparison of pelleting lines

Table L-1: Characteristics of the SRF product and product recoveries for the process lines

Line #	Product characteristics				Product recovery	
	Moisture content	Ash content	LHV$_{wet}$	SRF Selling price	Organic fraction	Scrap metal
	(wt.%)	(wt.%)	(MJ/kg)	(R/ton)	(%)	(%)
BC	5.1%	9.0%	28.9	1330	92.1%	96.0%
1	4.4%	14.8%	25.9	1190	100.0%	80.0%
2	14.4%	12.9%	23.0	1050	78.0%	64.0%
3	4.9%	11.1%	28.2	1300	92.1%	80.0%
4	5.1%	8.6%	29.0	1330	91.9%	98.2%
5	5.1%	9.0%	28.9	1330	92.1%	86.4%
6	5.1%	9.0%	28.9	1330	92.1%	96.0%
7	4.9%	11.1%	28.2	1300	92.1%	72.0%
8	4.4%	14.8%	25.9	1190	100.0%	80.0%
9	4.6%	13.0%	26.4	1210	99.7%	96.5%
10	5.1%	9.2%	28.9	1320	91.9%	96.5%
11	4.6%	12.8%	26.5	1210	100.0%	96.0%

L.2. Efficiency and economic comparison of pelleting lines

Table L-2: Process efficiencies and economic considerations of process lines

Line #	Process Efficiency			Economic considerations			
	MC	GEC	NEC	TCI	Revenue	OPEX	Result
	(wt. %)	(%)	(%)	(R Mil)	(R mil/y)	(R mil/y)	(-)
BC	43.5%	97.7%	84.0%	R 39.7	R 3.40	R 3.20	Profit
1	50.1%	100.0%	86.0%	R 40.4	R 3.48	R 2.53	Profit
2	43.7%	87.5%	80.2%	R 31.9	R 2.80	R 2.60	Profit
3	44.6%	97.7%	86.2%	R 38.7	R 3.32	R 3.17	Profit
4	43.2%	97.5%	86.0%	R 39.6	R 3.41	R 3.20	Profit
5	43.5%	97.7%	86.2%	R 38.8	R 3.34	R 3.18	Profit
6	43.5%	97.7%	86.2%	R 38.8	R 3.40	R 3.16	Profit
7	44.6%	97.7%	86.2%	R 38.8	R 3.27	R 3.18	Profit
8	50.1%	100.0%	88.3%	R 39.5	R 3.48	R 2.50	Profit
9	48.9%	99.9%	88.1%	R 40.3	R 3.56	R 2.52	Profit
10	43.5%	97.5%	86.0%	R 39.6	R 3.40	R 3.19	Profit
11	48.9%	100.0%	88.3%	R 39.5	R 3.56	R 2.49	Profit

L.3. Key profitability indicators of process lines

Table L-3: Key profitability indicators of process lines

Line #	Result	Net result	ROI	PB	NPV$_{25}$	IRR
	(-)	(R mil/y)	(%)	(years)	(R Mil)	(%)
BC	Profit	R 0.203	-3.09	136	-R 31.4	-8.87
1	Profit	R 0.949	0.55	29	-R 29.3	-0.12
2	Profit	R 0.204	-2.83	108	-R 25.1	-7.72
3	Profit	R 0.155	-3.31	173	-R 30.8	-10.08
4	Profit	R 0.213	-3.03	128	-R 31.3	-8.59
5	Profit	R 0.166	-3.26	162	-R 30.8	-9.76
6	Profit	R 0.239	-2.88	112	-R 30.6	-7.91
7	Profit	R 0.093	-3.62	287	-R 31.1	-12.46
8	Profit	R 0.986	0.84	28	-R 28.4	0.29
9	Profit	R 1.038	1.00	27	-R 28.9	0.51
10	Profit	R 0.211	-3.04	130	-R 31.3	-8.64
11	Profit	R 1.066	1.24	26	-R 28.2	0.83

Note: The "Key performance indicators" header spans all columns except "Line #".

Appendix M. 500 °C pyrolysis process

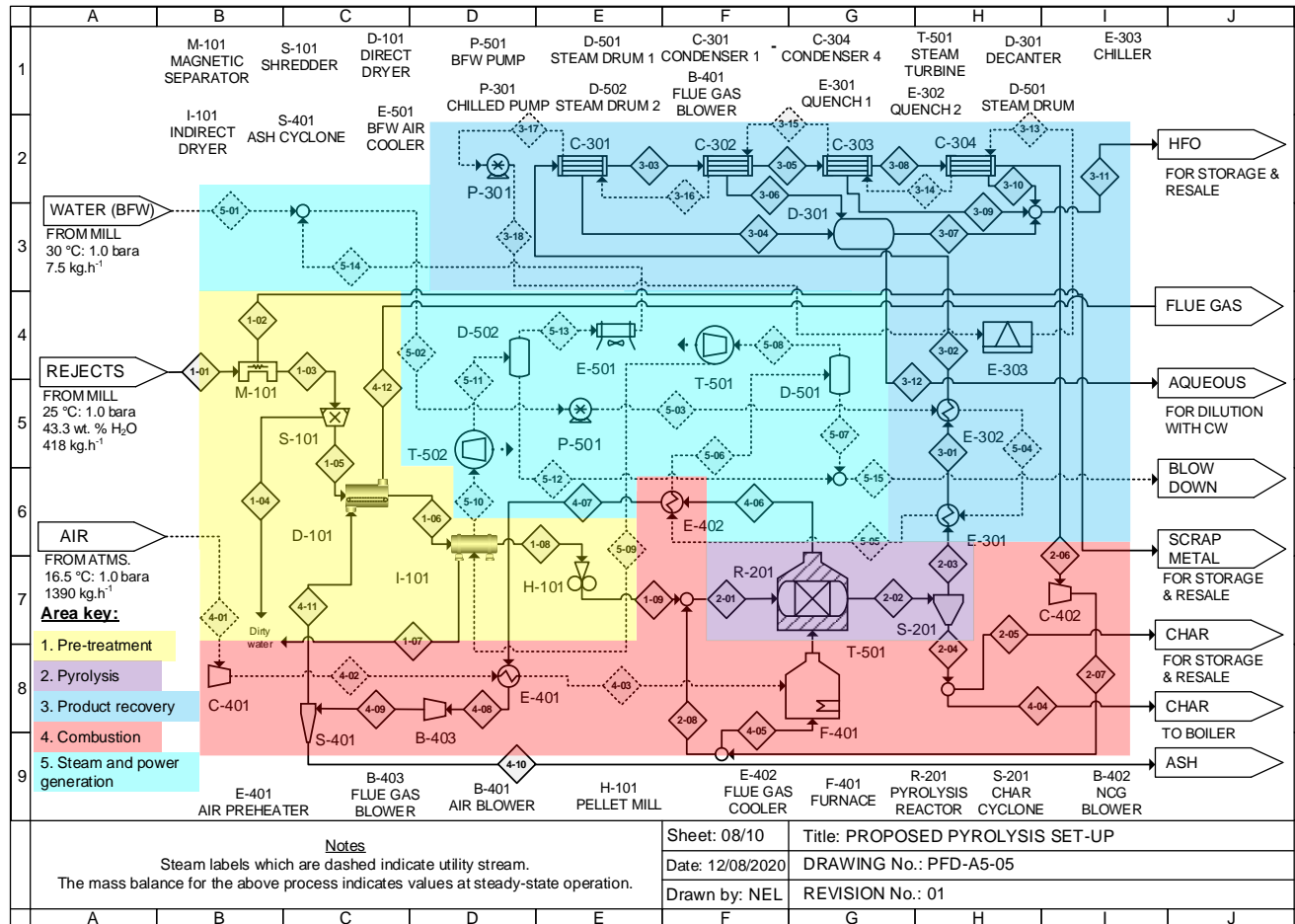## M.1. Process Flow diagram

Figure M-1: Process flow diagram for the 500 °C pyrolysis process

M.2. Utility flowrate and equipment duties

Table M-1: Utility flowrates and equipment duties for the 500 °C pyrolysis process

Area	Equip no.	Equipment name	Utility	Utility flowrate	Utility Duty	Elec. Duty
-	-	-	-	(kg/h)	(kW)	(kW)
Pretreatment	M-101	Magnetic Separator	-			
	S-101	Shredder	Elec.			4.10
	D-101	Direct Dryer	Elec.			6.90
	I-101	Indirect dryer	MPS	800	67.6	
	H-101	Pellet Mill	Elec.			9.23
Pyrolysis	R-201	Pyrolysis reactor	Furnace			1.46
	S-201	Char Cyclone	-			
Product recovery	E-301	Quench 1	BFW	807	-23.79	
	E-302	Quench 2	BFW	807	-22.28	
	C-301	Condenser 1	RW	488	-5.02	
	C-302	Condenser 2	RW	488	-17.9	
	C-303	Condenser 3	RW	488	-0.192	
	C-304	Condenser 4	RW	488	-0.0379	
	D-301	Decanter	-			
	P-301	Chilled Pump	Elec.			0.0135
	E-303	Chiller	Elec.	*C.O.P = 4		92.7
Combustion	B-402	NCG blower	Elec.			0.345
	B-401	Air Blower	Elec.			12.0
	E-401	Air Preheater	PS		67.1	
	F-401	Furnace	NCG	41	302	
	E-402	Flue gas cooler	BFW	807	-525	
	B-403	Flue gas blower	Elec.			15.0
	S-401	Ash Cyclone	-			
Heat generation	P-501	BFW pump	Elec.			2.23
	D-501	Steam drum	-			
	T-501	Steam Turbine	Power gen.			-61.4
	T-502	Steam Turbine 2	Power gen.			-33.1
	E-501	BFW air cooler	*Air*		-398.4	2.5

* S. PS-process stream; Elec.–electricity; MPS–medium pressure steam (5bar); RW–refrigerated water; CW-cooling water; BFW–boiler feed water.

M.3. Plant utility requirement

Table M-2: Plant utility requirement for the 500 °C pyrolysis process

Energy	Utility	Total energy (kW)	Generated (kW)	Required (kW)
Power	Electricty	146.4	94.4	52.0
Heating	MPS	67.6	67.6	0
	NCG	301.7	301.7	0
Cooling	BFW	571.0	571.0	-
	CW		-	0
	RW	23.2	23.2	-
	Air	398.4	-	398.4